UNIVERSITY OF ILLINOIS
URBANA

AERONOMY REPORT NO. 63

AN EVALUATION OF THE PARTIAL-REFLECTION TECHNIQUE AND RESULTS FROM THE WINTER 1971-1972 D REGION

By
L. C. da Silva
S. A. Bowhill

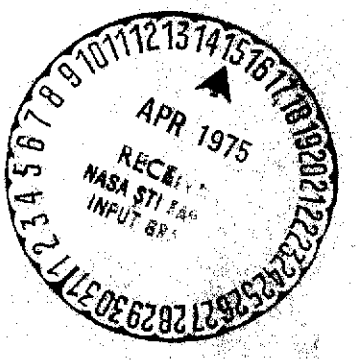

October 1, 1974

Library of Congress ISSN 0568-0581

Supported by
National Aeronautics and Space Administration
Grant NGR-14-005-181

Aeronomy Laboratory
Department of Electrical Engineering
University of Illinois
Urbana, Illinois

CITATION POLICY

The material contained in this report is preliminary information circulated rapidly in the interest of prompt interchange of scientific information and may be later revised on publication in accepted aeronomic journals. It would therefore be appreciated if persons wishing to cite work contained herein would first contact the authors to ascertain if the relevant material is part of a paper published or in process.

UILU-ENG 74 2506

A E R O N O M Y R E P O R T

N O. 63

AN EVALUATION OF THE PARTIAL-REFLECTION TECHNIQUE AND RESULTS FROM THE WINTER 1971-1972 D REGION

By

L. C. da Silva

October 1, 1974

Supported by
National Aeronautics
and Space Administration
Grant NGR-14-005-181

Aeronomy Laboratory
Departmentof Electrical Engineering
University of Illinois
Urbana, Illinois

ABSTRACT

Fundamental physical and chemical processes, and measurement techniques on the *D* region are reviewed. Design considerations about a partial-reflection system are made, and the main characteristics of the partial-reflection system at the University of Illinois are presented. The nature of the partial reflections are discussed, particularly reflections produced by gradients in electron density and by random fluctuations in a locally homogeneous random medium. Possible reasons for disagreement between partial reflections and rocket measurements are discussed. Some suggestions are made to improve partial-reflection data reduction, including the use of only maximums of the reflections and deconvolution of the data. The results of partial-reflection measurements at Wallops Island, Virginia during the 1971-1972 winter are presented and compared to rocket measurements.

TABLE OF CONTENTS

LIST OF TABLES

LIST OF FIGURES

1. THE IONOSPHERIC *D* REGION

1.1 *General Characteristics*

The ionospheric region between 50 and 90 km of altitude is known as the *D* region. Although the lowest part of the ionosphere, it is the least well understood, due to the complexity of the processes in effect and to the difficulty in making measurements.

The *D* region is characterized as a region of weakly ionized plasma with complex ionic structure. It is the only atmospheric region where both positive and negative ions are present in significant concentrations. Above 90 km, negative ions are quickly detached by ultraviolet solar radiation.

The electron densities are very small, of the order of 10^8 to 10^9 m^3 during the day, but because of collisions with the relatively dense neutral atmosphere, a strong attenuation is produced in HF electromagnetic waves propagating in this region.

Being primarily governed by solar radiation, the ionization of the *D* region almost disappears at night. The seasonal behavior of the ionization constitutes an exception to the solar control, and during some winter days very high electron densities are observed. Such abnormal behavior is part of the so-called winter anomaly, and will be discussed later.

The temperature structure shows a negative gradient with height, in an altitude region of 50 to 80 or 85 km, which is known as the mesosphere. The altitude of 85 km corresponds to the coldest level in the entire atmosphere (about 180°K in midsummer), and is known as the mesopause. Above the mesopause the gradient of temperature is positive, as a consequence of downward heat conduction from the thermosphere. During the winter the

temperature profile of the mesosphere shows strong fluctuations, and the minimum near 85 km is not clearly identified.

The mass of air that constitutes the *D* region is in turbulent motion, and the relative composition of the major neutral constituents is the same as that at ground level. Minor and ionized constituents do not follow this rule, due to the presence of sources and sinks.

In the remainder of this chapter, the principal aspects of the chemistry and dynamics of the *D* region, and the techniques of measurement of the more important parameters and constituents will be discussed.

1.2 *Sources of Ionization*

The *D* region is formed by the most penetrating radiations. The following sources are considered as important on its formation, and will be discussed below:

1) Solar Lyman-α radiation

2) Solar X-rays of wavelengths less than 10 Å

3) Galactic cosmic rays

1.2.1 *Solar Lyman-α.*

The strong solar radiation of Lyman-α (1216 Å) can penetrate the *D* region, due to the small absorption cross section of the atmosphere above 100 km of altitude, for this wavelength.

Lyman-α radiation can ionize only constituents with ionization potential less than 10 eV, in particular nitric oxide (ionization potential of 9.25 eV). *Nicolet and Aikin* [1960] estimated that the ionization of NO by Lyman-α is the major source of ionization in the altitude range of 65 to 85 km. Recent rocket measurements of NO concentration [*Meira*, 1971] confirmed the importance of Lyman-α in the formation of the *D* region. Calculated production functions of NO, using

the NO concentrations as measured by *Meira* [1971], are shown in Figure 1.1 [*Aikin*, 1972]. The role of Lyman-α as the principal ionizing source between 65 to 85 km during quiescent solar conditions is confirmed in this calculation.

1.2.2 *Solar X-rays of wavelength less than 10 Å.* All atmospheric constituents can be ionized by X-rays. X-ray photons with wavelengths greater than 10 Å are absorbed above 90 km, but photons with wavelengths less than 10 Å are able to penetrate the *D* region, that, in this way, can be considered as a tail of the *E* region.

The intensity of the solar X-ray radiation is extremely variable. Under quiet sun conditions, the intensity through the region of wavelengths less than 100 Å remains practically constant over a period of 24 hours. Over longer periods of time, however, considerable variations are observed for wavelengths less than 10 Å, and the intensity may change by a factor of 10 to 100 over a period of a few days [*Mandel'stam*, 1965]. During solar flares, a change in solar flux and spectral composition can be observed. The spectrum shifts towards shorter wavelengths, and sharp increases in the flux for $\lambda \leq 5$ Å are frequently observed. During a class I flare, the radiation intensity in the wavelength range of 1 to 8 Å can reach values of the order of 10 erg cm^2 s^1.

In Figure 1.1 a calculation of the ion-pair production function is shown for the solar fluxes and solar zenith angles listed in Table 1.1 [*Aikin*, 1972]. The curve X-ray I corresponds to quiescent conditions at low solar activity. During this time the contribution of X-rays to the ionization of the *D* region is negligible. Curve X-ray II corresponds to conditions of an X-ray enhancement event. Curve X-ray III shows the

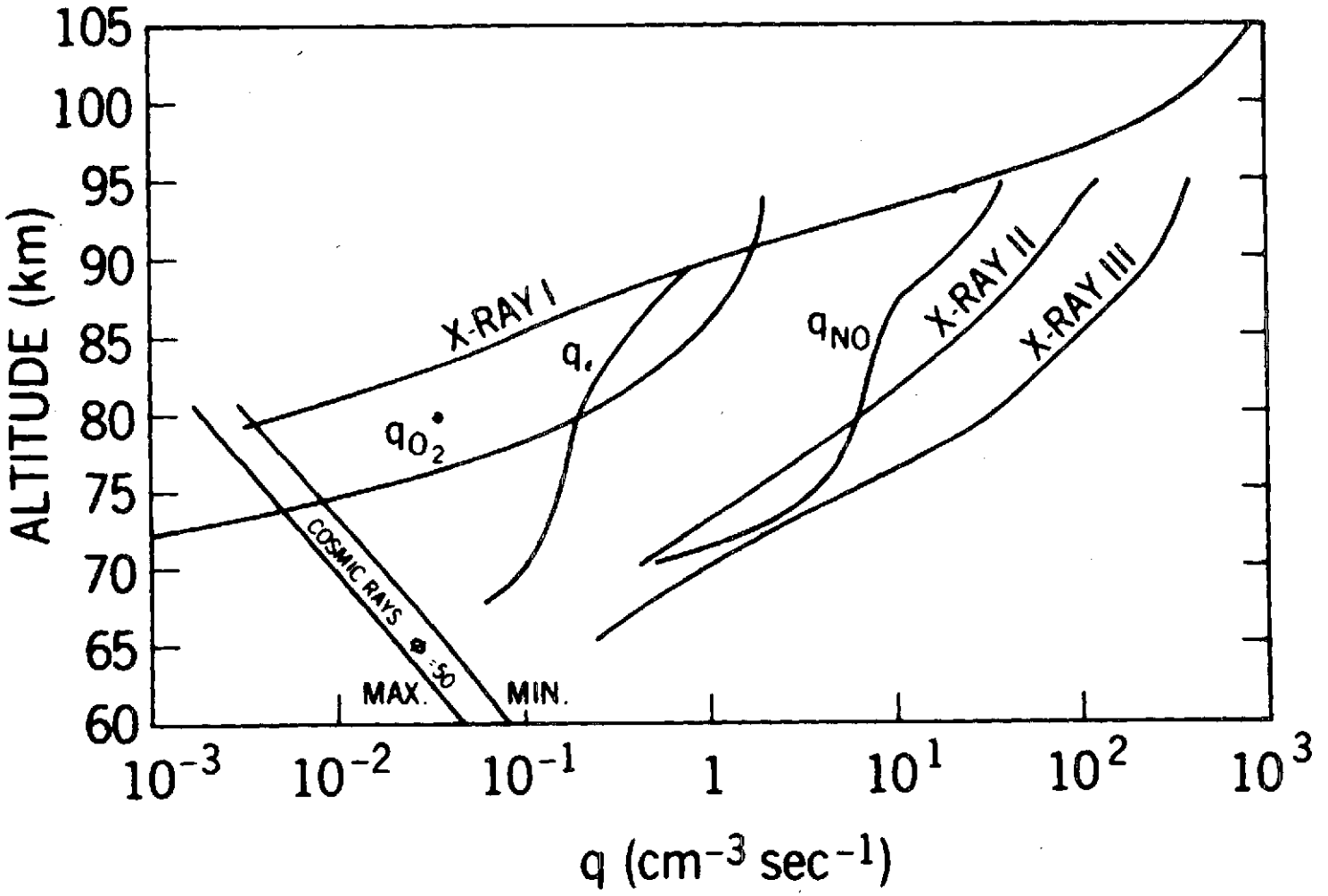

Figure 1.1 Ion-electron production functions produced by Lyman α (q_{NO}), X-rays (X-ray I, X-ray II and X-ray III), cosmic rays and ultraviolet radiation of wavelength less than 1118 Å (q_{O_2}). (From *Aikin* [1972]).

TABLE 1.1

X-ray fluxes and solar zenith angles corresponding to the electron-density profiles of Figure 1.1.

X-ray flux		Solar zenith
0.5-3 Å	1-8 Å	angle
	1.9×10^{-4}	53°
4.5×10^{-5}	5.8×10^{-3}	65°
1.2×10^{-3}	9.0×10^{-2}	68°

effect of X-rays during a class I flare. On such occasions X-rays are the dominant source of ionization down to 65 km.

1.2.3 *Galactic cosmic rays.* Galactic cosmic radiation (GCR) constitutes the most important source of ionization below 65 km [*Nicolet and Aikin*, 1960; *Webber*, 1962]. Calculated ion-electron production functions produced by galactic cosmic rays are shown in Figure 1.1 for maximum and minimum of solar activity, and a latitude of 50°.

1.2.4 *Solar ultraviolet radiation of wavelengths less than 1118 Å.* Wavelengths between 1216 Å and 1026.5 Å penetrate the *D* region in small intensities, so that the ionization of minor constituents by such radiation does not constitute an important source of ionization. The major constituents in ground state cannot be ionized by such radiation. If excited metastable species are present in sufficient concentrations, however, their ionization can contribute appreciably to the formation of the *D* region.

Ionization of $O_2(^1\Delta_g)$ by such mechanism has been suggested as a source of ionization of the *D* region. $O_2(^1\Delta_g)$ has an ionization threshold at a wavelength of 118 Å, and its ionization cross section is estimated as 3×10^{-18} cm^2. First calculations of the ion-electron production function resulted in a source as important as the ionization of NO by Lyman-α. In such calculations, however, atmospheric absorption by CO_2 was not considered. Ionization rates including CO_2 absorption [*Huffman et al.*, 1971] are of one order of magnitude smaller than the ionization produced by Lyman-α. A calculation of the ionization production function of $O_2(^1\Delta_g)$, including the absorption by CO_2 is shown in Figure 1.1.

1.3 D-*Region Chemistry*

The gases that constitute the atmosphere are chemically inert at low altitudes. In the ionosphere, however, they are excited and dissociated by solar radiation, and become extremely active. A multitude of reactions take place. The study of such reactions and the resulting distribution of neutral and ionized species is the objective of ionospheric chemistry.

As it is impossible, at the present state of knowledge to obtain a global model of the *D* region, involving all chemical reactions, normally particular models are developed, appropriate to a group of constituents, in a certain range of altitudes. It is usual to divide the *D*-region chemistry into positive-ion chemistry, negative-ion chemistry and neutral chemistry. Some aspects of each will be presented below. Electron loss processes encompasses both positive- and negative-ion chemistry, and will be presented in a separate section.

1.3.1 *Positive-ion chemistry.* The principal aspects and main problems related to the positive-ion chemistry of the *D* region have been presented in review papers by *Donahue* [1972] and *Thomas* [1974].

Mass spectrometric measurements of positive-ion composition of the *D* region have been successfully made since 1963 [*Narcisi and Bailey*, 1965]. The results obtained by Narcisi and Bailey are shown in Figure 1.2.

Above 82 km, 32^+, (O_2^+), and 30^+ (NO^+) are the dominant ions. Below 82 km, water cluster ions of mass 37^+ ($H^+ \cdot (H_2O)_2$) and 19^+ ($H^+ \cdot (H_2O)$) are the most predominant. It is possible that heavier hydrated ions of the form $H^+ \cdot (H_2O)_n$ are present, but they are dissociated by collisions with the rocket, and are not observed in the measurements. 28^+ (N_2^+) is observed in small quantities, since the ions formed by X-ray ionization of

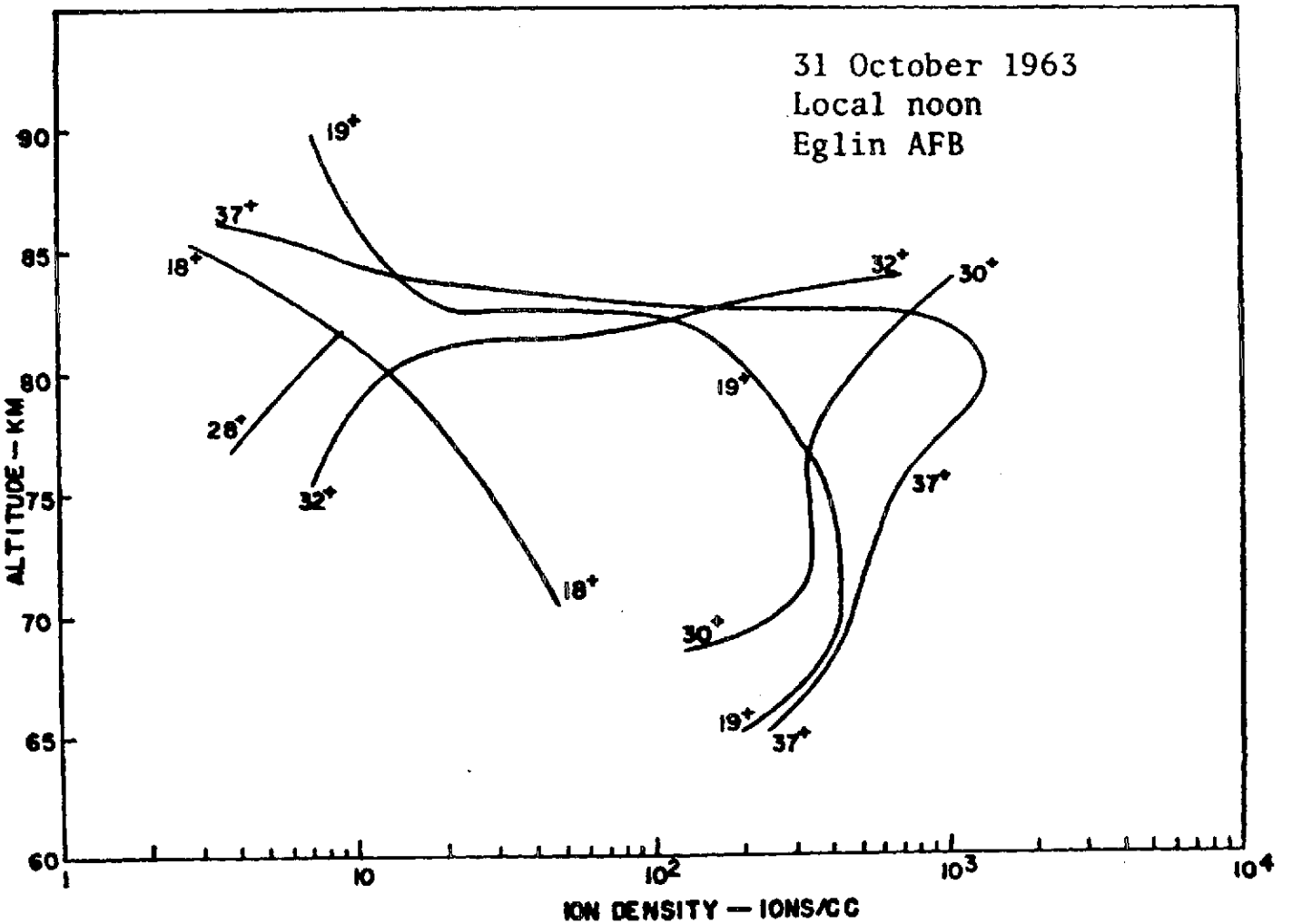

Figure 1.2 Positive-ion composition of the *D* region as measured by *Narcisi and Bailey* [1965].

N_2 disappear very rapidly by the reaction $N_2^+ + O_2 \rightarrow O_2^+ + N_2$. O_2^+ in turn dissociatively recombines with electrons or with negative ions.

The origin of the hydrated ions is one of the leading problems in *D*-region chemistry. *Fehsenfeld and Ferguson* [1969] suggested a scheme of reactions which is based on the formation of the cluster $NO^+ \cdot H_2O$ in a three-body reaction. This scheme was later supplemented by another starting with O_2^+ instead of NO^+ [*Ferguson and Fehsenfeld*, 1969]. The complete reaction scheme is shown in Figure 1.3 [*Donahue*, 1972].

The reaction $O_2^+ + O_2 + M \rightarrow O_4^+ + M$, the initial step in the proposed formation of the hydrated ions is a fast reaction in the lower ionosphere, and provides an effective way of changing O_2^+ ions in hydrated ions. Above 80 km in daytime the reaction $O_4^+ + O \rightarrow O_2^+ + O_3$ is very effective in reducing O_4^+ ions, and can explain the disappearance of hydrated ions near 82 km.

Recent calculations of the ionization rate of $O_2(^1\Delta_g)$ have shown that this ionization is much smaller below 80 km than believed before. As a result, the O_2^+ source will not be enough to explain the measured ion concentrations below 77 km.

The reaction scheme starting with NO^+ also presents some problems [*Donahue*, 1972]. In the first place, the first created ion is $H_3O^+ \cdot (H_2O)_2$, and not $H_3O^+ \cdot (H_2O)$, that has been observed to be the dominant ion; second, the conversion of NO^+ to the hydrates via the first three-body reactions is too slow, relative to the dissociative recombination of the cluster ions, and finally, if the NO measurements of *Meira* [1971] are correct, and if the ionization rate of NO is of about 10 cm^{-3} s^{-1}, as commonly accepted, NO^+ would be the dominant ion at 80 km, with density close to 3×10^3 cm^{-3}. This situation does not correspond to the facts.

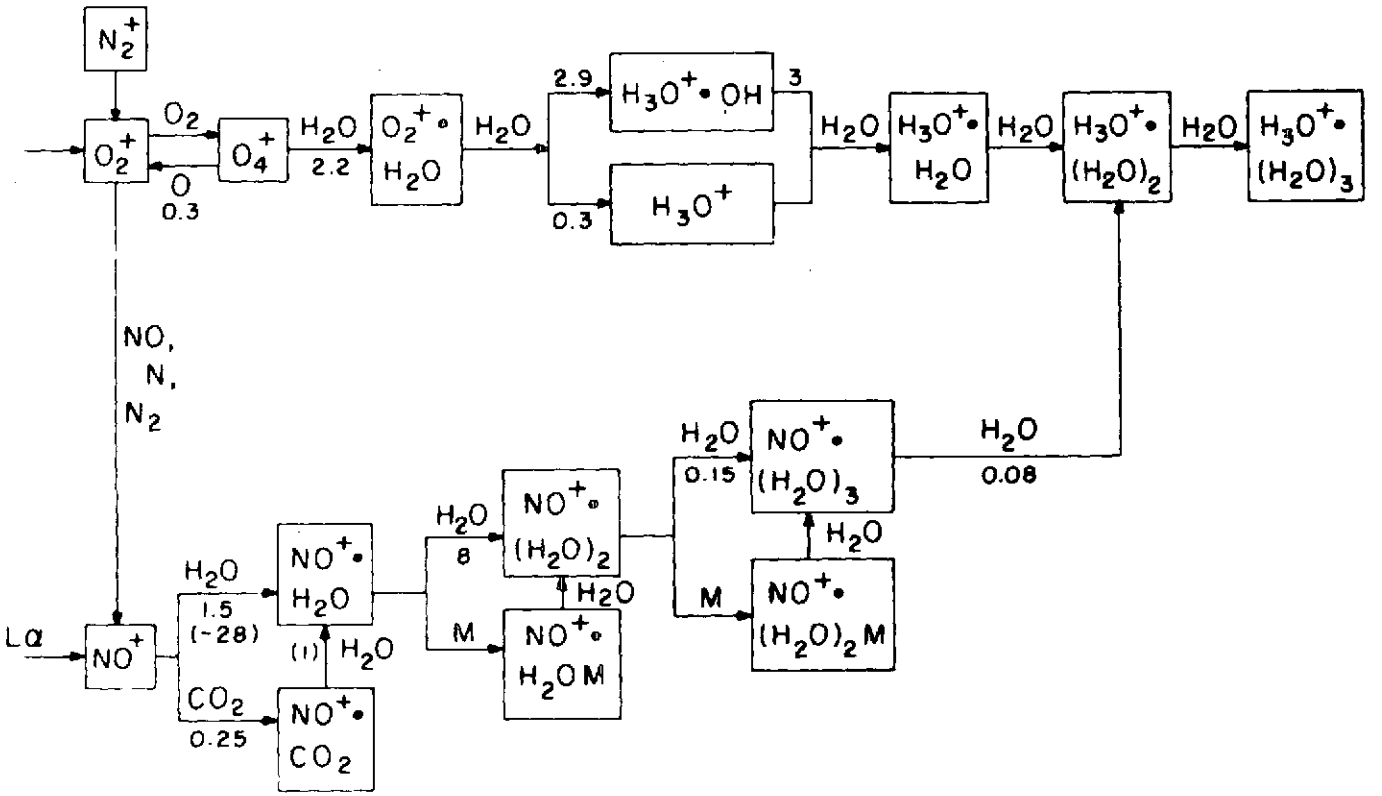

Figure 1.3 Reaction scheme for conversion of O_2^+ and NO^+ to hydrates. Three-body reaction rate constants in units of 10^{-28} cm^6 sec^{-1}. Two-body rate constants in units of 10^{-9} cm^3 sec^{-1} (From *Donahue* [1972]).

This problem would be solved if the ionization rate of NO by Lyman-α at 80 km were not as high as believed. *Donahue* [1972] suggests as possible explanations for a low ionization rate that the absorption of NO by a Lyman-α photon would not lead directly to NO^+, but rather to an excited state of NO, the ionization rate increasing by collisions at low altitudes, or that there would be a variation in the cross section of NO within the width of 1 Å of the Lyman-α line, the structure being a function of pressure.

1.3.2 *Negative-ion chemistry.* Measurements made up to the present time of negative-ion composition of the *D* region have yielded conflicting results [*Narcisi et al.*, 1972a; *Arnold et al.*, 1971]. Consequently the knowledge of the negative-ion chemistry is based on laboratory measurements and theoretical models. A review relating the most recent progress has been given by *Thomas* [1974].

1.3.3 *Electron loss processes.* The predominant electron loss source above 80 km is dissociative electron-ion recombination with NO^+ and O_2^+. At lower altitudes three-body reactions become important, and electron attachment to O_2 can be realized with N_2 or O_2 as the third body in the reaction.

The effective recombination coefficient, α_{eff}, can be measured at any occasion when a sudden variation in electron production is observed, as during solar flares [*Montbriand and Belrose*, 1972] and solar eclipses [*Sechrist*, 1970].

According to the results obtained by *Sechrist* [1970], above 80 km α_{eff} lies between 10^{-6} and 10^{-5}. The rapid variation with height of α_{eff} in this region corresponds to the gradient of electron density observed

near 85 km. Below 75 km, α_{eff} increases sharply from 4×10^{-5} to 10^{-3} cm^3 s^{-1}. Between 78 and 85 km, α_{eff} appears to be nearly constant with a value of about 4×10^{-5} cm^3 s^{-1}. The loss mechanisms in this altitude range are not well understood, but electron recombination with hydrated ions is probably the dominant electron loss process [*Reid*, 1970].

1.3.4 *Neutral chemistry.* *D*-region neutral chemistry is related to the chemical processes involving minor neutral constituents. All atmospheric constituents in the *D* region, with exception of O_2 and N_2 fall in the minor category. They include rare gases, metallic atoms such as Na, Ca, Al, Mg, Ni, Cr, Fe, and a number of molecules formed from the elements nitrogen, oxygen, hydrogen, and carbon.

To the present time, measurements of minor neutral constituents have been made by using particular techniques that are able to measure only one type of constituent. For atomic oxygen, for example, no reliable technique of measurement has been developed until now. As a result, our knowledge of the concentration of minor constituents is very unsatisfactory.

The chemistry of the most important minor netural constituents has been described in review papers by *Strobel* [1972] and *Thomas* [1974].

1.4 *Measurement Techniques*

The complexity of the parameters involved, the relatively high density of the atmosphere, and the small concentration of some of the most important constituents are some of the factors that contribute to the difficulty in performing *D*-region measurements. Satellites cannot be used, and measurements have to be made by using rocket or ground-based experiments.

Rockets have the disadvantage of giving only instantaneous information of the parameter involved, and are not well suited to time variation or synoptic measurements. Most *D*-region ground-based experiments, as will be described below, do not furnish the accuracy that would be desirable.

Because of the complexity of the processes involved, *D*-region measurements must be carefully coordinated, to take maximum advantage of the data obtained to the best theoretical interpretation, and in planning the next generation of experiments [*Bowhill*, 1969]. In the next sections the following types of measurements will be discussed: neutral structure and composition, ion density and composition, and electron density and collision frequency.

1.4.1 *Neutral structure and composition.* Measurements related to the neutral structure of the *D* region include measurements of density, neutral temperature, winds, minor neutral constituents and turbulence.

- Density measurements: Below the turbopause, measurements of gas density give the concentration of each major constituent, since the composition is nearly the same as at the ground.

Density profiles have been obtained by using falling spheres and pressure gauge experiments.

In the falling sphere experiment [*Bartman et al.*, 1956] a collapsed sphere is launched to a high altitude and then ejected and inflated after the rocket power has been exhausted and atmospheric drag has reached a tolerable magnitude.

Using falling sphere experiments *Faucher et al.* [1963, 1967] have performed several density measurements between the heights of 20 to 135 km; they estimated an error of about 4 percent at 110 km, increasing to 50 percent at 135 km.

Pressure gauges aboard rockets were used by *La Gow et al.* [1959] in the determination of air density to an altitude up to 210 km.

- Winds and neutral temperature: The most useful method of measuring winds and neutral temperature is the rocket-grenade method. The experiment is made by carrying aloft and ejecting grenades from rockets.

The fundamental parameters measured are the positions in space, the total travel time of sound waves to the ground, and angles of arrival of successive sound waves at an array of microphones located on the ground. From these parameters, wind velocities and temperature can be determined.

The grenade experiment has been used successfully several times, and a large amount of data obtained [*Stroud et al.*, 1960].

The accuracy of the measurement is limited by errors in measurements of the sound arrival times, and the resulting error below 75 km is generally less than $\pm$ 15° in wind direction. For higher altitudes, the intensity of the sound at the ground is so weak that the errors sometimes increase by a factor of 10.

- Minor neutral constituents: No technique has been developed to the present time that is able to measure different minor neutral constituents simultaneously. Mass spectroscopy has not been able to detect minor constituents in the *D* region. The information we have is the result of measurements made by rather specialized techniques, usually only applicable to one particular constituent, or by indirect means. Most measurements have been made by using absorption spectroscopy and glow emissions.

Absorption spectroscopy has been used successfully in measurements of ozone.

Diurnal distributions of ozone were measured by *Johnson et al.* [1952], *Weeks and Smith* [1968], *Reed* [1968], *Hays et al.* [1972] and

Miller and Ryder [1973]; nocturnal distributions were obtained by *Carver et al.* [1966].

Dayglow emissions have been used in measurements of sodium and nitric oxide.

Sodium profiles were obtained by *Donahue and Meier* [1967] by measuring the brightness of the sodium *D* lines as a function of altitude, using rocket-borne photometers.

Ground-based measurements of sodium dayglow brightness with Zeeman photometers have given information about the total concentration and time variations of atmospheric sodium [*Blamont and Donahue*, 1964].

Barth [1964], *Pearce* [1969], and *Meira* [1971] obtained NO concentrations in rocket experiments, by measuring the dayglow emission of NO in the gamma bands, using scanning ultraviolet spectrometers aboard rockets.

- Turbulence: Turbulence parameters have been measured by release of chemicals in the atmosphere [*Zimmerman*, 1965] and from reflections of radio waves from meteor trails [*Greenhow and Neufeld*, 1959]. Sodium and other chemicals have been released from rockets. The sodium trail is observed at twilight due to resonant scattering of 5890 Å sunlight. Some other chemicals have been used that produce a chemiluminescent trail. Turbulence parameters are obtained by taking pictures of the trail and analyzing its spreading as a function of time. The spread of the trail is due to molecular diffusion, wind shear and turbulence. There are some problems in interpreting the results, since the pictures taken contain only two-dimensional information, and the passage of the rocket introduces a pertubation in the atmosphere, and can alter the turbulent regime.

1.4.2 *Ion composition and density.* Measurements of positive-ion composition have been successfully performed several times, by using

rocket-borne mass spectrometers [*Narcisi and Bailey*, 1965; *Narcisi et al.*, 1972a, b; *Krankowsky et al.*, 1972]. Measurements of negative-ion composition in the *D* region, that have been carried out by *Narcisi et al.* [1972a] and *Arnold et al.* [1971], produced conflicting results; such measurements are very difficult to be made, due to the interactions of the ions with the structure of the rocket and spectrometers.

Ion densities have been measured by different kinds of probes. *Narcisi and Bailey* [1965] used a spherical electrostatic analyzer, that consists of a spherical collector surrounded by a concentric wire mesh grid. When the collector has a negative polarization, and the grid is at the rocket potential, the collector current is proportional to the positive-ion density. *Hale et al.* [1968] used parachute-borne blunt probes in measurements of ion concentrations.

1.4.3 *Electron density and collision frequency measurements.* The techniques of measurement of electron density and collision frequency can be classified into rocket and ground-based techniques.

- Rocket techniques: The first rocket measurements of electron density of the *D* region were obtained as early as 1947 [*Seddon*, 1953], utilizing the Doppler effect. Since then different techniques have been developed and combined, so that rocket measurements became the most effective way of measuring electron density and collision frequency in the lower ionosphere.

Rocket techniques utilize effects introduced by the ionosphere on propagation of radio waves, or current probes. The radio propagation experiments are based on Doppler effect, Faraday rotation, pulse delay and absorption, and on phase variations. Several measurement systems have been developed.

The University of Illinois, in cooperation with GCA Corporation, developed a measurement system incorporating both differential absorption and Faraday rotation, and a Langmuir probe. Since 1964 several successful measurements have been performed using this system. *Bowhill* [1965] has described the propagation experiment. The Langmuir probe, that will be discussed below, adds height resolution to the measurement.

- Langmuir probe: The Langmuir probe is a direct current instrument, that works by collecting charged particles in a plasma, by using a collector a few volts positive (in electron-density measurements) or negative (in positive-ion measurements). The probe current can give, in this way, an indication of electron density and of ion number density. Its usefulness at altitudes below 100 km, however, is severely limited by the lack of an adequate theory to describe the collection of electrons and ions by a space vehicle when the mean free path of the particles is not much larger than the Debye length. Such a problem has been solved by using Langmuir probes simultaneously with radio propagation rocket measurement, as described before. The Langmuir probe in such simultaneous measurements has the advantage of increasing the height resolution to an order of 10 m.

- Ground-based experiments: Ground-based electron density and collision frequency measurements have been obtained from the following: VLF propagation, incoherent scattering, cross modulation and partial reflection.

Only the partial-reflection technique will be discussed here. Information about the other techniques can be obtained on review papers [*Fejer*, 1970; *Sechrist*, 1974].

- Partial reflection: The partial-reflection technique is based on the measurement of weak reflections produced by small irregularities in the D region. If an HF pulse is sent to the ionosphere, a series of small reflections are observed between the heights of 50 and 90 km. If pulses with polarization corresponding to the ordinary and extraordinary modes of propagation are transmitted, from the ratios of the amplitudes, or from the phase of the reflections of the two modes, electron densities can be calculated, if a collision frequency profile is assumed.

Weak reflections produced by irregularities in the ionosphere were observed by *Dieminger* [1952], by examining conventional ionograms. Such reflections were used for the first time to calculate electron densities by *Gardner and Pawsey* [1953]. The technique of Gardner and Pawsey is based on the measurement of the amplitude of the reflections, and for this reason sometimes called a differential absorption technique. *Belrose* and *Burke* [1964] introduced the generalized magnetoionic theory in the expressions for calculation of electron densities, and developed the experimental techniques. A theory based on the work of Belrose and Burke will be presented below.

If the reflection produced at a height h is due to a small discontinuity in the refractive index, the coefficient of reflection is given by:

$$R_{o,x} = \left(\frac{n_2 - n_1}{n_2 + n_1} \right)_{o,x} \tag{1.1}$$

where n_2 and n_1 are the refractive index immediately above and below the irregularity, and the indices o and x refer to the ordinary and extraordinary modes of propagation. In expression (1.1) it was assumed that

the ionosphere is horizontally stratified, and that the propagation is quasi-longitudinal, so that the wave equation is decoupled for the ordinary and extraordinary modes, and the classical Fresnel expression for the coefficient of reflection can be used.

As the reflection observed are very small, it can be written: $n_2 \cong n_1 \cong n$, and $n_2 - n_1 = dn$, resulting:

$$R_{o,x} = \frac{dn_{o,x}}{2n_{o,x}} \tag{1.2}$$

The expressions for the refractive indices are given by the generalized Appleton-Hartree magnetoionic formulas [*Sen and Wyller*, 1960], for quasi-longitudinal approximation:

$$n^2_{o,x} = \left[\mu_{o,x} - \frac{jc\ K_{o,x}}{\omega}\right]^2 = 1 - \frac{\omega_o^2(\omega \pm \omega_L)}{\omega\nu^2} C_{3/2}\left[\frac{\omega \pm \omega_L}{\nu}\right] - j\,\frac{5}{2}\,\frac{\omega_o^2}{\omega\nu} C_{5/2}\left[\frac{\omega \pm \omega_L}{\nu}\right] \tag{1.3}$$

where $\omega = 2\pi f$, f being the operating frequency;

$\omega_L = 2\pi f_h \cos\theta$, f_h being the gyrofrequency, and θ the angle between the earth's magnetic field and the path of propagation;

ω_o is the plasma frequency;

$C_{3/2}(x)$, $C_{5/2}(x) = C_p(x)$ are integrals which have been tabulated by *Burke and Hara* [1963];

c is the velocity of light in free space; and

ν is the collision frequency of monoenergetic electrons.

Assuming that the irregularities are produced only by fluctuations in electron density, and not in collision frequency, it results from (1.2) and (1.3).

$$\frac{|R_x|}{|R_o|} = \left[\frac{\left\{\frac{\omega-\omega_L}{\nu} C_{3/2}\left(\frac{\omega-\omega_L}{\nu}\right)\right\}^2 + \left\{\frac{5}{2} C_{5/2}\left(\frac{\omega-\omega_L}{\nu}\right)\right\}^2}{\left\{\frac{\omega+\omega_L}{\nu} C_{3/2}\left(\frac{\omega+\omega_L}{\nu}\right)\right\}^2 + \left\{\frac{5}{2} C_{5/2}\left(\frac{\omega+\omega_L}{\nu}\right)\right\}^2} \right]^{1/2} \tag{1.4}$$

where $|R_o|$ and $|R_x|$ are the amplitudes of the ordinary and extraordinary coefficients of reflection, respectively.

The intensity of the signal reflected at a height h, when received at the ground is given by:

$$A_{o,x} \propto |R_{o,x}| \exp\left[-2 \int_0^h (K_{o,x}) dh \right] \tag{1.5}$$

and the ratio of the intensities of the extraordinary to ordinary signals is given by:

$$\frac{A_x}{A_o} = \frac{|R_x|}{|R_o|} \exp\left[-2 \int_0^h (K_x - K_o) dh \right] \tag{1.6}$$

If reflections from two different heights h_1 and h_2 are measured, it can be written:

$$\Delta \ln \left(\frac{A_x}{A_o}\right) = \Delta \ln \left(\frac{|R_x|}{|R_o|}\right) - 2 \int_{h_1}^{h_2} (K_x - K_o) dh \tag{1.7}$$

where

$$\Delta \ln\left(\frac{A_x}{A_o}\right) = \ln\left(\frac{A_x}{A_o}\right)_2 - \ln\left(\frac{A_x}{A_o}\right)_1$$

$$\Delta \ln \frac{|R_x|}{|R_o|} = \ln\left(\frac{|R_x|}{|R_o|}\right)_2 - \ln\left(\frac{|R_x|}{|R_o|}\right)_1$$

the indices 1 and 2 referring to the heights h_1 and h_2, respectively.

Taking the distance h_2-h_1 sufficiently small, the factors K_x and K_o can be assumed constants in the interval h_2-h_1, resulting:

$$\Delta \ln(A_x/A_o) = \Delta \ln(R_x/R_o) - 2(K_x-K_o)\Delta h \qquad (1.8)$$

where $\Delta h = h_2-h_1$.

The value of $K_{o,x}$ is given by:

$$K_{o,x} = \frac{\omega}{c} \mathrm{Im}(n_{o,x}) \cong \frac{5}{4} \frac{Ne^2}{m\varepsilon_o c\nu} C_{5/2} \frac{\omega \pm \omega_L}{\nu} = F_{o,x} N \qquad (1.9)$$

where N is the electron density.

From expressions (1.8) and (1.9), it results

$$N = \frac{\Delta \ln \frac{|R_o|}{|R_x|} - \Delta \ln (A_x/A_o)}{2(F_x-F_o)} \qquad (1.10)$$

Expression (1.10) can be used in the determination of the average electron density between the heights h_1 and h_2. The quantities $|R_x|/|R_o|$, F_x and F_o are obtained from equations (1.4) and (1.9), if a collision frequency profile is assumed.

Some comments are necessary about the signal processing techniques and the theory used.

The received signals are produced from reflections of transmitted pulses with width between 25 and 50 μ sec. Considerations of bandwidth and height resolution limits the lower and upper values of the pulse width. The pulse repetition rate normally used ranges from 0.5 to 60 sec^{-1}, depending on the processing capabilities of the system. Average values of the scattering cross sections at height intervals of approximately 1 km must be obtained from such signals. The average scattering cross sections are determined in the following ways:

1) By measuring the amplitudes of the received signals corresponding to a given height in every sample, and taking the average power over all samples:

$$A_{o,x} = \sqrt{\frac{\sum_{1}^{M} (a_{o,x})_m^2}{M}} \tag{1.11}$$

where M is the number of samples, $(a_{o,x})_m$ is the amplitude of the received signal, from a given height, in the m-th sample, and $A_{o,x}$ is the average value of $a_{o,x}$. Several ways of reducing the influence of noise are used, and some of them will be discussed in Chapter 2.

As the pulse width is finite, reflections from a height h are really produced in a height interval of $\pm Wc'/4$, W being the pulse width, and c' the velocity of light in the medium. The average value of the signals measured at a height h, in this case, will be representative of the scattering cross section at this height if the reflections are equally distributed over the interval $\pm Wc'/4$, during the sampling period, and if

the scattering cross section per unit volume does not change very rapidly with height. The consequences of a breakdown of the above assumptions will be discussed in Chapter 4.

2) By measuring only the peaks of the received signals, and taking the average of the measured peaks at each height. In this procedure it is assumed that the peaks of the signals correspond to reflections at a given height, and are not the result of interference of signals reflected from different heights. In practice, this method offers the disadvantage that normally only a few reflections are observed from certain height intervals, principally between 76 and 80 km. As a result long sampling and processing times are necessary. The influence in the electron-density profiles of using one or the other of the above methods will be discussed in Chapter 4.

The theory of scattering used in the determination of the ratio $|R_x|/|R_o|$ is a second point that deserves some comments.

The ratio $|R_x|/|R_o|$ was obtained by assuming that the reflections are produced by irregularities over height intervals much smaller than one wavelength, and that the atmosphere is horizontally stratified, at least over a region comparable to the first Fresnel zone. If the reflections are produced by irregularities distributed continually over the height interval, if there are a great number of discrete irregularities in the volume occupied by the pulse, or if the atmosphere is not horizontally stratified, a new model of reflectors must be introduced, or the use of equation (1.4) must be justified.

Belrose and Burke [1964] showed that reflections produced by irregularities distributed over a volume are related to reflections produced by a small discontinuity by a geometric factor, that is the same for both the

ordinary and extraordinary modes, and in consequence the ratio $|R_x|/|R_o|$ should be the same for both models of reflectors. This result, however, depends on assuming that the collision frequency and correlation function of the irregularities remain constant over the reflection volume, and that the atmosphere is horizontally stratified.

The effect of irregularities in the refractive index produced by irregularities in collision frequency was considered by *Piggott and Thrane* [1966]. As shown by *Gallet* [1955], however, if the irregularities are caused by adiabatic turbulent mixing on the gradient of electron density, the pressure fluctuations, and consequently the collision frequency fluctuations, are orders of magnitude smaller than the electron-density fluctuations.

Flood [1968] extended the theory of partial reflections by considering a reflector model consisting of irregularities continuously distributed over a homogeneous background medium. It was assumed an ionosphere horizontally stratified over an area at least equal to the first Fresnel zone, and quasi- longitudinal propagation.

If the above assumptions are valid, the wave equation is decoupled for the ordinary and extraordinary modes of propagation and the scattering cross section can be obtained by using the same techniques developed for scattering from an isotropic medium [*Tatarski*, 1961; *Booker*, 1959]. The expression obtained by Flood for the ratio A_x^2/A_o^2 is given by:

$$\frac{A_x^2}{A_o^2} = \frac{[y_x^2\ C_{3/2}(y_x) + \frac{25}{4} C_{5/2}(y_x)]C_{5/2}(y_o)\{1 - \exp[-\frac{5}{2} C_{5/2}(y_x) \left(\frac{Ne^2\tau}{m\varepsilon_o \nu}\right]]\}}{[y_o^2\ C_{3/2}(y_o) + \frac{25}{4} C_{5/2}(y_o)]C_{5/2}(y_x)\{1 - \exp[-\frac{5}{2} C_{5/2}(y_o)\ \frac{Ne^2\tau}{m\varepsilon_o \nu}]\}} \cdot$$

$$\exp\{-[\frac{5e^2}{m\varepsilon_o\, c} \int_0^{h-c\tau/4} \frac{N(h)}{\nu(h)} \left(C_{5/2}(y_x) - C_{5/2}(y_o)\right) dh]\} \qquad (1.12)$$

where $y_x = \omega - \omega_L/\nu$, $y_o = \omega + \omega_L/\nu$, τ is the pulse width, e is the charge of the electron, m is the mass of the electron, and c the velocity of light in free space. Figure 1.4 shows electron-density profiles obtained from the same A_x/A_o profile, by applying the theories of *Belrose and Burke* [1964] and *Flood* [1968]. The difference between the two profiles is at most 100 percent. As pointed out by *Holt* [1969], if the differential absorption inside the scattering volume is not too great, Flood's theory reduces to Belrose and Burke's theory. If the differential absorption inside the scattering volume is great and changes with altitude, the two theories will give results considerably different. Such a situation occurs normally above 80 km.

Cohen [1971] developed an expression for the scattering cross section for a reflector model including the following characteristics:

a) There is a finite number of irregularities distributed in a random way;

b) The irregularities are uncorrelated;

c) The ionosphere is horizontally stratified.

Assuming that the probability of occurrence of M different irregularities follow a Poisson distribution, Cohen arrived at the following expression for $A^2_{o,x}$:

$$A^2_{o,x} = \gamma \left(\frac{c\tau}{2}\right) |\bar{a}|^2 \int_{\tau_B}^{\tau_B+\tau} \left[\left(\frac{e^2 \delta N(ch/2)}{\varepsilon_o m\omega\nu(ch/2)}\right)^2 \right.$$

$$\left. \{[y_{o,x}\, C_{3/2}(y_{o,x})]^2 + [5/2\; C_{5/2}(y_{o,x})]^2\} \exp\{-4 \int_0^{ch/2} K_{o,x}\, dh\} \frac{dh}{\tau} \right] \quad (1.13)$$

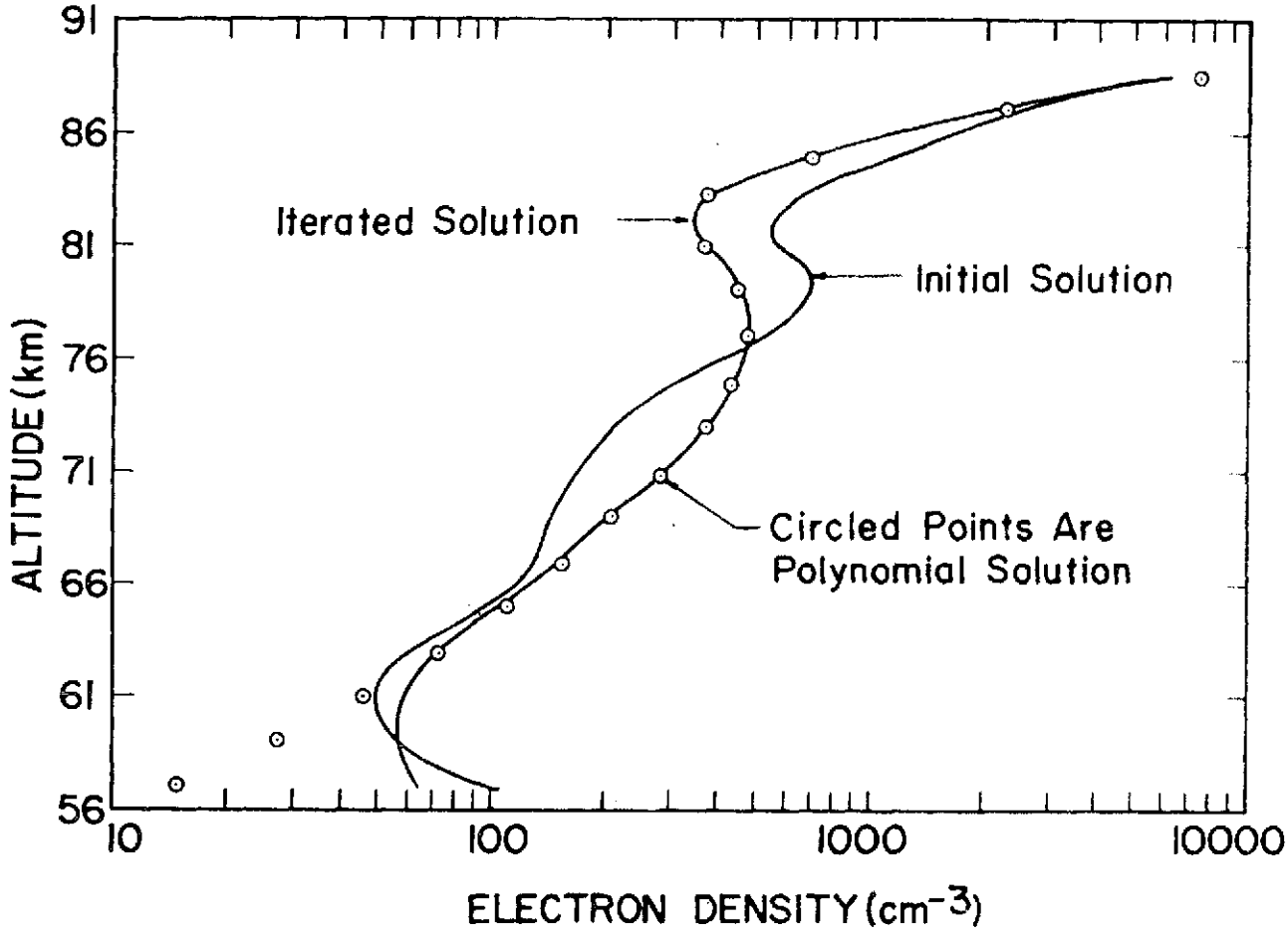

Figure 1.4 Electron-density profiles obtained using *Flood* [1968] theory (-o--o-) and *Belrose and Burke* [1964] theory (——). (From *Flood* [1968]).

where the variation of electron density of the irregularities is supposed to have a height dependence of the form $\Delta N(h) = \beta N(h) g(h)$ being the constant $g(h)$ a geometric factor; γ is the average number of irregularities per unit length, which was assumed to be a constant independent of height; $|\bar{a}|$ is a geometrical factor; τ is the pulse duration, and the other symbols are as defined before.

In Chapter 4 the problem of comparison of different scattering theories will be discussed again.

The real structure of the irregularities is not known, and thus it is not possible to define the more appropriate model. The problem of determination of the structure of the irregularities will be discussed in Chapter 4.

If the ionosphere is not horizontally stratified, there will be a coupling between the ordinary and extraordinary modes. If a pulse with one mode of polarization is transmitted, it will be depolarized, and reflections containing both modes will result. The wave equation in such a case cannot be separated, and its solution is very difficult. An approximate solution for the scattering cross section of a magnetoionic medium containing continuously distributed irregularities over a homogeneous background was developed by *Simonich and Yeh* [1971]. In the model of Simonich and Yeh the collision frequency was assumed as zero, and so the results cannot be applied directly to partial reflections. The wave equation was solved by using an approximate technique developed by *Lighthill* [1960]. The calculated scattering cross sections show that for the range of parameters encountered in partial-reflection experiments, the results are practically the same of *Flood's* [1968] theory.

Coupling between the ordinary and extraordinary modes in a horizontally stratified medium where the propagation is not longitudinal was discussed by *Connolly and Tanenbaum* [1972].

The results of *Connolly and Tanenbaum* [1972] show that for a horizontally stratified ionosphere, and for an electron density of 10^{10} m^{-3}, the coupling coefficient is always less than 3 percent. This is not large enough to be considered in partial-reflection calculations, since the error introduced is much smaller than the imprecision of the technique.

Until now only electron-density determinations based on measurements of amplitude of the reflections were discussed. *Von Biel et al.* [1970] developed a method of determining electron densities from the differential phase between the ordinary and extraordinary reflections, using the same model of reflector and the same approximations of *Flood* [1968], and utilizing measurements of amplitude of the reflections at different directions to determine indirectly the phase. The electron-density profiles obtained are very similar to the profiles measured by Flood's differential absorption technique, as should be expected, since both are based on the same theory.

Austin [1971] developed a method of determination of electron densities by measuring directly the phase difference between the ordinary and extraordinary reflections.

1.5 *Comparison of Electron-Density Profiles Obtained by Different Techniques.*

A comparison of electron-density profiles obtained by different techniques has been given by *Sechrist* [1974]. Differences between partial reflection and rocket measurements are of particular importance for this

work. Such differences occur principally for heights greater than 75 km, where partial-reflection profiles show a tendency to produce a valley in electron density that is not observed in rocket profiles. Above 80 km partial-reflection profiles are normally too low if compared to rocket profiles. Such differences will be discussed in Chapter 4.

1.6 *The Winter Anomaly: Theories and Experiments.*

The exceptionally high absorption of HF radio waves that is observed in some winter days at middle latitudes is known as the winter anomaly.

It was first observed by *Appleton* [1937] and later confirmed by several workers [*Appleton and Piggott*, 1948, 1954; *Dieminger*, 1952].

The causes of the winter anomaly remain unexplained until now. Several theories have been suggested, however, to explain its existence. These theories are basically related to:

a) An increase in electron production due to an increased concentration of NO;

b) Decreased electron loss by a change in the dissociative recombination process;

c) Increased electron production due to an increase in precipitated energetic electrons.

The theories related to items a and b above assume a meteorological origin to the winter anomaly. Studies of *Bossolasco and Elena* [1963] and *Gregory* [1965] have demonstrated that the increases in *D*-region absorption are correlated with increases in the temperature at the 10 millibar (30 km) level of the stratosphere.

Geisler and Dickinson [1968] suggested that the winter anomaly would be produced by enhancements of NO concentrations, and that such enhancements would be caused by vertical transport resultant of planetary waves.

A second possible meteorological cause of the winter anomaly is related to variations in electron loss rates. *Reid* [1970] and *Sechrist* [1970] arrived at the conclusion that the principal electron loss mechanism around 80 km is probably recombination with molecular or hydrated ions. *Sechrist* [1970] suggested that changes in mesospheric water vapor content could alter the concentration of hydrated ions, and consequently the electron loss rate. *Reid* [1970] suggested that besides the 37^+ ions observed by *Narcisi and Bailey* [1965] there are heavier hydrated ions in the mesosphere, as 55^+, 73^+, etc., that are not observed in rocket measurements because they are fragmented by the passage of the rocket. More complex ions would have higher recombination coefficients, since they have more degrees of freedom. Increases in mesospheric temperature would be sufficient to break up the larger ions, reducing the electron loss rate.

Maehlum [1967] showed correlations between satellite measurements of precipitated energetic electrons and days of high absorption, and advocated the theory that the winter anomaly is produced by precipitated electrons. *Geller and Sechrist* [1971] calculated the electron production produced by precipitating electrons necessary to explain the observed electron densities during days of high absorption and concluded that a very localized production rate of electrons would be required, and that the production rate at 80 km should be over 100 cm^3 s^{-1}. That is not probable.

Measurements of the winter anomaly have been in most cases obtained only by absorption measurements. *Belrose* [1966] obtained electron-density profiles during the winter by means of a partial-reflection experiment. A rocket electron-density profile during a day of high absorption was

obtained by *Mechtly and Smith* [1968]. The complexity of the factors involved in the winter anomaly, however, makes necessary simultaneous measurements of several parameters. A coordinated ground-based and rocket experiment was carried out in January and February of 1967 at Wallops Island, Virginia [*Sechrist et al.*, 1969]. The experiment included ground-based ionosonde and radio-wave absorption measurements to determine the days of high and low absorption, and rocket measurements of temperature, winds and electron density. The electron-density profiles obtained by *Sechrist et al.* [1969] are shown in Figure 1.5.

Figure 1.6 shows the rocket-grenade temperature and winds for the normal day (February 3, 1967) and for the anomalous day (January 31, 1967).

The electron-density profile for the anomalous winter day was very similar to electron-density profiles obtained during summer for the same zenith angle. The temperature profiles on normal and anomalous days were significantly different, with a warming occurring on the anomalous day above 70 km. The results of the experiment supported a meteorological origin to the winter anomaly.

During winter of 1970-1971, a coordinated rocket experiment was performed by the members of the Ionosphere Research Laboratory of Pennsylvania State University and the Atmospheric Sciences Laboratory of White Sands Missile Range, New Mexico [*Mitchell et al.*, 1972]. The experiment intended to measure electron and positive-ion densities, neutral temperature, winds, ozone concentrations and neutral air densities on three different days, two of them preferably anomalous, and one a control day. The measurements were performed on January 22, 1971

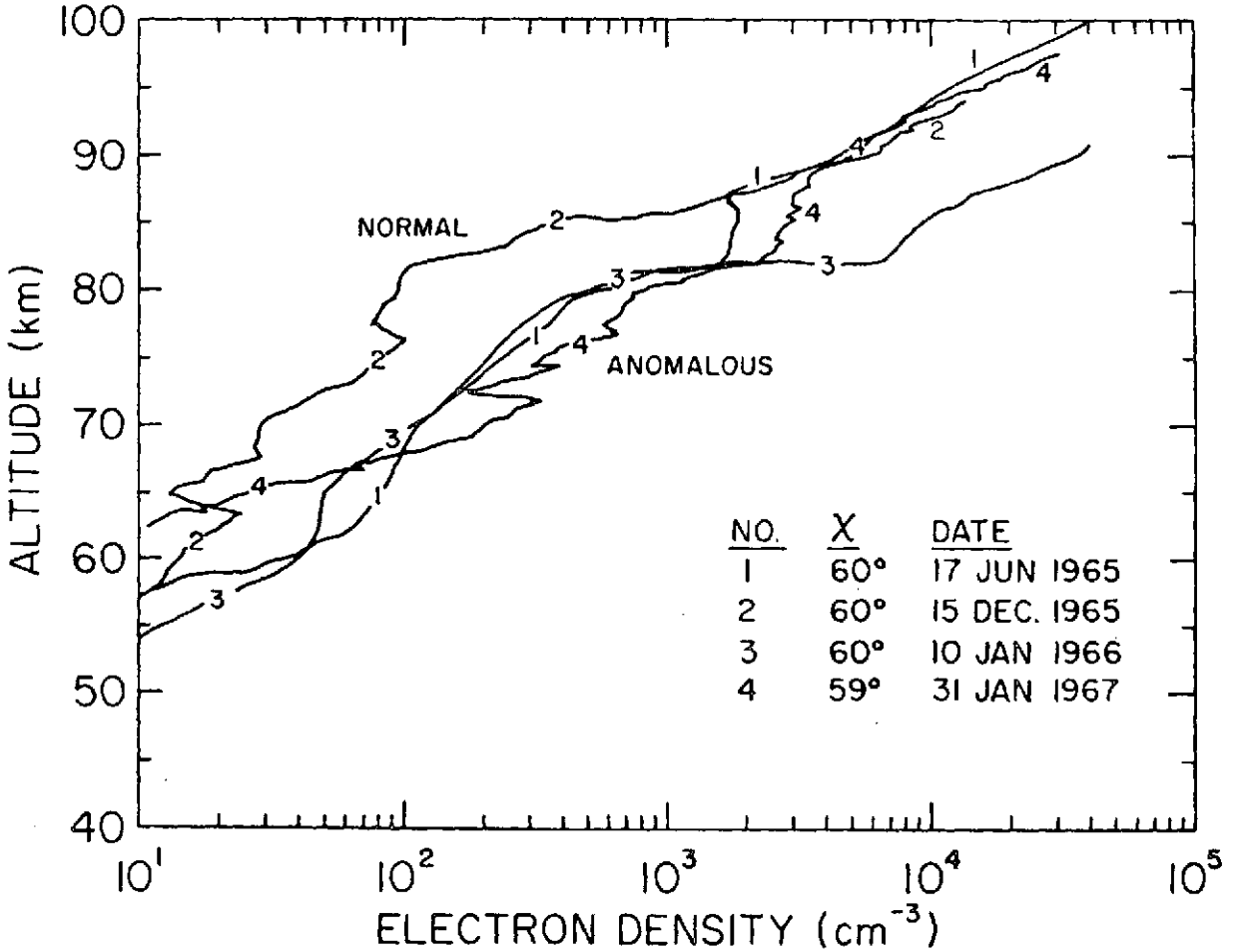

Figure 1.5 Rocket electron-density profiles comparing summer values with normal and anomalous winter electron densities. (From *Sechrist et al.* [1969]).

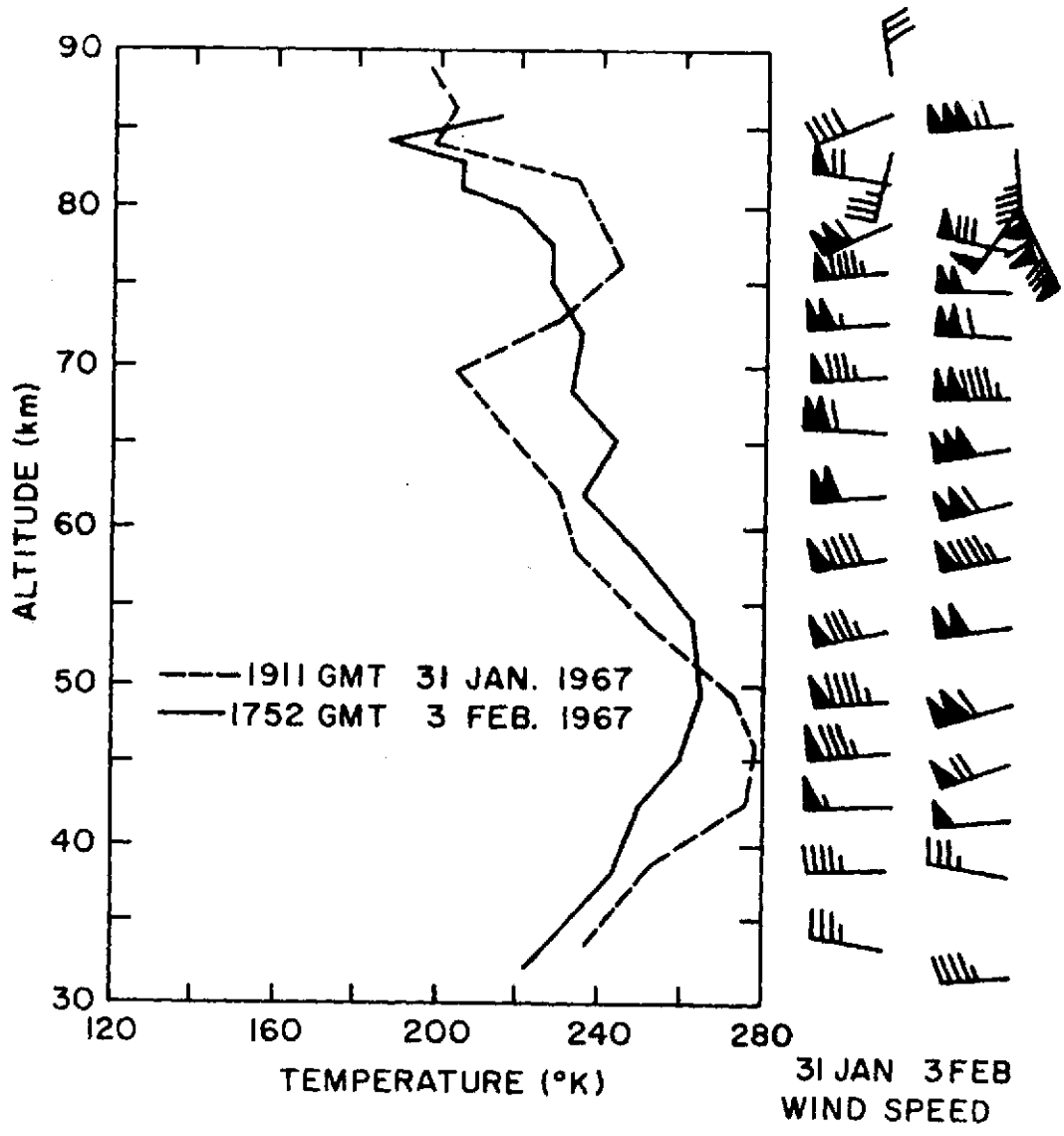

Figure 1.6 Rocket-grenade temperatures and winds for a normal (February 3, 1967) and anomalous winter day (January 31, 1967) at Wallops Island. (From *Sechrist et al.* [1969]).

and January 26, 1971, anomalous days, and on February 1, 1971, the control day. *Mitchell et al.* [1972] suggested that the anomalous absorption on January 22 was probably related to meteorological phenomena, and apparently was characterized by a decrease in the electron loss rate, and the other anomalous day was possibly related to a solar disturbance, and was accompanied by an increase in detachment.

During the 1971-1972 winter the University of Illinois conducted another coordinated experiment for measurements of the winter anomaly at Wallops Island. The description of the experiment and analysis of some of the results obtained will be made in Chapter 5.

1.7 *Statement of the Problem*

As discussed in the sections above, for a better understanding of the *D*-region processes it is necessary to develop new techniques of measurements, and to improve the accuracy of the existing techniques. One of the most important parameters to be measured is the electron density, in particular its time and spatial variations, and the small-scale structure of electron-density profiles. The partial-reflection technique, being a ground-based technique, and relatively inexpensive, is particularly suitable to this type of measurement. The accuracy and limitations of the partial-reflection technique, however, are not very well known at the present time. The real structure of the irregularities producing the reflections is not known. The range of validity of the scattering theories and signal processing methods used, for example, must be examined critically. The appearance of minimums in electron density between 75 and 80 km is another point that deserves attention.

It is the purpose of the present work to make an evaluation of the partial-reflection technique, to analyze the range of validity of the

theories used, to extend the scattering theory to a locally homogeneous random medium, to verify the possible reason for disagreement between rocket and partial-reflection profiles, to improve the signal analysis techniques, and to present and discuss results of partial-reflection measurements made during the winter 1971-1972.

In Chapter 2 the specifications and signal processing methods for a partial-reflection system will be discussed and the system in use by the University of Illinois will be discussed in Chapter 3.

In Chapter 4 a theory of scattering in a locally homogeneous random medium, will be developed. A medium like this is observed above 80 km, where the large gradients in electron density make the *D* region depart considerably from a homogeneous medium, as is normally assumed in partial-reflection measurements. Comparisons of the developed theory with the classical theories used in partial reflection will be made. The possible influence of the scattering theories in the electron-density profiles will be discussed. The influence of a strong dependence on height of the scattering cross section will be studied.

In Chapter 5 results of partial-reflection measurements obtained during the winter 1971-1972 will be presented and discussed.

2. DESIGN CONSIDERATIONS FOR A PARTIAL-REFLECTION SYSTEM

In this chapter will be discussed the specifications of the transmitter, receiver, antenna system and signal processing methods, adequate to partial-reflection measurements. The nature of the received signals will be presented initially, and based on its characteristics, the desired specifications of the system will be analyzed.

2.1 *The Nature of the Received Signals*

Partial-reflection signals are the result of small reflections, produced at heights between 50 and 90 km altitude. The incident signals are HF pulses, of width between 10 and 50 μsec, with polarization corresponding to the ordinary and extraordinary modes of propagation. The reflection coefficient of the ionosphere is very small in this height range, going from approximately 10^{-6} at the lower altitudes to 10^{-3} near 90 km. Measured values of the reflection coefficients will be presented in Chapter 5. The number of reflections observed on each sample is normally small between 60 and 75 km, and increases above this height. As a result, isolated reflections can be observed below 75 km, but the amplitude of the signals increases steadily with height above approximately 80 km. Shown in Figure 2.1 is a sample of the received signals for the ordinary and extraordinary modes of propagation.

The small reflection coefficient below 75 km, and the strong absorption for the extraordinary mode above 80 km, make the received signals very weak, and some signal processing system able to detect signals with a signal-to-noise ratio close or below 1 must be used, in order to obtain a better utilization of the received data, principally at low altitudes.

The dynamic range of the amplitudes of the signals is very large, the signals being, on the average, at 80 km, approximately 20 times greater

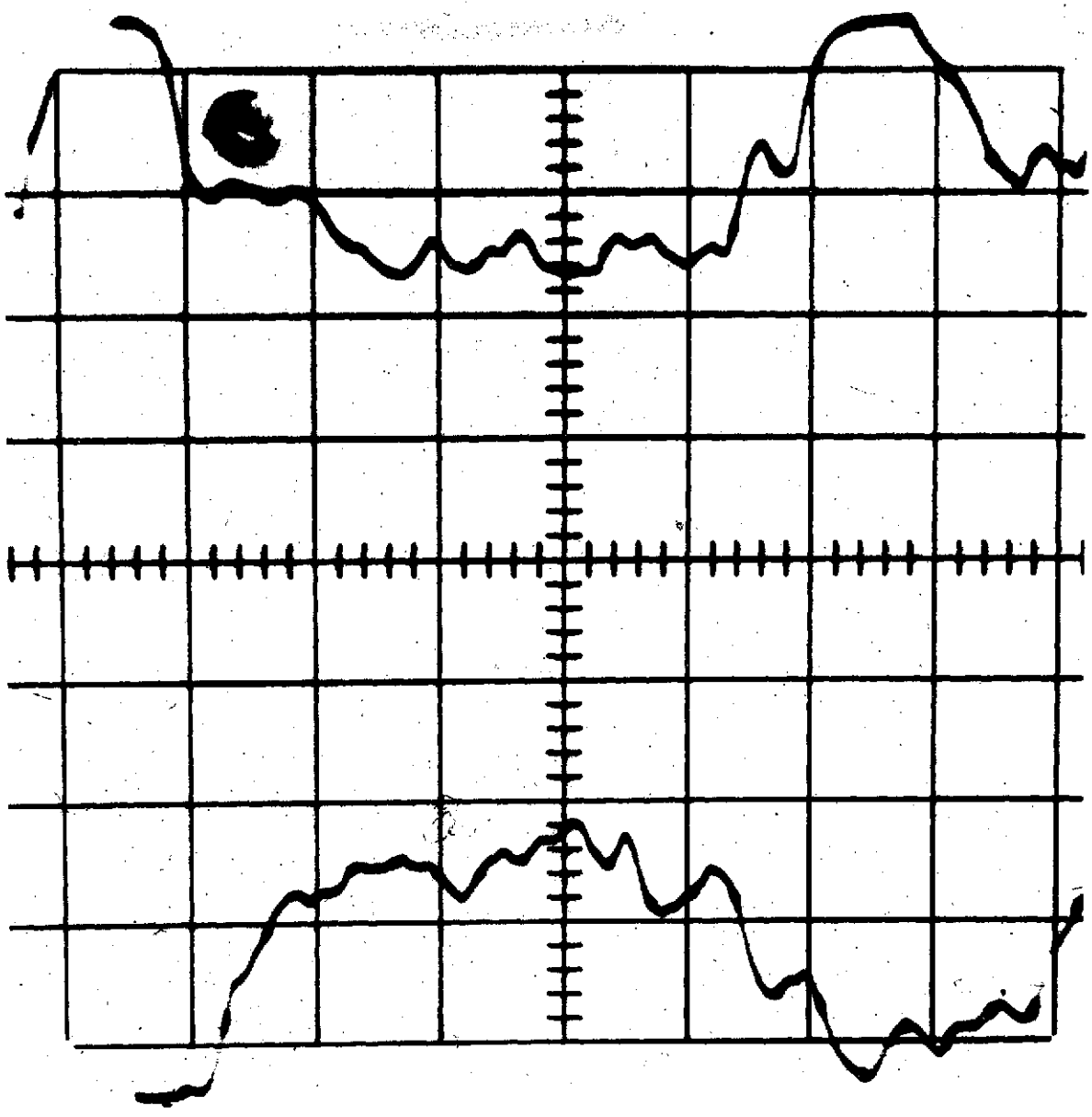

Figure 2.1 Sample of received signal. The upper trace corresponds to ordinary polarization and the lower trace corresponds to extraordinary polarization. The vertical center line of the graticule is the 60 km mark, with height increasing to the right; each centimeter represents 15 km [*Pirnat and Bowhill*, 1968].

than at 60 km. Besides that, the fading of the signals produces a large fluctuation of amplitudes at the same height. As a result, amplitude fluctuations as large as 50 dB must be detected. Such fluctuations impose some restrictions on the specification of the receiver, that will be discussed in Section 2.3. A sample of the variations of amplitude of the ordinary and extraordinary signals for reflections from 82 km altitude is shown in Figure 2.2. It is observed that the signals present a fading with a correlation time of approximately 4 sec.

The correlation coefficients between the A_o and A_x signals at the same height, and between A_o signals at heights 1.5 and 3.0 km apart, are shown in Table 2.1, for the data obtained on January 28, 1972, at 12:00 hours, local time, at Wallops Island, Va. The average A_o and A_x amplitudes, the noise amplitude, and the electron densities obtained from the same data used in Table 2.1 are shown in Table 2.2. The noise amplitude is the result of averaging the power of noise from samples collected between the heights of 40 and 44.5 km, where partial reflections are not present. It is observed that at low altitudes the A_o and A_x signals are very well correlated. The correlation decreases with altitude, and is very poor for altitudes above 80 km. Such low correlation coefficients cannot be explained by the presence of noise, since the signal-to-noise ratio at 81 km, for example, is approximately 5, as shown in Table 2.2. *Austin* [1971] suggested that the low correlation coefficients at higher altitudes could be the result of the different group velocities of the ordinary and extraordinary modes. The height of reflection of the signals is determined by assuming that both signals propagate with the velocity of light in free space. As a result, at higher altitudes, reflections considered from the same height, are

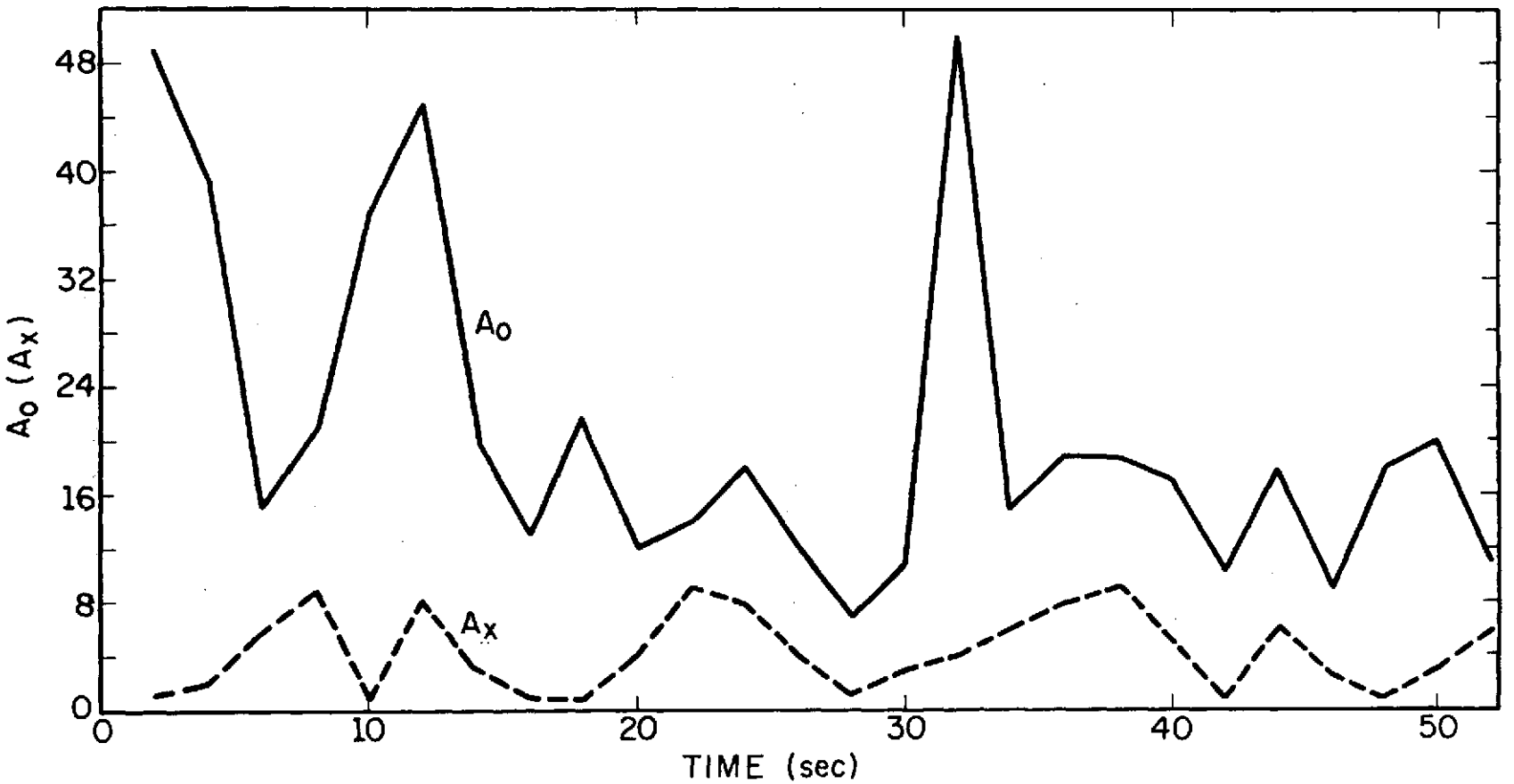

Figure 2.2 Variation as a function of time of reflections from 82 km altitude, for the data obtained on May 7, 1971 at 7:30 h, local time, at Urbana, Illinois.

TABLE 2.1

Correlation coefficients between A_O and A_x, at the same height, and between A_O signals separated by 1.5 and 3.0 km, for the data obtained on January 28, 1972, at 12:00 hours, local time, at Wallops Island, Virginia.

Height (km)	Correlation coefficient		
	A_O-A_x	$A_O(h)$-$A_O(h$-1.5km)	$A_O(h)$-$A_O(h$-3km)
63	0.917	0.942	0.769
64.5	0.918	0.856	0.527
66	0.872	0.758	0.305
67.5	0.827	0.715	0.483
69	0.878	0.868	0.685
70.5	0.923	0.909	0.682
72	0.923	0.886	0.577
73.5	0.895	0.836	0.455
75	0.832	0.767	0.343
76.5	0.652	0.734	0.424
78	0.411	0.851	0.599
79.5	0.255	0.867	0.373
81	0.182	0.574	0.142
82.5	0.042	0.694	0.502
84	0.016	0.889	0.683
85.5	<0.01	0.904	0.730
87	<0.01	0.932	0.767
88.5	<0.01	0.927	0.927
90	<0.01	0.998	0.998

TABLE 2.2

A_O, A_x and electron densities for the data obtained on January 28, 1972, at 12:00 hours, local time, at Wallops Island, Va. No sample received was rejected or reached saturation of the receiver.

Height (km)	Average A_O	Average A_x	Electron density (m^{-3})
63	10.0	15.7	1.19×10^8
64.5	10.2	16.3	1.20×10^8
66	9.9	16.3	4.90×10^7
67.5	10.6	18.2	1.32×10^8
69	13.3	22.8	1.44×10^8
70.5	17.2	28.5	1.25×10^8
72	19.5	31.6	1.34×10^8
73.5	19.7	30.9	1.56×10^8
75	18.8	27.7	3.08×10^8
76.5	17.8	22.4	6.15×10^8
78	19.3	17.4	6.41×10^8
79.5	22.5	15.2	5.22×10^8
81	25.6	14.2	1.31×10^9
82.5	36.1	13.1	2.99×10^9
84	74.0	12.5	2.10×10^9
85.5	123.4	13.7	5.85×10^8
87	164.3	16.7	-
88.5	186.5	19.4	-
90	182.4	20.2	-
Average noise: - 5.4			

really produced from different heights. The error in the determination of height, however, is much less than 1.5 km, as will be shown in Chapter 4; Table 2.2 shows that above 80 km, the A_o signals for heights separated by 1.5 km are very well correlated. So the justification of Austin for the low correlation coefficients between A_o and A_x does not seem reasonable. *Von Biel et al.*, [1970] calculated the correlation coefficient between the ordinary and extraordinary reflections that would be produced by volume scattering, instead of a sharp reflector, and showed that in this case the correlation coefficient can assume very small values. A second indication of reflections produced by volume scattering is the good correlation coefficient between A_o signals separated by 1.5 or 3.0 km, as shown in Table 2.2.

2.2 *Sources of Errors in the Determination of the Electron-Density Profiles.*

The sources of error in partial-reflection measurements will be discussed in this section in order to specify the system in a way of minimizing such errors. Errors directly produced by an inadequate choice of the model of reflector were shown in Chapter 1 and will not be discussed further.

The expression for the determination of the average electron density between heights h_1 and h_2 is given by equation (1.10) that will be repeated below:

$$N = \frac{\log[(R_x/R_o)_2/(R_x/R_o)_1] - \log[(A_x/A_o)_2(A_x/A_o)_1]}{2(F_x - F_o)} \tag{2.1}$$

where

$$\frac{R_x}{R_o} = \left\{ \frac{[\frac{\omega-\omega_L}{\nu} C_{3/2}(\frac{\omega-\omega_L}{\nu})]^2 + [\frac{5}{2} C_{5/2}(\frac{\omega-\omega_L}{\nu})]^2}{[\frac{\omega+\omega_L}{\nu} C_{3/2}(\frac{\omega+\omega_L}{\nu})]^2 + [\frac{5}{2} C_{5/2}(\frac{\omega+\omega_L}{\nu})]^2} \right\}^{1/2} \tag{2.2}$$

and

$$F_{o,x} = \frac{5}{4} \frac{e^2}{m\varepsilon_o c\nu} C_{5/2} \left(\frac{\omega \pm \omega_L}{\nu}\right) \tag{2.3}$$

Errors are produced by imprecisions in the measurement of the ratio $(A_x/A_o)_2/(A_x/A_o)_1$, in the determination of $(R_x/R_o)_2/(R_x/R_o)_1$, that depends on the choice of the model of reflector and on the previous knowledge of the collision frequency profile, and in the choice of the collision frequency profile, that alters both the factors $(R_x/R_o)_2/(R_x/R_o)_1$ and $(F_x - F_o)$. Imprecisions in the measurement of $(A_x/A_o)_2/(A_x/A_o)_1$ are the results of errors introduced by noise, or by wrong interpretation of the received data. This second class of errors will be discussed in Chapter 4.

The percentage of error produced by the factor $(R_x/R_o)_2/(R_x/R_o)_1$ can be expressed by:

$$\frac{\Delta N}{N} = \frac{\Delta R}{[\log(R) - \log(A)]R} \tag{2.4}$$

where $A = (A_x/A_o)_2/(A_x/A_o)_1$ and $R = (R_x/R_o)_2/(R_x/R_o)_1$.

It is observed that the percentage of error increases as the factor $\log(R) - \log(A)$ decreases. Such a situation occurs at low altitudes where the electron density is small. Consequently, electron-density calculations become very imprecise at lower altitudes, principally below 60 km. If the frequency of the HF pulses is increased, the denominator in equation (2.4) decreases, and the percentage of error $\Delta N/N$ increases. The tolerable error $\Delta N/N$, assuming a given error $\Delta R/R$, imposes a restriction on the maximum frequency to be utilized for measurements over a given range of altitudes.

The lower limit of the frequency to be utilized is imposed by the attenuation of the extraordinary signal, that will make its amplitude to reach the minimum value detectable by the receiving system utilized. As the attenuation of the extraordinary signal affects principally reflections from higher altitudes, and errors due to imprecisions in the determination of R are more pronounced at lower altitudes, a given frequency of operation will be suitable for measurements only over a given range of altitudes. For a complete measurement of the D region, from 50 to 90 km, more than one frequency should be used, for better results.

To estimate the value of the error produced by imprecisions in the determination of the ratio $(R_x/R_o)_2/(R_x/R_o)_1$, the following calculation was performed. The electron densities and collision frequencies shown in Table 2.3 were taken as a reference. They are representative of rocket profiles during conditions of maximum and minimum of solar activity. It was assumed that reflections were produced by sharp reflectors spaced by 2.0 km, and the resultant R_x/R_o profile was calculated, for frequencies of 2.66 and 5.0 MHz. The corresponding A_x/A_o profiles were obtained from the collision frequencies listed in Table 2.3. From the (A_x/A_o) and (R_x/R_o) profiles, the electron densities were calculated, reproducing, evidently, the data of Table 2.3. After that, the ratio $(R_x/R_o)_2/(R_x\ R_o)_1$ was changed by ± 2, 4 and 10%, and the error introduced in electron density was verified. The results are shown in Figures 2.3 to 2.6. As expected, the error increases at lower altitudes, and for measurements below 70 km, $(R_x/R_o)_2/(R_x/R_o)_1$ must be determined with a precision of at least 2%. As can be observed in Figure 2.6, the frequency of 5.0 MHz is impracticable for partial-reflection measurements, even at heights of 90 km, for conditions of minimum solar activity.

TABLE 2.3

Electron densities and collision frequencies used as a reference for the calculation of errors in electron-density measurements produced by imprecisions in the determination of the ratio $(R_x/R_O)_2/(R_x/R_O)_1$, as shown in Figures 2.3 to 2.6. The electron densities of column (a) correspond to conditions of maximum of solar activity, and column (b) to minimum of solar activity.

Height	Electron density (m^{-3})		Col. Freq.
(km)	(a)	(b)	sec^{-1}
60	$2.5x10^7$	$1.0x10^7$	$2.5x10^7$
62	$3.5x10^7$	$1.0x10^7$	$1.7x10^7$
64	$4.0x10^7$	$2.0x10^7$	$1.2x10^7$
66	$6.0x10^7$	$3.0x10^7$	$7.5x10^6$
68	$1.0x10^8$	$3.0x10^7$	$5.5x10^6$
70	$2.0x10^8$	$4.0x10^7$	$4.5x10^6$
72	$3.0x10^8$	$5.0x10^7$	$3.0x10^6$
74	$4.0x10^8$	$6.0x10^7$	$2.5x10^6$
76	$5.0x10^8$	$7.0x10^7$	$1.8x10^6$
78	$6.0x10^8$	$1.0x10^8$	$1.3x10^6$
80	$8.0x10^8$	$1.0x10^8$	$9.0x10^5$
82	$1.0x10^9$	$1.0x10^8$	$6.0x10^5$
84	$4.0x10^9$	$3.0x10^8$	$4.5x10^5$
86	$5.0x10^9$	$6.0x10^8$	$3.5x10^5$
88	$8.0x10^9$	$3.0x10^9$	$2.5x10^5$
90	$1.0x10^{10}$	$6.0x10^9$	$1.5x10^5$

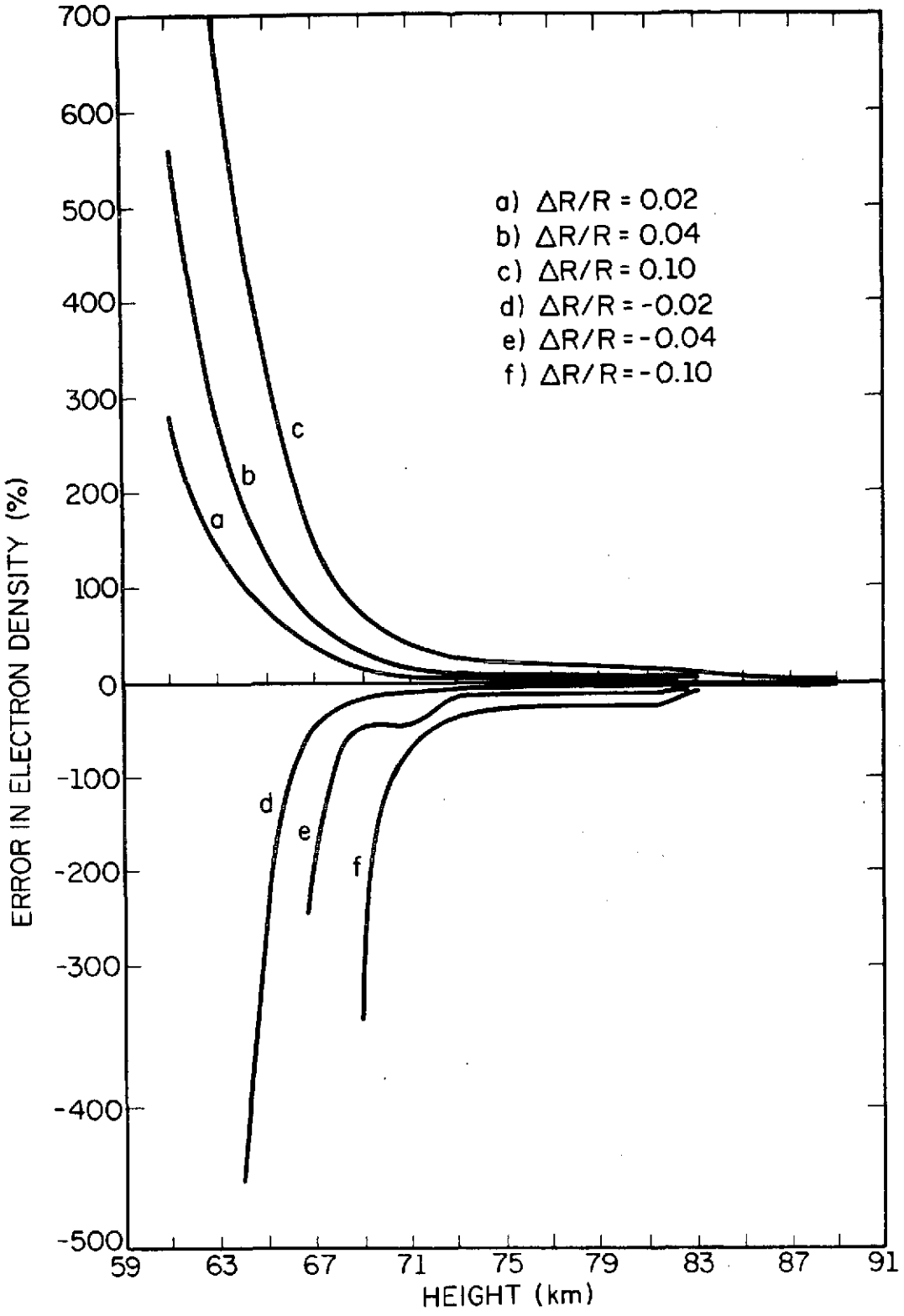

Figure 2.3 Error in electron density produced by errors of ±2, 4 and 10% in the ratio $(R_x/R_O)_2/(R_x/R_O)_1$, for the frequency of 2.66 MHz, electron densities and collision frequencies listed on Table 2.3 (column a), corresponding to conditions of maximum solar activity.

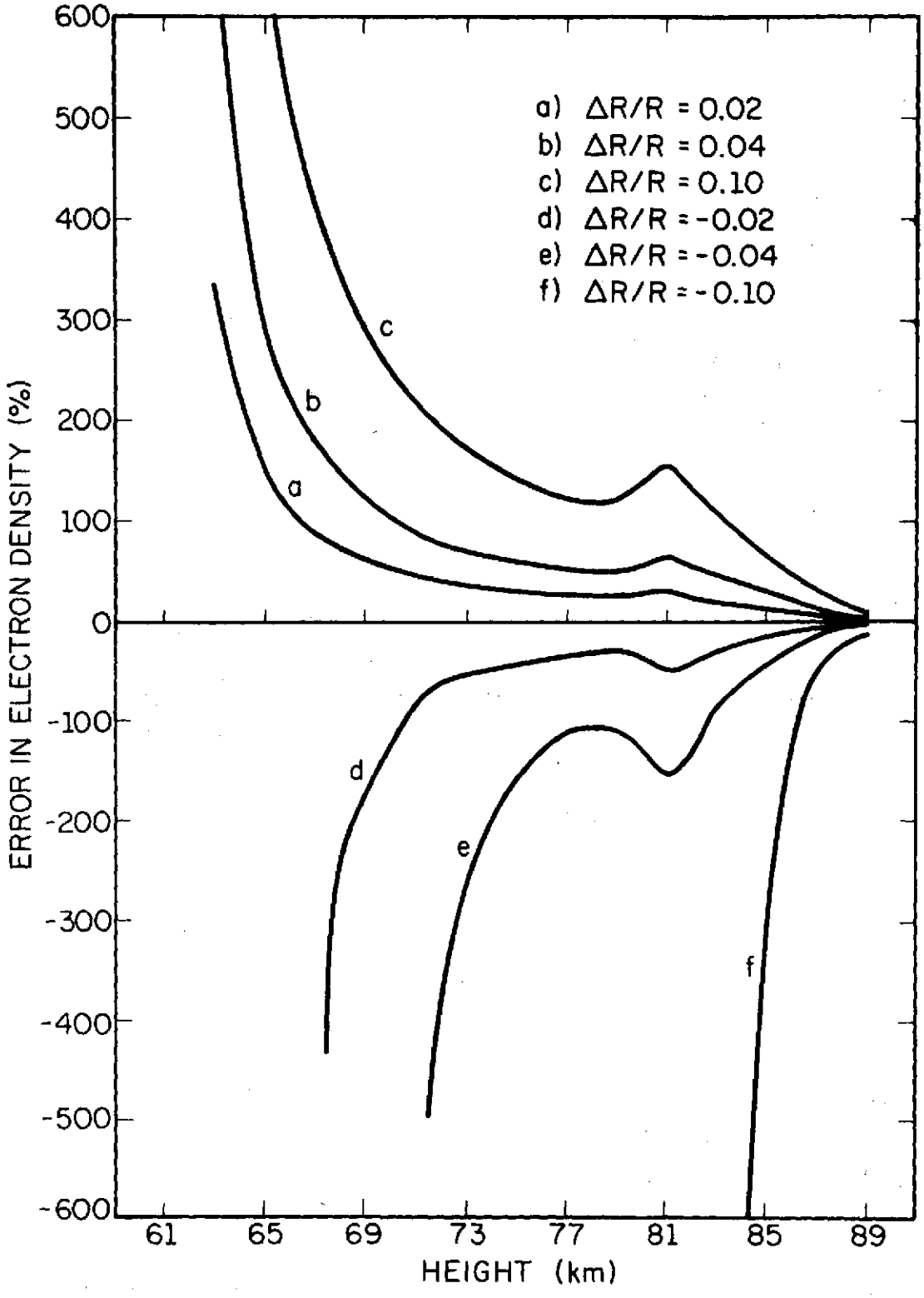

Figure 2.4 Error in electron density produced by errors of ±2, 4 and 10% in the ratio $(R_x/R_o)_2 / (R_x/R_o)_1$, for a frequency of 2.66 MHz, electron densities and collision frequencies listed on Table 2.3 (column b), corresponding to conditions of minimum of solar activity.

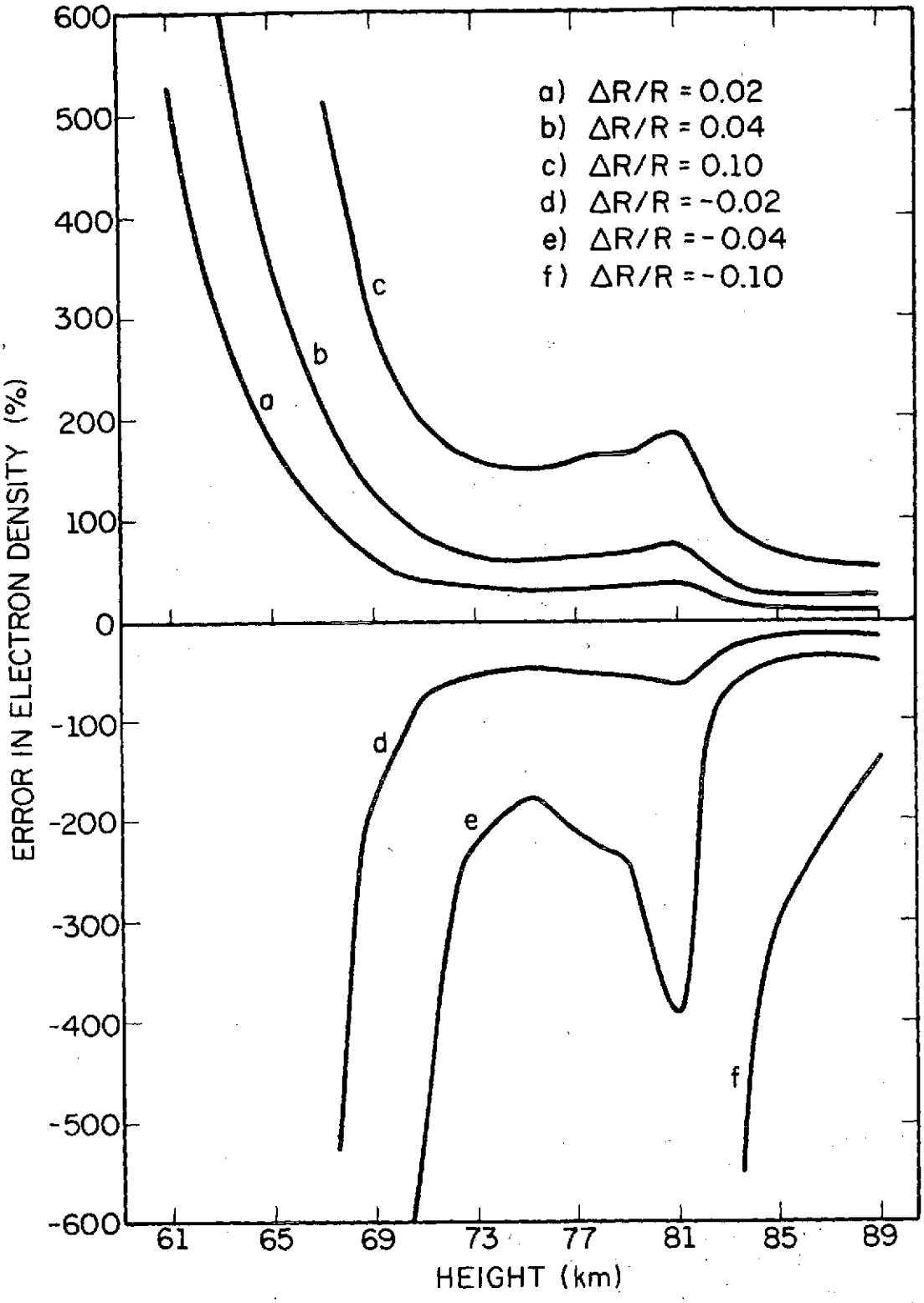

Figure 2.5 Error in electron density produced by errors of ±2, 4 and 10% in the ratio $(R_x/R_O)_2/(R_x/R_O)_1$, for a frequency of 5.0 MHz, electron densities and collision frequencies listed in Table 2.3 (column a), corresponding to conditions of maximum solar activity.

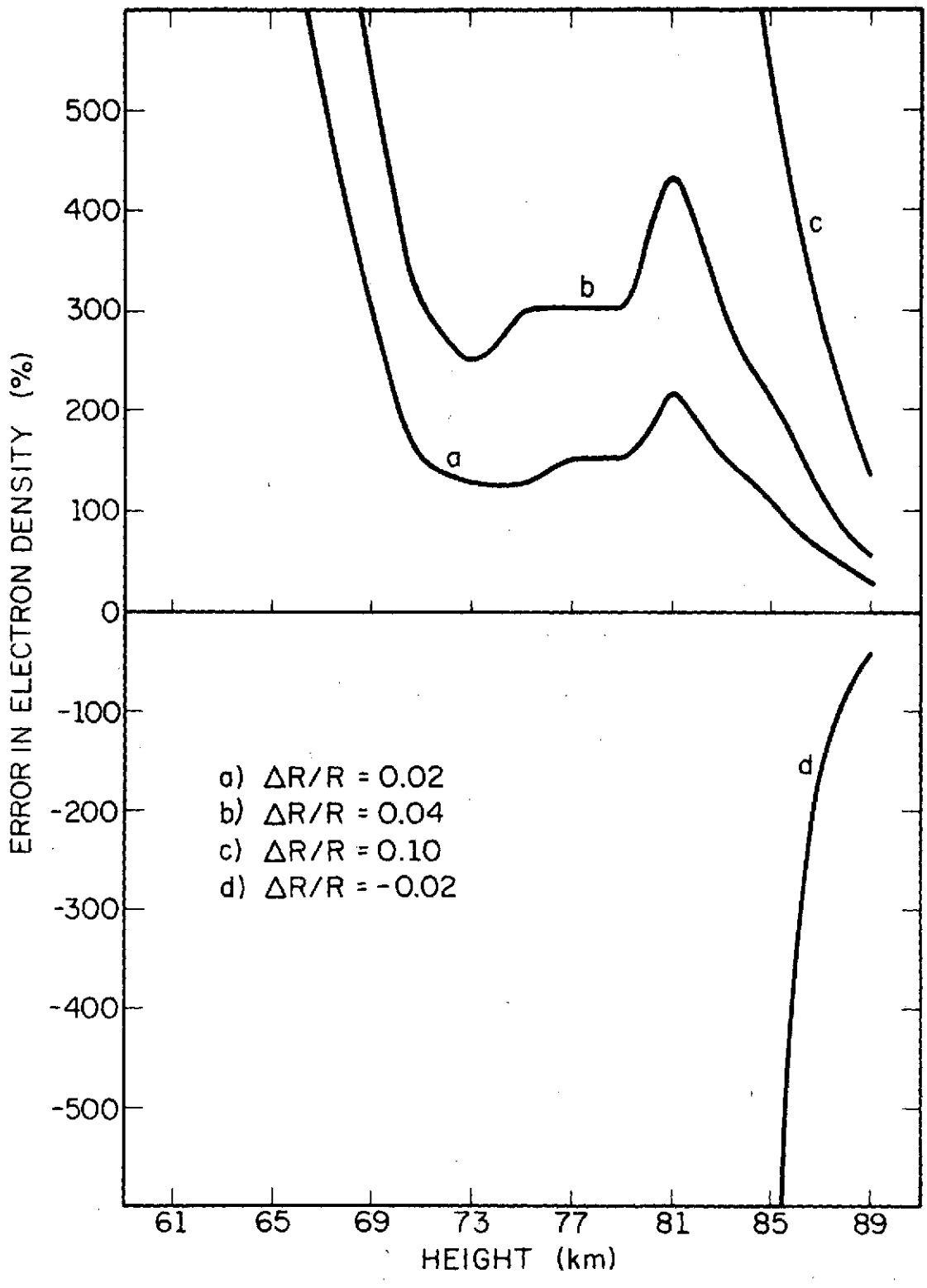

Figure 2.6 Error in electron density produced by errors of ±2, 4 and 10% in the ratio $(R_x/R_o)_2/(R_x/R_o)_1$, for a frequency of 5.0 MHz, electron densities and collision frequencies listed on Table 2.3 (column b), corresponding to conditions of minimum of solar activity.

The error produced by the ratio $(A_x/A_o)_2/(A_x/A_o)_1$ is given by:

$$\frac{\Delta N}{N} = \frac{-\Delta A}{[\log(R) - \log(A)]A} \tag{2.5}$$

This expression is similar to equation (2.4), that gives the error produced by $(R_x/R_o)_2/(R_x/R_o)_1$, so that the same discussion made above applies to the present case. It should be noted, that for a frequency of operation of 2.66 MHz, and at lower heights, the error in the determination of $(A_x/A_o)_2/(A_x/A_o)_1$ has to be less than 2%. Such tolerance will impose restrictions on the signal processing method to be used, as will be discussed in Section 2.6.

An expression for the error introduced by imprecisions on the determination of the collision frequency, ν, would be too involved, since ν appears in the factors $(R_x/R_o)_2/(R_x/R_o)_1$, and (F_x-F_o). The influence of the value of ν in the calculation of electron densities can be better observed from an analysis of Figure 2.7. In Figure 2.7 a plot of electron density as a function of A is shown, using as a parameter the values of collision frequency at heights h_2 and h_1, that are assumed to be separated by 1.5 km. If a given value of A is considered, the influence of the values of collision frequency on the calculation of electron densities can be obtained by taking the values of electron density corresponding to different curves, each one corresponding to a pair of values of ν, at heights h_1 and h_2. It is observed, that even if the collision frequency is changed by a large amount (from curves a to b, for example, the collision frequencies change from 2.4×10^7 and 1.8×10^7 s^{-1} to 1.7×10^7 and 1.08×10^7 s^{-1}), the corresponding variation of electron density is not very large. As a

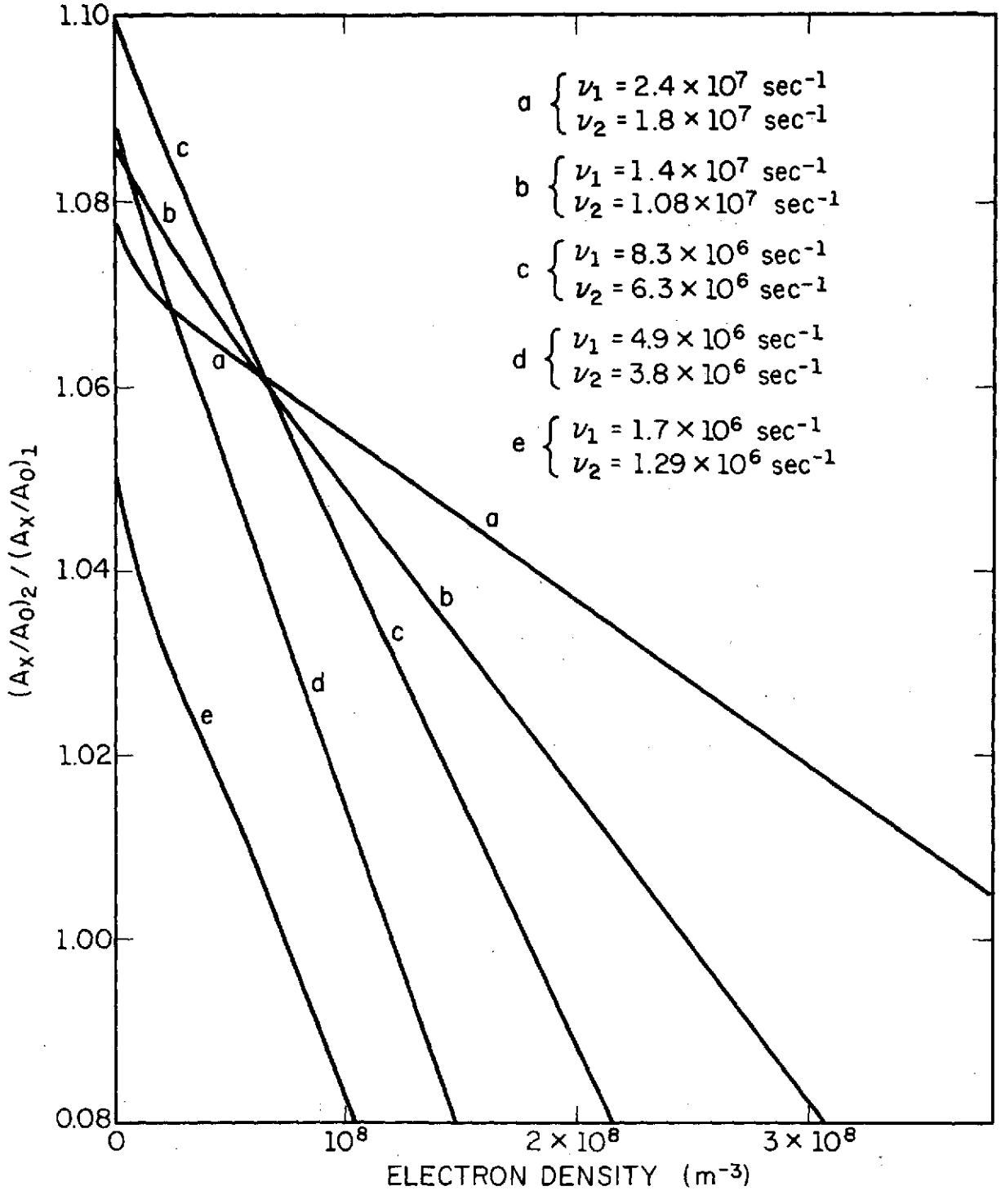

Figure 2.7 Electron density as a function of the ratio $(A_x/A_o)_2/(A_x/A_o)_1$, for different values of collision frequency.

consequence, the choice of the collision frequency model to be used is not very critical.

2.3 *The Receiver*

The most stringent specifications for a receiver to be used in partial reflection are the dynamic range and the linearity of the receiver. Saturation of the signals can produce serious errors in the measurement, and as the amplitude of the reflections cover a very wide range, the receiver to be used must be linear over a range of at least 40 dB, with a tolerance in linearity of at most 10%. Such specification imposes some limitations on the design of the intermediate stage, responsible for non-linearities of large input signals, and on the detector, responsible for non-linearities of small input signals. The minimum input signal to be detected is limited by atmospheric noise, and not by the receiver noise, and as a consequence, the sensitivity is not an important specification.

The bandwidth is given by the expression

$$bW = 1/W \tag{2.6}$$

where W is the width of the transmitted pulse. Such width is limited on the lower side by the increase of the necessary bandwidth, with deterioration of the signal-to-noise ratio, and increase in interference produced by spurious frequencies. On the upper side, the width of the pulse is limited by the height resolution of the measurement. A pulse of 50 μsec, for example, occupies a height range of 7.5 km. Pulse widths used in the existing partial-reflection systems range from 25 to 50 μsec, corresponding to bandwidths of 40 to 20 kHz. For a better height resolution, 25 μsec or less should be

used all the times that the signal-to-noise ratio is good enough. A pulse width of 10 μsec, corresponding to a bandwidth of 100 kHz should be tried, principally for a comparative analysis of electron-density profiles obtained with different pulse widths. A more flexible partial-reflection receiver should be able to have its bandwidth adjusted in order to operate with pulse widths of 10, 25 and 50 μsec. Phase distortion must be kept in a low level, in order to avoid distortion of the pulse, so that single tuned circuits are recommended in the design of the IF stage.

The frequencies utilized on partial-reflection measurements are very close to the broadcast and commercial services bands. To avoid interference from such frequencies, a passband filter must be added to the front end of the receiver, with a bandwidth of approximately 400 kHz, and an attenuation of at least 50 dB for frequencies 200 kHz outside the bandwidth.

The rejection of image and spurious frequencies of the receiver must be of at least 90 dB.

2.4 *The Transmitter*

The specifications to be discussed in the transmitter are the power output and the pulse repetition rate.

The necessary power output can be determined from the following expression:

$$P_t = P_r + L_s \quad , \quad \text{in dB} \tag{2.7}$$

where P_t is the output power, P_r is the received power and L_s is the system loss, that is given by:

$$L_s = L_p + L_a - G_t - G_r + L_h + R_i \tag{2.8}$$

where L_p is the free space loss, given by:

$$L_p = 20 \log\{\frac{4\pi f}{c} s\} \tag{2.9}$$

f being the frequency, c the velocity of light, s the ray path, L_a is the ionospheric absorption, G_r and G_t the gains of the receiving and transmitting antennas, L_h are the ohmic losses in the transmission lines, and R_i the reflection coefficient of the ionosphere.

The necessary received power P_r depends on the minimum signal-to-noise ratio that the system is able to process, on the atmospheric noise at the receiver location, and on the bandwidth of the receiver.

The power of noise is given by [*Davies*, 1965]:

$$P_n = F_a + B - 204 \quad \text{dB/w} \tag{2.10}$$

where F_a is the external noise power available from a noiseless antenna, expressed in decibels above KT_o, where K is Boltzmann's constant and $T_o = 288.39$ °K is a reference temperature, which is the noise generated in a unit bandwidth by a thermal source in a temperature T_o, and $B = 10 \log(b)$, b being the bandwidth. The values of F_a are given in the literature (CCIR Report No. 322).

Based on the above expressions, the power necessary to a transmitter to be located at Urbana, Illinois will be calculated below.

The following parameters will be considered:

Receiving and transmitting antenna gains: 20 dB, each one;

Minimum signal-to-noise ratio acceptable: 1;

Ohmic loss in the transmission lines: 3 dB;

Frequency of operation: 2.66 MHz;

bandwidth: 40 kHz (25 μsec pulses).

Since the smallest reflections are produced in the height range of 60 to 70 km, a height of 65 km will be used in the calculations, resulting in a free space loss L_p = 92 dB.

The noise factor F_a, for winter conditions, during the morning, is 23 dB [*Davies*, 1965]. Assuming that a reflection coefficient of the ionosphere of 3×10^{-6} must be detected, a transmitter power of at least 100 kw must be used.

The pulse repetition rate ideally should be equal to the inverse of the correlation time of the noise, that is equal to the inverse of the bandwidth, assuming a white noise at the input. Two practical reasons, however, limit this ratio:

1) As the repetition rate increases, the average power to be delivered by the transmitter increases;
2) Between the reception of the ordinary signal and the transmission of the extraordinary signal, a switching device must change the polarization of the antennas from one mode to the other; the time of operation of such a device is a limiting factor in the pulse repetition rate.

Taking into consideration the above restrictions, a reasonable pulse repetition rate can be considered as 50 double pulses per second. Such a rate, for a transmitter with a power output of 300 kw, and a pulse width of 25 μsec, implies an average power output of 750 w.

2.5 *The Antenna System*

The directivity of the antennas is an important factor in the design of a partial-reflection system, in order to avoid a strong contribution of

oblique reflections to the received signals. Assuming that all the transmitted power is uniformly distributed over the main lobe of the antenna, the reflections received from a height h will be produced by a volume with an average width of $2htg(\theta/2)$, where θ is the width of the main lobe, and a height $cW/2$, where c is the velocity of light, and W the pulse width. The indetermination produced by the pulse width, in height, is equal to $cW/2$, and the indetermination in height produced by the finite angle of radiation of the antenna is given by $h[1-\cos(\theta/2)]$, as can be observed in Figure 2.8. If the main lobe of the antenna is of 20°, for reflections from 80 km altitude and a pulse width of 25 μsec the scattering volume will have dimensions of 2.75 km of height and 28 km of width. The indetermination in height produced by the lobe of the antenna will be 1.3 km, smaller than the height of the scattering volume, that depends only on the width of the transmitted pulse. An antenna lobe of 20°, in this case, is enough for partial-reflection measurements, and will keep contributions of oblique reflections at a low level.

An attenuation of secondary lobes of at least 20 dB must be obtained, in order to reduce the reflections produced by such lobes by at least 40 dB, if both the receiving and transmitting antennas have the same characteristics.

The antennas must operate with the polarizations corresponding to the ordinary and extraordinary modes of propagation. A switch device must be incorporated to the antenna system in order to change the polarization from one mode to the other. Since the polarizations used are circular, an array of cross dipoles is the most convenient type of antenna for partial reflection.

In the design of the antennas, the same antenna can be used for transmission and reception, or independent antennas can be used. The first

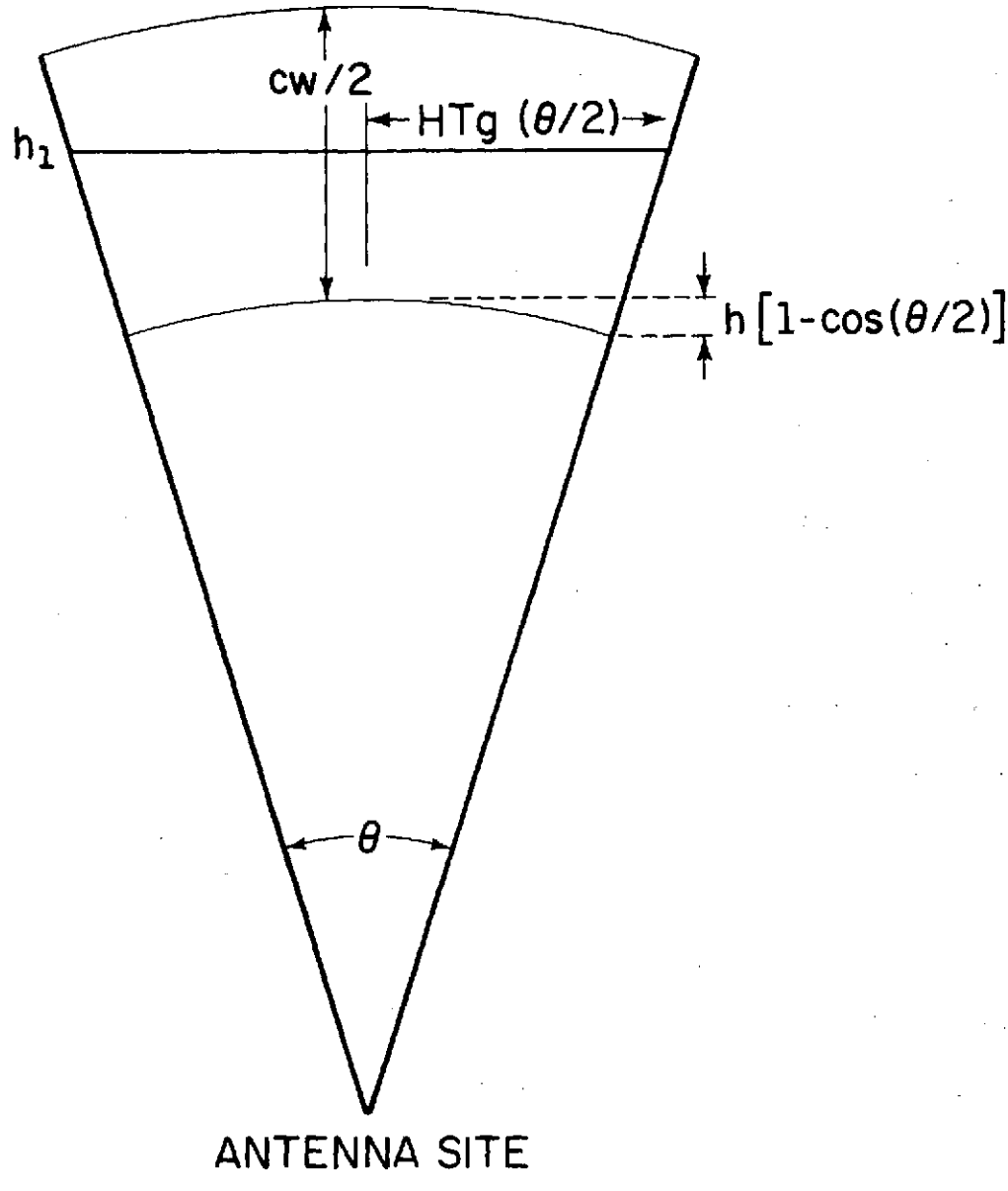

Figure 2.8 Main lobe of the antenna, showing the volume occupied by the pulse.

solution implies the use of a decoupling device between the receiver and the transmitter. An example of such a device is the transmission line bridge shown in Figure 2.9 [*Westcott*, 1948]. The use of a single antenna, although more economical, gives less flexibility to the system. If two antennas are used, there is the possibility of transmitting one mode of polarization and receiving a different mode. Such type of operation is convenient for phase measurements [*Von Biel et al.*, 1970], and for measurements of rejection of the undesired mode of propagation of the antennas.

2.6 *The Signal-Processing System*

The relatively high correlation time of the reflections (4 to 5 sec, approximately), permits the use of a series of signal processing methods, in order to improve the effective signal-to-noise ratio of the received signals. Due to the limitations of the partial-reflection systems in operation, however, the advantages of such methods have not been fully exploited to the present time. Most of the processing techniques used in Thomson-scatter experiments, for example, could be adapted to partial-reflection measurements. In the system in operation at the University of Illinois, some techniques have been introduced, by using the correlation function of the signals [*D. R. Ward and S. A. Bowhill*, private communication], and integration of the signals, as in the present work. The integration method will be discussed in Chapter 3.

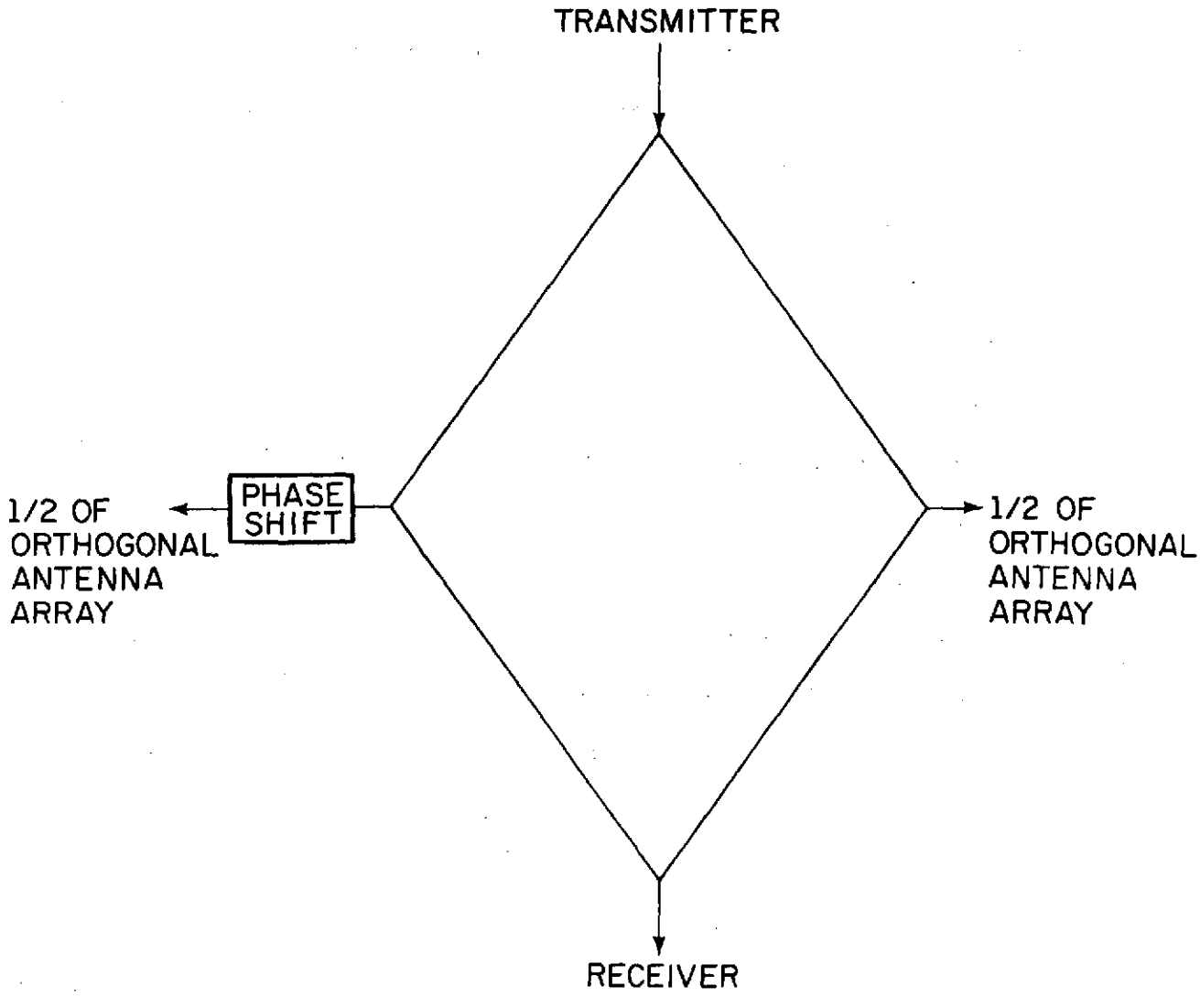

Figure 2.9 Transmission line bridge.

3. THE PARTIAL-REFLECTION SYSTEM AT THE UNIVERSITY OF ILLINOIS

3.1 *Characteristics of the Equipment*

The partial-reflection system in operation by the University of Illinois, at Urbana, at the time the present work was made, is described in detail by *Henry* [1966] and by *Pirnat and Bowhill* [1968], and had the following characteristics:

Transmitter:

Peak power: ~ 50 kW

Frequency: - 2.66 MHz

Pulse width: - adjustable between 20 and 50 μsec

Output impedance: - 50 ohm, unbalanced

Receiver:

Noise figure: - 3 dB, maximum

Selectivity: - 25 kHz between -6 dB points, as shown in Figure 3.1

Linearity: - according to Figure 3.2

Recovery time: - 200 msec for the receiver to drop into noise after 0.1 volts RMS at the signal frequency applied at the input is removed

RF input impedance: - 50 ohm, unbalanced.

As can be observed in Figure 3.2, the linearity of the receiver is not good enough for partial-reflection applications. To compensate for the effects of non-linearity, two subroutines, VALUE and LINAP, were included in the computer program that calculated electron density. Such subroutines are listed in Appendix II. The subroutine VALUE is a list of the values of input signals at the receiver, TU(I), the corresponding values of output signals, TUO(I), and the ratios of increments at the input and output,

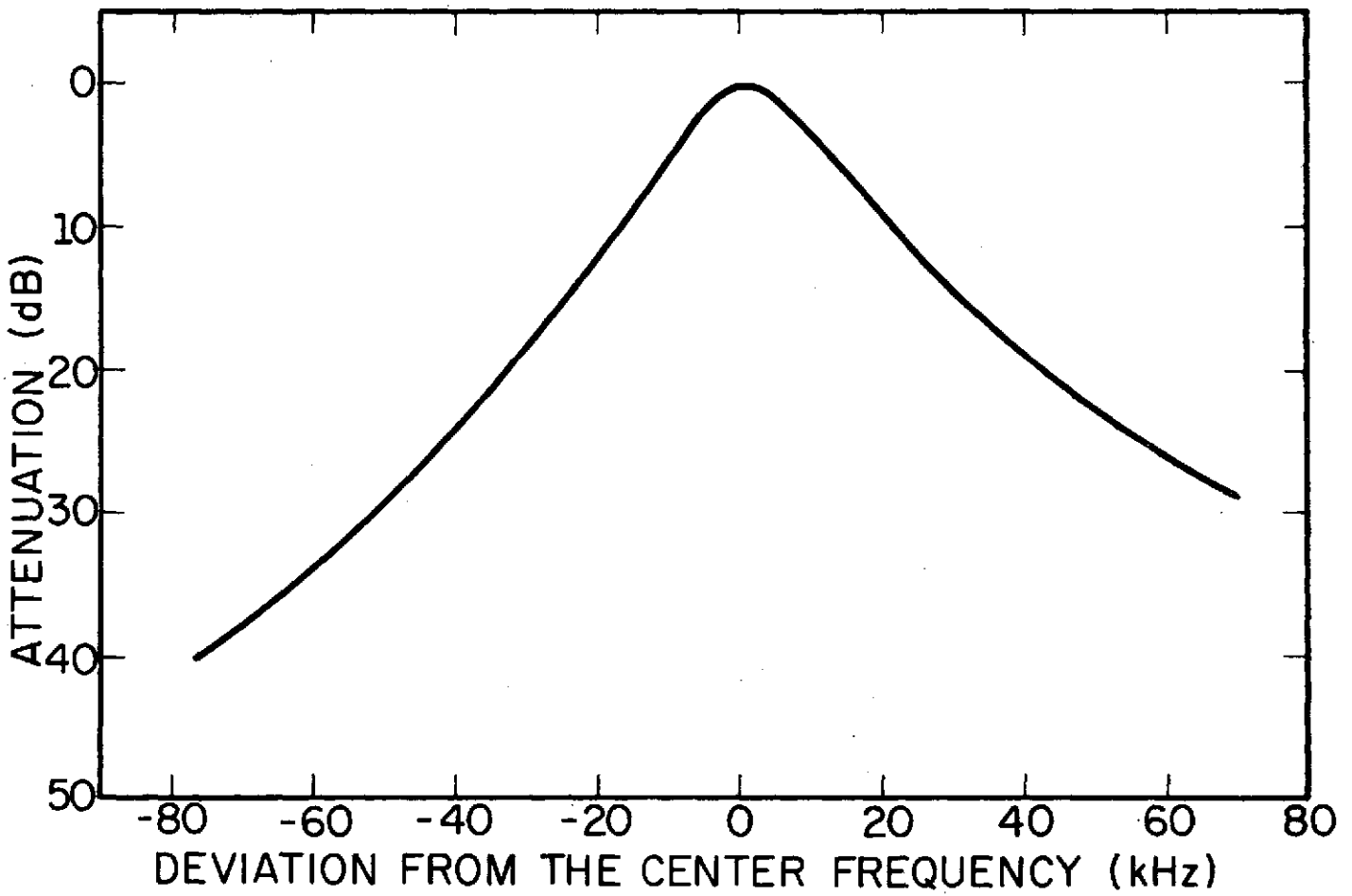

Figure 3.1 Selectivity curve of the receiver.

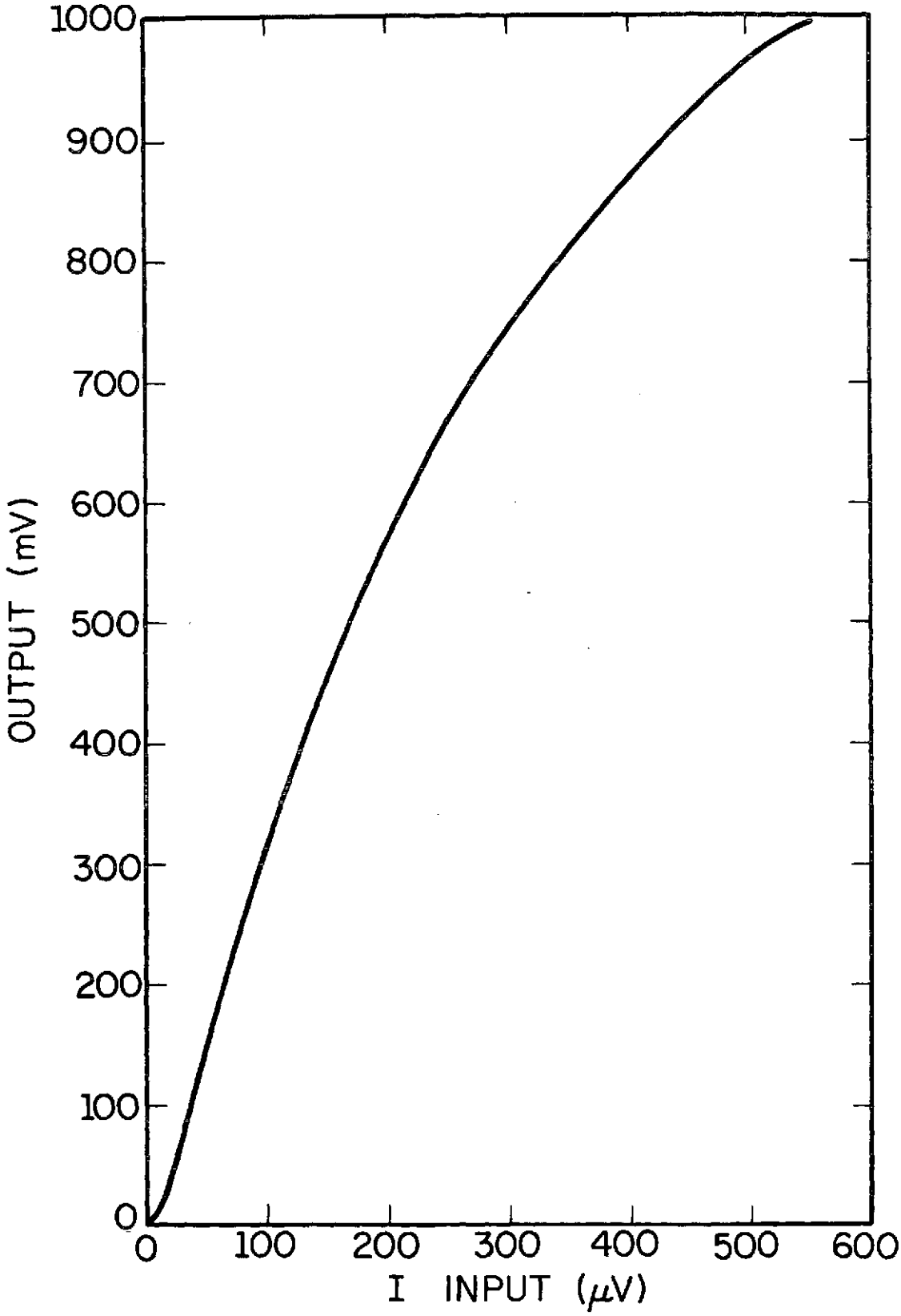

Figure 3.2 Output voltage as a function of input voltage of the receiver.

S(I). The subroutine LINAP uses the data listed in VALUE to transform output signals into the corresponding input signals, that are used in the calculations of electron densities, eliminating in this way the effects of non-linearity of the receiver. The subroutine LINAP employs a linear interpolation between two of the values tabulated in VALUE to perform the linearization.

The dynamic range of the receiver is not enough for measurements of electron densities between 60 and 90 km, saturation generally occurring for reflections above 84 km. To overcome such a problem, a programmed attenuator, adjustable between 0 and 30 dB, was introduced at the input of the receiver. This attenuator operates only on alternating frames, and when it is used, the output data consists of two interconnected sets of data, one with the attenuator on, and the other with the attenuator off. The inconvenience of such a method is that only one-half of the measured samples are used in the calculation of electron density at each height. The computer program PROAT calculates electron densities using the data obtained as described above.

Using the above method of data collection it was possible to obtain electron-density profiles between the heights of 70 and 90 km, without saturation of any sample. Figure 3.3 shows two electron-density profiles obtained in this way.

The antenna system is composed of two independent arrays for transmission and reception. Each array consists of two sub-arrays of 30 parallel half-wave dipoles. The sub-arrays are prependicular to each other. A schematic diagram of the two antennas is shown in Figure 3.4. Switching between the ordinary and extraordinary modes of polarization is controlled by the polarization reversal control, operated by a pulser.

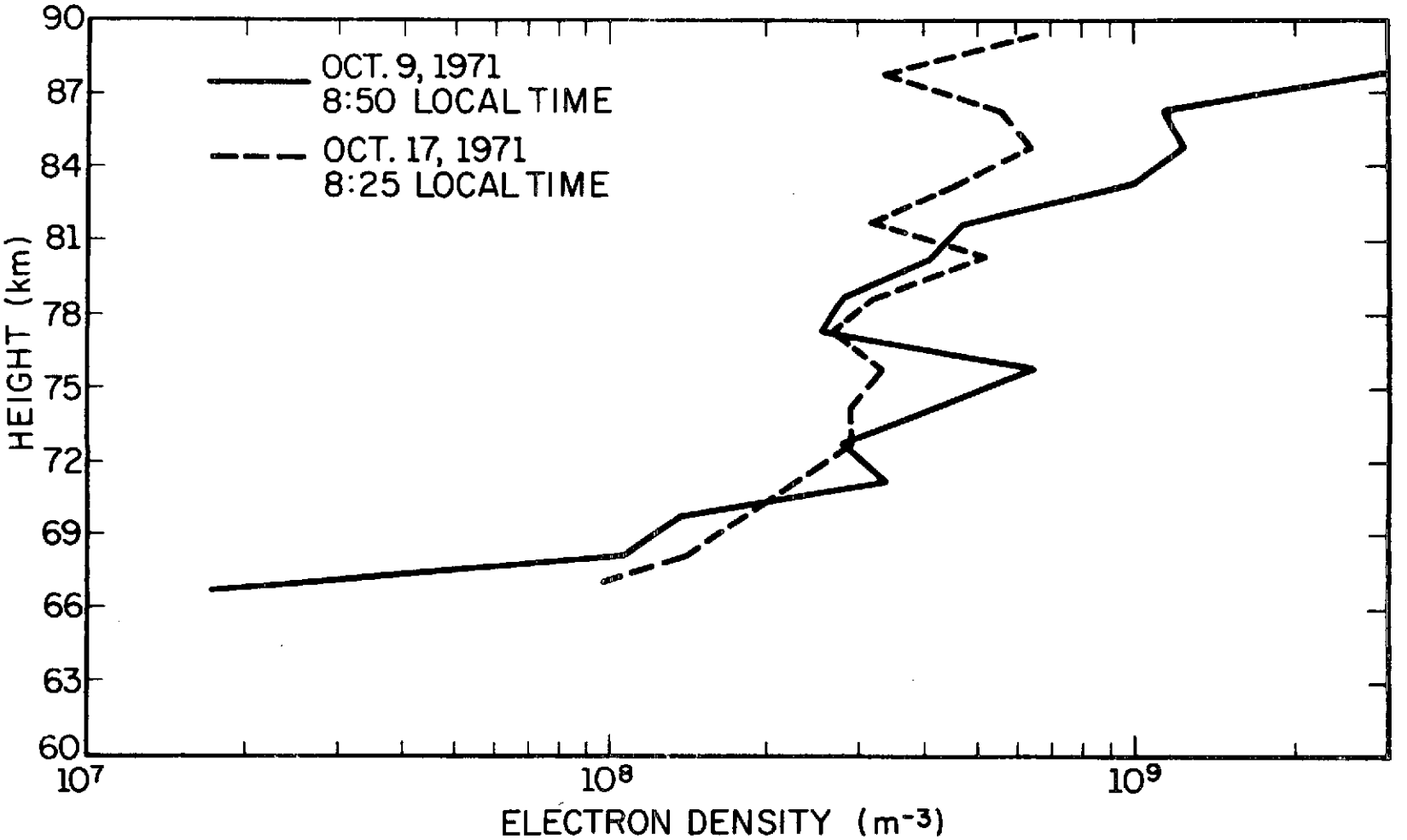

Figure 3.3 Electron-density profiles obtained with a programmed attenuator at the input of the receiver, at the University of Illinois, Urbana, Illinois, on October 9, 1971 at 8:50h, local time (a), and October 17, 1971 at 8:25h local time (b).

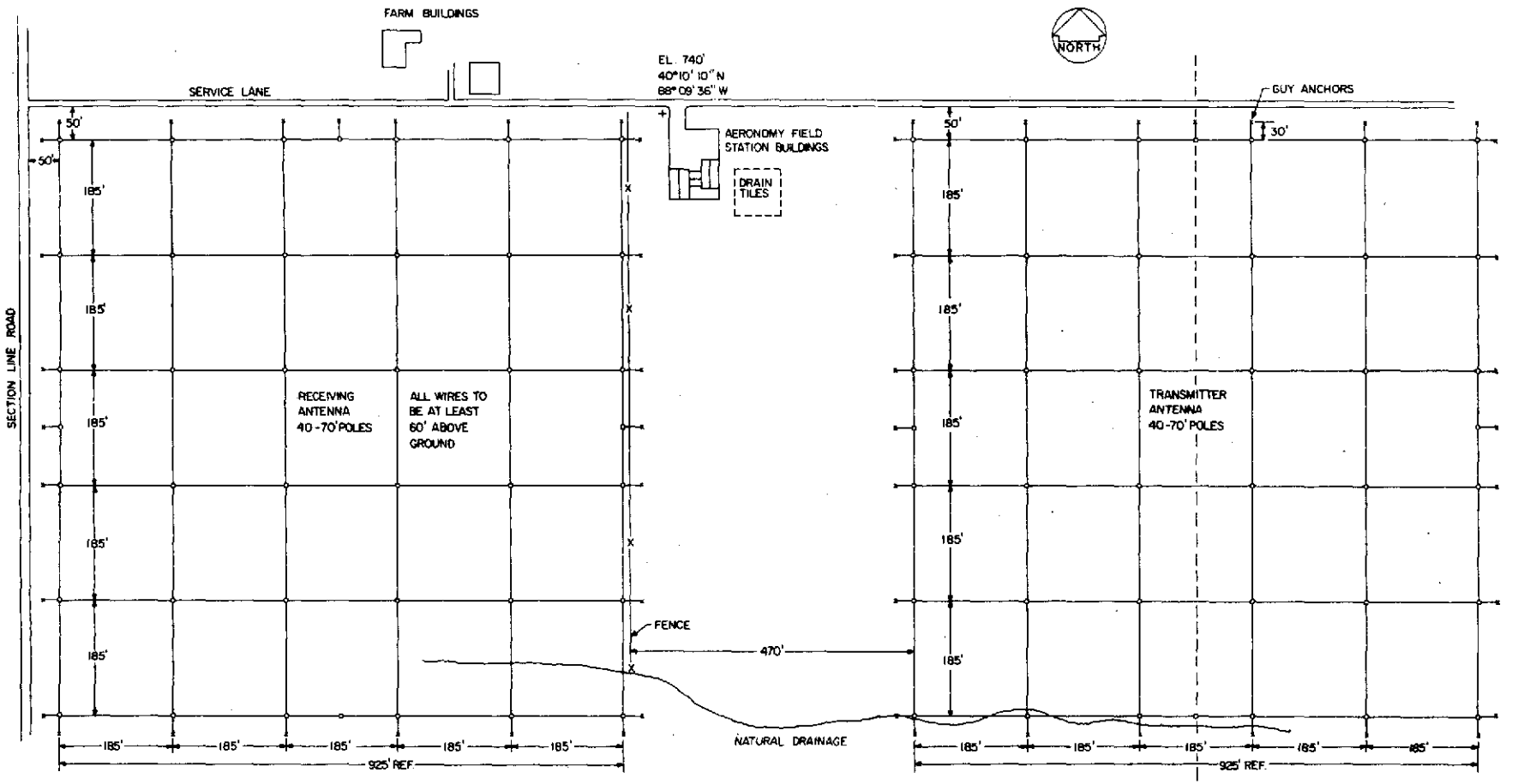

Figure 3.4 Antenna layout (From *Henry* [1966]).

For the operation of the partial-reflection system at Wallops Island, Virginia, the receiver and transmitter were installed in a van, and a new antenna was constructed. A single antenna was used, consisting of two perpendicular sub-arrays of four short dipoles. Isolation between transmitter and receiver was obtained by means of a transmission line bridge, as shown in Figure 2.9. At the input of the receiver, as an additional protection, it was placed the diode circuit shown in Figure 3.5. This diode circuit is operated by a pulser, and opens the input of the receiver all the time, with exception of the time interval between 20 and 300 μsec after a pulse is transmitted.

The measured gain of the antenna used at Wallops Island [*G. W. Henry, Jr.*, private communication] was approximately 16 dB.

3.2 *The Signal Processing System*

In the system operated by the University of Illinois, the output of the receiver is coupled to an analog-to-digital converter, that for each reflection takes 21 samples of signal, from 60 to 90 km, with a height interval of 1.5 km, and four samples of noise, corresponding to the height interval between 40 and 44.5 km, where reflected signals are absent. The sampled signals are fed to a PDP-15 digital computer, and stored on magnetic tapes. The sampling and storage systems are described in detail by *Birley and Sechrist* [1971].

The data are processed by a computer program, PROAX, that is listed in Appendix II. The processing system is based on taking the average power of signal at each height, and subtracting it from the average power of noise, that is obtained from the samples measured in the interval corresponding to the heights between 40 and 44.5 km. In this way, the average signal $A_{o,x}(h)$

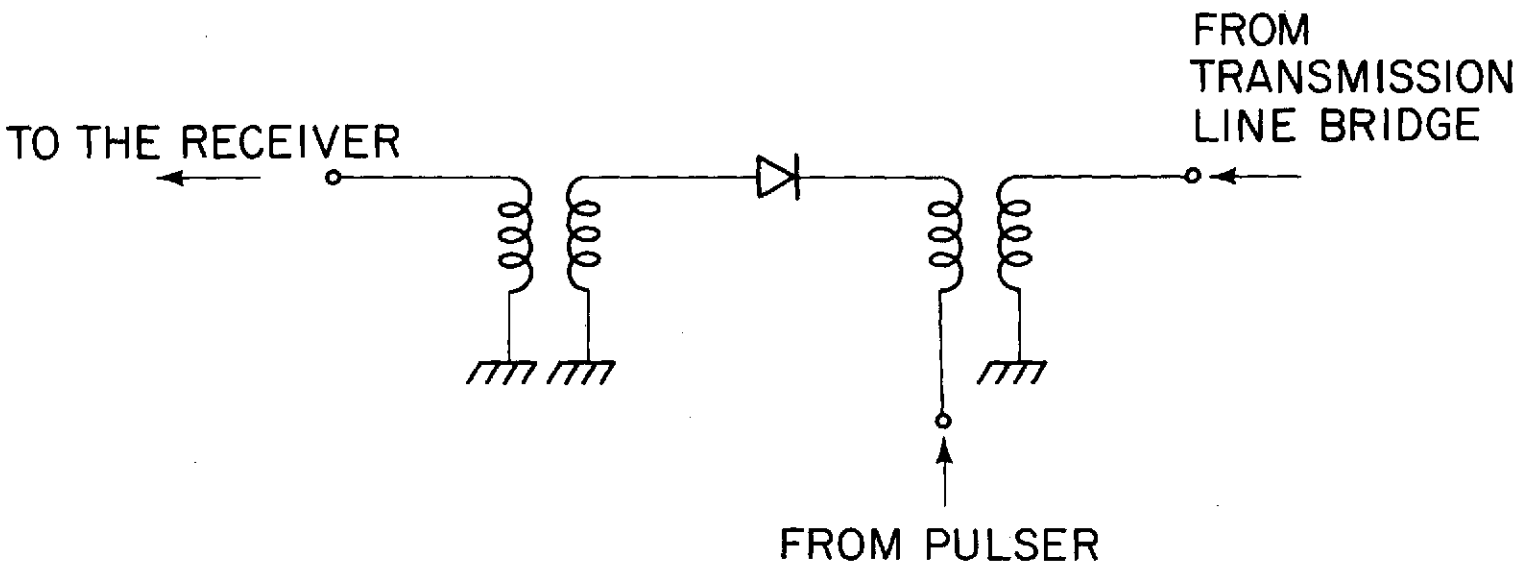

Figure 3.5 Diode circuit used to protect the receiver from overload.

from a height h is given by:

$$A_{o,x}(h) = \sqrt{\frac{\sum_n a^2_{o,x}(h)_n - \sum_n n^2_{o,x,n}}{N}} \qquad (3.1)$$

where N is the number of samples taken, $a_{o,x}(h)_n$ is the amplitude of the ordinary (extraordinary) signal received from a height h, in the n-th sample, $n_{o,x,n}$ is the average amplitude of noise in the n-th sample, for the ordinary (extraordinary) frame, and is given by:

$$n_{o,x,n} = \sqrt{\frac{\sum_{m=1}^{4} n^2_{o,x,n,m}}{4}} \qquad (3.2)$$

$a_{o,x,n,m}$ corresponding to the m-th sample of the four samples of noise taken during each frame.

It was observed that besides the Gaussian noise, an impulsive noise, probably produced by nearby power transmission lines, appeared on the signals. An example of such a noise is shown in Figure 3.6.

The integration procedure expressed by equation (3.1) is effective in eliminating a Gaussian noise, but not an impulsive noise.

The impulsive noise observed is characterized by a rapid fading, and normally does not appear on successive frames at the same height. This characteristic was used to minimize its influence on the averaging of the signals, in the following way: each sample from a given height, $a_{o,x}(h)_n$ is compared with the sample from the same height in the frame immediately before, $a_{o,x}(h)_{n-1}$. If the difference $a_{o,x}(h)_n - a_{o,x}(h)_{n-1}$ is greater

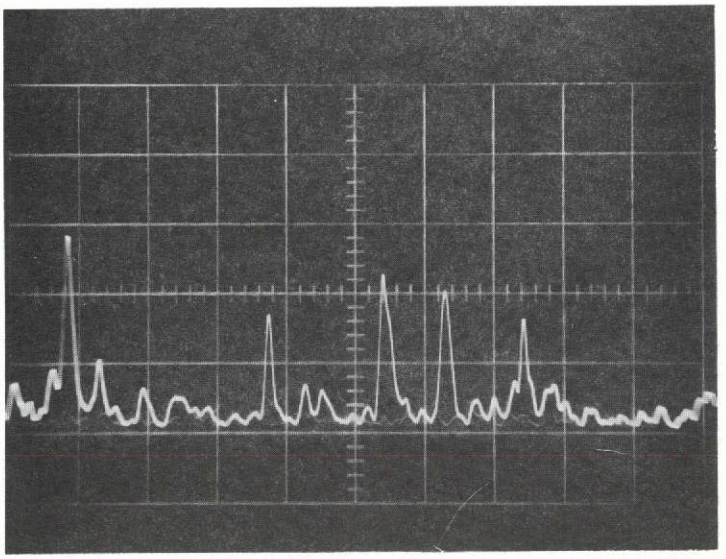

Figure 3.6 Sample of received impulsive noise. The horizontal scale is of 0.2 msec per graticule.

than a specified value, that is an input of the processing program, for the height h, h - 1.5 km, or h + 1.5 km, the sample is rejected, since such a rapid fading corresponds probably to the presence of impulsive noise.

Too noisy frames, produced principally by lightning, are also rejected. If the average noise on two consecutive frames, one ordinary and the other extraordinary, exceeds a given value, both frames, for all the 21 heights, are rejected.

The signals used in the above computations are linearized signals, obtained from the subroutines VALUE and LINAP, described before.

Once the average A_o and A_x are obtained, electron densities are calculated by calling the subroutine CALC, that is listed in Appendix II.

The number of samples necessary to the calculation of an electron-density profile can be obtained from the expression of the statistical uncertainty associated with the total power $A^2_{o,x}(h)$ at a given height, that is given by:

$$\Delta A^2_{o,x}(h) = \pm \sqrt{\frac{(A^2_{o,x}(h))^2 + (n^2)^2}{N}} \qquad (3.3)$$

where n^2 is the average power of noise, and N the number of samples taken. Using as the minimum signal-to-noise acceptable 1, and an uncertainty in the total power $A^2_{o,x}(h) = 0.04\ A^2_{o,x}(h)$, it results $N = 5000$ samples.

3.3 *Results Obtained*

Using the system and the processing method described above, it was possible to obtain reliable electron-density measurements down to a height of 63 km, taking approximately 5000 samples for each profile. Figure 3.7 shows two electron-density profiles obtained in this way, on August 8, 1971,

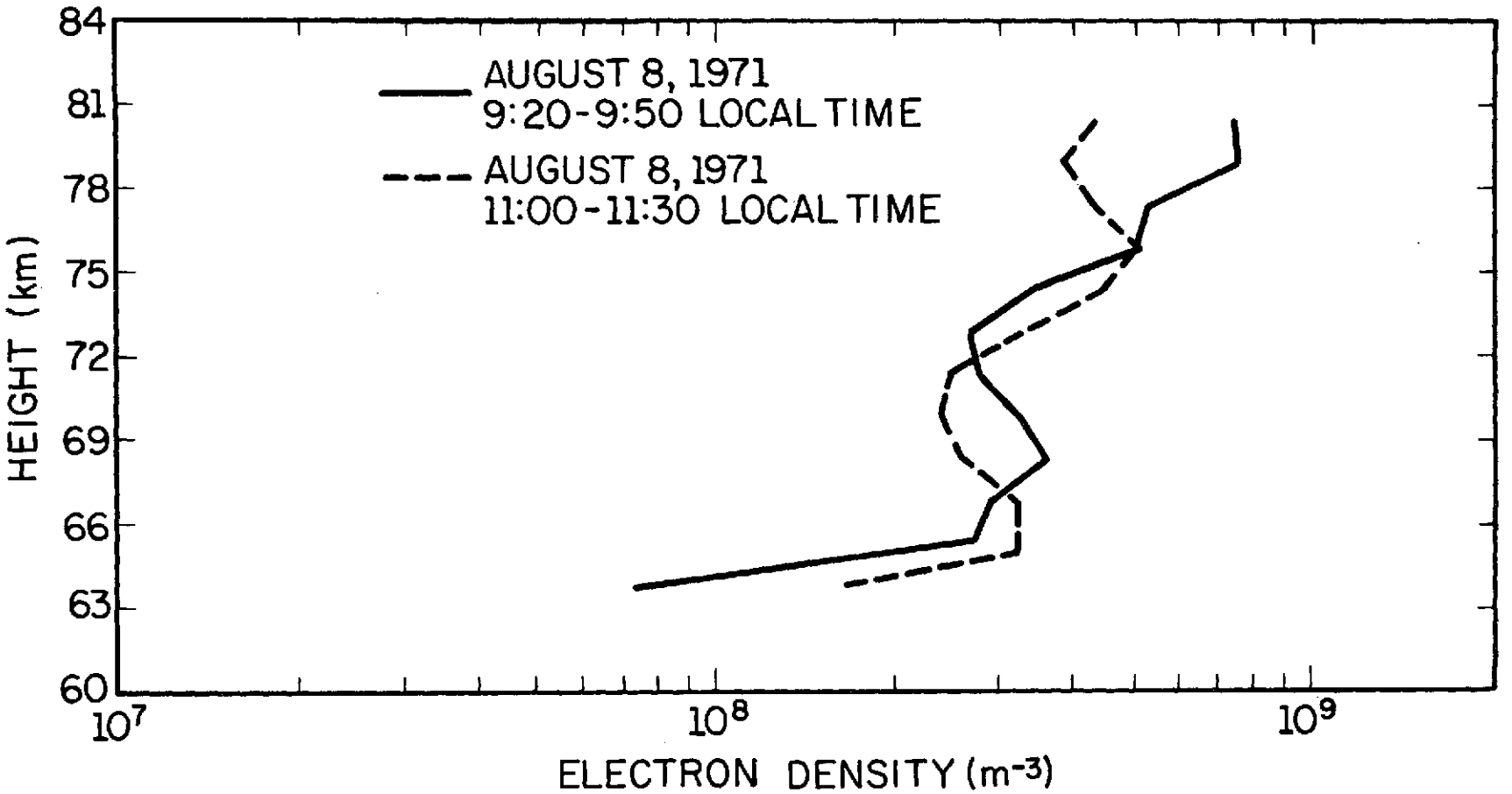

Figure 3.7 Electron-density profiles at low altitudes obtained at Urbana, Illinois.

between 9:20 and 9:50, local time, and on August 8, 1971 between 11:00 and 11:30, local time, at Urbana, Illinois. In Table 3.1 the corresponding values of average noise, number of samples taken, $A_o(h)$ and $A_x(h)$ are shown. In Chapter 5 a more detailed analysis of the results obtained will be made.

3.4 *Suggested Improvements in the Urbana System*

The main limitation of the system in operation at Urbana, is the poor linearity of the receiver. The subroutines VALUE and LINAP that correct the non-linearity are relatively slow, and most of the processing time is taken by them. In consequence, the processing of an electron-density profile with 5000 samples takes approximately 30 minutes of computer time. A more linear receiver, besides saving processing time, and permitting an increase in the number of collected samples, would permit obtaining profiles from 60 to 80 km without the use of a programmed attenuator, if the dynamic range of the receiver is increased to at least 40 dB. The necessary modifications on the receiver implies a new design of the IF and detector stages.

A second important improvement in the system would be an increase of the pulse repetition rate. In the system used now, the pulse repetition rate is limited by the average output power of the transmitter in two double-pulses per second. If the power output of the transmitter were increased, the repetition rate could be increased up to 20 double-pulses per second, this second limitation being imposed by the recovery time of the switching device that changes the polarization of the antennas from the ordinary to the extraordinary mode. A system with a speed of 20 double-pulses per second would be able to take 12,000 samples in 10 minutes, improving the precision of the measured profiles, principally at low altitudes.

TABLE 3.1

Values of A_x, A_o, A_x/A_o average noise and number of samples taken, corresponding to the electron-density profiles of Figure 3.3.

Height	August 8, 71 9:20-9:50 h			August 8, 71 10:00-11:30 h		
km	A_o	A_x	A_x/A_o	A_o	A_x	A_x/A_o
60	17.5	28.0	1.60	30.2	40.0	1.33
61.5	20.1	32.2	1.60	47.2	66.9	1.42
63	24.6	39.7	1.61	75.1	114.6	1.53
64.5	31.4	53.6	1.71	115.2	180.5	1.57
66	48.6	80.6	1.66	159.8	237.7	1.48
67.5	71.9	112.2	1.56	196.5	270.4	1.38
69	108.4	147.1	1.36	223.0	283.6	1.27
70.5	146.4	172.5	1.18	224.0	284.4	1.17
72	167.7	174.3	1.04	244.9	257.8	1.05
73.5	179.9	164.4	0.91	226.1	200.1	0.89
75	174.1	131.7	0.76	218.5	148.0	0.68
76.5	165.7	94.3	0.57	220.7	111.7	0.51
78	165.9	71.4	0.43	223.7	90.7	0.41
79.5	200.0	60.2	0.30	231.6	79.5	0.34
81	257.3	57.8	0.22	258.6	75.5	0.29
	Average noise: - 21.8 4824 samples taken 51 frames rejected			Average noise: - 27.8 5040 samples taken 82 frames rejected		

Finally, an increase of the peak power output of the transmitter to 300 kw would permit an increase in the sensitivity of the system.

4. PARTIAL REFLECTIONS IN THE PRESENCE OF GRADIENTS OF ELECTRON DENSITY

Observation of partial reflection and rocket electron-density profiles above 75 km shows the following characteristics:

1) Partial-reflection measurements frequently present valleys in the electron-density profiles between 75 and 85 km, as can be verified on the profiles of Figures 4.1 to 4.3, obtained at Urbana, and on the results published by several experimenters [*Belrose and Burke*, 1964; *Von Biel et al.*, 1970].

2) The A_o profile in this height range shows a strong increase with altitude of the scattering cross section per unit volume. Figures 4.4 to 4.6 show the A_o profiles corresponding to the electron-density profiles of Figures 4.1 to 4.3.

3) Above 80 km partial reflections produce electron densities that are too low if compared to rocket measurements.

4) Rocket profiles above 75 km are characterized by small changes with height up to 80 km where sharp gradients in electron density are observed [*Bowhill*, 1969].

Such differences between rocket and partial-reflection measurements will be investigated in this chapter. It will be shown that the gradients in electron density observed in rocket profiles can be responsible for the increase in the A_o profiles near 80 km, and that in a region where the scattering cross section is a strong function of altitude, classical methods of partial-reflection data processing can introduce errors great enough to explain the observed differences.

The gradients in electron density can give a two-fold contribution, to partial reflections:

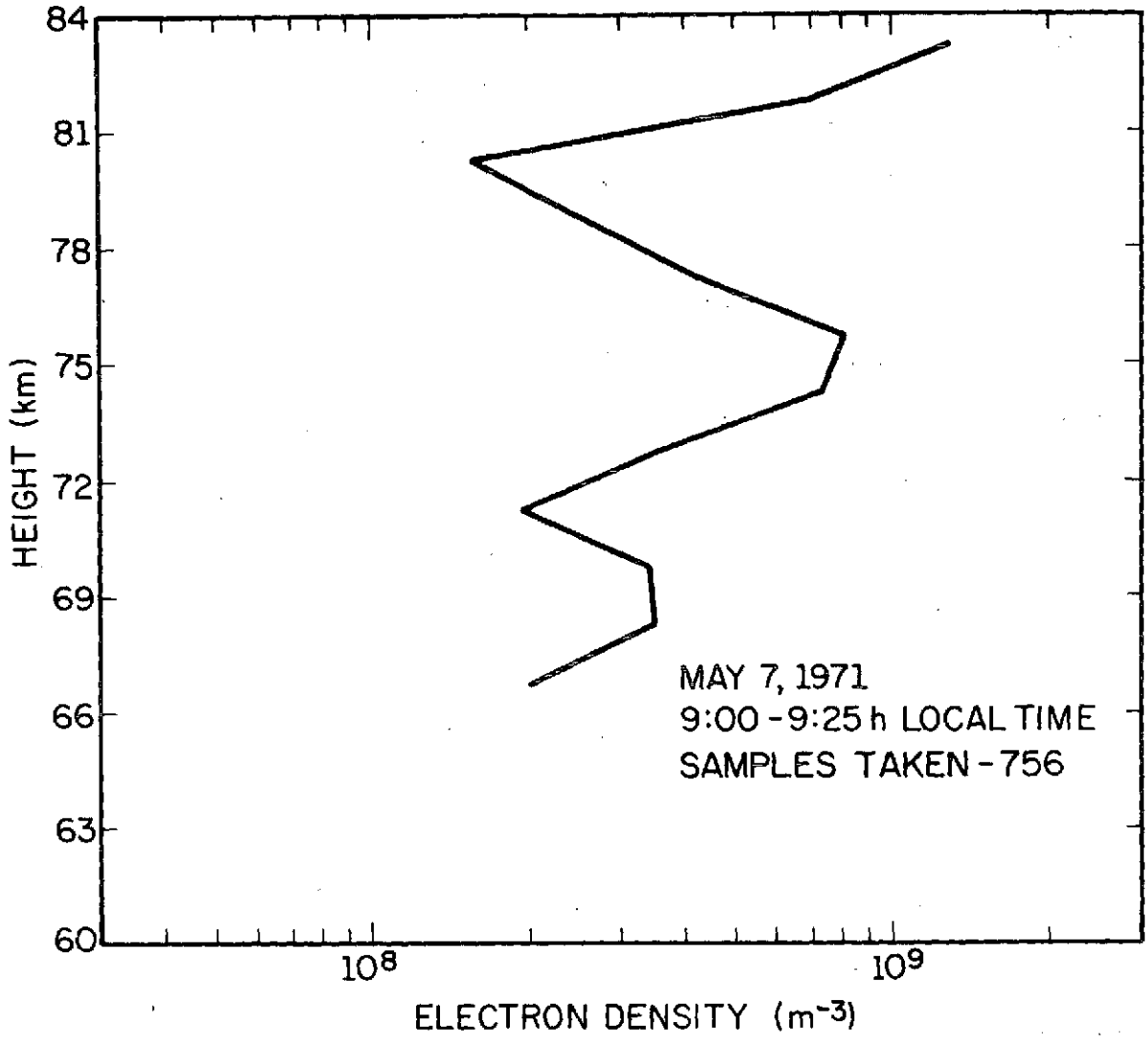

Figure 4.1 Electron-density profile obtained at the University of Illinois Urbana, Ill., on May-7-71, at 9:00h; local time. Valleys of electron density are observed near 71 and 80 km.

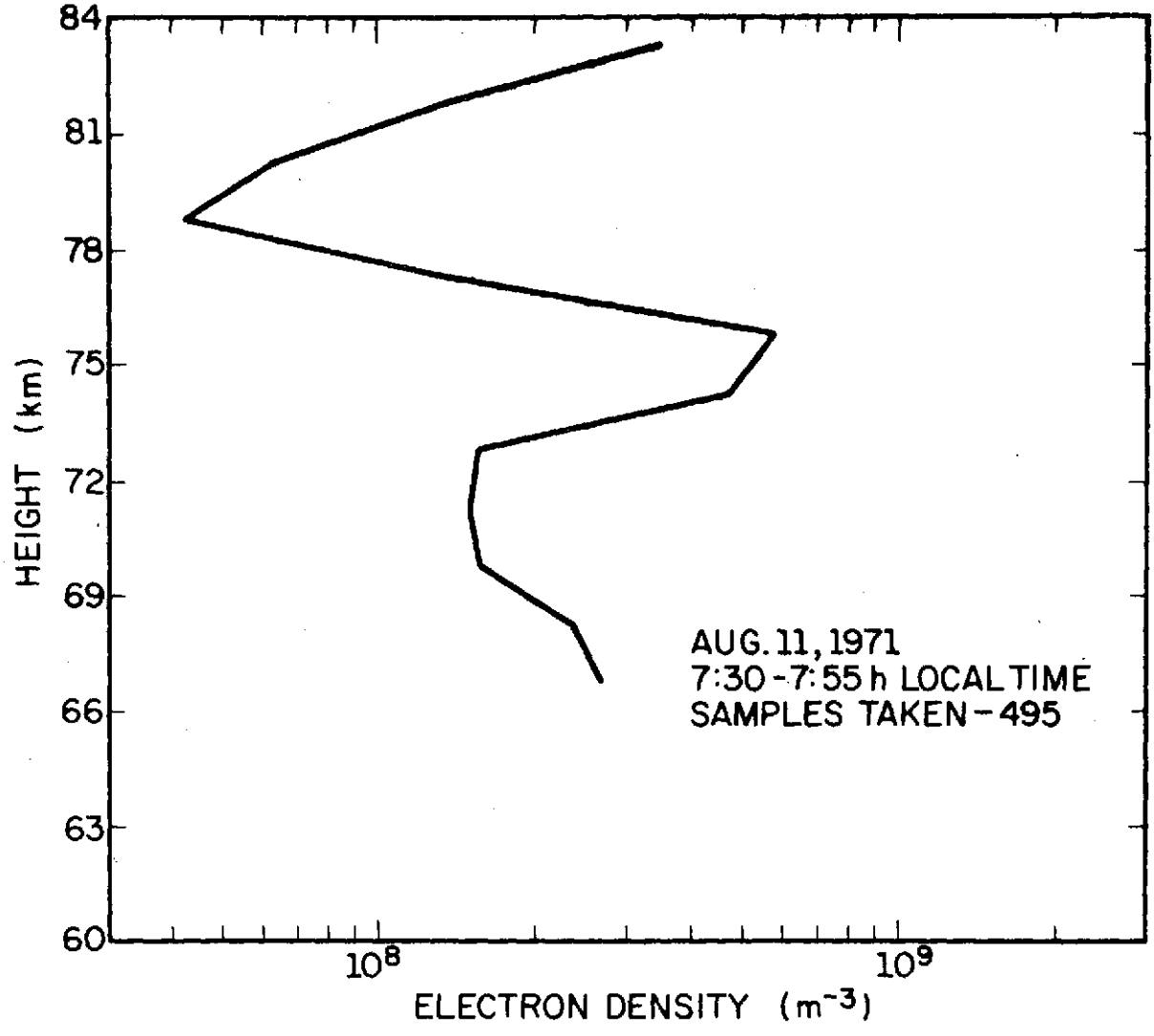

Figure 4.2 Electron-density profile obtained at the University of Illinois, Urbana, Ill., on August-11-71, at 7:30h, local time. A valley of electron density is observed near 80 km.

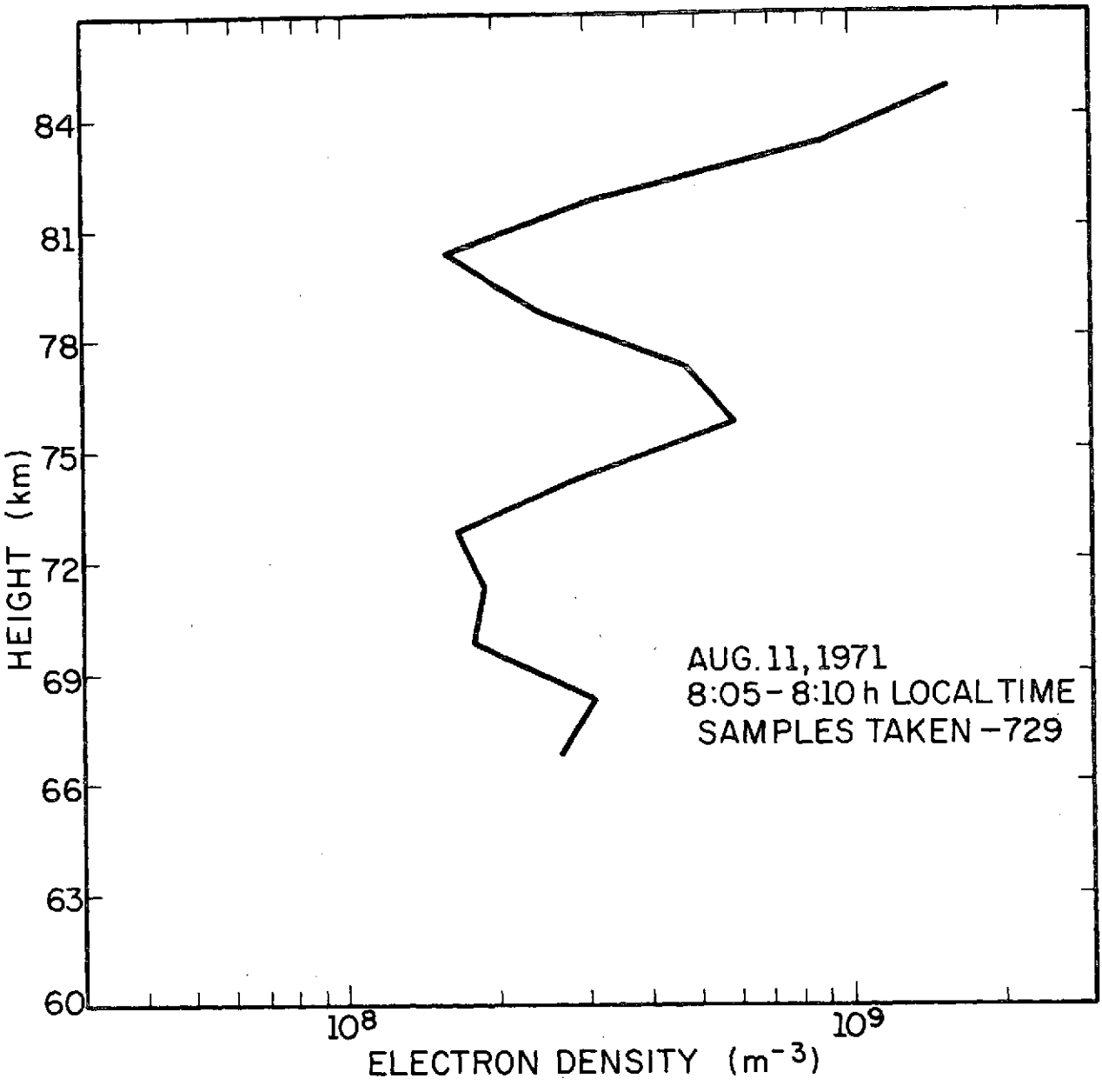

Figure 4.3 Electron-density profile obtained at the University of Illinois, Urbana, Ill. on August-11-71, at 8:05h, local time. Valleys of electron density are observed near 70 and 80 km.

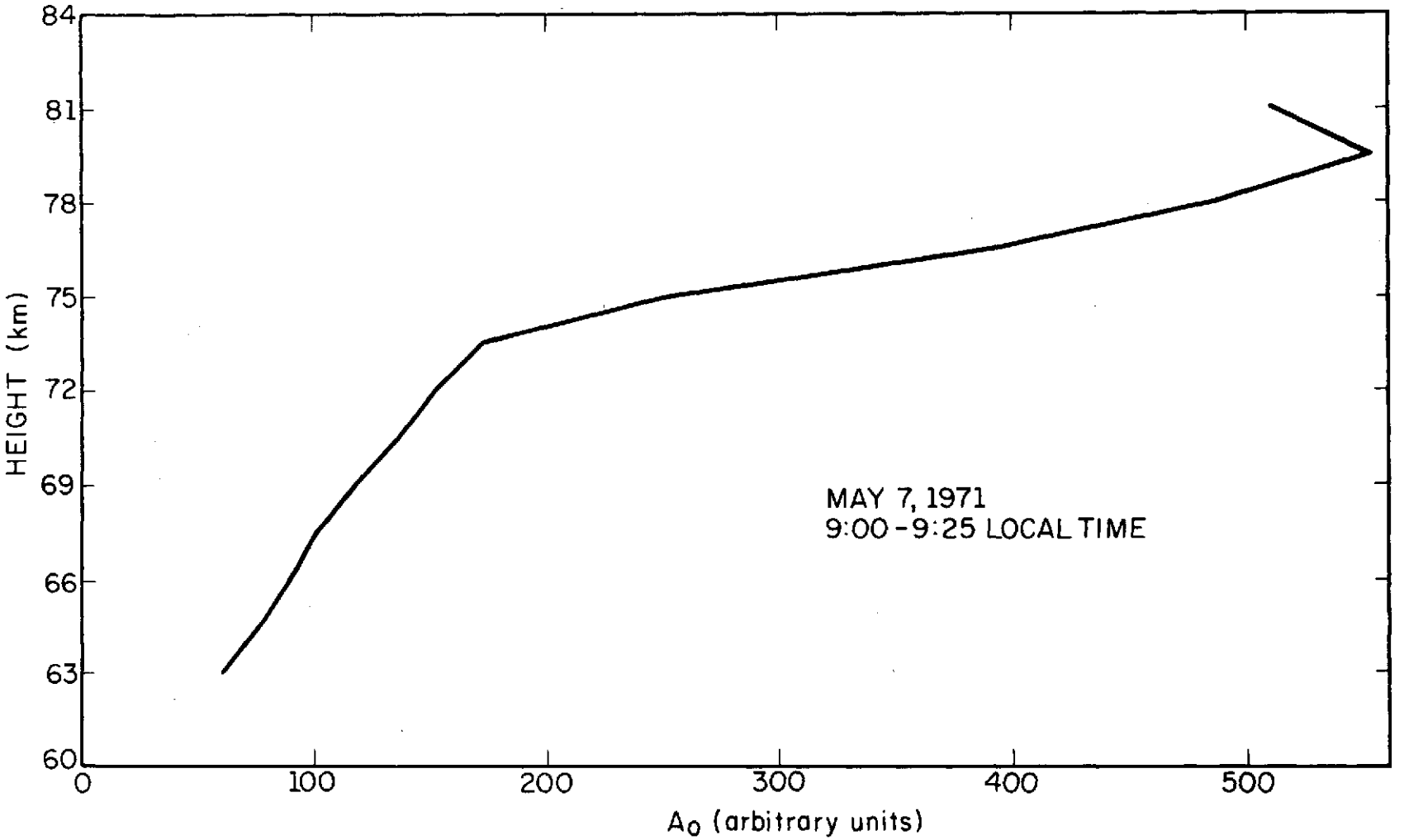

Figure 4.4 A_o profile corresponding to the electron-density profile of Figure 4.1.

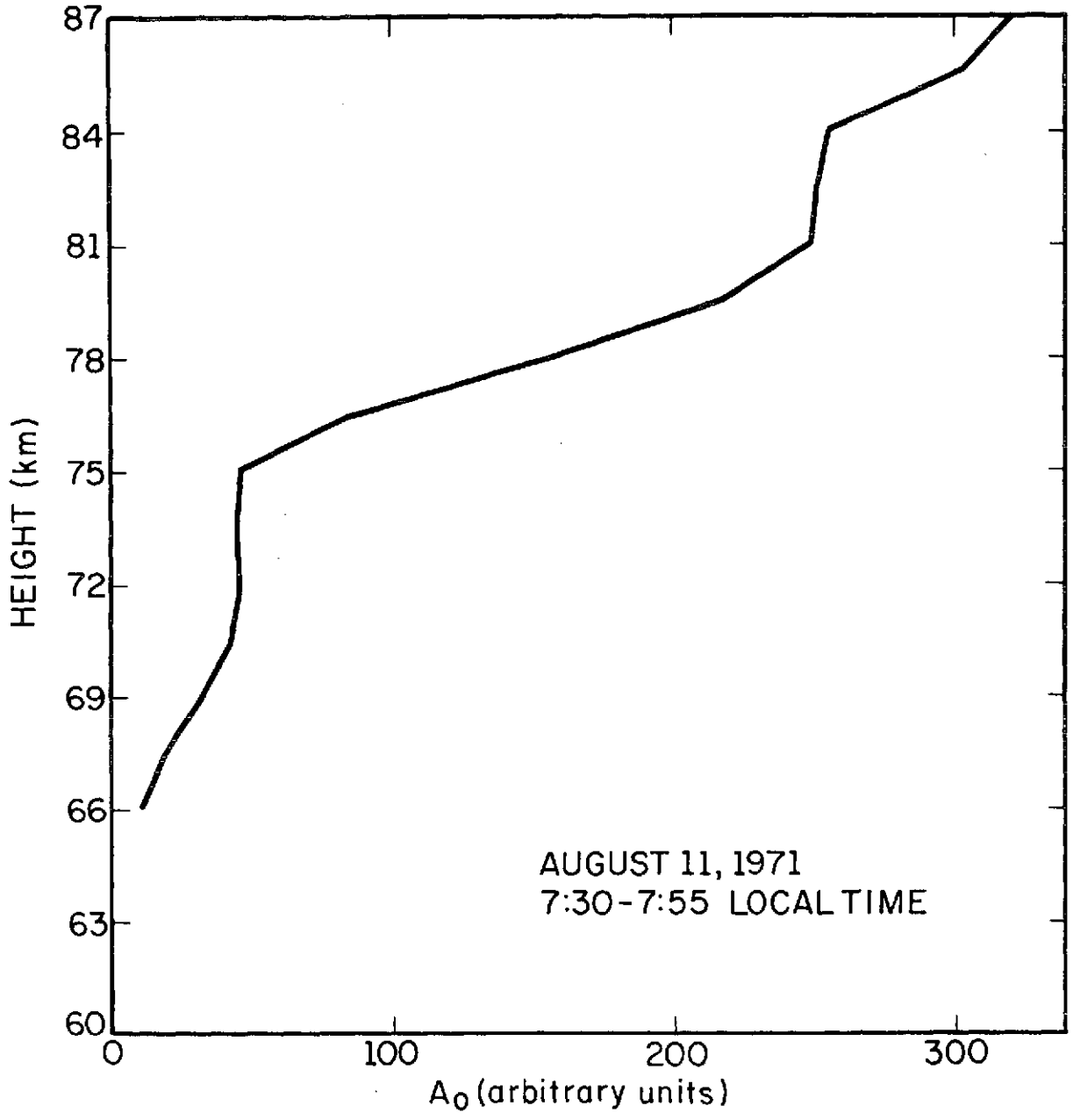

Figure 4.5 A_O profile corresponding to the electron-density profile of Figure 4.2.

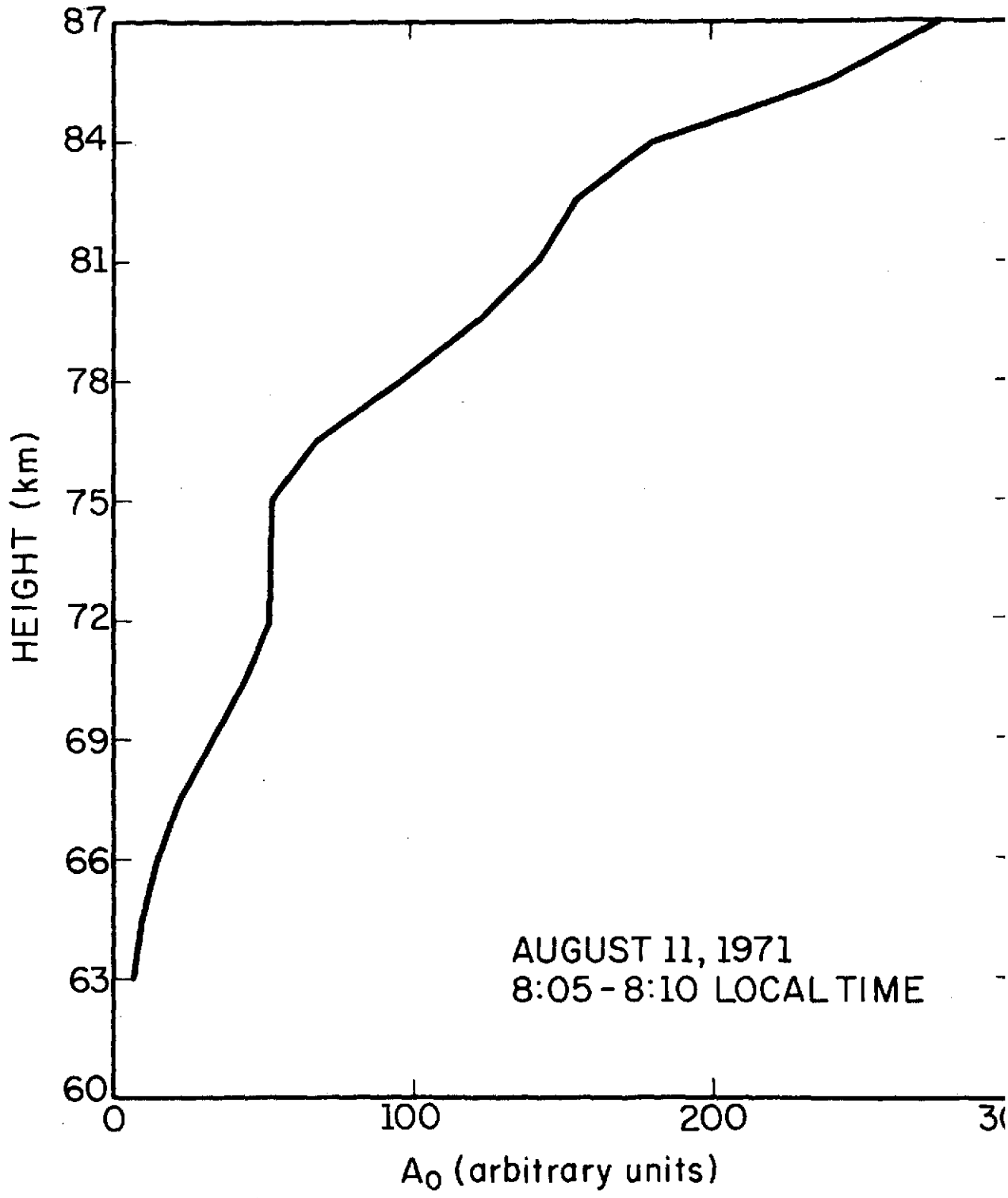

Figure 4.6 A_o profile corresponding to the electron-density profile in Figure 4.3.

C-2

1) The gradient itself produces reflections, due to changes in the refractive index;

2) If there is turbulence, eddies with different electron densities will be mixed, and reflections will result from the random medium produced in this way.

If such reflections are strong enough, they can be responsible for the changes in the scattering cross section near 80 km.

The theories currently used in partial-reflection calculations do not take into account a medium as the one described above. *Belrose and Burke* [1964] assumed reflections produced by a sharp irregularity, and *Flood* [1968] assumed a random medium with a homogeneous background.

The influence of the height dependence of the scattering cross section on the values of the calculated electron densities will be discussed in Section 4.1. It will be shown that the calculated electron-density profiles depend on the width of the transmitted pulse, and that "fictitious valleys", very similar to that observed in the measurements, can appear on the profiles. The dependence of partial-reflection profiles on the pulse width has been already discussed by *Coyne and Belrose* [1973]. In Section 4.2 the reflection coefficients produced by gradients in electron density will be calculated, for gradients of the magnitude of that observed on rocket profiles. In Section 4.3 the theory of scattering in a random medium will be extended to the case of electron-density fluctuations in a locally homogeneous background medium. Results will be compared with the theories of *Belrose and Burke* [1964], *Flood* [1968] and *Cohen* [1971]. Possible influences of the correlation function of the irregularities on the ratio $|R_x/R_o|$ will be verified. The relative contribution of random

irregularities and of gradients in electron density to partial reflections will be discussed. In Section 4.4 the nature of the irregularities producing partial reflections will be analyzed and in Section 4.5 some suggestions to overcome the influence of the finite pulse width on partial-reflection calculations, and experimental results, will be presented.

4.1 *Partial Reflections in a Region where the Scattering Cross Section is a Function of Altitude.*

Observation of A_o profiles, as shown in Figures 4.4 to 4.6 shows that the scattering cross section per unit height changes sharply with heights above 78 km. Such sharp increase in scattering cross section has been observed in practically all partial-reflection measurements [*Gardner and Pawsey*, 1953; *Belrose and Burke*, 1964].

The changes in scattering cross section with height are really greater than the changes observed in the A_o profiles, since A_o is the result of integration of reflections produced over a height interval $cW/2$, where c is the velocity of light in the medium, and W is the pulse width. To study the influence of changes in the scattering cross section on the calculated electron-density profiles, two models of scattering cross section per unit volume as a function of height will be considered:

1) The scattering cross section per unit volume has a constant value σ_1 below a height h_a, σ_2 between the heights h_a and h_b, and σ_3 above the height h_b. Discontinuities are observed at h_a and h_b, as shown in Figure 4.7a;

2) The scattering cross section per unit volume is a constant σ_1 below a height h_a, changes exponentially to a value σ_2 at a height h_b, and has a constant value σ_3 above h_b, as shown in Figure 4.7b.

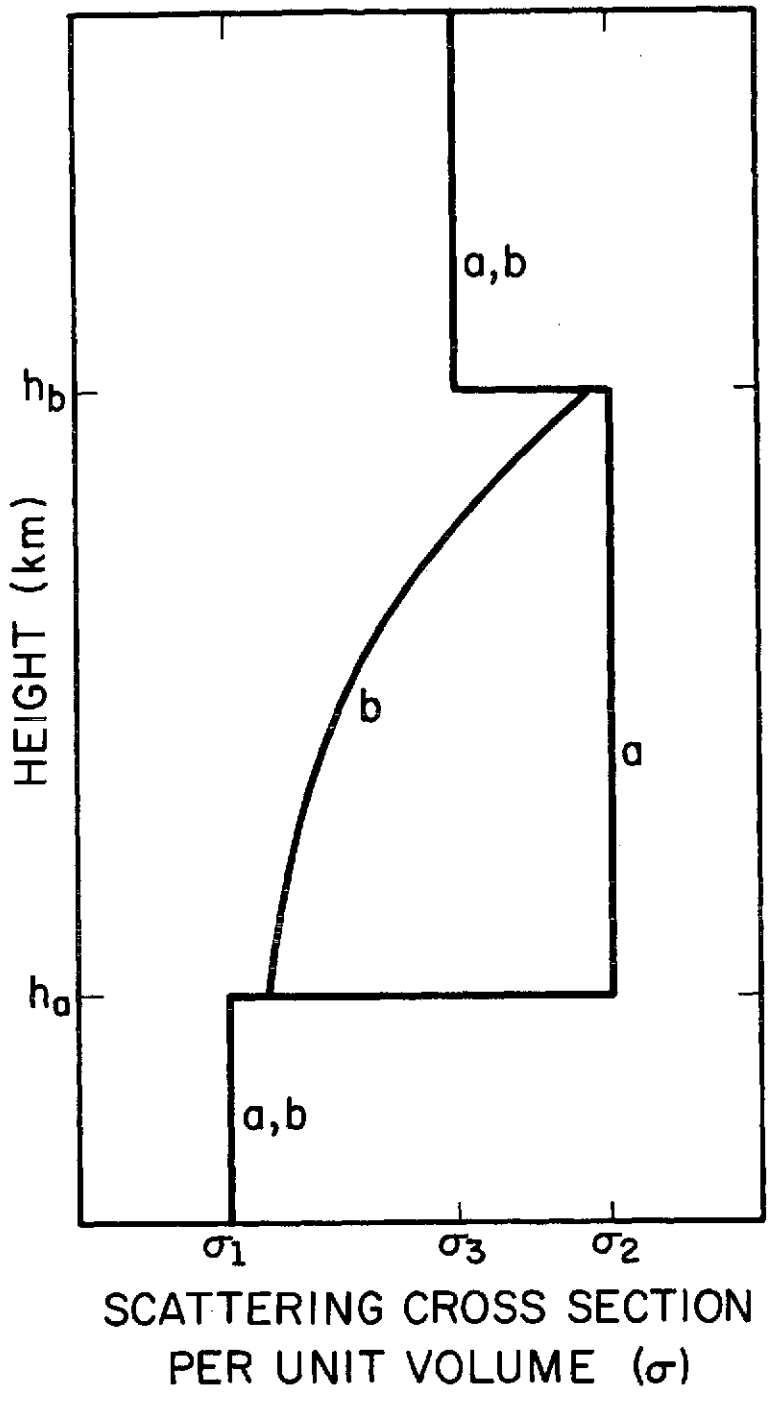

Figure 4.7 Scattering cross-section per unit volume profiles used on the calculations of Section 4.1.

For both models it will be assumed that the electron density and collision frequency, N_r and ν, are constant over the region of interest. The A_x/A_o profiles that would result from a plane wave pulse propagating vertically in such a medium will be obtained, and, from such profiles, electron densities will be calculated using the theory of *Belrose and Burke* [1964]. The real electron density N_r will be compared to the calculated electron densities.

4.1.1 *Partial reflections in a region where the scattering cross section per unit volume changes in steps.* If a plane wave pulse is incident on the ionosphere, the amplitude of the reflected pulse will be given by

$$A^2(h_1) = D \int_{h_1 - \frac{Wc}{4}}^{h_1 + \frac{Wc}{4}} \sigma(h)\, A_{in}^2 \cdot \exp \int_0^{h_1} \{-4a\, dh\} dh \qquad (4.1)$$

where $A^2(h_1)$ = reflected power

A_{in}^2 = incident power

a = attenuation coefficient

D = average width of the volume V occupied by the pulse

W = width of the incident pulse

h_1 = height of the center of the pulse

$\sigma(h)$ = scattering cross section per unit volume

c = velocity of light in the medium.

For the scattering cross section per unit volume profile of Figure 4.7a with $h_b - h_a \leq Wc/4$, it results

-For $h_1 \leq h_a - Wc/4$

$$\frac{A^2(h_1)}{A_{in}^2} = \frac{\sigma 1}{2\alpha} \sinh(\alpha We)\ \exp(-4\alpha h_1) \tag{4.2}$$

-For $h_b - We/4 \geq h_1 \geq h_a - We/4$

$$\frac{A^2(h_1)}{A_{in}^2} = \frac{(\sigma_2-\sigma_1)}{4\alpha}\exp(-4\alpha h_a) + \left\{\frac{\sigma_1\ \exp(\alpha We) - \sigma_2\ \exp(-\alpha We)}{4\alpha}\right\}\exp(-4\alpha h_1) \tag{4.3}$$

-For $h_a + We/4 \geq h_1 \geq h_a - We/4$

$$\frac{A^2(h_1)}{A_{in}^2} = \frac{(\sigma_2-\sigma_1)}{4\alpha}\ \exp(-4\alpha h_a) + \left(\frac{\sigma_3-\sigma_2}{4\alpha}\right)\ \exp(-4\alpha h_b)$$

$$+ \left\{\frac{\sigma_1\ \exp(\alpha We) - \sigma_3\ \exp(-\alpha We)}{4\alpha}\right\}\ \exp(-4\alpha h_1) \tag{4.4}$$

-For $h_a + We/4 \geq h_1 \geq h_a + We/4$

$$\frac{A^2(h_1)}{A_{in}^2} = \frac{(\sigma_3-\sigma_2)}{4\alpha}\ \exp(-4\alpha h_b) + \left\{\frac{\sigma_2\ \exp(\alpha We) - \sigma_3\ \exp(-\alpha We)}{4\alpha}\right\}\exp(-4\alpha h_1) \tag{4.5}$$

-For $h_1 \leq h_b + We/4$

$$\frac{A^2(h_1)}{A_{in}^2} = \frac{\sigma_3\ \sinh(\alpha We)}{2\alpha}\ \exp(-4a h_1) \tag{4.6}$$

If both characteristic modes of propagation are transmitted, the ratio of the amplitudes of the reflected signals, A_x/A_o, can be obtained from equations (4.2) to (4.6), using for α the following expressions, for the ordinary and extraordinary modes, respectively

$$\alpha_o = \frac{5}{4} \frac{N_e^2}{\varepsilon_o mc\nu} C_{5/2}\left(\frac{\omega+\omega_L}{\nu}\right) \tag{4.7}$$

$$\alpha_x = \frac{5}{4} \frac{N_e^2}{\varepsilon_o mc\nu} C_{5/2}\left(\frac{\omega-\omega_L}{\nu}\right) \tag{4.8}$$

The quasi-longitudinal approximation being assumed.

The ratio of the scattering cross sections, σ_x/σ_o, is given by *Belrose and Burke* [1964]

$$\frac{\sigma_x}{\sigma_o} = \frac{\left\{\left(\frac{\omega-\omega_L}{\nu}\right) C_{3/2}\left(\frac{\omega-\omega_L}{\nu}\right)\right\}^2 + \left\{\frac{5}{2} C_{5/2}\left(\frac{\omega-\omega_L}{\nu}\right)\right\}^2}{\left\{\left(\frac{\omega+\omega_L}{\nu}\right) C_{3/2}\left(\frac{\omega+\omega_L}{\nu}\right)\right\}^2 + \left\{\frac{5}{2} C_{5/2}\left(\frac{\omega+\omega_L}{\nu}\right)\right\}^2} \tag{4.9}$$

In the case considered here, the collision frequency is constant, and the ratio σ_x/σ_o will be constant.

Figures 4.8 and 4.9 show the A_o and A_x/A_o profiles for a pulse width of 50 μsec, an electron density of 10^9 m^{-3}, a collision frequency of 7.7×10^5 s^{-1}, typical of heights near 80 km, and the following scattering cross sections per unit volume:

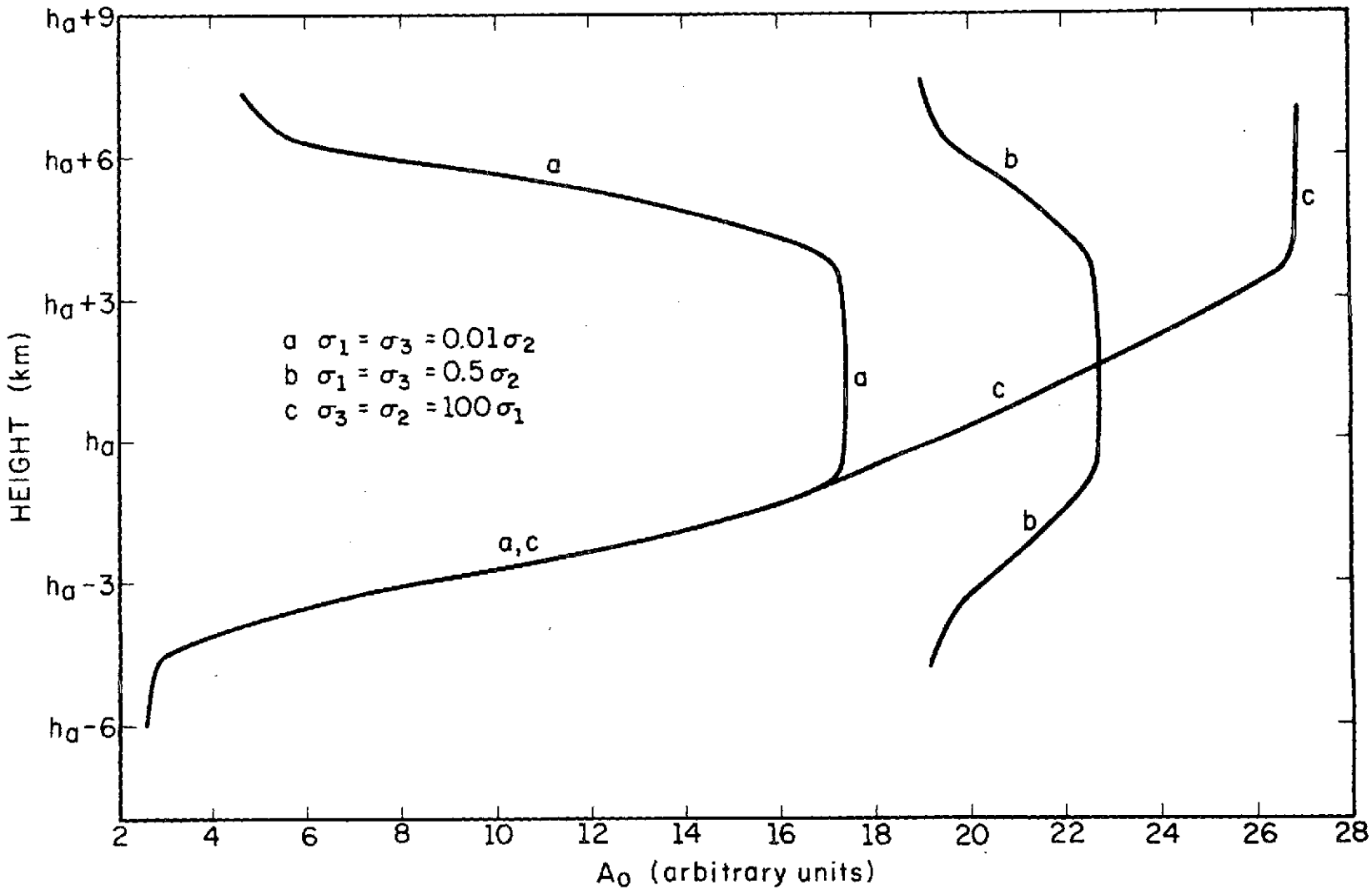

Figure 4.8 Calculated A_o profiles, for a region where the electron density is of 10^9 m^{-3}, the collision frequency 7.7×10^5 s^{-1}, and the scattering cross-section per unit volume profile is that shown on Figure 4.7a, with $\sigma_1 = \sigma_3 = 0.01\ \sigma_2$, (*a*), $\sigma_1 = \sigma_3 = 0.5\ \sigma_2$, (*b*), and $\sigma_3 = \sigma_2 = 100\ \sigma_1$, (*c*).

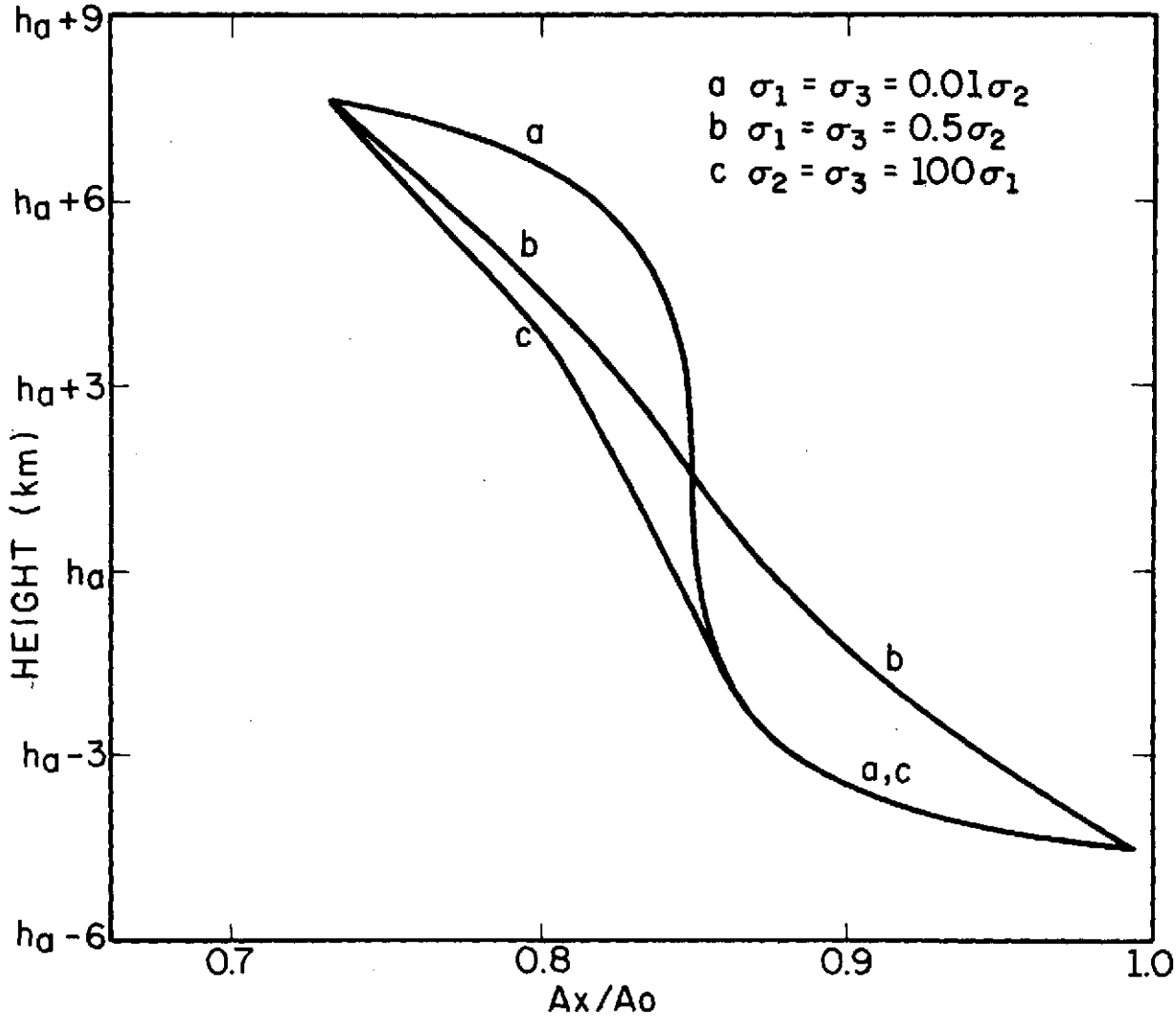

Figure 4.9 A_x/A_o profiles corresponding to the A_o profiles of Figure 4.8.

1) $\sigma_{1o} = \sigma_{3o} = 0.01\ \sigma_{2o}$, $h_b - h_a = 3$ km

2) $\sigma_{1o} = \sigma_{3o} = 0.5\ \sigma_{2o}$, $h_b - h_a = 3$ km

3) $\sigma_{2o} = \sigma_{3o} = 100\ \sigma_{1o}$, $h_b - h_a = 3$ km

The index o refers to the ordinary mode.

Electron-density profiles calculated from the A_x/A_o profiles of Figure 4.9 by using *Belrose and Burke's* [1964] theory are shown in Figure 4.10. It must be noticed that the real electron density is constant and equal to 10^9 m^{-3}. As it is observed, variations of the scattering cross section with height, and the finite pulse width, can produce valleys in a region where the real electron density is constant. The depth of the valley can be as great as 2.5×10^{-2} of the real value, as in Figure 4.10a; even if the scattering cross section changes only by a factor of 2, as in Figure 4.10b (and in this case A_o changes only by a factor of 1.25), the depth of the valley will be of 0.7 of the real value of the electron density.

A comparison of Figure 4.10 with Figures 4.1 to 4.3 shows a great similarity between experimental results and model calculations. In Figure 4.3, for example, the electron density changes from 6×10^8 at 75.7 km to 1.6×10^8 at 80.2 km; the average A_o changes from 52 to 75 km to 140 at 81 km. Such variations are comparable to the theoretical results of Figures 4.10c and 4.8c.

To analyze the influence of changes of the pulse width in partial-reflections measurements, electron-density calculations were made for a region where the real electron density is 10^9 m^{-3}, the collision frequency 7.7×10^5 s^{-1}, using pulses of 50 and 25 μsec, for the following changes

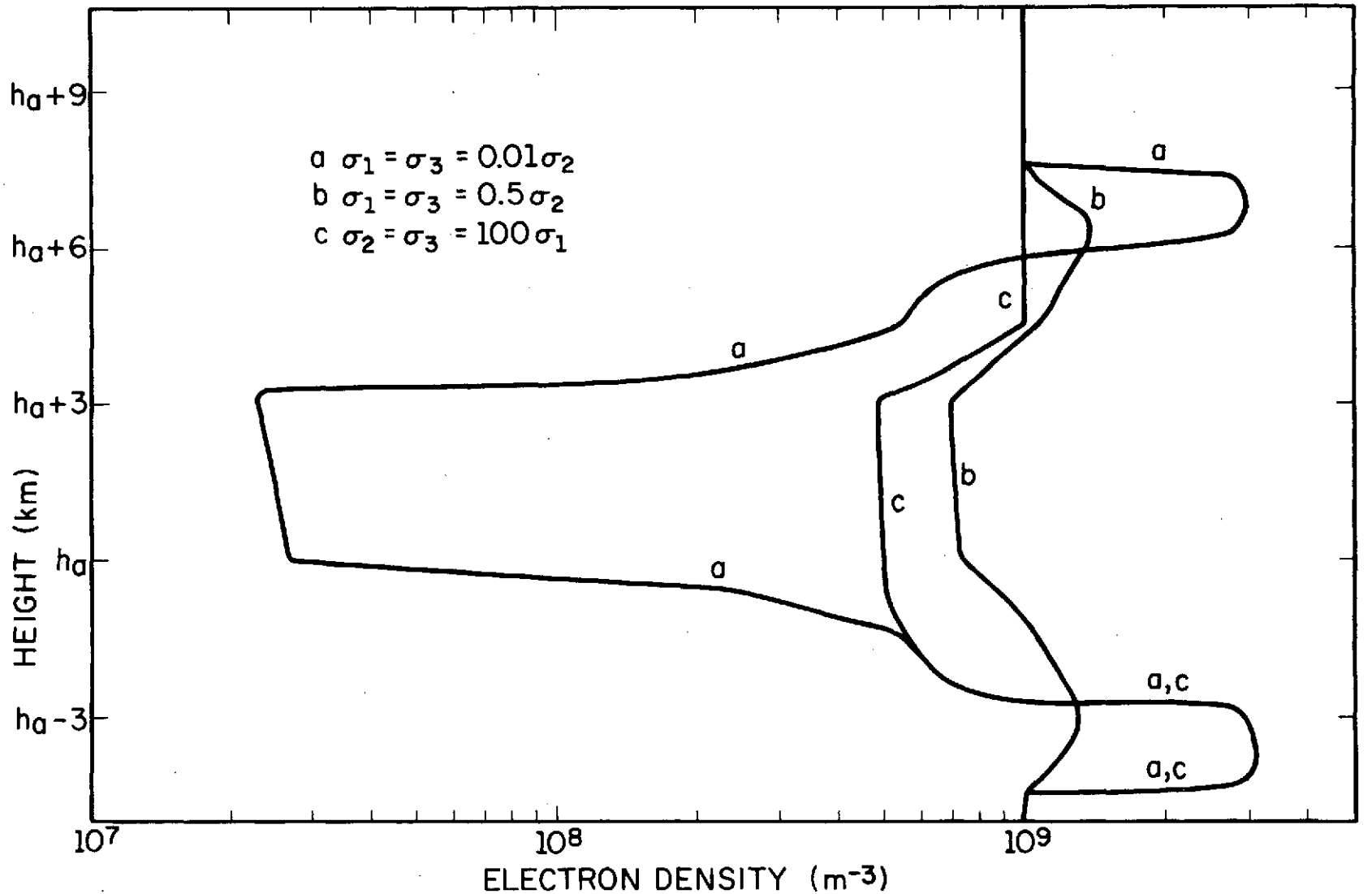

Figure 4.10 Electron-density profiles obtained from the A_x/A_o profiles in Figure 4.9.

in backscattering cross section

a) $\sigma_1 = \sigma_3 = 0.01\ \sigma_2$

b) $\sigma_2 = \sigma_3 = \frac{10}{3}\ \sigma_1$

The results are shown in Figure 4.11. Figure 4.12 shows an experimental measurement, made by *Belrose* [1971], using the same pulse widths. Experimental and theoretical results agree very well, again. In both cases the depth of the valley is practically independent of the pulse width, but for the 25 μsec pulse, the valley appears at higher altitudes, and is narrower.

The above calculations show that the knowledge of A_o profiles is necessary to the interpretation of partial-reflection results. Every time the average A_o changes rapidly with height, valleys observed in electron-density profiles cannot be considered as real, but may be a consequence of changes in the scattering cross section and of the finite pulse width.

4.1.2 *The scattering cross section per unit volume changes exponentially as a function of height.* The scattering cross section per unit volume to be considered is shown in Figure 4.7b and is given by:

$\sigma(h) = \sigma_1 \qquad h < h_a$

$\sigma(h) = \exp(\beta h) \qquad h_b \geq h \geq h_a$

$\sigma(h) = \sigma_3 \qquad h \geq h_b$

The reflected power, as obtained from equation (4.1) is given by:

-If $h_1 \leq h_a - Wc/4$

$$\frac{A^2(h_1)}{A_{in}^2} = \frac{\sigma_1}{2\alpha} \sinh(\alpha Wc)\ \exp(-4\alpha h_1) \tag{4.10}$$

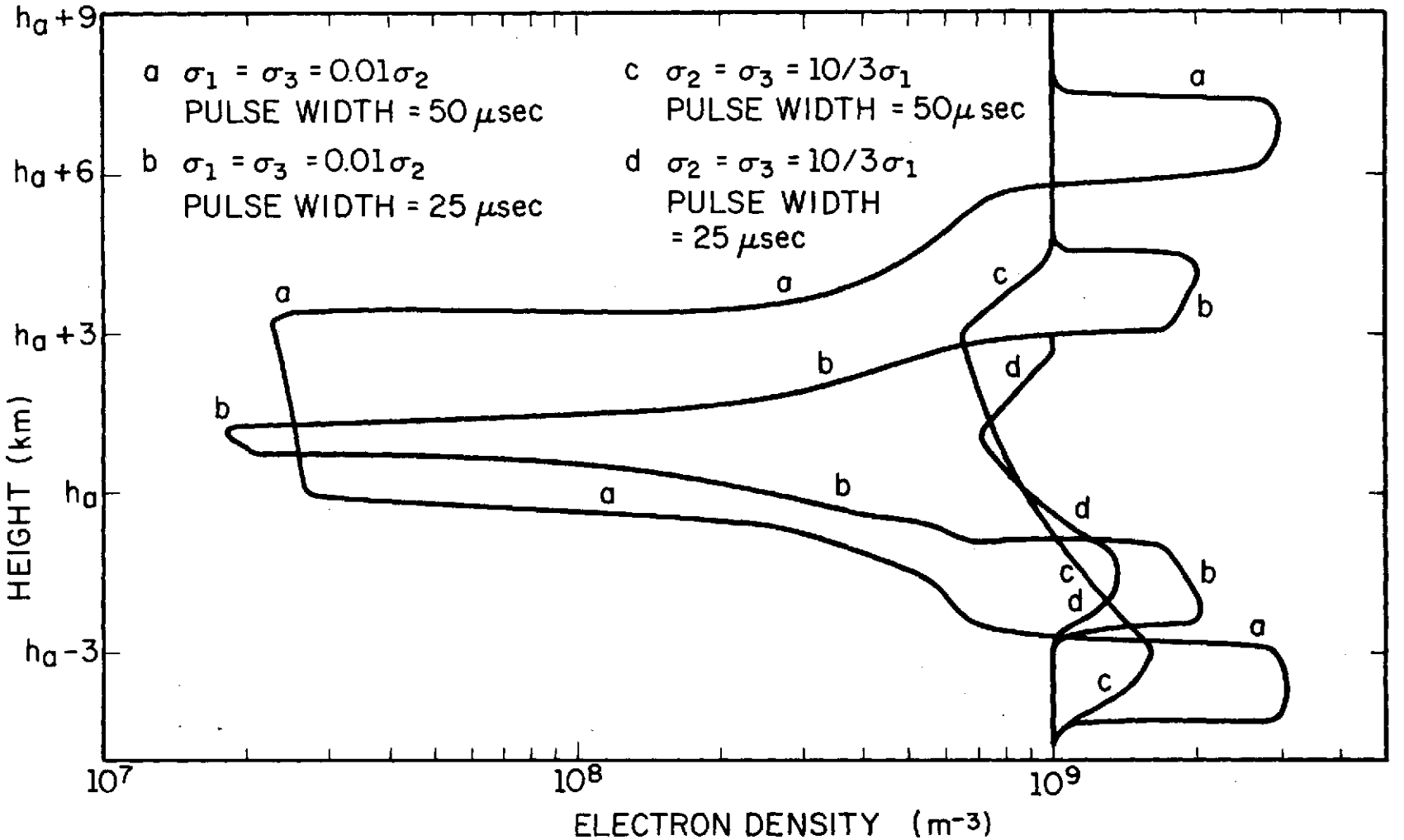

Figure 4.11 Electron-density profiles calculated using Belrose and Burke's theory, for a region where the real electron density is of 10^9 m^{-3}, the collision frequency 7.7 x 10^5 sec^{-1}, the scattering cross section per unit volume profile is that shown on Figure 4.7, with $\sigma_1 = \sigma_3 = 0.01\ \sigma_2$, pulse widths of 50 μsec, (*a*), and 25 μsec, (*b*), and with $\sigma_2 = \sigma_3 = \frac{10}{3}\ \sigma_1$, pulse widths of 50 μsec, (*c*), and 25 μsec, (*d*).

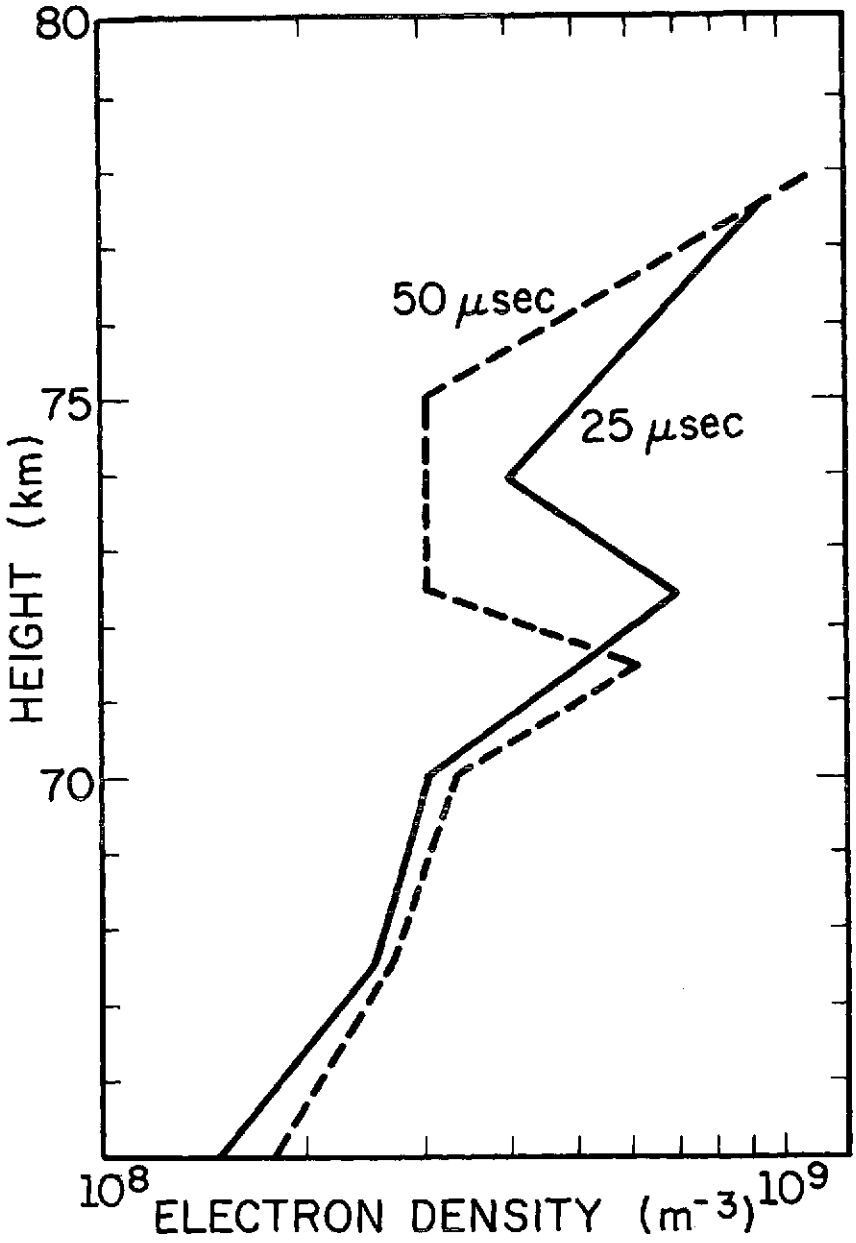

Figure 4.12 Electron density measurements obtained experimentally by *Belrose* [1971] using pulses of 50 and 25 μsec.

-If $h_b - We/4 \geq h_1 \geq h_a - We/4$

$$\frac{A^2(h_1)}{A_{in}^2} = \frac{\sigma_1}{4\alpha}\{\exp(-4\alpha(h_1 - \frac{We}{4})] - \exp(-4\alpha h_a)\}$$

$$+ \frac{1}{(\beta - 4\alpha)} \exp[(\beta - 4\alpha)(h_1 + \frac{We}{4})] - \exp[(\beta - 4\alpha)h_a]\} \quad (4.11)$$

-If $h_a + We/4 \geq h_1 \geq h_b - We/4$

$$\frac{A^2(h_1)}{A_{in}^2} = \frac{\sigma_1}{4\alpha}\{\exp[-4\alpha(h_1 - \frac{We}{4})] - \exp(-4\alpha h_a)\} + \frac{1}{(\beta-4\alpha)}\{\exp[(\beta-4\alpha)h_b] - \exp[(\beta-4\alpha)h_a]\}$$

$$+ \frac{\sigma_1}{4\alpha}\{\exp(-4\alpha h_b) - \exp[-4\alpha(h_1 - \frac{We}{4})]\} \quad (4.12)$$

-If $h_b + We/4 \geq h_1 \geq h_a + We/4$

$$\frac{A^2(h_1)}{A_{in}^2} = \frac{1}{(\beta-4\alpha)} \exp[(\beta-4\alpha)h_b] - \exp[(\beta-4\alpha)(h_1 - \frac{We}{4})]\}$$

$$+ \frac{\sigma_3}{4\alpha}\{\exp(-4\alpha h_b) - \exp[-4\alpha(h_1 - \frac{We}{4})]\} \quad (4.13)$$

-If $h_1 \geq h_b + We/4$

$$\frac{A^2(h_1)}{A_{in}^2} = \frac{\sigma_3}{2\alpha} \sinh(\alpha We) \exp(-4\alpha h_1) \quad (4.14)$$

Equations (4.10) to (4.14) can be used in the calculation of electron densities as would be measured from partial reflections, using the same procedure as in Section 4.1.1. Figure 4.13 shows the electron-density profiles obtained for the case where the real electron density is 10^9 m^{-3}, the collision frequency 7.7×10^5 s^{-1}, the pulse width 50 μsec, and the following scattering cross section per unit volume profiles:

1) $\sigma_{1o} = 1$, $\beta_o = 1.63 \times 10^{-3}$, $\sigma_{3o} = \exp(-\beta_o h_b) = 100$

$h_a = 0$ $h_b = 3$ km

2) $\sigma_{1o} = 1$, $\beta_o = 1.63 \times 10^{-3}$, $\sigma_{3o} = 1$

$h_a = 0$, $h_b = 3$ km

3) $\sigma_{1o} = 1$, $\beta_o = 7.66 \times 10^{-4}$, $\sigma_{3o} = 1$

$h_a = 0$, $h_b = 3$ km

The results are essentially the same as obtained in Section 4.1.1, and they show that deep valleys in electron density can be produced even in the case where the scattering cross section per unit volume changes continually with height.

4.2 *Reflections Produced by Gradients in Electron Density.*

As discussed before, the scattering cross section of the ionosphere increases sharply at altitudes near 80 km. Such altitudes are characterized by gradients in the electron-density profiles, as can be observed in rocket measurements. On this item the reflection coefficient produced by gradients will be calculated, in order to verify if they have enough magnitude to explain the observed partial reflections. Initially it will be assumed that the electron density changes linearly with altitude, and a full-wave calculation will be applied to the determination of the

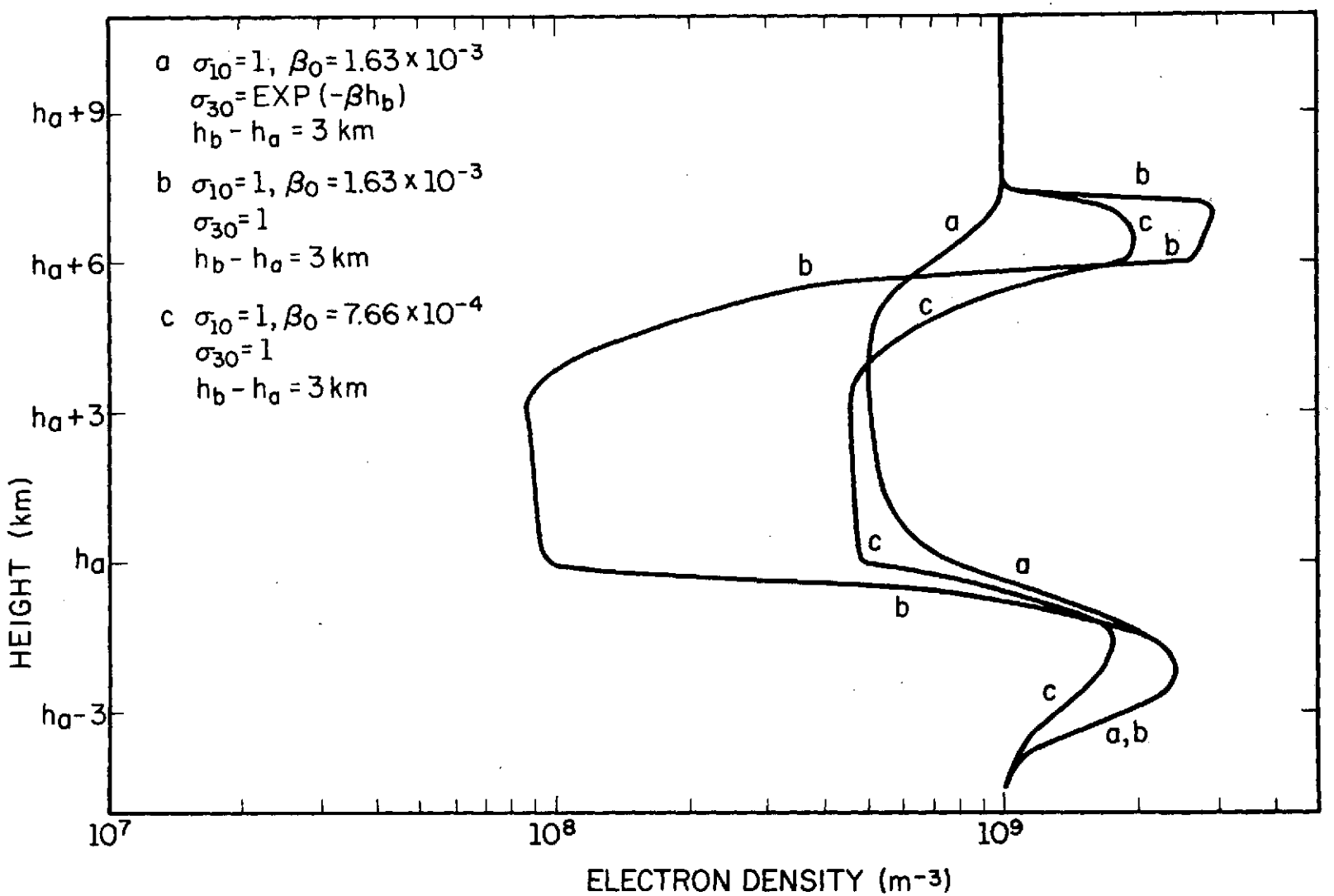

Figure 4.13 Electron-density profiles calculated using *Belrose and Burke's* [1964] theory, for a region where the real electron density is 10^9 m^{-3}, the collision frequency 7.7 x 10^5 sec^{-1}, and the scattering cross-section profile is that shown on Figure 4.7b, with h_a-h_b = 3 km, and with σ_{1o} = β_0 = 1.63 x 10^{-3}, σ_{3o} = exp(-βh_b), β_0 = 7.66 x 10^{-4} σ_{3o} = 1, (c).

reflection coefficients. After that, an approximate solution will be applied to different geometries of electron-density profiles.

4.2.1 *Reflections from gradients with a linear variation in electron density.* The model of reflector utilized in this item is shown in Figure 4.14. The electron density is constant above a height h_2 and below a height h_1, and increases linearly with height between h_1 and h_2. The collision frequency is assumed constant, the ionosphere horizontally stratified and the propagation quasi-longitudinal. For such a simple model it is possible to find an analytical solution for the reflection coefficients, avoiding numerical calculations.

As the propagation is longitudinal, and the ionosphere horizontally stratified, the solution of the wave equation can be written as [*Budden*, 1960]

1) If $h \leq h_1$

A plane wave solution:

$$E_{o1} = \exp\{ - i\, k_0 n_{1o}\, (h-h_1)\} + R_o \exp\{i\, k_0 n_{1o}(h-h_1)\} \qquad (4.15a)$$

$$H_{o1} = i\, n_{1o} \exp\{- i\, k_0 n_{1o}(h-h_1)\} - i\, n_{1o}\, R_o \exp\{i\, k_0 n_{1o}(h-h_1)\} \qquad (4.15b)$$

$$E_{x1} = \exp\{- i\, k_0 n_{1x}(h-h_1)\} + R_x \exp\{i\, k_0 n_{1x}(h-h_1)\} \qquad (4.16a)$$

$$H_{x1} = i\, n_{1x} \exp\{- i\, k_0 n_{1x}(h-h_1)\} - i\, n_{1x}\, R_x \exp\{i\, k_0 n_{1x}(h-h_1)\} \qquad (4.16b)$$

where $k_0$is the wave number in free space, $R_{o,x}$ is the reflection coefficient, $n_{o,x}$ is the refractive index for heights equal or below h_1, the

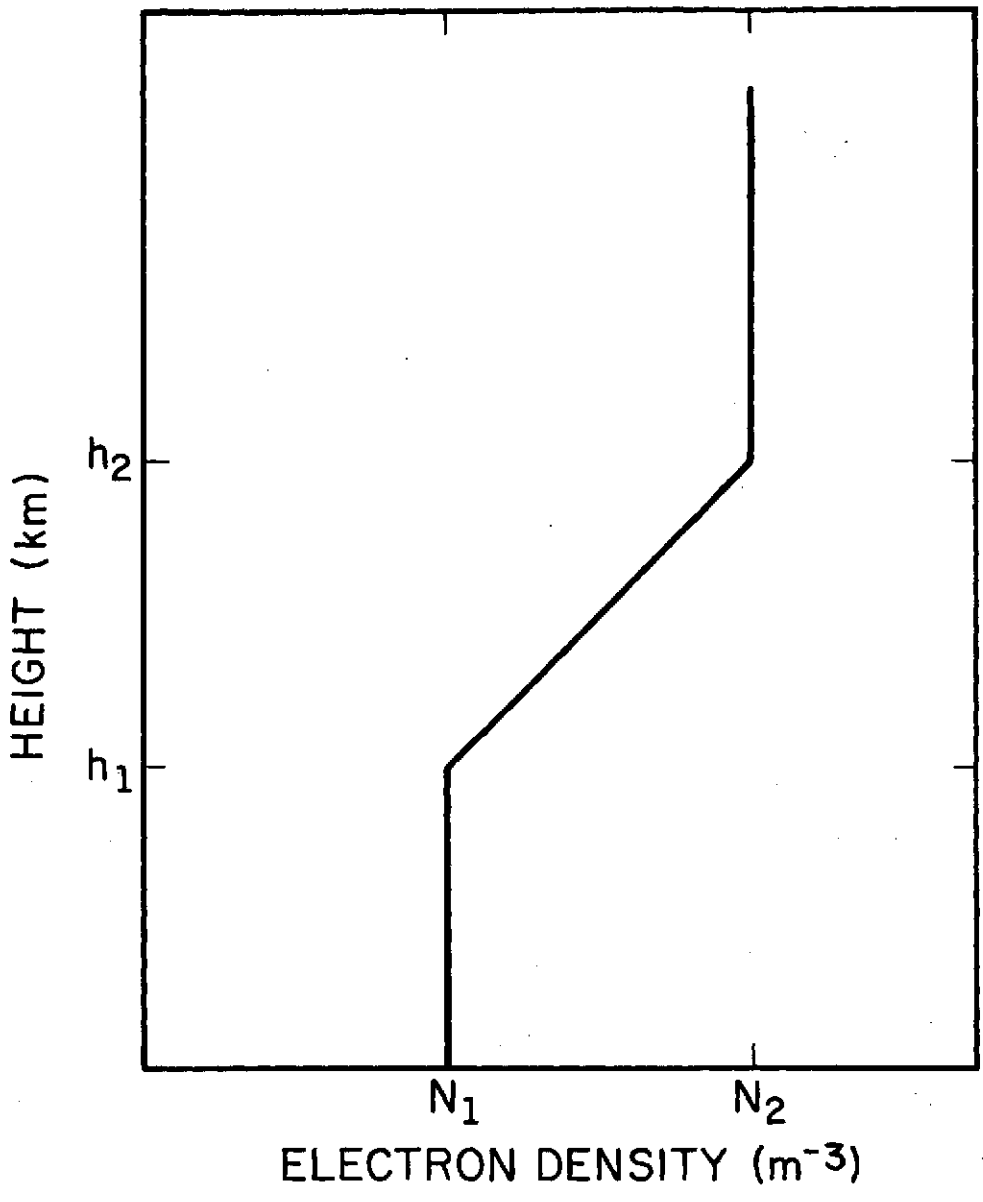

Figure 4.14 Model of reflector used on the calculations Section 4.2.1.

indices o and x referring to the ordinary and extraordinary modes of propagation, respectively.

2) If $h \geq h_2$

A plane wave solution:

$$E_{o3} = C_o \exp\{- k_0 i\, n_{2o}(h-h_2)\} \tag{4.17a}$$

$$H_{o3} = i\, n_{2o}\, C_o \exp\{i\, k_0 n_{2x}(h-h_2)\} \tag{4.17b}$$

$$E_{x3} = C_x \exp\{- i\, k_0 n_{2x}(h-h_2)\} \tag{4.18a}$$

$$H_{x3} = i\, n_{2x}\, C_x \exp i\, k_0 n_{2x}(h-h_2)\} \tag{4.18b}$$

where $n_{2o,x}$ is the refractive index for heights equal or above h_2, the indices o and x referring to the ordinary and extraordinary modes of propagation.

The solution to the wave equation in a medium with linear variation in electron density is given by *Budden* [1960], and will be extended below to include the *Sen-Wyller* [1960] expressions for the refractive index.

The refractive index of the medium for quasi-longitudinal approximation, is given by equation (1.3) that will be repeated below

$$n^2_{o,x} = 1 - \frac{\omega_o^2}{\omega\nu^2}(\omega \pm \omega_L)\, C_{3/2}\left(\frac{\omega \pm \omega_L}{\nu}\right) - i\,\frac{5}{2}\,\frac{\omega_o^2}{\nu}\, C_{5/2}\left(\frac{\omega \pm \omega_L}{\nu}\right) \tag{4.19}$$

The height dependence of the electron density can be expressed by

$$N = \beta(h - h_o)$$

β and h_o being constants. As a result $n^2_{o,x}$ can be written as

$$n^2_{o,x} = 1 - \gamma_{o,x}(h-h_o) \tag{4.20}$$

where

$$\gamma_{o,x} = \left[\frac{(\omega \pm \omega_L)}{\omega \nu^2} C_{3/2}\frac{\omega \pm \omega_L}{\nu} - i\,\frac{5}{2}\,\frac{1}{\nu}\,C_{5/2}\frac{\omega \pm \omega_L}{\nu}\right]\frac{e^2\beta}{\varepsilon_o m} \tag{4.21}$$

As a consequence the wave equation has the form

$$\frac{d^2 E_{o,x}}{dh^2} + k_o^2[1 - \gamma_{o,x}(h-h_o)] = 0 \tag{4.22}$$

Taking

$$\tau_{o,x} = (k_o^2\,\gamma_{o,x})^{1/3}\,(h-h_o - 1/\gamma) \tag{4.23}$$

and substituting equation (4.23) into equation (4.22) it results

$$\frac{d^2 E_{o,x}}{d\,\tau^2_{o,x}} = \tau_{o,x}\,E_{o,x} \tag{4.24}$$

Equation (4.24) is the Airy's equation whose solution $A_i(\tau_{o,x})$ and $B_i(\tau_{o,x})$ are discussed in *Budden* [1960].

Using the solution $A_i(\tau_{o,x})$ and $B_i(\tau_{o,x})$, the electric and magnetic fields can be written as

$$E_{o,x} = B1_{o,x}\,A_i(\tau_{o,x}) + B2_{o,x}\,B_i(\tau_{o,x}) \tag{4.25}$$

$$H_{o,x} = -1/k_o \{B1_{o,x} A_i'(\tau_{o,x}) + B2_{o,x} B_i'(\tau_{o,x})\}(k^2 \gamma_{o,x})^{1/3} \qquad (4.26)$$

Where

$$A_i'(\tau_{o,x}) = \frac{d A_i(\tau_{o,x})}{d \tau_{o,x}} \quad \text{and} \quad B_i'(\tau_{o,x}) = \frac{d B_i(\tau_{o,x})}{d \tau_{o,x}}$$

Applying the boundary conditions at h_1 and h_2, using equations (4.15) to (4.18), (4.25) and (4.26) for the fields, the following expression is obtained

$$\frac{1 + R_{o,x}}{1 - R_{o,x}} = \frac{n_{1o,x}[\alpha_{o,x} A_i(\tau 1_{o,x}) + B_i(\tau 1_{o,x})]}{i(\frac{\gamma_{o,x}}{k_o})\{\alpha_{o,x} A_i'(\tau 1_{o,x}) + B_i'(\tau 1_{o,x})\}} \qquad (4.27)$$

where

$$\alpha_{o,x} = \frac{i(\frac{\gamma_{o,x}}{k_o})^{1/3}\{B_i'(\tau 2_{o,x}) - n_{2o,x} B_i(\tau 2_{o,x})\}}{n_{2o,x} A_i(\tau 2_{o,x}) - i(\frac{\gamma_{o,x}}{k_o})^{1/3} A_i'(\tau 2_{o,x})} \qquad (4.28)$$

$\tau_{1o,x}$ = value of $\tau_{o,x}$ at height h_1

$\tau_{2o,x}$ = value of $\tau_{o,x}$ at height h_2.

The reflection coefficients, R_o and R_x can be determined from equations (4.27) and (4.28).

Plots of $|R_o|$, $|R_x|$ and $|R_x/R_o|$ as a function of $h_2 - h_1$ are shown in Figures 4.15 and 4.16, for the case where the electron density changes from 2.5×10^9 m^{-3} to 3×10^9 m^{-3}, the collision frequency is 2.15×10^5 s^{-1}, the frequency is of 2.66 Mhz, and the distance $h_2 - h_1$ changes from zero to 150 m. If the electron density changes from 6×10^8 m^{-3} to 7×10^9 m^{-3} over a distance of 2 km, values typical of rocket profiles near 80 km, for the same frequency and collision frequency as above, the results are $R_o = -3.7 \times 10^{-6} + i\ 3.9 \times 10^{-6}$ and $R_x = -2.4 \times 10^{-4} - i\ 1.8 \times 10^{-4}$.

The results show that reflections produced by gradients in electron density are of the same order of magnitude of measured partial reflections. Resonances are observed, for distances close to a multiple of half wavelengths. The situation is the same as in a transmission line with characteristic impedance changing as a function of length. The difference between the wavelengths of the ordinary and extraordinary modes produces minimums and maximums in $|R_x/R_o|$. If enough number of samples are taken, minimums and maximums tend to cancel, and the average $|R_x/R_o|$ will be the same as if $h_2 - h_1 = 0$, that is, a sharp reflector as in *Belrose and Burke's* [1964] theory. The changes of the ratio $|R_x/R_o|$ as a function of the geometry of the irregularities show that in partial-reflection measurements it is necessary to take the average value of A_o and A_x over all samples received, without rejecting samples with low signal-to-noise ratio or samples that reach the saturation of the receiver. If only a few percent of the samples reach the saturation of the receiver, even if the ordinary and the corresponding extraordinary samples are rejected, a bias can be introduced on the average A_o and A_x, producing errors in the calculated electron densities. Such a situation is exemplified in Figure 4.17. Figure 4.17a

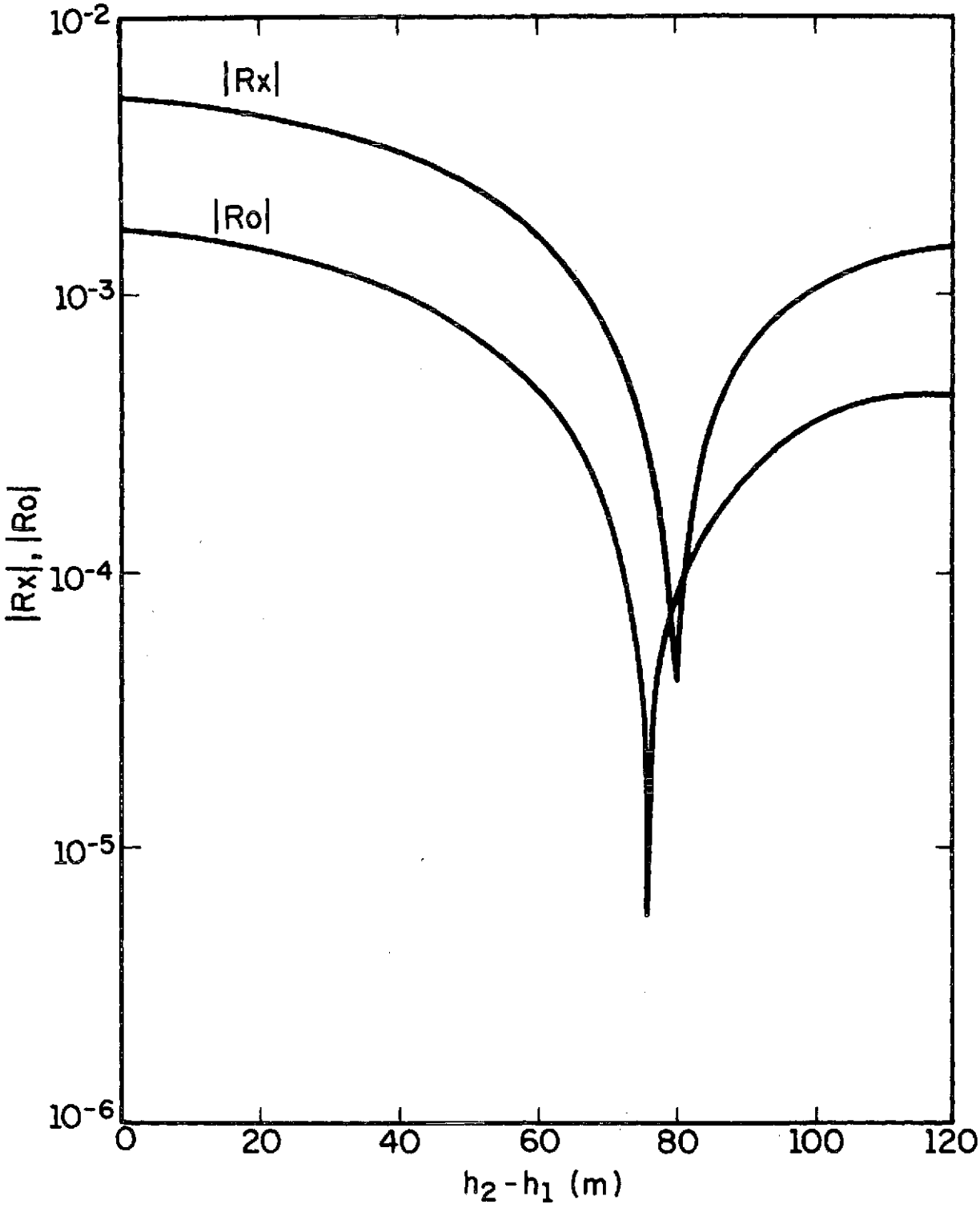

Figure 4.15 $|R_x|$ and $|R_o|$ as a function of the height interval h_2-h_1, for reflections produced by a gradient in electron density as shown in Figure 4.14, for a frequency of 2.66 MHz, an electron density changing from 2.5 x 10^9 m-3, and a collision frequency of 2.15 x 10^5 s^{-1}.

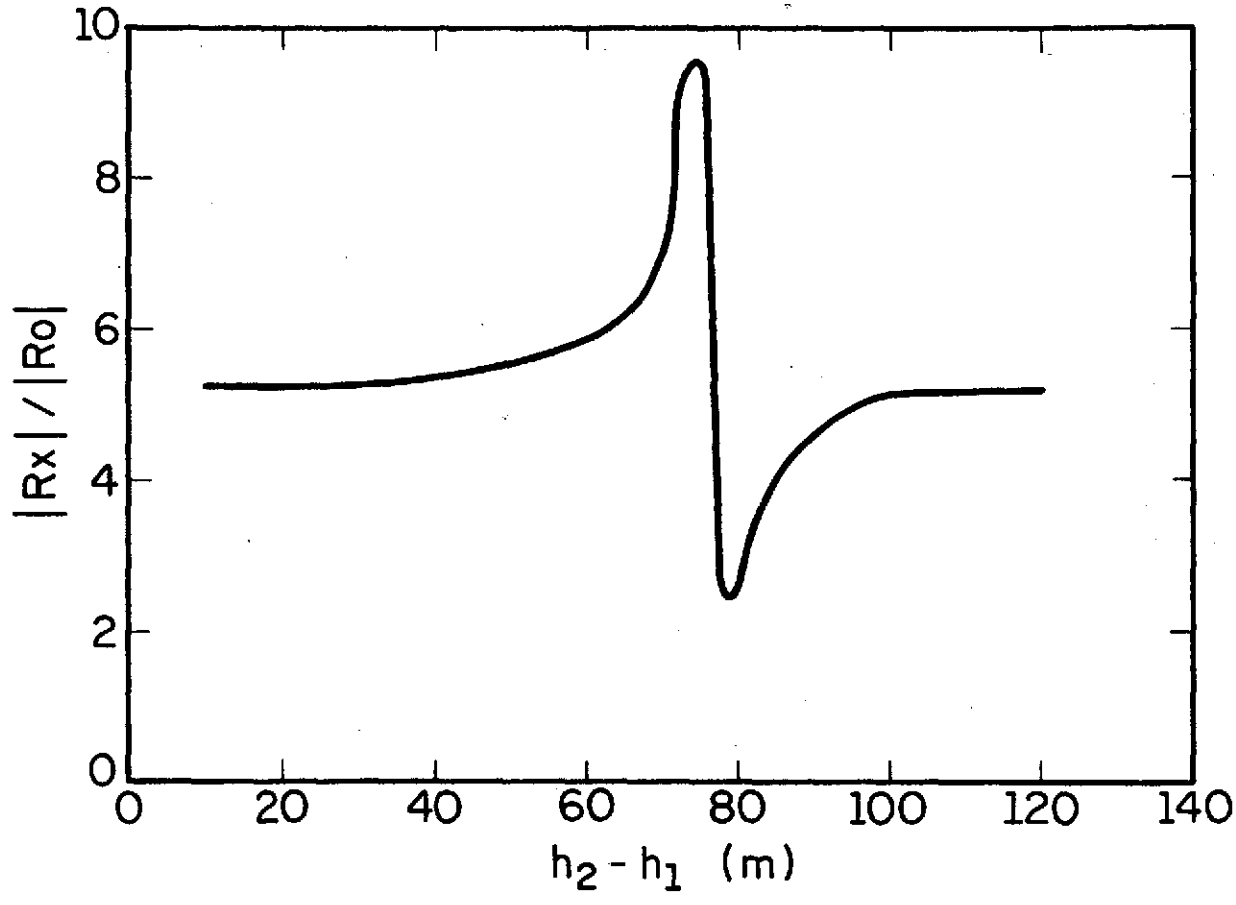

Figure 4.16 $|R_x/R_o|$ profile corresponding to the $|R_x|$ and $|R_o|$ profiles of Figure 4.15.

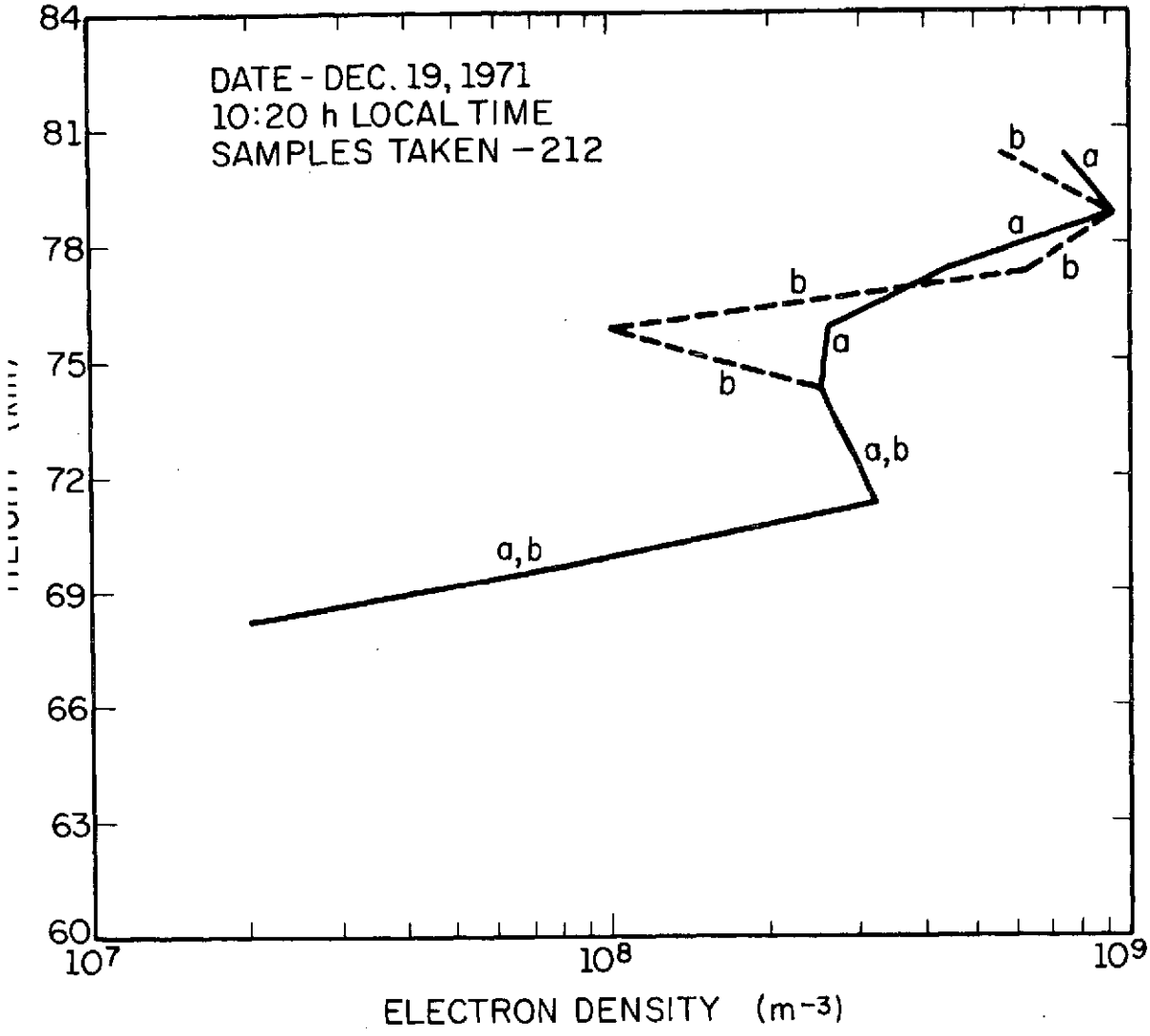

Figure 4.17 Electron densities calculated using all samples received (a) and rejecting all samples above 300 mV at the output of the receiver (b).

shows an electron-density profile obtained at Wallops Island, Virginia using all the samples received, with the receiver gain adjusted to avoid saturation of any sample. Figure 4.17b shows the electron-density profile calculated from the same data, but rejecting all samples that reached a value greater than 300 mV at the output of the receiver, in a simulation of a receiver with a saturation level of 300 mV. In the processing of the data, if one ordinary sample was rejected because of excessive amplitude, the corresponding extraordinary sample was also rejected, to avoid an additional bias on averaging the data. The number of samples rejected at each height is shown on Table 4.1. As it is observed the rejection of some samples can introduce serious errors on the calculated electron density.

At 76.5 km, for example, only one sample was rejected. The electron density between 75 and 76.5 km, however, changed from 2.55×10^8 m^{-3} to 10^8 m^{-3}. At 81 km, 9 samples were rejected. The electron density between 79.5 and 81 km changed from 7.5×10^8 m^{-3} to 5.7×10^8 m^{-3}.

Reflections produced by gradients in electron density could explain some of the preferred heights of reflection observed in partial-reflection measurements by some experimenters [*Gregory*, 1961].

Preferred heights of reflection have been confirmed on the Urbana measurements, as seen in the histograms of occurrence of maxima in the A_o profiles shown in Figures 4.18 and 4.19, and that correspond to the electron-density profiles of Figures 4.1 and 4.3. It is observed that heights of occurrence of a maximum of reflections in the histograms are associated to valleys on the electron-density profiles. Such association is one more indication that the valleys are not real, but produced by variations in the scattering cross section with height.

TABLE 4.1

Number of samples rejected at each height, in the calculation of the electron-density profile of Figure 4.17b.

HEIGHT (km)	NUMBER OF SAMPLES REJECTED
67.5	1
69.0	0
70.5	0
72.0	0
73.5	0
75.0	0
76.5	1
78.0	0
79.5	0
81.0	9

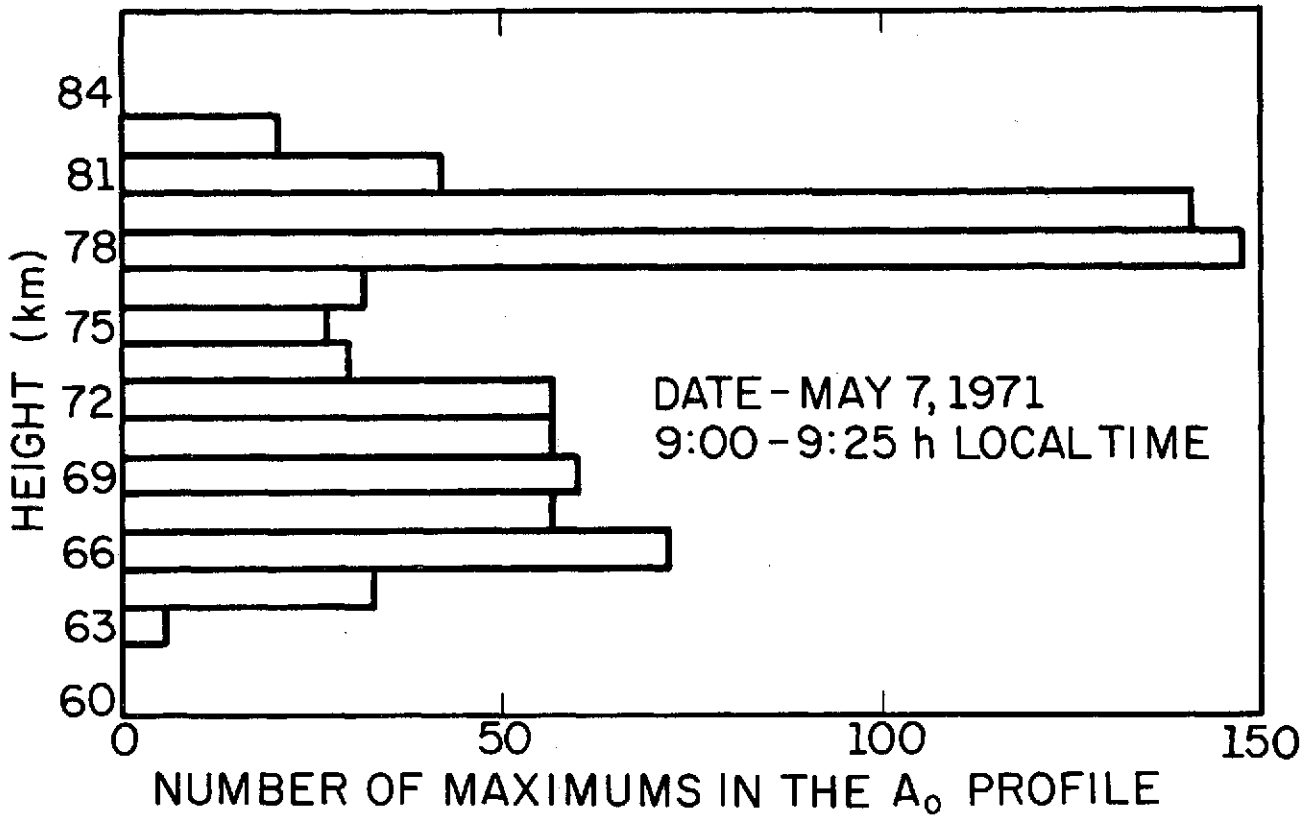

Figure 4.18 Histogram of occurrence of maximums in the A_o profiles for the data used in the calculation of the electron density profiles of Figure 4.1. It is observed that the valleys in electron density of Figure 4.1, near 71 and 80 km, correspond to an increase in the number of maximums in A_o at the same heights.

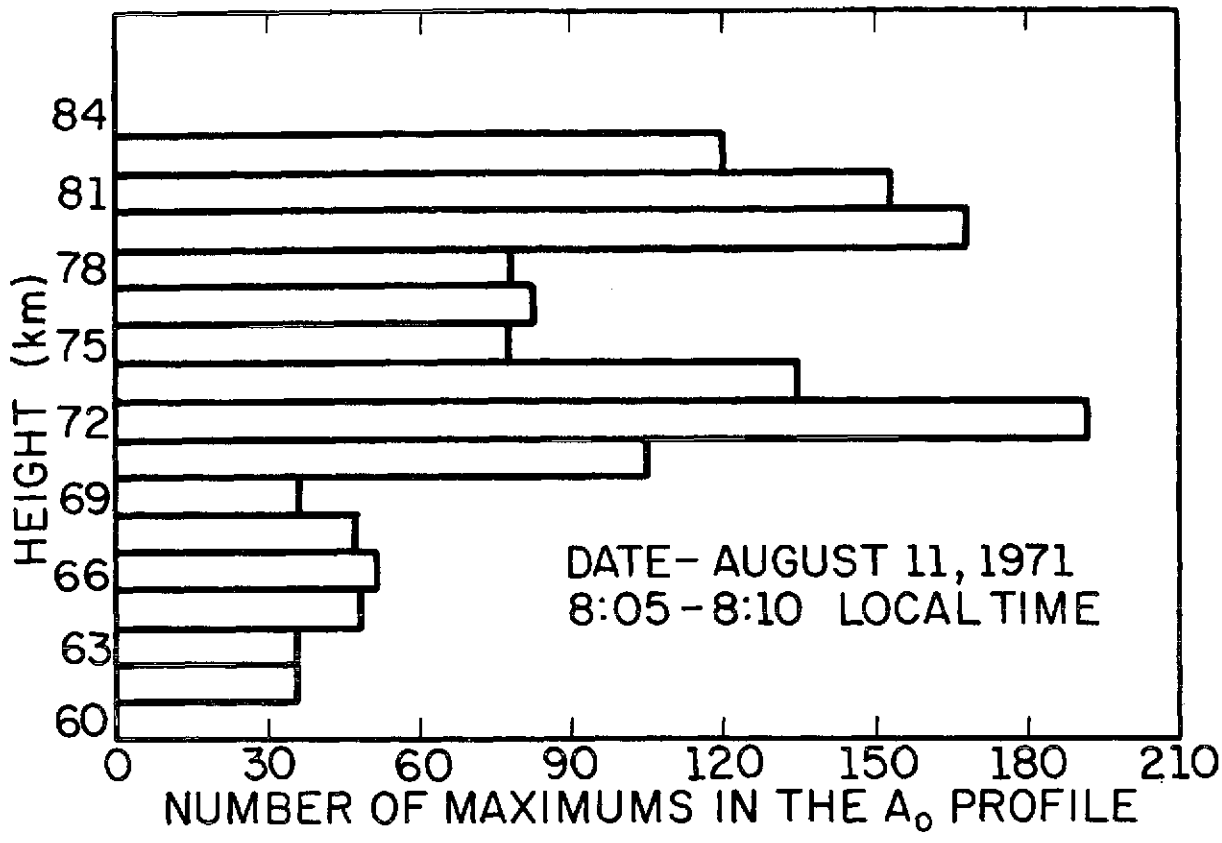

Figure 4.19 Histogram of occurrence of maximums in the A_o profiles, for the data used in the calculation of the electron-density profile of Figure 4.3. Valleys in the electron-density profile of Figure 4.3, near 80 km corresponds to an increase in the number of maximums in A_o at the same height.

4.2.2 *Reflections produced by gradients in electron density: - an approximate solution.* The full wave solution presented in Section 4.2.1 is possible only for particular geometries of the electron-density profile. As partial reflections are very weak, however, a first order approximation can be applied to the determination of the reflection coefficients, and results obtained for an arbitrary geometry. The solution of the problem is presented by *Collin* [1966] for the case of an isotropic medium, and can be extended to a horizontally stratified magnetoionic medium, for quasi-longitudinal propagation, as will be shown below.

The electron-density profile can be approximated by infinitesimal steps dN over distances dh, as shown in Figure 4.20.

Each discontinuity dN will produce a reflection coefficient given by

$$dR_{o,x} = \frac{dn_{o,x}}{2n_{o,x}} \tag{4.29}$$

If second order reflections are not considered, the total reflection coefficient is given by:

$$R_{o,x} = \frac{1}{2}\int_0^L e^{-2ik_o n_{o,x} h} \frac{d}{dh}(\ln n_{o,x})dh \tag{4.30}$$

where L is the length of the reflector.

If the height dependence of $n_{o,x}$ is known, $R_{o,x}$ can be readily evaluated from integration of equation (4.30).

As examples, the reflection coefficient will be calculated for three different geometries. The indices o and x will be dropped from the equations, and the results can be applied to the ordinary or extraordinary

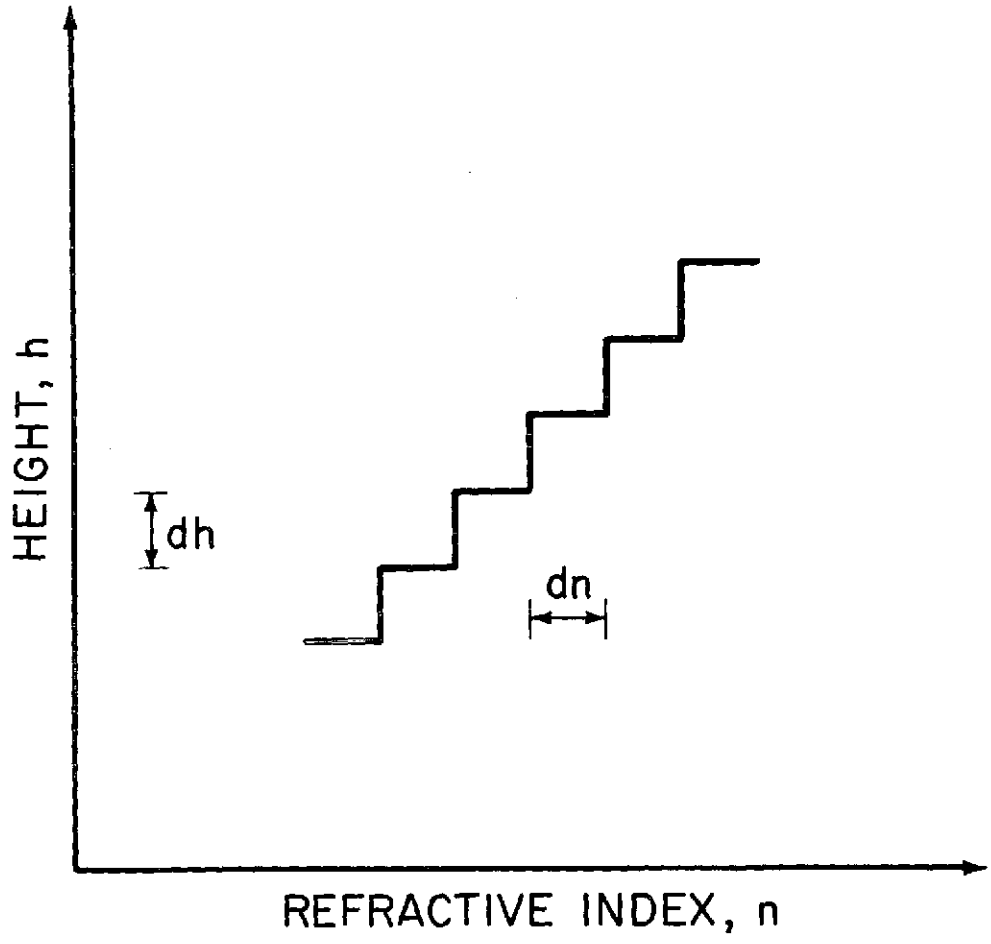

Figure 4.20 Approximation of the electron-density profile by infinitesimal changes dN over height interval dh, as used on the calculations of Section 4.2.2.

modes, depending on the expression used for the refractive index n.

1) The electron density is an exponential function of height between heights zero and h_1, and constant outside this range.

In this case the refractive index is given by:

$$n = n_0 \exp\left\{\frac{\ln(n_1/n_0)}{h_1}\, h\right\} \tag{4.31}$$

where n_0 and n_1 are the refractive indices at heights zero and h_1, respectively. Substituting equation (4.31) into (4.30), it results:

$$R = \frac{1}{2} \exp(-in_0k_0h_1) \ln \frac{1}{0} \frac{\sin(k_0n_0h_1)}{k_0n_0h_1} \tag{4.32}$$

where n was assumed as a constant equal to n_0 in the exponential factor, in performing the integration of equation (4.30).

A normalized plot of $|R|$ as a function of the height interval h_1 is shown in Figure 4.21. The results are similar to that obtained on item 3.2.1.

2) The refractive index has the following height dependence:

$$n = n_0 \exp 2\left[\left(\frac{h}{h_1}\right) \ln\left(\frac{n_1}{n_0}\right)\right], \quad 0 \leq h \leq \frac{h_1}{2} \tag{4.33a}$$

$$n = n_0 \exp\left\{\left[\frac{4h}{h_1} - \frac{2h^2}{h_1^2} - 1\right] \ln\left(\frac{n_1}{n_0}\right)\right\}, \quad \frac{h_1}{2} \leq h \leq h_1 \tag{4.33b}$$

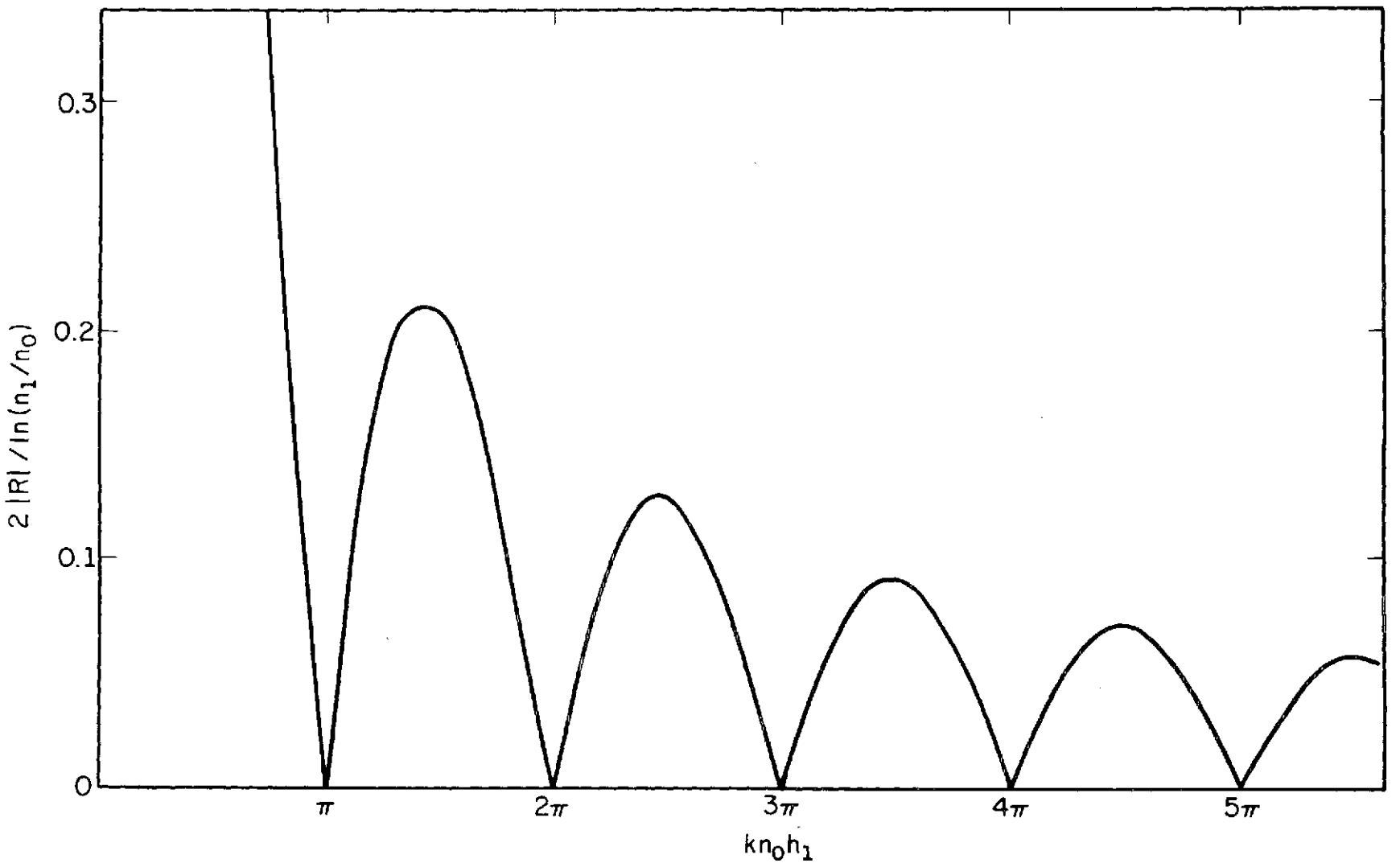

Figure 4.21 Normalized plot of reflection coefficient, a function of the length of the reflector, for the case where the refractive index is given by $n = n_0 \exp\left[\frac{\ln(n_1/n_0)}{h_1} h\right]$.

Substituting equations (4.33a) and (4.33b) into equation (4.30), and performing a straightforward integration it results:

$$R = \frac{1}{2} \exp(-in_0 k_0 h_1) \ln\left(\frac{n_1}{n_0}\right) \left[\frac{\sin(n_0 k_0 h_1)}{n_0 k_0 h_1}\right]^2 \tag{4.34}$$

A normalized plot of $|R|$ as a function of the height interval h_1 is shown in Figure 4.22.

Observation of Figures 4.21 and 4.22 shows that the rate of change of $|R|$ as a function of the height interval h_1 depends on the geometry of the irregularity. As a consequence the variations of $|R_x/R_o|$ as a function of h_1 will also depend on this geometry.

3) The refractive index changes between heights zero and π/γ as a function:

$$n = n_A \exp[\alpha \cos(\gamma h)] \tag{4.35}$$

and is constant outside this height interval. This profile is characterized by having no discontinuity in the refractive index or in the first derivative of the refractive index with height.

If equation (4.34) is substituted into equation (4.30) one gets:

$$R = \frac{\alpha \exp\left[\frac{-ik_0 n_0 \pi}{\gamma}\right]}{\left(\frac{2k_0 n_0}{\gamma}\right)^2 - 1} \cos\left(\frac{k_0 n_0 \pi}{\gamma}\right) \tag{4.36}$$

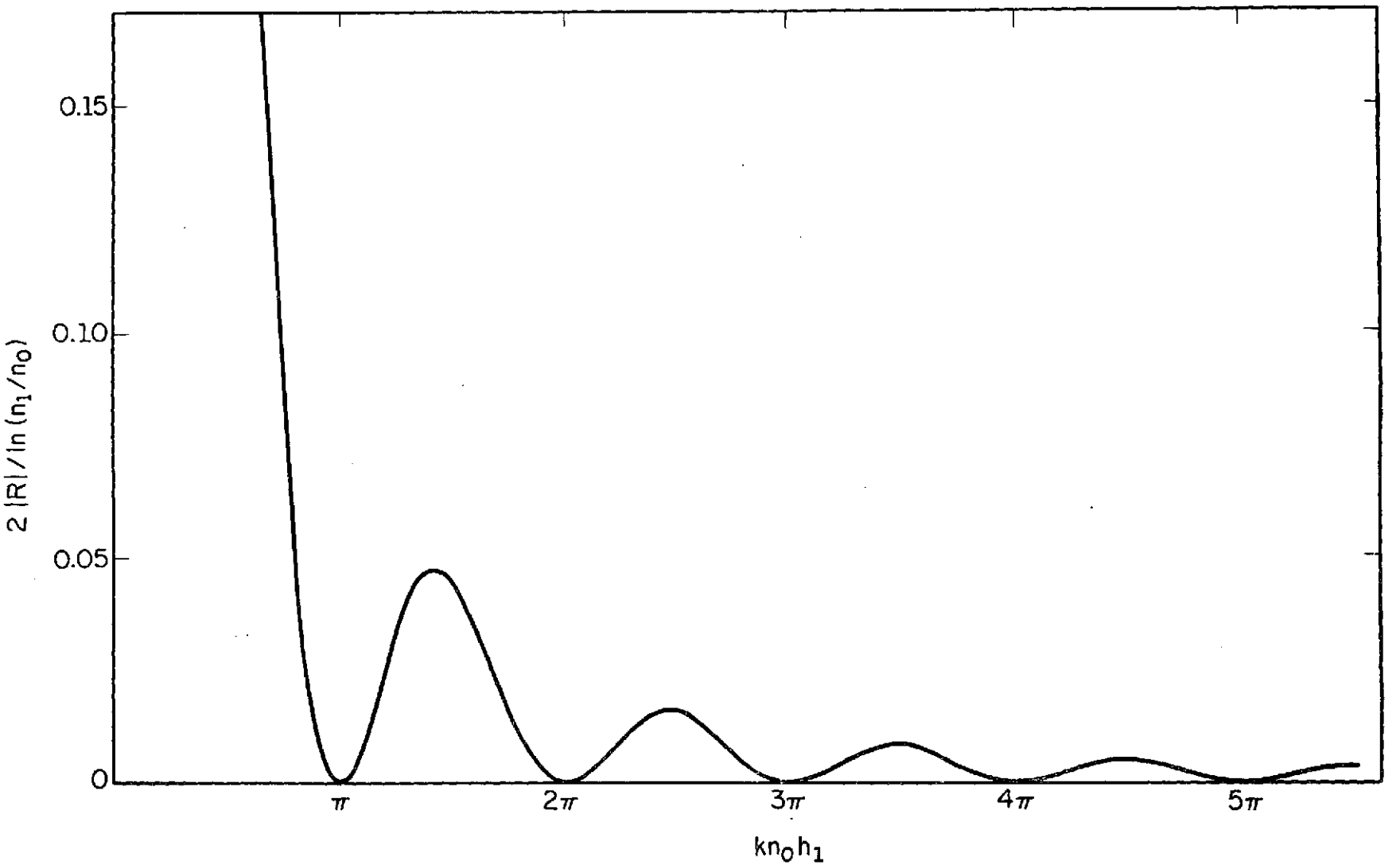

Figure 4.22 Normalized plot of the reflection coefficient as a function of the length of the reflector, for the case where the refractive index is given by equation (4.33).

A normalized plot of R as a function of π/γ is shown in Figure 4.23. The results show that resonances appear even in the case where no discontinuity in the refractive index or in the first derivative of the refractive index are observed.

In all the three cases shown above the amplitude of the reflection coefficient is proportional to $\ln(n_1/n_0)$, n_1 and n_0 being the refractive indices at the bottom and at the top of the irregularity, respectively.

Rocket electron-density profiles near 65 km show electron-density gradients where $\ln(n_1/n_0)$ is of approximately one order of magnitude below $\ln(n_1/n_0)$ observed near 80 km. Partial reflections at 65 km are one order of magnitude below partial reflectors near 80 km.

Such reflections, in this case, can also be explained by gradients in electron density.

Belrose and Burke [1964] considered the electron-density profiles as proportional to the A_o profiles at low altitude, assuming that the reflection coefficient is proportional to the electron density. It should be noted, however, that the A_o profile is the result of integration of reflections over a height range equal to one-half of the pulse width, and is not proportional to the scattering cross-section profile, being a function of the pulse width. Even if the reflection coefficient is proportional to the electron density, the gradient of electron density with height should be sharper than the corresponding gradient in the A_o profile.

4.3 *Scattering from Random Irregularities in a Locally Homogeneous Background Medium*

Contributions to partial reflections of reflections produced by random irregularities in electron density near 80 km altitude will be discussed in

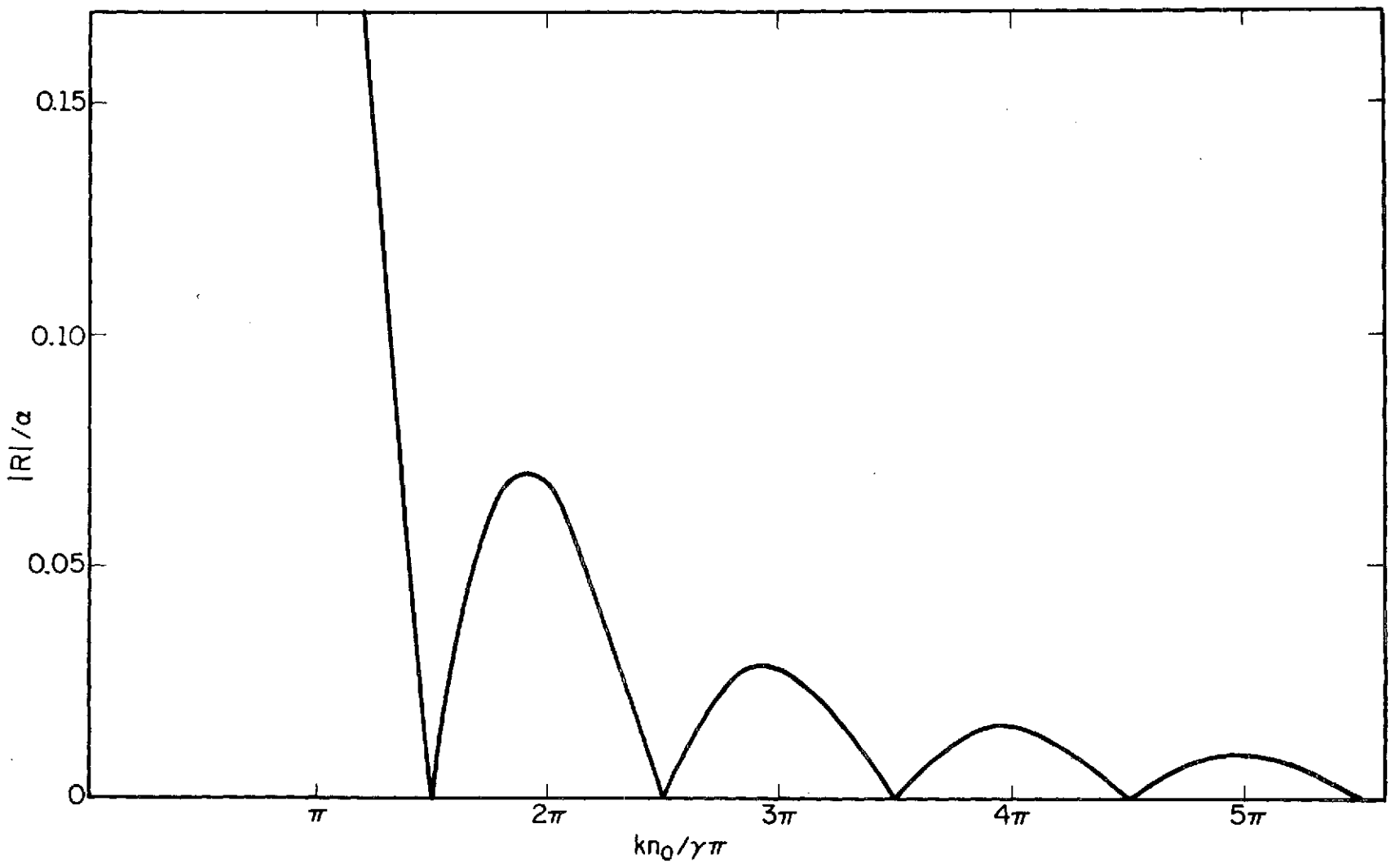

Figure 4.23 Normalized plot of the reflection coefficient as a function of the length of the reflector, for the case where the refractive index is given by equation (4.35).

this section. The background medium is characterized by a sharp gradient in electron density, and so it departs considerably from a homogeneous medium. To analyze such reflections, the theory of scattering will be extended to the case of a locally homogeneous background medium. The method of analysis will be similar to that used by *Tatarski* [1961] and applied to partial reflections by *Flood* [1968].

4.3.1 *Scattering cross section of random irregularities in a locally homogeneous background medium.* The model of reflector to be considered is characterized by weak irregularities superposed to a horizontally stratified, slowly varying, background medium. The medium will be assumed initially as isotropic, and the scattering cross section will be determined.

The refractive index of the medium can be written as:

$n(h) = \overline{n}(h) + n_1(\vec{R})$, if $\vec{R}$ is inside a volume V

$n(h) = \overline{n}(0)$, for points outside a volume V

where $\overline{n}(h)$ is the average value of $n(h)$, and $n_1(\vec{R}) << \overline{n}(h)$, for points inside V, that will be assumed as having a lower boundary at the plane $h = 0$.

Taking a time variation given by the factor $\exp(-i\omega t)$ the Maxwell equations have the following form, in a medium without currents or charges:

$$\nabla \times \vec{E} = i\omega\mu\vec{H} \tag{4.37a}$$

$$\nabla \times \vec{H} = -i\omega\varepsilon_0 n^2 \vec{E} \tag{4.37b}$$

$$\nabla \cdot n\vec{E} = 0, \quad \text{or} \quad \vec{\nabla} \cdot \vec{E} = -2\vec{E} \cdot \nabla(\ln n) \tag{4.37c}$$

The wave equation can be written as

$$\nabla^2\vec{E} + k_0{}^2 n^2 \vec{E} + 2\,\nabla[\vec{E} \cdot \nabla(\ln n)] = 0 \tag{4.38}$$

If a series solution of the type $\vec{E} = \vec{E}_0 + \vec{E}_1 + \vec{E}_2 + \ldots$ is assumed, and a first order approximation used (Born's approximation) the electric field is given by

$$\vec{E} = \vec{E}_0 + \vec{E}_1 \tag{4.39}$$

Substituting equation (4.39) into equation (4.38) and collecting terms of the same order of magnitude it results:

$$\nabla^2\vec{E}_0 + k_0^2\, \bar{n}(h)^2\, \vec{E}_0 = 0 \tag{4.40a}$$

$$\nabla^2\vec{E}_1 + k_0^2\, \bar{n}(h)^2\, \vec{E}_1 = -2k_0^2\, \bar{n}(h) n_1(\vec{R}) - 2\nabla[\vec{E}_0 \cdot \nabla \ln(n(h))] \tag{4.40b}$$

Equation (4.40a) has the well-known W.K.B. solution

$$\vec{E}_0 = \vec{A}_0\, \bar{n}(h)^{-1/2} \exp\left\{ i\, k_0 \int_0^h \bar{n}(h)\,dh \right\} \tag{4.41}$$

Where the incident wave is assumed propagating vertically, and consequently the vector $\vec{A}$ is on the horizontal plane. It should be noted that the use of the WKB solution implies in not considering reflections produced by the background medium. Such reflections, however, were discussed in Section 4.2.

Substituting the value of $\vec{E}$ given by equation (4.41) into equation (4.40b) the following equation for the scattered field is obtained:

$$\nabla^2 \vec{E}_1 + k_0^2 \, \bar{n}(h)^2 \, \vec{E}_1 = - 2k_0^2 \bar{n}(h)^{1/2} \, n_1(\vec{R}) \, \exp\left\{ i \, k_0 \int_0^h \bar{n}(h) dh \right\}$$

$$- 2\nabla \left\{ \bar{n}(h)^{-1/2} \exp[i \, k_0 \int_0^h \bar{n}(h) dh] \, \vec{A}_0 \cdot \nabla \, [\ln(\bar{n}(h))] \right\} \qquad (4.42)$$

To solve equation (4.42) the Green's function will be determined. The Green's equation is given by:

$$\nabla^2 \, G(\vec{R},\vec{R}') + k_0^2 \, \bar{n}(h)^2 \, G(\vec{R},\vec{R}') = -4\pi\delta(\vec{R}-\vec{R}') \qquad (4.43)$$

The solution of equation (4.43) is given by *Liu* [1967] and has the following expression:

$$G(\vec{R},\vec{R}') = i\sqrt{\frac{k_0}{2\pi r \sin\theta_0}} \exp\left(\frac{-i\pi}{4}\right) \int_{\Gamma_2} \exp\left\{ i \, k_0 [r \sin\theta \sin\theta_0 - \omega(\theta)] \right\}$$

$$\cdot \quad \frac{\sqrt{\sin\theta} \cos\theta}{[q(h) \, q(h')]^{1/2}} \, d\theta \quad , \quad \text{for} \; -\infty < h < h' \qquad (4.44)$$

where $r = |\vec{R}-\vec{R}'|$, $q^2(h) = \bar{n}(h)^2 - \sin^2\theta$, θ_0 is shown in Figure 4.24, the path of integration Γ is shown in Figure 4.25, and

$$\omega(\theta) = \int_{h'}^{h} [\bar{n}^2(\tau) - \sin^2\theta]^{1/2} \, d\tau \qquad (4.45)$$

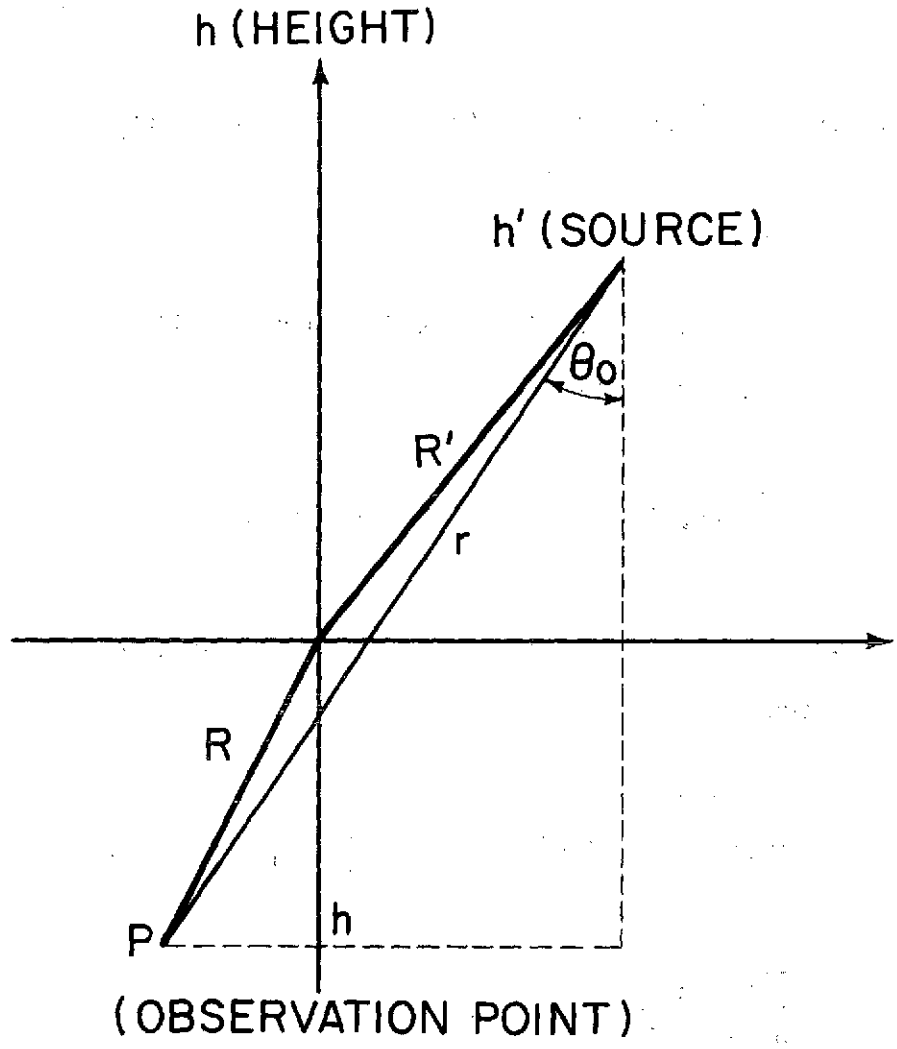

Figure 4.24 Geometry of the source and observation points used in the determination of Green's function, equation (4.46).

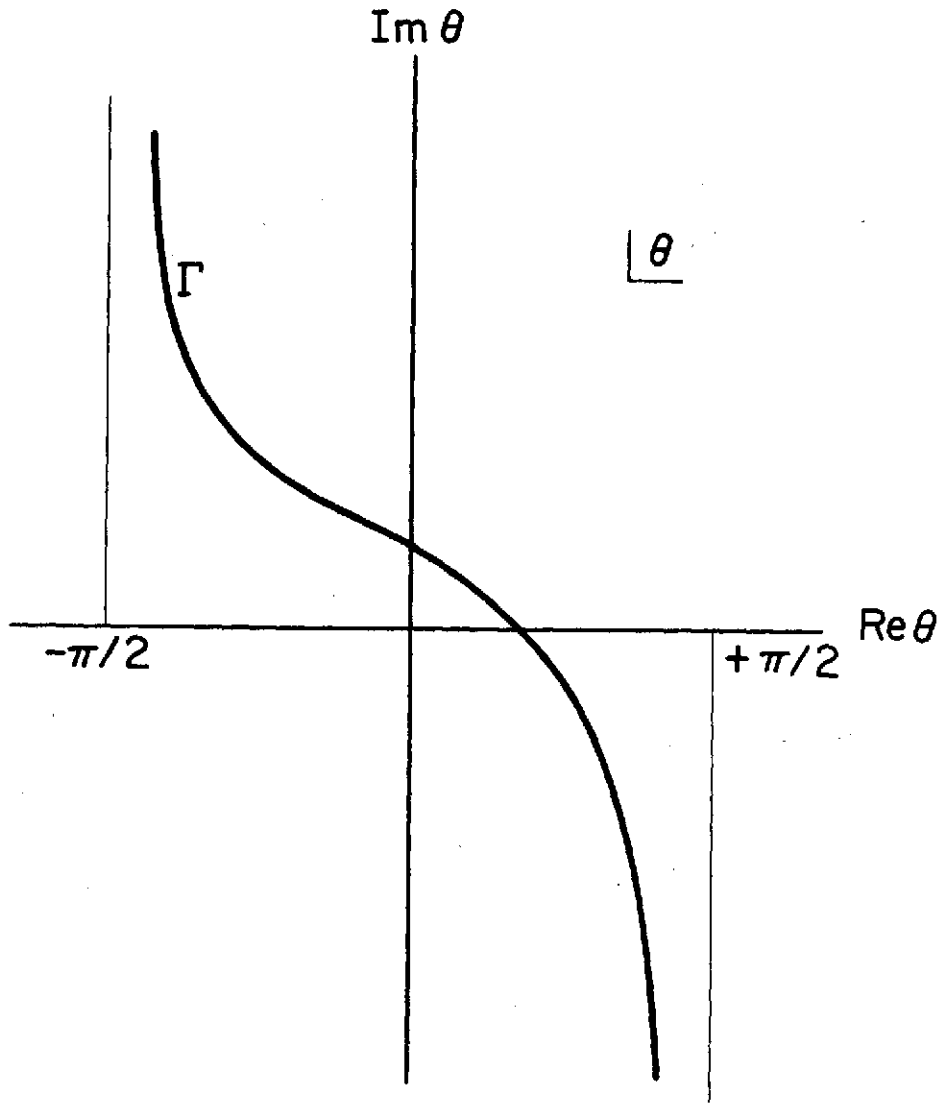

Figure 4.25 Path of integration, Γ, of the integral in equation (4.46).

Integration of equation (4.44) can be performed by the saddle-point method. The integral can be put in the form:

$$G(\vec{R},\vec{R}') = \int_{\Gamma_2} R(\theta)\, \exp[\gamma f(\theta)]\, d\theta \tag{4.46}$$

Where

$$F(\theta) = i\sqrt{\frac{k_0}{2\pi r\, \sin\theta_0}}\, \exp\left(\frac{-i\pi}{4}\right) \frac{\sqrt{\sin\theta}\, \cos\theta}{[q(h)\, q(h')]^{1/2}} \tag{4.47a}$$

$$\lambda = i\, k_0 r \tag{4.47b}$$

$$f(\theta) = \sin\theta\, \sin\theta_0 - \frac{\omega(\theta)}{r} \tag{4.47c}$$

The saddle point is given by:

$$\left.\frac{df(\theta)}{d\theta}\right|_{\theta=\theta_s} = f'(\theta_s) = 0 \tag{4.48}$$

Taking $\bar{n}(h) = \bar{n}(o) + \gamma(h)$, where $\gamma(h) \ll \bar{n}(o)$.

It results from equations (4.47c) and (4.50)

$$f'(\theta_s) = \cos\theta_s\, \sin\theta_0 - \frac{\sin\theta_s\, \cos\theta_s}{[\bar{n}(0)^2 - \sin^2\theta_s]^{1/2}} \cos\theta_0 + \frac{1}{2r} \int_h^{h'} \frac{\gamma \sin\theta_s\, \cos\theta_s\, dh}{[\bar{n}(0)^2 - \sin^2\theta_s]^{3/2}} = 0 \tag{4.49}$$

or, as $\gamma \ll 1$

$$\cos\theta_s \sin\theta_0 - \frac{\sin\theta_s \cos\theta_s}{[\bar{n}(0)^2 - \sin^2\theta_s]^{1/2}} \cos\theta_0 \cong 0 \tag{4.50}$$

Resulting

$$\sin\theta_s \cong \bar{n}(0) \sin\theta_0 \tag{4.51}$$

Performing the saddle-point integration it results

$$G(\vec{R},\vec{R}') = \frac{\bar{n}(0)}{r} \exp\{i\, k_0 \vec{r}\, \bar{n}(0)\} \exp\left\{i\, k_0 \int_0^{h'} [\bar{n}(h) - \bar{n}(0)]dh\right\} \tag{4.52}$$

Using the Green's function (4.52) the solution for the scattered field $\vec{E}_1$, in equation (4.41) is given by

$$\vec{E}_1 = \frac{-2k_0^2 \bar{n}(0) \exp(i\, k_0 \bar{n}(0) R)\vec{A}_0}{4\pi R} \int_V n_1(\vec{R}')\ \bar{n}(h')^{1/2} \exp\left\{i\, k_0 \int_0^{h'} \bar{n}(h)dh\right\} \cdot$$

$$\cdot \exp\{-i\, k_0 \bar{n}(0)\vec{m}\cdot\vec{R}'\} \exp\{i\, k_0 \int_0^{h'} [\bar{n}(h) - \bar{n}(0)]dh\}\, dV'$$

$$- \frac{\bar{n}(0) \exp(i\, k_0 \bar{n}(0) R)}{2\pi R} \int_{V'} \nabla\{\bar{n}(h')^{-1/2} \exp[i\, k_0 \int_0^{h'} \bar{n}(h)dh]\vec{A}_0 \cdot \nabla \ln(n_1(\vec{R}'))\}$$

$$\exp\{-i\, k_0 \vec{m}\cdot\vec{R}'\} \cdot \exp\{i\, k_0 \int_0^{h'} [\bar{n}(h) - \bar{n}(0)]dh\}dV' \tag{4.53}$$

where the following approximation was introduced:

$$\exp(i\, k_0\, r) = \exp(i\, k_0\, R) \exp(-i\, k_0\, \vec{m}\cdot\vec{R}') \tag{4.54}$$

$\vec{m}$ being a unit vector in the direction of $\vec{R}$.

The second term in the second member of equation (4.53), in a first order approximation, produces a component of the electric field in the direction of $\vec{r}$. Such longitudinal component is annulled by the longitudinal part of the first term of the second member of equation (4.53) and does not contribute to the scattered power. This statement is proven in Appendix I. As a result it can be written

$$\vec{E}_1 = \frac{-2k_0^2\ \bar{n}(0)\ \exp(i\ k_0\ \bar{n}(0)R)}{4\pi R}\ I \tag{4.55}$$

where

$$I = \int_{V'} n_1(\vec{R}')\ \bar{n}(h')^{1/2}\ \exp\{i\ k_0 \int_0^{h'} \bar{n}(h)dh\}\ \exp\{-i\ k_0 \bar{n}(0)\vec{m}\cdot\vec{R}'\}$$

$$\cdot\ \exp\{\ i k_0 \int_0^{h'} [\bar{n}(h)\ -\ \bar{n}(0)]dh\}\ dV' \tag{4.56}$$

The $\vec{H}_1$ field can be determined from (4.37a)

$$\vec{H}_1 = \frac{1}{i\omega\mu}\ \nabla\ x\ \vec{E}_1 \quad , \quad \text{or}$$

$$\vec{H}_1 = \frac{2k_0^2\ \bar{n}(0)}{i\pi 4\omega\mu}\ \nabla\ x\left\{\frac{\vec{A}_0}{R}\ \exp\{i\ k_0\ \bar{n}(0)R\}I\right\}$$

$$\cong \frac{2k_0^3\ \bar{n}(0)^2}{4\pi R\omega\mu}\ \exp\{i\ k_0\ \bar{n}(0)R\}\ I\cdot(\vec{m}\ x\ \vec{A}_0) \tag{4.57}$$

The Poynting vector is given by

$$\vec{S} = \frac{\vec{E}_1 \times \vec{H}_1^*}{2} = \frac{2k_0^5\,\bar{n}(0)^3}{(4\pi)^2\,\omega\mu R^2}\, I\, I^*\, [\vec{A}_0 \cdot \vec{A}_0 - (\vec{m}\cdot\vec{A}_0)]\vec{m} \tag{4.58}$$

and the flux of power density in the direction of $\vec{m}$ is given by

$$S_m = \vec{S} \cdot \vec{m} = \frac{2k_0^5\,\bar{n}(0)^3}{(4\pi)^2\,\omega\mu R^2} A_0^2 \sin^2\chi\, II^* \tag{4.59}$$

where χ is the angle between the direction of the incident field, $\vec{E}_o$, and the direction of observation, $\vec{r}$.

The average power density in the direction of $\vec{m}$ is given by

$$\bar{S}_m = \frac{2k_0^5\,\bar{n}(0)^3}{(4\pi)^2\,\omega\mu R^2} A_0^2 \sin^2\chi\, \overline{II^*} \tag{4.60}$$

where the bar means average.

For the scattering cross section, σ, defined by

$$\sigma = \frac{\text{Scattered power per unit solid angle, per unit volume}}{\text{Incident power per unit area}}$$

for following expression results

$$\sigma = \frac{4k_0^4\,\bar{n}(0)^3}{(4\pi)^2} \cdot \frac{\overline{II^*}}{V} \sin^2\chi \tag{4.61}$$

This product $\overline{II^*}$ is given by

$$\overline{II^*} = \int_{V_1}\int_{V_2} \bar{n}(h_1)^{1/2}\bar{n}^*(h_2)^{1/2}\,\overline{n_1(R_1)n_1^*(R_2)}\,\exp\{-i\,k_0\bar{n}(0)\vec{m}\cdot\vec{R}_1\}$$

$$\cdot\,\exp\{i\,k_0\bar{n}(0)h_1\}\,\exp\{2\,i\,k_0\int_0^{h_1}[\bar{n}(h_1)-\bar{n}(0)]dh_1\}\cdot\exp\{i\,k_0\bar{n}^*(0)\vec{m}\cdot\vec{R}_2\}$$

$$\cdot\,\exp\{-i\,k_0\bar{n}^*(0)h_2\}\exp\{-2i\,k_0\int_0^{h_2}[\bar{n}(h_2)-\bar{n}^*(0)]dh_2\}dV_1dV_2 \qquad (4.62)$$

$\overline{n_1(R_1)n_1^*(R_2)}$ can be identified as the correlation function of the refractive index, $B_n(\vec{R}_1,\vec{R}_2)$.

For a general medium equation (4.62) cannot be integrated, unless the analytical expression of $B_n(\vec{R}_1,\vec{R}_2)$ is known.

A slowly varying medium, however, can be assumed as a locally homogeneous random medium [*Tatarski*, 1961], and $B_n(\vec{R}_1,\vec{R}_2)$ can be written as

$$B_n(\vec{R}_1,\vec{R}_2) = \sigma^2\left(\frac{\vec{R}_1+\vec{R}_2}{2}\right)\,b_n(\vec{R}_1-\vec{R}_2) \qquad (4.63)$$

Substituting equation (4.63) into equation (4.62), and introducing the new coordinates

$$\vec{R}_S = \frac{\vec{R}_1+\vec{R}_2}{2} \qquad (4.64a)$$

$$\vec{R}_e = R_1 - R_2 \tag{4.64b}$$

It results

$$\overline{II^*} = \int_{V_S}\int_{V_e} \bar{n}(h_S+\frac{h_e}{2})^{1/2}\ \bar{n}^*(h_S-\frac{h_e}{2})^{1/2}\ \sigma^2(R_S)\ \exp\{i\ k_0\vec{b}\cdot\vec{R}_e[Re(\bar{n}(0))]\}$$

$$\exp\{-2k_0[Im(\bar{n}(0))]\vec{b}\cdot\vec{R}_S\}\exp\{2ik_0\int_0^{h_S+h_e/2}[\bar{n}(h) - \bar{n}(0)]dh\}$$

$$\cdot\ \exp\{-2ik_0\int_0^{h_S-h_e/2}[\bar{n}^*(h) - \bar{n}^*(0)]dh\}\ \exp\{i\ k_0[Re(\bar{n}(0))]h_e$$

$$\cdot\ \exp\{2k[Im(\bar{n}(0))]h_S\}\cdot b_n(R_e)dV_S\ dV_e \tag{4.65}$$

where $k_0\vec{b} = (\vec{k}_0 - k_0\vec{m})$, *Re* and *Im* mean real and imaginary parts, respecitvely. For a homogeneous random medium without losses, $\bar{n}(h)$ is real and constant, and $\overline{II^*}$ reduces to

$$\overline{II^*} = \bar{n}\int_{V_S}\int_{V_e} b_n(R_e)\ \exp\{i\ k_0\vec{b}\ \cdot\ \vec{R}_e\ \bar{n}(0)\}\ dV_S\ dV_e$$

$$\cong \bar{n}\ V\ \Phi_n(\vec{k}_0\bar{n} - k\ \bar{n}\ \vec{m}) \tag{4.66}$$

where $\Phi_n(\vec{k}_0\bar{n} - k_0\bar{n}\ \vec{m})$ is the spectral density of power.

In this case the scattering cross section reduces to the well-known expression:

$$\sigma = \frac{4k_0^4\ n^{-4}}{(4\pi)^2}\ \sin^2\chi\ \ \Phi_n\ (\vec{k}_0\bar{n} - k_0\bar{n}\ \vec{m}) \tag{4.67}$$

If the background medium is not homogeneous, equation (4.65) can be solved if $n(h)$ is known. Assuming a linear variation with height:

$$\bar{n}(h) = 1 - \alpha(h - h_0) \quad , \quad h \geq 0 \tag{4.68a}$$

$$\bar{n}(h) = 1 + \alpha h_0 \quad , \quad h \leq 0 \tag{4.68b}$$

it results

$$\overline{II^*} = \int_{V_S} \sigma^2(R_S) \exp 2k_0(Im\alpha)\ (h_S^2 - \vec{b} \cdot \vec{R}_S\, h_0)\} \cdot$$

$$\cdot \int_{V_e} \bar{n}(h_S + \frac{h_e}{2})^{1/2}\ \bar{n}^*(h_S - \frac{h_e}{2})^{1/2}\ b_n(R_e) \exp\{i\, k_0[\vec{b}\cdot\vec{R}_e\ Re(\bar{n}(0))]$$

$$- 2(Re\alpha)h_e h_S]\} \exp\{(Im\alpha)\ \frac{h_e^2}{2}\} dV_e\ dV_S \tag{4.69}$$

The factors $\bar{n}(\frac{h_e}{2} + h_s)^{1/2}$, $\bar{n}^*(h_s - \frac{h_e}{2})^{1/2}$ and $\{\exp\ (Im\alpha)\frac{h_e^2}{2}\}$ can be considered as a constant in the integration in V_e, since $b_n(R_e)$ goes to zero very rapidly. Recognizing $\int_V \exp\{i\vec{k}_0\vec{R}\} b_n(R) dV = \Phi_{\omega o}(\vec{k}_0)$ the power spectrum of $n_1(R)$, it results:

$$\overline{II^*} = \int_{V_S} \sigma^2(R_S)\ \exp\{2k_0(Im\alpha)\,(h_S^2 - \vec{b}\cdot\vec{R}_S\, h_0)\}\ \bar{n}(h_S)^{1/2} \cdot \bar{n}^*(h_S)^{1/2} \tag{4.70}$$

$$\Phi_{\omega 0}\{k_0[Re\ \bar{n}(0)]b_x, k_0[Re\ \bar{n}(0)]b_y,\ k_0[Re\ \bar{n}(0)]b_z - 2\ (Re\,\alpha)h_S]\}\, dV_s$$

For backscattering:

$$\overline{II^*} = \int_{V_S} \sigma^2(R_S)\ \exp\{4k_0 \int_0^{h_S} [Im\ \bar{n}(h)]dh\}\ \Phi_{\omega o}\{2k_0\ [Re\ \bar{n}(h_S)]\}$$

$$\cdot\ \bar{n}(h_S)^{1/2}\ \bar{n}^*(h_S)^{1/2} dV_S \tag{4.71}$$

and

$$\sigma = \frac{4k_0^4\ \bar{n}(0)^3}{16\pi^2} \cdot \frac{1}{V} \int_{V_S} \bar{n}(h_S)^{1/2}\ \bar{n}^*(h_S)^{1/2} \sigma^2(R_S)$$

$$\cdot\ \exp\{4k_0 \int_0^{h_S} [Im(\bar{n}(h))]dh\}\ \Phi_{\omega o}\{2k_0\ [Re\ \bar{n}(h)]\}\ dV_S \tag{4.72}$$

4.3.2 *Application to partial reflections.* For quasi-longitudinal propagation, for the ordinary and extraordinary modes of propagation,

$$\Phi_{\substack{\omega o \\ o,x}} = \frac{1}{4}\ [y_{o,x}^2\ C_{3/2}^2(y_{o,x}) + \frac{25}{4}\ C_{5/2}^2(y_{o,x})]\ \Phi_{\omega N} \tag{4.73}$$

Where $\Phi_{\omega N}$ is the power spectrum of the electron-density fluctuations, and $y_{o,x} = \dfrac{\omega \pm \omega_L}{\nu}$. From equation (4.72) and (4.73) it results for reflections produced by a pulse of width W, centered at a height h_o:

$$\sigma_{o,x} = \frac{k_0^4\ n(0)^4}{16\pi^2}\ [y_{o,x}^2\ C_{3/2}(y_{o,x}) + \frac{25}{4}\ C_{5/2}^2(y_{o,x})]\ \frac{1}{V} \int_V \exp\{4k_0 \int_{h_o-CW/4}^{h_o+CW/4} Im(\bar{n}_{o,x}(h))]dh\}$$

$$\Phi_{\omega N}\{2k_0\ [Re(\bar{n}_{o,x}(h))]\}dV \tag{4.74}$$

The signals A_o and A_x measured at ground are given by:

$$A_{o,x} = \sigma_{o,x} V \exp\{2 \int_0^{h_o - CW/4} k_0 [Im\ \bar{n}(h)]dh\} \tag{4.75}$$

The ratio $(A_x/A_o)^2$ is given by:

$$\left(\frac{A_x}{A_o}\right)^2 = \frac{\sigma_x}{\sigma_o} \exp\{2 \int_0^{h_o - CW/4} (K_x - K_o)dh\} \tag{4.76}$$

Where

$$K_{x,o} = k_0\{Im\ \bar{n}_{o,x}(h)]\} \tag{4.77}$$

Using the expression of $\sigma_{o,x}$ given by equation (4.74) it results:

$$\left(\frac{A_x}{A_o}\right)^2 = \frac{[y_x^2\ C_{3/2}^2(y_x) + \frac{25}{4}\ C_{5/2}^2(y_x)]}{[y_o^2\ C_{3/2}^2(y_o) + \frac{25}{4}\ C_{5/2}^2(y_o)]} \frac{\int_V \exp\{4 \int_{h_o - CW/4}^{h_o + CW/4} k_x dh\} \Phi_{\omega N}\{2k_0 [Re\bar{n}_x(h)]\}dV}{\int_V \exp\{4 \int_{h_o - CW/4}^{h_o + CW/4} k_o dh\} \Phi_{\omega N}\{2k_0 [Re\bar{n}_o(h)]\}dV}$$

$$\cdot \exp\{2 \int_0^{h_o - CW/4} (K_x - K_o)dh\} \tag{4.78}$$

If the background electron density does not change inside the volume V,

equation (4.78) reduces to:

$$\left(\frac{A_x}{A_o}\right)^2 = \frac{[y_x^2\, C_{3/2}^2(y_x) + \frac{25}{4}\, C_{5/2}^2(y_x)]}{[y_o^2\, C_{3/2}^2(y_o) + \frac{25}{4}\, C_{5/2}^2(y_o)]} \cdot \exp\{4 \int_{h_o-CW/4}^{h_o+CW/4} (K_x - K_o)dh\}$$

$$\cdot \exp\{2 \int_0^{h_o-CW/4} (K_x - K_o)dh\} \qquad (4.79)$$

That is identical to the results obtained by *Flood* [1968].

If the irregularities are uncorrelated, equation (4.78) takes the form

$$\left(\frac{A_x}{A_o}\right)^2 = \frac{[y_x^2\, C_{3/2}^2(y_x) + \frac{25}{4}\, C_{5/2}^2(y_x)]}{[y_o^2\, C_{3/2}^2(y_o) + \frac{25}{4}\, C_{5/2}^2(y_o)]} \quad \frac{\int_V \exp\{4 \int_{h_o-CW/4}^{h_o+CW/4} K_x\, dh\}\, dV}{\int_V \exp\{4 \int_{h_o-CW/4}^{h_o+CW/4} K_o\, dh\}\, dV}$$

$$\exp\{2 \int_0^{h_o+CW/4} (K_x - K_o)dh\} \qquad (4.80)$$

Such expression is similar to that developed by *Cohen* [1971].

As a numerical application, the ratios A_x/A_o were calculated at 78.5 and 81.5 km for a pulse of 20 μsec, a collision frequency of $7.7 \times 10^5\ s^{-1}$ and the electron-density profile shown in Figure 4.26. The following power spectrums were assumed: A Gaussian spectrum ($\Phi_{\omega N} = \exp(-a^2k^2/2)$, with a = 0, 50 and 70 m), and a power law spectrum ($\Phi_{\omega N} = k^{-n}$, n = 11/3 and 6).

With the values of A_x/A_o obtained, the electron density between 78.5 and 81.5 km was calculated using *Belrose and Burke's* [1964] theory. For

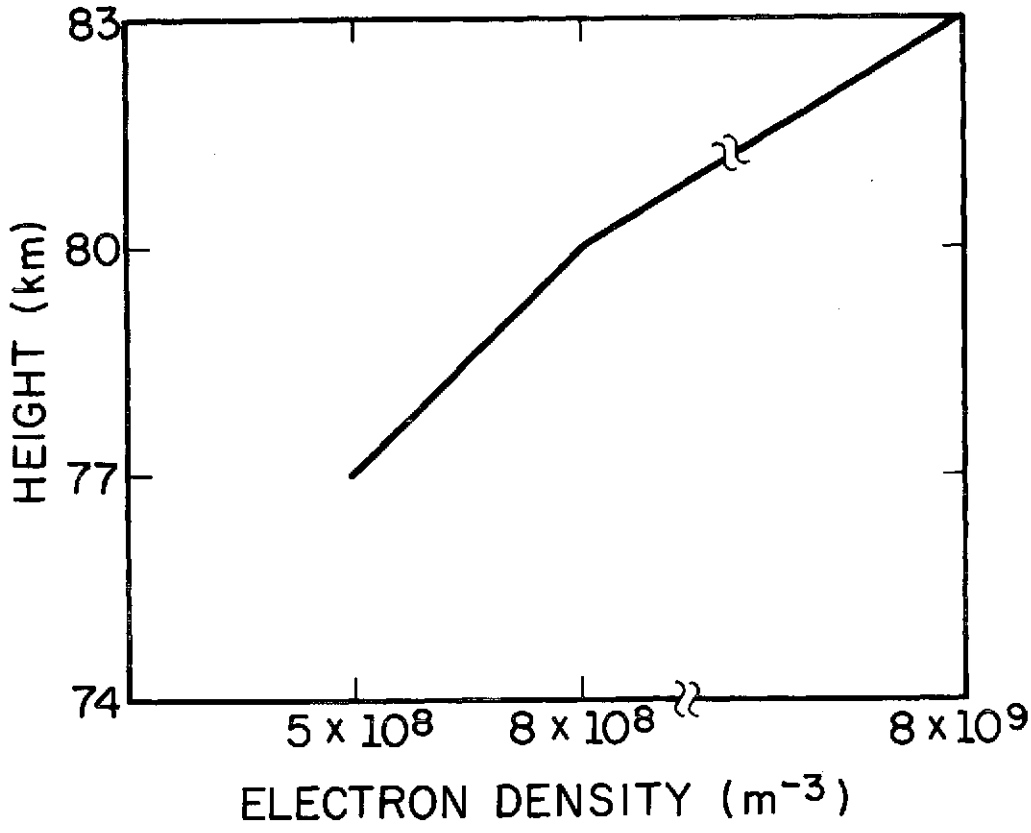

Figure 4.26 Electron-density profile used on the calculations of Section 4.3.

comparison, the electron density was calculated assuming the existence of sharp reflectors at 78.5 and 81.5 km, instead of a random medium. The results are shown in Table 4.2. They show that if the power spectrum is a Gaussian spectrum, with the parameter as great or equal to 50 m, a serious error can be produced in the calculation of electron densities using Belrose and Burke's theory. If the power spectrum is a power law spectrum, such error will be small.

4.3.3 *Electron-density fluctuations necessary to produce partial reflections.* An estimate of the fluctuations of electron density necessary to produce partial reflections of amplitude comparable to the observed reflections can be obtained from equation (4.67), for altitudes above 80 km, since for such heights the losses produce a small effect on the value of the scattering cross section for the ordinary mode, and in a first approximation, the background medium can be considered as homogeneous.

If the power spectrum is of the form

$$\Phi_n(\vec{k}) = 2(\pi)^{3/2} L^3 \cdot \exp(-\frac{\overline{n}^2}{2} k_0^2 L^2) \cdot \overline{n_1^2} \qquad (4.81)$$

it results from equations (4.67) and (4.81), for the scattering cross section of the ordinary mode:

$$\sigma_o = \frac{4k_0^4 \overline{n}_o^4}{(4\pi)^2} \cdot (2\pi)^{3/2} L^3 \exp(-\frac{\overline{n}_o^2}{2} k_0^2 L^2) \cdot \overline{n_{1o}^2} \qquad (4.82)$$

Where the angle χ in equation (4.67) was taken as 90° (back-scattering), and $\overline{n_{1o}^2}$ is given by:

TABLE 4.2

Electron-density calculations using *Belrose and Burke's* theory [1964], for reflections produced by sharp reflectors and by a random medium, for the electron-density profile of Figure 4.26, and a collision frequency of 7.7×10^5 sec^{-1}.

	Sharp Reflector =	Gaussian Spectrum a=0	Gaussian Spectrum a=50m	Gaussian Spectrum a=70m	Power Law Spectrum n=11/3	Power Law Spectrum n=6
$\ln[(A_x/A_o)_2]$ / $\ln[(A_x/A_o)_1]$		-0.683	-0.43	-0.05	-0.66	-0.65
Electron density at 80 km (m^{-3})	1.5×10^9	1.1×10^9	0.69×10^9	0.12×10^9	1.03×10^9	1.02×10^9

$$\overline{n_{1o}^2} \cong \frac{\overline{(\Delta x)^2}}{4(1+Y)^2} \tag{4.83}$$

where

$$\sqrt{\overline{(\Delta x)^2}} = \frac{N_1 e^2}{\varepsilon_o m\omega^2} \tag{4.84}$$

N_1 being the r.m.s. electron-density fluctuation.

If the transmitting antenna has a lobe with an angle θ, the transmitted pulse with W, and the irregularities are distributed over all the volume occupied by the pulse, the power back-scattered per unit angle solid per unit incident power density, from a height h is given approximately by

$$R_o^2 = \frac{V}{h^2}\sigma_o \cong \pi\left(\sin\frac{\theta}{2}\right)^2 \cdot \frac{WC}{2}\sigma_o \tag{4.85}$$

If R_o is known, the value of $\overline{N}_1$ can be determined from equations (4.82) and (4.85). A plot of $\overline{N}_1/R_o$ is shown in Figure 4.27, for a pulse of 50 μsec, and antenna lobe of 15°, a background electron density of 10^9 m^{-3}, a frequency of 2.66 MHz, and a gyrofrequency of 1.5 MHz.

As will be shown in Chapter 5, the reflection coefficient for the ordinary mode, near 80 km, is of the order of 10^{-5}, and the electron density of the order of 10^9 m^3. From Figure 4.27 we conclude that, if $L \leq 50$ m, fluctuations of electron density of the order of 0.1 percent will be enough to produce such reflections.

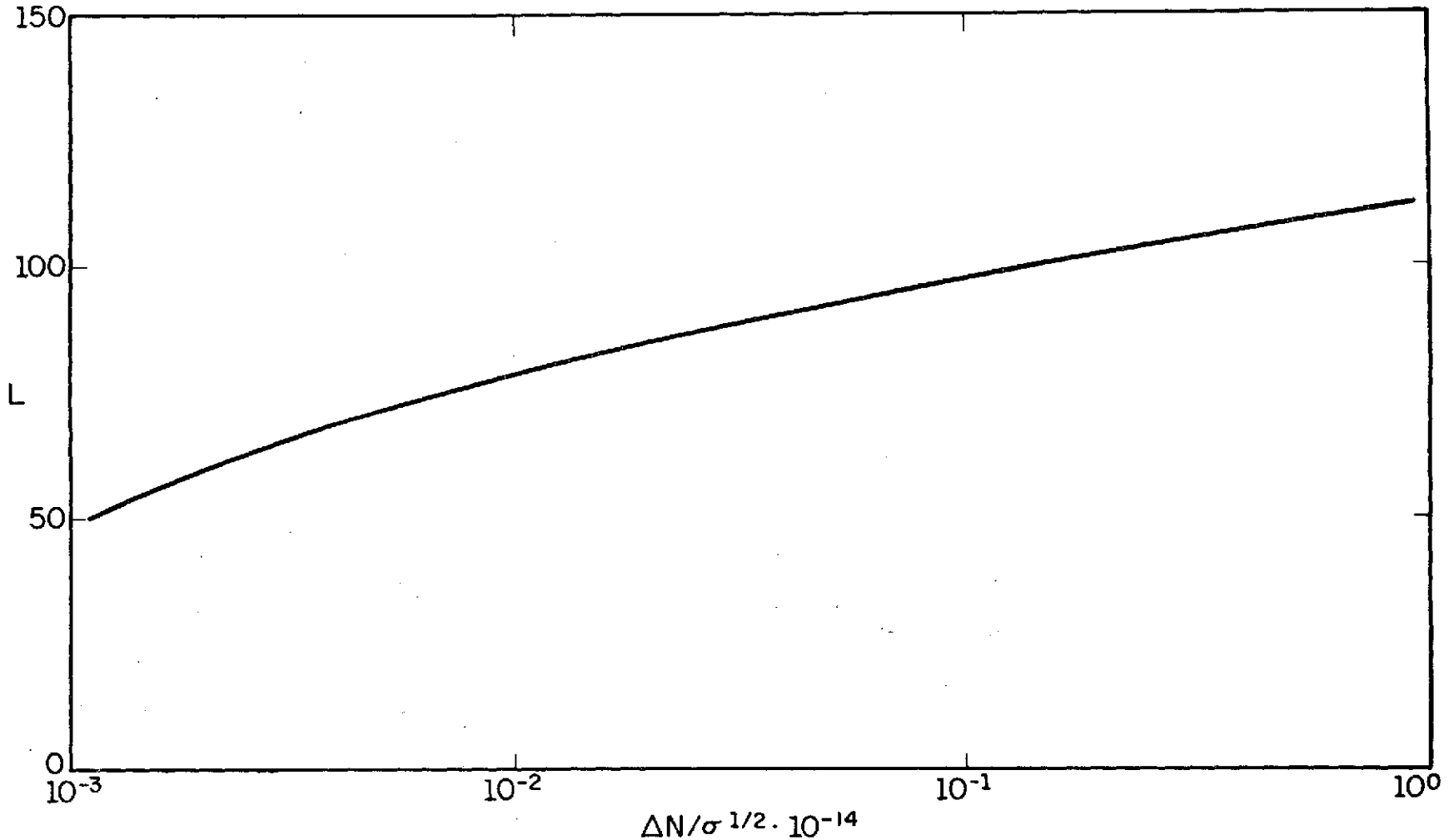

Figure 4.27 Normalized plot of fluctuation of electron density, for a power spectrum of the form $\Phi_n(\vec{k}) = (2\pi)^{3/2} L^3 \exp(-\frac{\bar{n}^2}{2} k_o^2 L^2) \overline{n_1^2}$, as a function of the parameter L.

4.4 *The Nature of the Irregularities*

The choice of the best model of reflector for partial reflections is impaired by the lack of knowledge of the real structure of the irregularities producing reflections. *Belrose and Burke* [1964] arrived at the conclusion that the reflections are produced by isolated reflections and not by a turbulent medium. Such conclusion was based on the fact that reflections produced by pulses of different width showed maximums at the same height, and more defined minimums for the narrower pulses, and that reflections produced by pulses with different frequencies (40 kHz apart) showed similar structures.

Further work, however, [*Belrose*, 1970] indicated that the reflection mechanism is probably produced by a combination of turbulent and isolated scatters. *Gregory* [1961] observed that the reflections are produced principally from the heights of 55, 61, 66, 74 and 86 km. *Von Biel et al.* [1970], based on the correlation coefficient between the ordinary and extraordinary reflections, suggested that the reflections are produced by small irregularities distributed over all the volume occupied by the pulse.

Fraser and Vincent [1970] studied the irregularities of the *D* region by measuring the phase variation of the received signals and the space and time correlations of the ground diffraction pattern. Sixty percent of all the 70-80 km and 20 percent of the 80-90 km reflections were coherent echoes. During the winter, reflections showing a pronounced stratification were observed near 85 km.

Manson et al. [1969] based on small irregularities in electron-density profiles published by *Mechtly and Smith* [1968] concluded that the

isolated irregularities of the rocket profiles are sufficient to explain the partial reflections. It should be noted, however, that the irregularities observed on rocket profiles are at least partially produced by the precession of the rocket, which changes the angle of attack of the current probe with the ionosphere, producing variations of current that are not really produced by irregularities. In the interpretation of the rocket data such irregularities cannot be taken into account.

Von Biel [1971], measuring the amplitude distribution of the received signals observed that below 80 km the echo amplitude distributions are predominantly Rayleigh-like in character, suggesting that they are produced by a turbulent medium.

Above 80 km the distribution approximates to a Rice distribution with the Rice parameter increasing with height, showing that above 80 km there is a contribution of coherent scattering. Such conclusion supports the theory that above 80 km the scatters are at least in part produced by gradients in electron density.

As can be concluded from the available information about the structure of the irregularities, that was summarized above, further work must be done on the subject.

4.5 *Electron-Density Calculations for a Region with Sharp Gradients in Electron Density*

In Sections 4.2 and 4.3 it was shown that the received signals $A_o(h)$ and $A_x(h)$, in some circumstances, do not represent the scattering cross section at the height h.

To overcome such a problem, at least two solutions can be tried:

1) To use only maximums of the a_o and a_x profiles in the calculation of the electron densities,

2) To deconvolute the average A_o and A_x profiles.

($a_{o,x}$ is the signal recieved from one sample, and $A_{o,x}$ the average of $a_{o,x}$.) Both solutions will be discussed below.

4.5.1 *Electron-density calculations using only maxima of the* a_o *and* a_x *profiles.* If a maximum on the a_o and a_x profiles at a height is considered as produced by a reflection from this height, and not the result of phase interference of waves reflected from different heights, the $A_{o,x}$ profiles obtained by averaging only the signals measured at such maximums will be representative of the scattering cross-section profile. A measurement made by this method, besides being based on the above assumption has the inconvenience that only a few maximums are observed on each received sample, they are not equally distributed over all heights, and as a consequence a great number of samples has to be taken to obtain a reasonable number of samples at each height. The sampling and processing time in this case becomes very large.

An electron-density profile obtained by the method above described, at the partial-reflection system of the University of Illinois is shown on Figure 4.28a. Table 4.3 shows the total number of samples and the number of maximums observed at each height. The electron-density profile obtained from the same samples, but averaging all the signals at 1.5 km of interval is shown in Figure 4.28b, for comparison.

The criteria used to consider a signal at a height h as a maximum was the following:

$$a_{o,x}(h) > a_{o,x}(h+1.5) \tag{4.86a}$$

$$a_{o,x}(h) > a_{o,x}(h-1.5) \tag{4.86b}$$

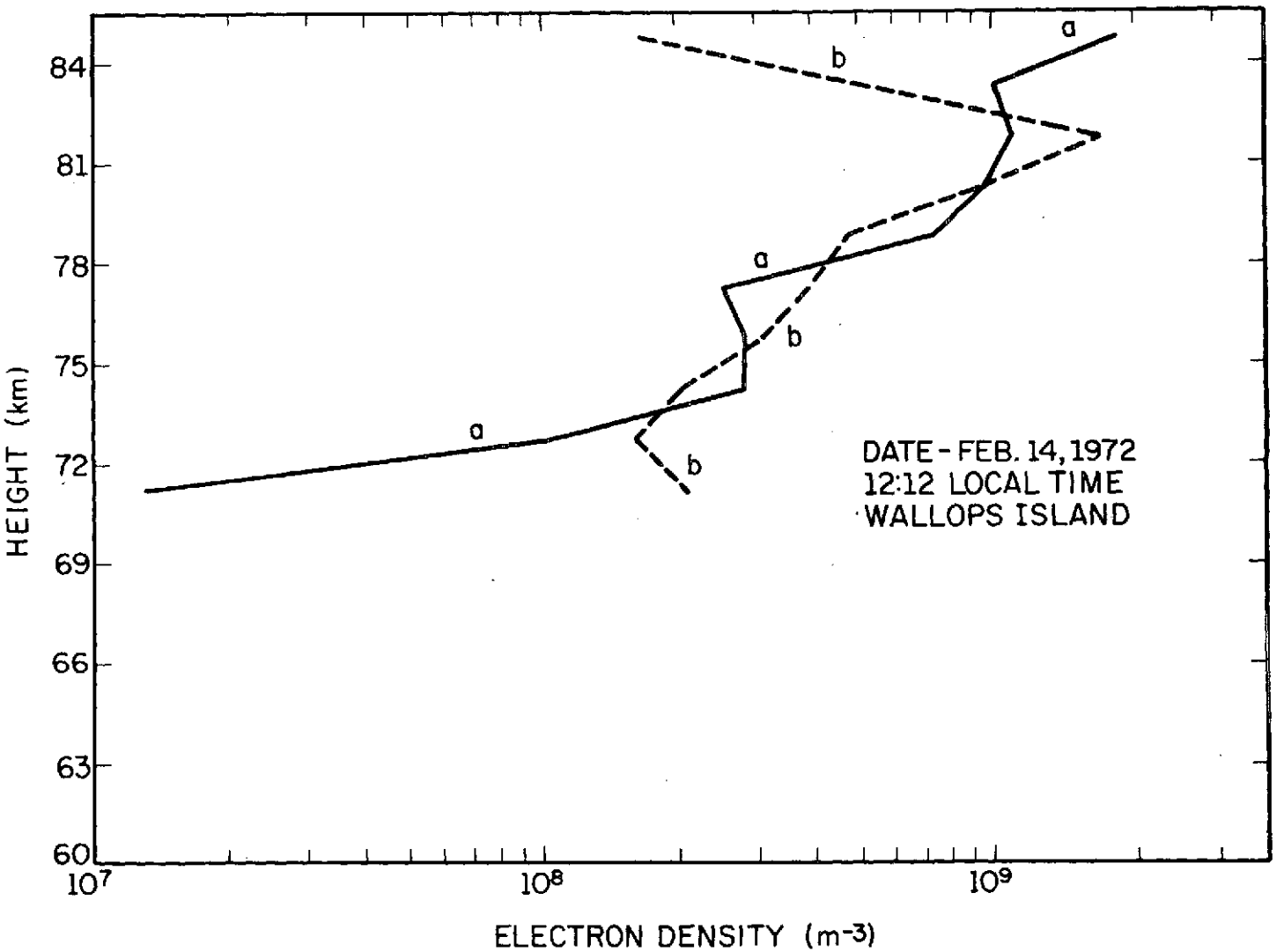

Figure 4.28 Electron-density profiles measured at Wallops Island, Virginia, on Feb-14-1972, at 12:12 local time, using only maximums of the A_O and A_x signals, (a), or averaging all the samples at 1.5 km of height interval, (b).

TABLE 4.3

Number of maximums observed at each height, in the data used in the calculation of the electron-density profiles of Figure 3.28.

Height (km)	Number of maximums in the A_o profiles	Number of maximums in the A_x profiles
69	145	150
70.5	137	127
72	185	202
73.5	170	190
75	170	196
76.5	165	187
78	132	166
79.5	195	149
81	62	132
82.5	191	141
84	263	182
85.5	247	224
Total number of samples		1,584

Observation of Figure 4.28a and 4.28b shows that the processing method can alter significantly the resultant electron-density profile. The profile of Figure 4.28a, obtained using only maximums of the a_o and a_x profiles shows a steep gradient above 84 km that is not observed on the profile of Figure 4.28b, obtained by the method described in Chapter 2.

Below 75 km the profile of Figure 4.28a presents lower electron densities than the profile of Figure 4.28b.

The signal processing method using only the maximums of the received signals, although time consuming, should be considered in partial-reflection systems having a transmitter with a rapid pulse repetition rate (order of 10 s^{-1}) and a capability of processing the number of samples necessary to get an electron-density profile (order of 15,000) in a reasonable time.

4.5.2 *Deconvolution of the* A_o *and* A_x *profiles.* Each received sample a_o or a_x from a given height is given by the expression:

$$a^2_{o,x}(h) = \int_{-\infty}^{+\infty} s(\tau-h)\ \sigma(\tau)d\tau \qquad (4.87)$$

Where $\sigma(\tau)$ is the waveform of the transmitted pulse and $\sigma(\tau)$ is the scattering cross section per unit volume.

If integral equation (4.87) is solved, the scattering cross section as a function of height can be obtained. A solution to this equation, and consequently the deconvolution of the A_o and A_x profiles was given by *Austin et al.* [1969] and *Coyne and Belrose* [1973].

As the reflections from different heights are not correlated, equation (4.87) can be averaged without taking the phase of $\sigma(\tau)$ into

consideration, resulting:

$$A^2_{o,x} = \int_{-\infty}^{+\infty} \overline{\sigma}_{o,x}(\tau)\ s(\tau-h)d\tau \qquad (4.88)$$

Equation (4.88) is a Fredholm integral equation of first kind, and admits oscillatory solutions. Such solutions, although mathematically plausible, do not correspond to the physical solution of the problem. To avoid the oscillations it is necessary to know with great precision the variations of A_o and A_x with altitude, from the lowest to the highest level, and to determine precisely the waveform of the transmitted pulse.

The solutions are particularly sensitive to the values of $A_{o,x}(h)$ at lower altitudes, and small variations of such values will produce solutions with oscillations growing with height. Due to limitations on the precision of the measurement of $A_{o,x}(h)$ at lower heights, where the signal-to-noise ratio is low, all the attempts made during the execution of the present work to deconvolute the $A_{o,x}(h)$ profiles did not produce reliable results. Due to the importance of this subject for partial reflection, and the convenience of further work to improve the deconvolution technique, the method used and the results obtained will be discussed below.

Methods of deconvolution of physical data have been discussed by several authors [*Stone*, 1962; *Grisson et al.*, 1968; *Ritchie and Anderson*, 1966]. A review of such methods is made by *Rareck* [1969].

The technique used in decovoluting the $A_{o,x}(h)$ profiles was that given by *Grisson et al.* [1966]. In this technique, the integral equation (4.88) is approximated by the following series:

$$A(h)^2 = \sum_{i}^{n} \sigma_i \, s_i(h) C_i \Delta \tag{4.89}$$

Where the subscripts o,x were dropped, the region of integration was sub-divided into n sub-regions of width $\Delta = h_2 - h_1$, and the coefficients C_i are chosen to yield an approximation of the integral given by Simpson's rule. $\sigma(h)$ has been replaced by a set of expansion coefficients σ_i.

To determine σ_i an error function is defined by

$$E = S_1 + \gamma S_2 \tag{4.90}$$

where S_1 is the sum of the squares of the deviations

$$S_1 = \sum_{j=1}^{m} [(A_j - \sum_{i=1}^{m} \sigma_i \, s_i(h_j) \, C_i \Delta)^2] \tag{4.91}$$

between the series of equation (4.89) and the experimental data.

The term S_2 is given by

$$S_2 = \sum_{i=k+1}^{n-1} k \, R_{k_i}^2 \tag{4.92}$$

where R_{ki} is the remainder after k terms in the approximate Taylor series expansion for σ_{i+1} in terms of the previous coefficients

$$\sigma_{i+1} \cong \sigma_i + \delta(\sigma)\Delta + \delta^2(\sigma) \frac{\Delta^2}{2!} + \ldots\ldots \delta^k(\sigma) \frac{\Delta^k}{k!} + R_{k_i} \tag{4.93}$$

The term $\delta^k(\sigma)$ represents the k-th derivative of the function set $\{\sigma_i\}$.

S_2 is a positive definite quantity whose magnitude is a direct measure of the continuity of the solution $\{\sigma_i\}$. The solution is obtained by minimizing the error E, for a given choice of γ, and given by the simultaneous system of equations

$$\frac{\partial E}{\partial \sigma_i} = 0 \qquad i = i, \tau, \ldots n \tag{4.94}$$

By adjusting the value of γ one imposes a continuity requirement on the solution and reduces the fluctuations to a certain degree.

The computer program to deconvolute the $A_{o,x}(h)$ profile by using the above method is in Appendix II (DECOMM). The results obtained were not reliable, and even adjusting γ over a wide range, the oscillations appear on the solutions, and as the oscillations on the $A_o(h)$ and $A_x(h)$ profiles are not in phase, they produce large fluctuations in the A_x/A_o ratio. In Figure 4.29 it is shown an electron-density profile obtained by the method described above (Figure 4.28a) and by using the program PROAX (Figure 4.29b).

4.5.3 *Correction for the different group velocities of the modes of propogation.* The different group velocities for the extraordinary and ordinary modes of propagation can be an additional source of error in the determination of electron-density profiles above 80 km, since in the signal processing of partial reflections $A_o(h)$ and $A_x(h)$ are obtained by assuming that both signals propagate with the velocity of light in free space up to the height h. In Figure 4.30 the group velocities v_{go} and v_{gx} for both modes of propagation as a function of electron density are shown. It is observed that for $N \geq 10^9$ m^{-3} the difference between v_{go} and v_{gx} has to be taken into consideration. If the wave propagates 1.5 km in a region where

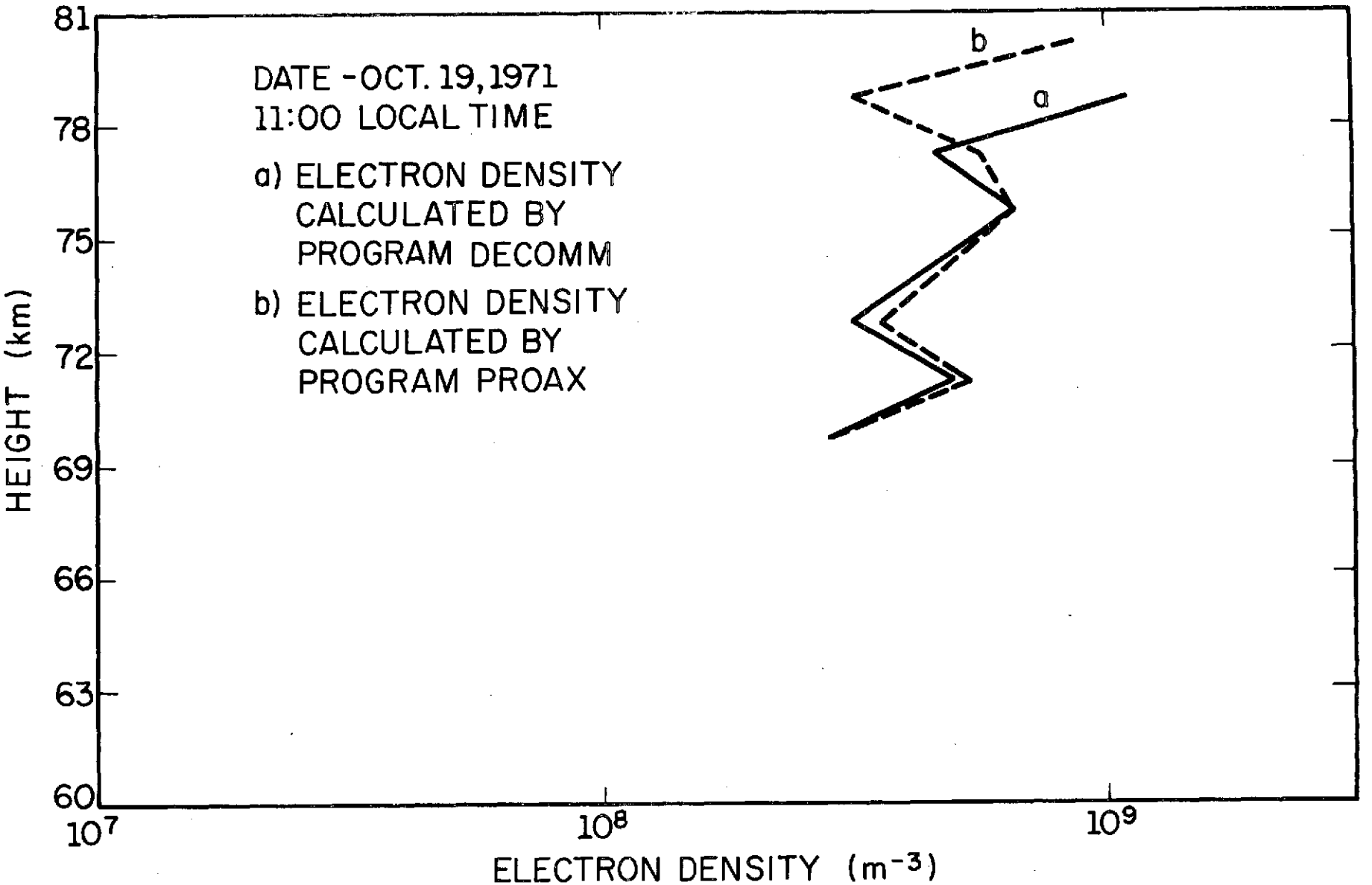

Figure 4.29 Electron-density profiles obtained by the programs PROAX (a) and DECOMM (b) measured at Urbana, Illinois, on October 19, 1971, at 11:00 A.M. local time.

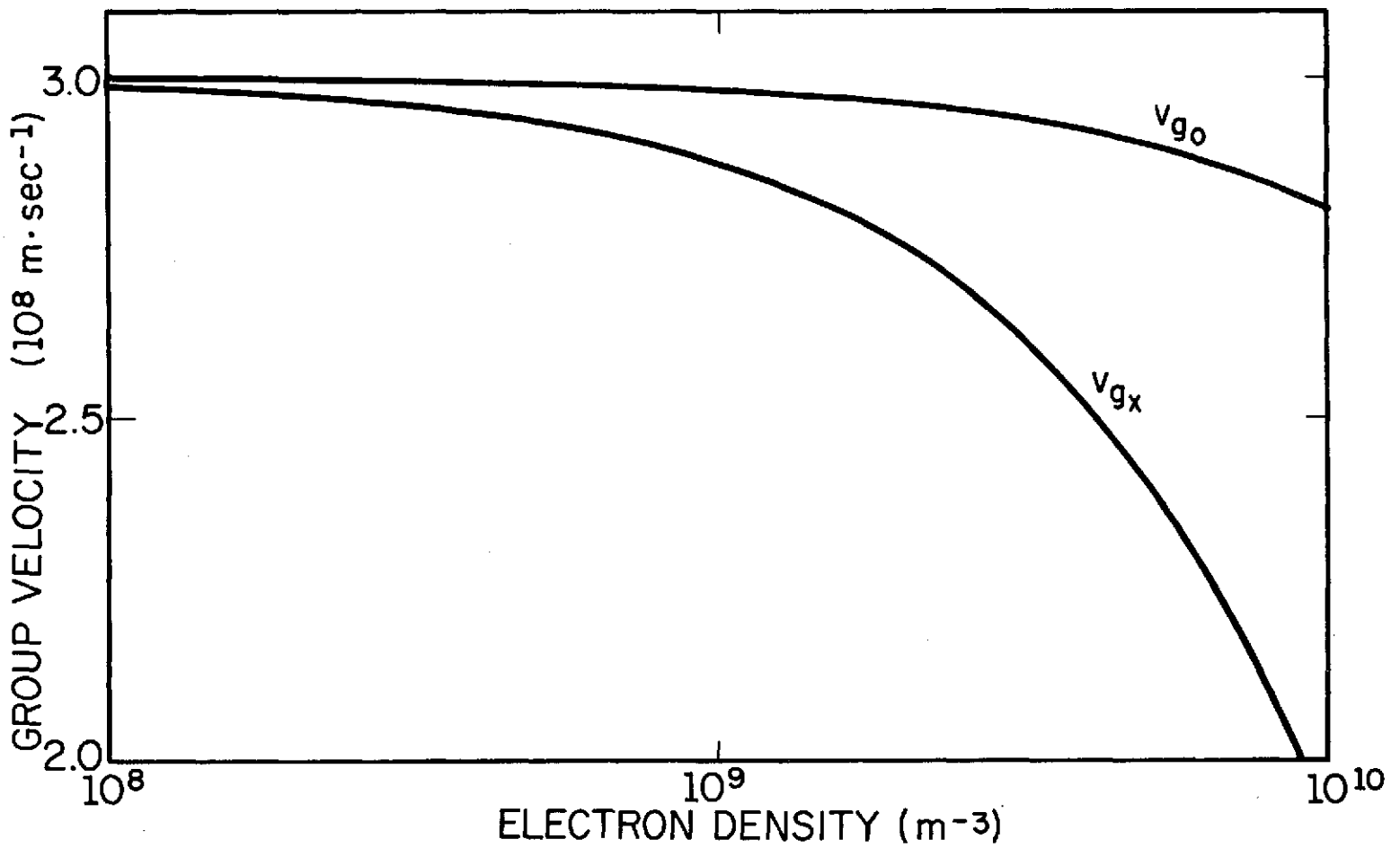

Figure 4.30 Group velocities for the ordinary and extraordinary modes of propagation, as a function of electron density, for a collision frequency of 10^5 s^{-1}.

$N = 5 \times 10^9$ m^{-3}, for example, the error in the determination of $A_x(h)$ will be of 180 m. If the $A_x(h)$ profile changes considerably over this distance, the corresponding A_x/A_o profile will be in error.

In an attempt to compensate this difference in propagation velocities computer program "RETARD" was developed. In this program, that is listed in Appendix II the corrected value of A_x at a height h, is taken as

$$A_{xr}(h) = A_x(h) + v_{gx}(h) \frac{A_x(h+1.5) - A_x(h)}{(1.5 \times 10^3/c_o)} \qquad (4.95)$$

where c_o is the velocity of light in free space. The corrected value of $A_x(h)$ is obtained by making a linear interpolation between two measured values, at heights separated by 1.5 km.

To calculate $v_{gx}(h)$ it is necessary to know the electron density at this height, and to determine the electron density it is necessary to know $A_{xr}(h)$. This problem is solved on the program RETARD by an iteration technique. The electron density is initially calculated by taking $A_{xr}(h) = A_x(h)$. With this value of electron density, $A_{xr}(h)$ is calculated using equation (4.95). The value of electron density is recalculated, and a new $A_{xr}(h)$ determined, until the value of electron density before and after a correction of $A_{xr}(h)$ shows a difference of less than 15 percent, that is considered as satisfactory in the present calculations. Electron-density calculations with and without correction for the different group velocities are shown in Figure 4.31. The profile of Figure 4.31a was calculated using the program PROAX, described in Chapter 2. The profile of Figure 4.31b was calculated using the program RETARD.

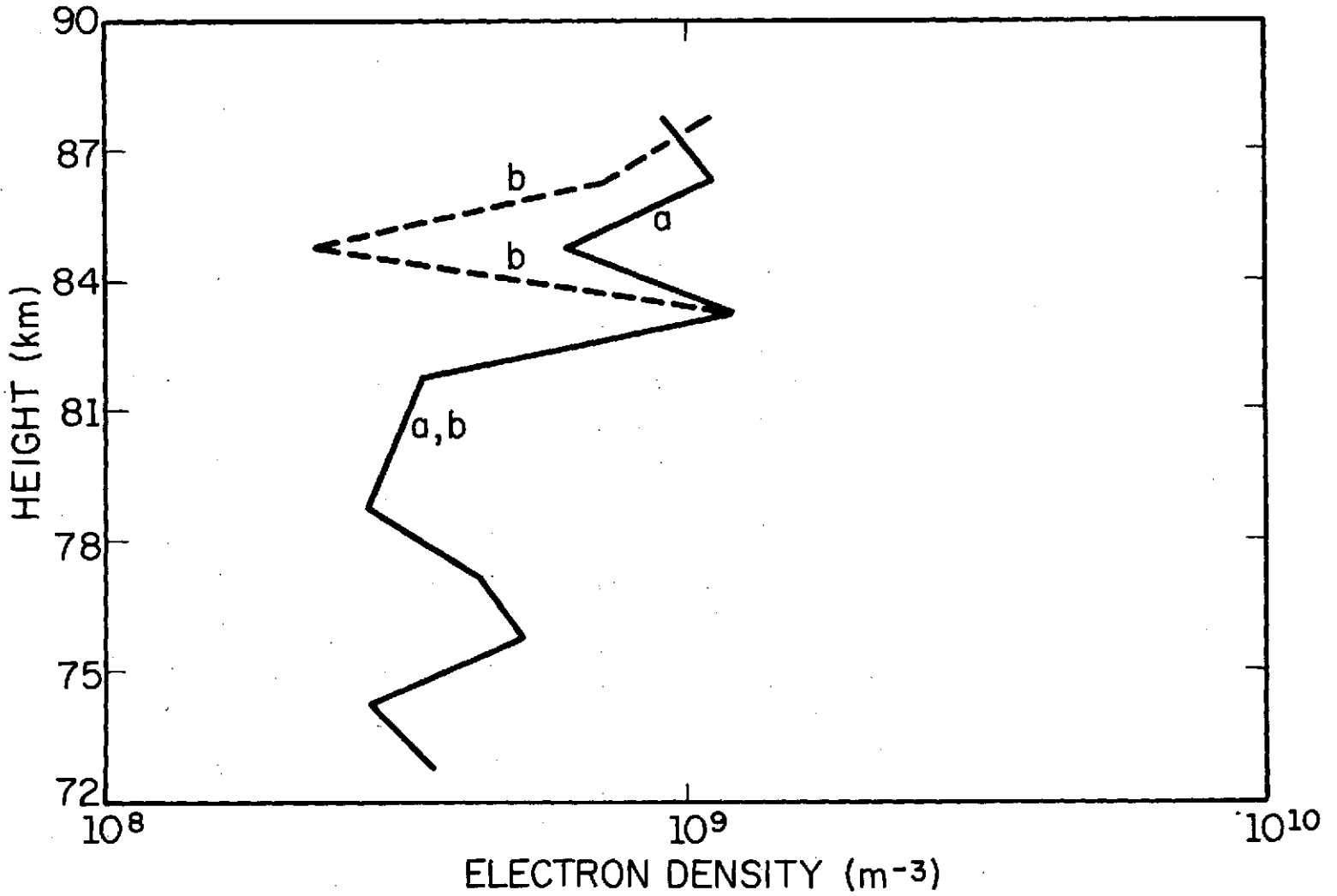

Figure 4.31. Electron-density profiles measured at Urbana, Illinois, on October 8, 1971, at 9:20 A.M. local time, using the programs PROAX (b) and RETARD (b).

5. PARTIAL-REFLECTION MEASUREMENTS DURING THE 1971-1972 WINTER

During the 1971-1972 winter, a coordinated rocket program, headed by the University of Illinois, was established to study the winter variability of the *D* region through measurements of electron density, ion composition, pressure and temperature, at Wallops Island, Virginia. It was decided to make measurements on three different days, with the following characteristics:

a) a day of low ionization of the *D* region;

b) a day of high ionization, with no magnetic disturbances during at least 8 days prior to the measurement;

c) a day of high ionization, during magnetic disturbances.

The rocket measurements were performed only at the low ionization day, on January 31, 1972, since no day attending the specifications of the items b and c above were observed during January and February of 1972.

To determine the conditions required for a given day, several measurements were made every day by different workers in United States and Canada, and the results sent to Wallops Island.

The measurements performed were the following: vertical absorption at 1.8 and 3.3 Mhz, oblique absorption at 2.2 Mhz, VLF phase, A_x/A_o ratio at 76 km, at Ottawa, Canada and Raleigh, North Carolina, 10 mb temperature, A index, particle precipitation, solar radiation fluxes, and electron-density profiles by partial reflection at Wallops Island.

In this chapter will be presented the results of the partial-reflection measurements made at Wallops Island, by the University of Illinois.

The equipment used is described in Chapter 3. Electron densities were normally measured from 9 to 13 o'clock, local time, with exception of a few

days when interference problems or hardware defects prevented the measurements. On the average, 10 profiles were taken each day. The profiles were obtained from 513 frames, each one corresponding to one ordinary and one extraordinary sample. The pulse repetition rate used was 2 double pulses per second, and consequently, each electron density corresponds to the average over approximately 4 minutes. When strong interference was observed during a measurement, it was interrupted and started again when the interference level reached a reasonable level. As a result, some profiles were obtained over a period of time greater than 4 minutes. The pulse width used was of 50 μsec.

Results obtained during the month of October of 1971, at Urbana, Illinois, using the partial-reflection system of the University of Illinois, that is described in Chapter 3, are also presented in this chapter.

5.1 *Partial Reflections in October, 1971*

The electron densities at 70.5, 75 and 78 km, measured at Urbana, Illinois, for the month of October, 1971, are shown in Figure 5.1. The electron densities presented are the median electron densities obtained from measurements performed at solar zenith angles between 65 and 55°. The electron density at each height is the result of averaging electron densities measured at two adjacent heights, separated by 1.5 km. The A_x/A_o ratios, at 69, 76.5 and 82.5 km, for a solar zenith angle of approximately 60° are shown in Figure 5.2.

As can be verified from Figure 5.1, some variability, although not strong, was observed in this month. The ionization on October 14, for example, was approximately 50 percent greater than on October 13.

On some days, measurements were made during all the morning, including sunrise time. One of such measurements, made on October 14, is shown in

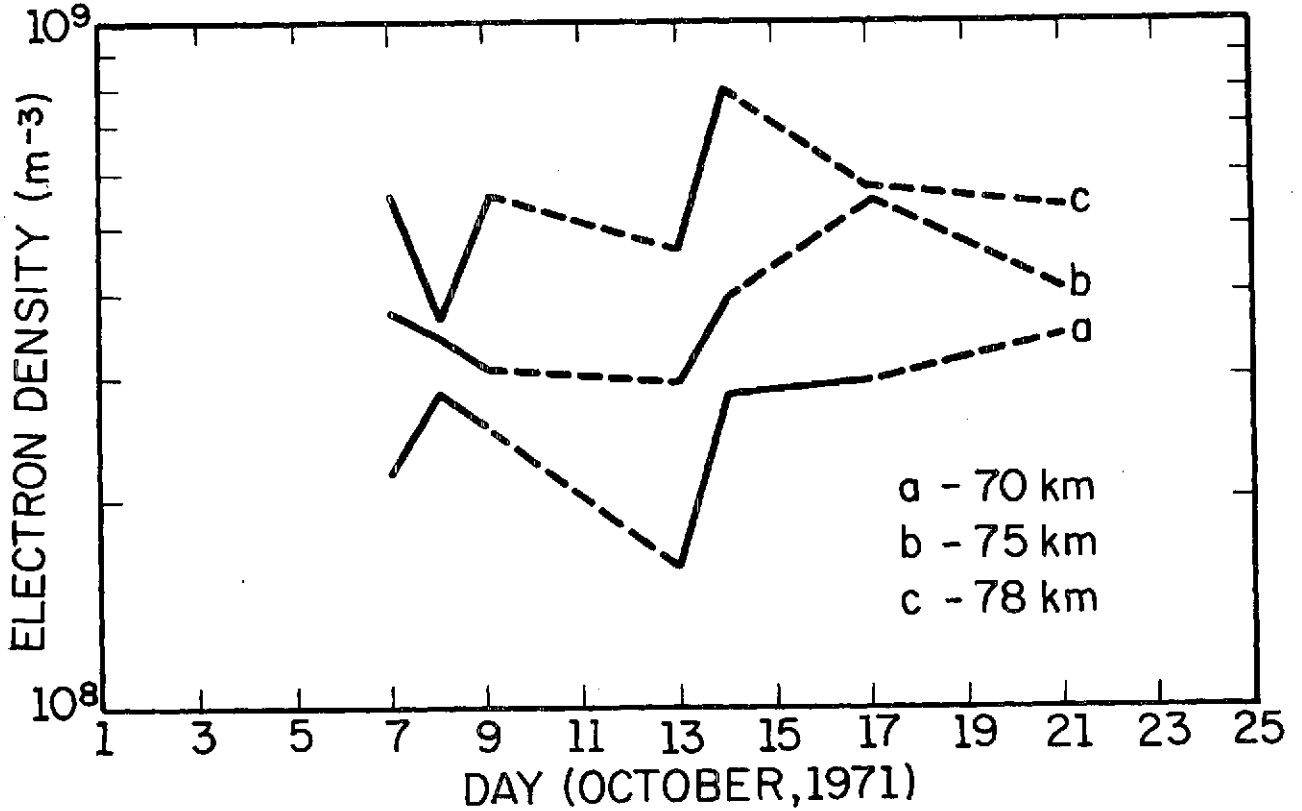

Figure 5.1 Daily median electron densities for the month of October, 1971 at 70, 75, and 78 km of altitude, solar zenith angles between 65 and 50 degrees, measured at Urbana, Illinois.

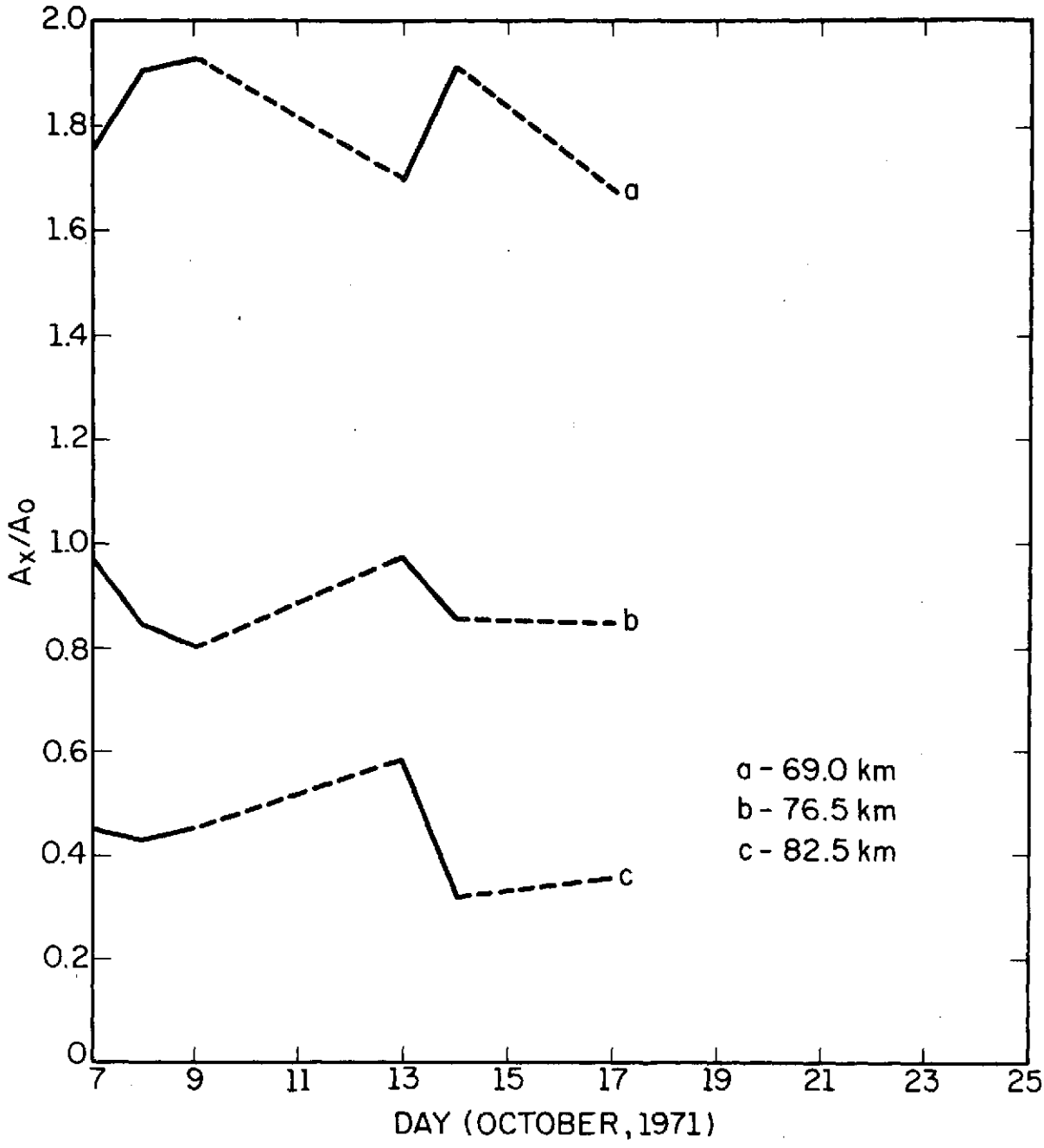

Figure 5.2 A_x/A_o ratios for the month of October, 1971, at 69, 76.5 and 82.5 km of altitude, solar zenith angle of approximately 60°.

Figure 5.3. For solar zenith angles above 80° no reflections above the noise level were observed between 65 and 80 km, but strong reflections were measured above this height. Reflections between 65 and 75 km were observed only for solar zenith angles below 70°. During sunrise, reflections produced by the *C* layer, at heights between 60 and 64.5 km were observed. One example of such reflections is shown in Figure 5.4, where the A_o profile measured on October 14 is plotted, for a solar zenith angle of 87°. Reflections above the noise level are observed at 61.5, 63 and 64.5 km, and above 81 km.

Reflections from the *C* layer during sunrise is a good way of measuring the collision frequency at lower altitudes, since at that altitude the ionospheric absorption is very small, one can take $A_x/A_o \cong R_x/R_o$, and from this ratio calculate the collision frequency. For the data obtained on October 14, collision frequency of 2.0×10^7 s^{-1} was calculated at 63 km.

5.2 *Partial Reflections in December, 1971*

The median electron densities at 70, 75 and 78 km for the month of December, 1971 are shown in Figure 5.5. The median was obtained for solar zenith angles between 70 and 60°. The A_x/A_o ratios, at 69, 76 and 82.5 km, for a solar zenith angle of approximately 60° are shown in Figure 5.6.

Two periods of low absorption, on December 8 to 10 and December 15 to 17, and two periods of high absorption, on December 12 to 13 and December 18 to 19 were observed. The variation from low to high absorption showed a periodic behavior, with a period of approximately 6 days. Figure 5.7 shows the median electron-density profiles during a day of high absorption, December 12, and a day of low absorption, December 9. It can

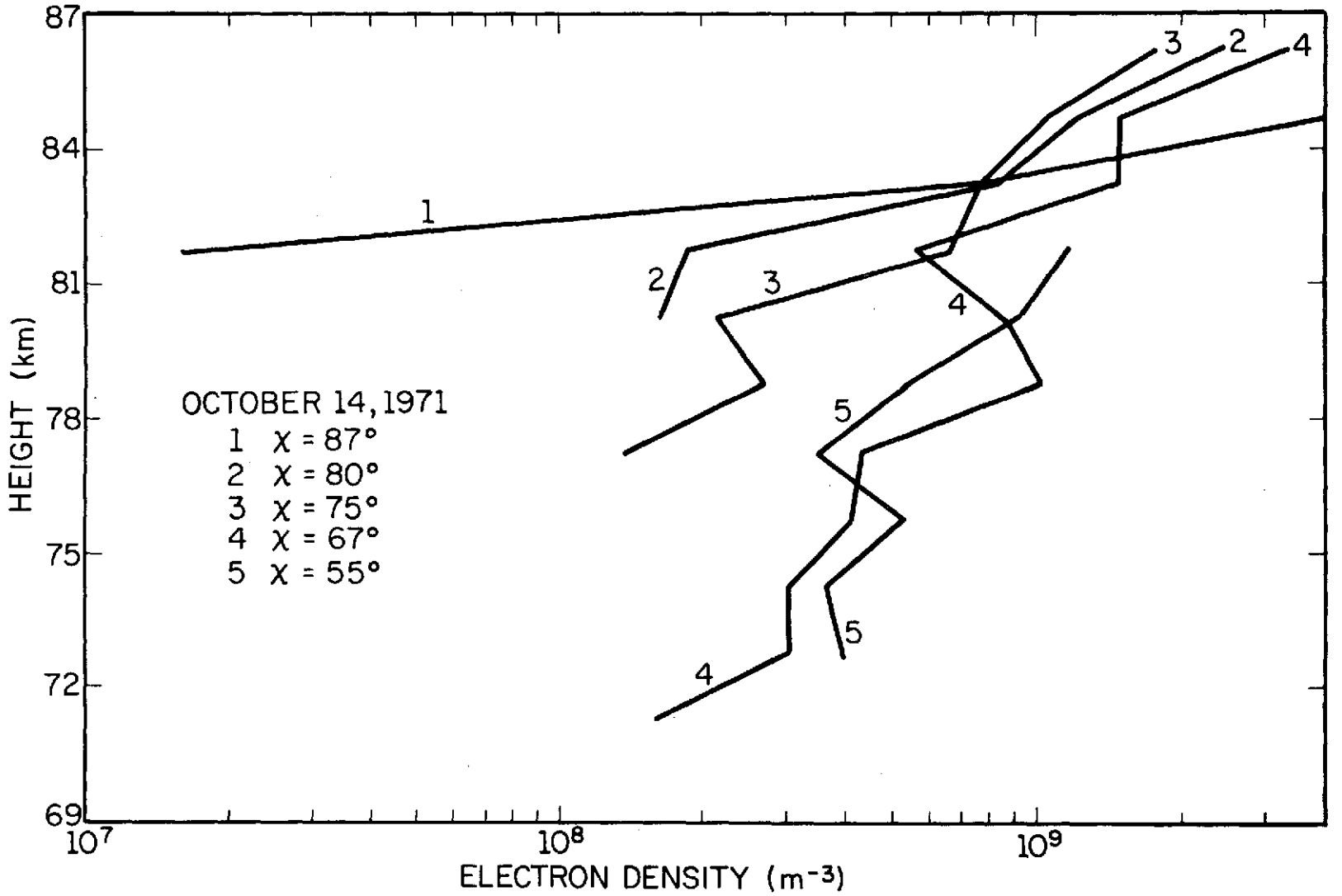

Figure 5.3 Solar zenith angle variation of electron densities, at Urbana, Ill., on October 14, 1971.

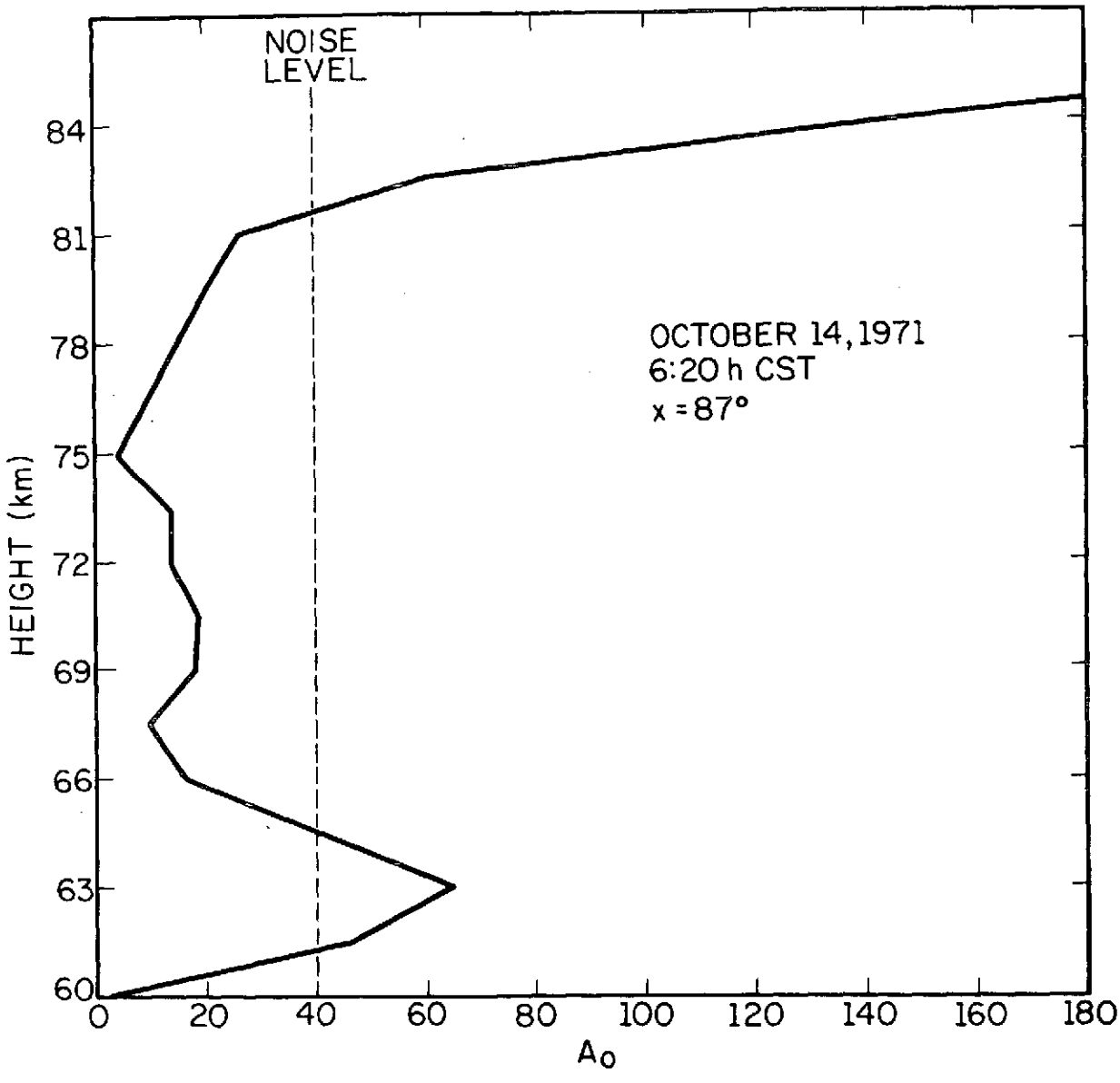

Figure 5.4 A_o profile measured on October 14, 1971, at a solar zenith angle of 87°.

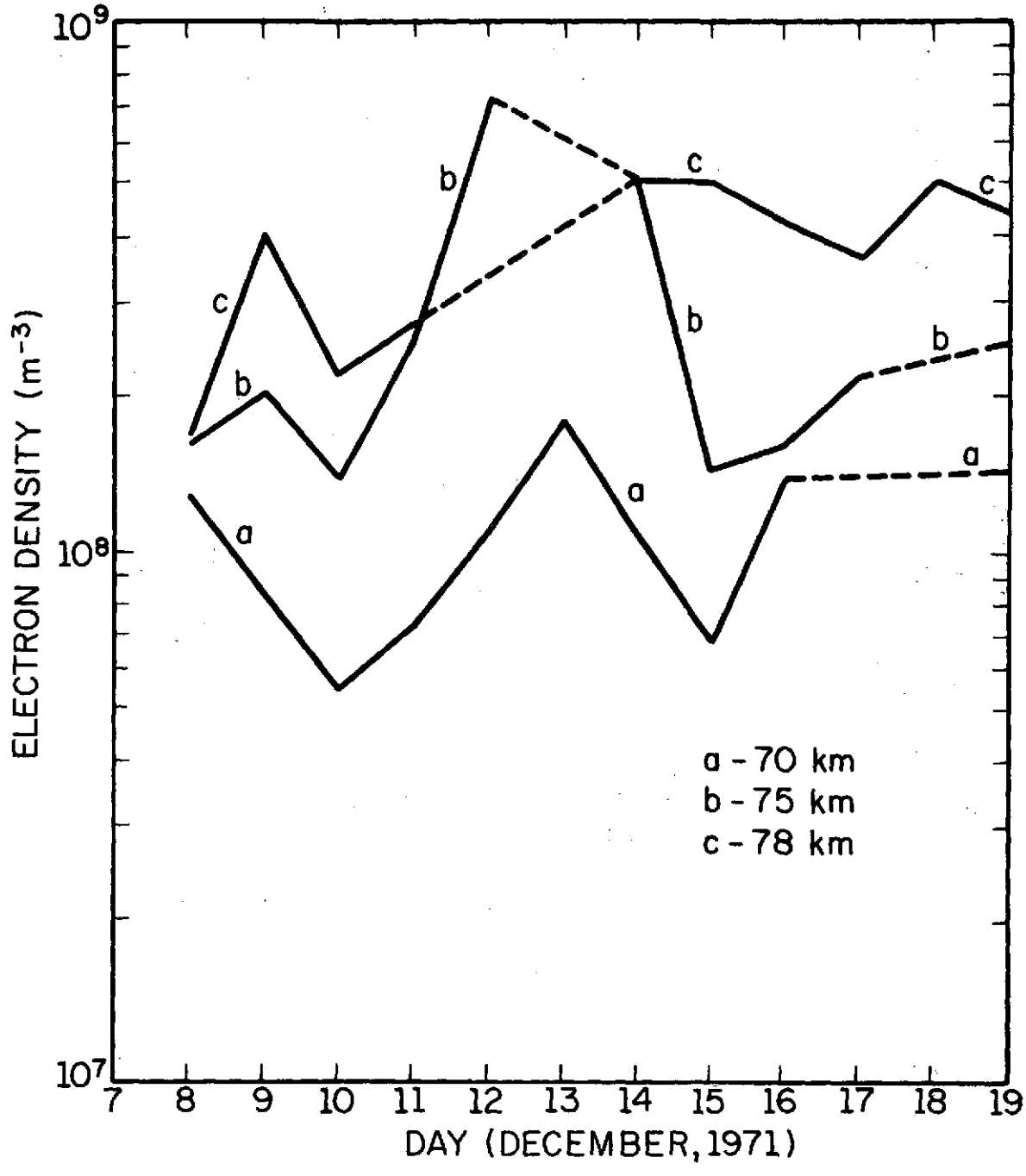

Figure 5.5 Daily median electron densities, for the month of December, 1971, at 70, 75 and 78 km altitude, solar zenith angles between 70 and 60°, measured at Wallops Island, Virginia.

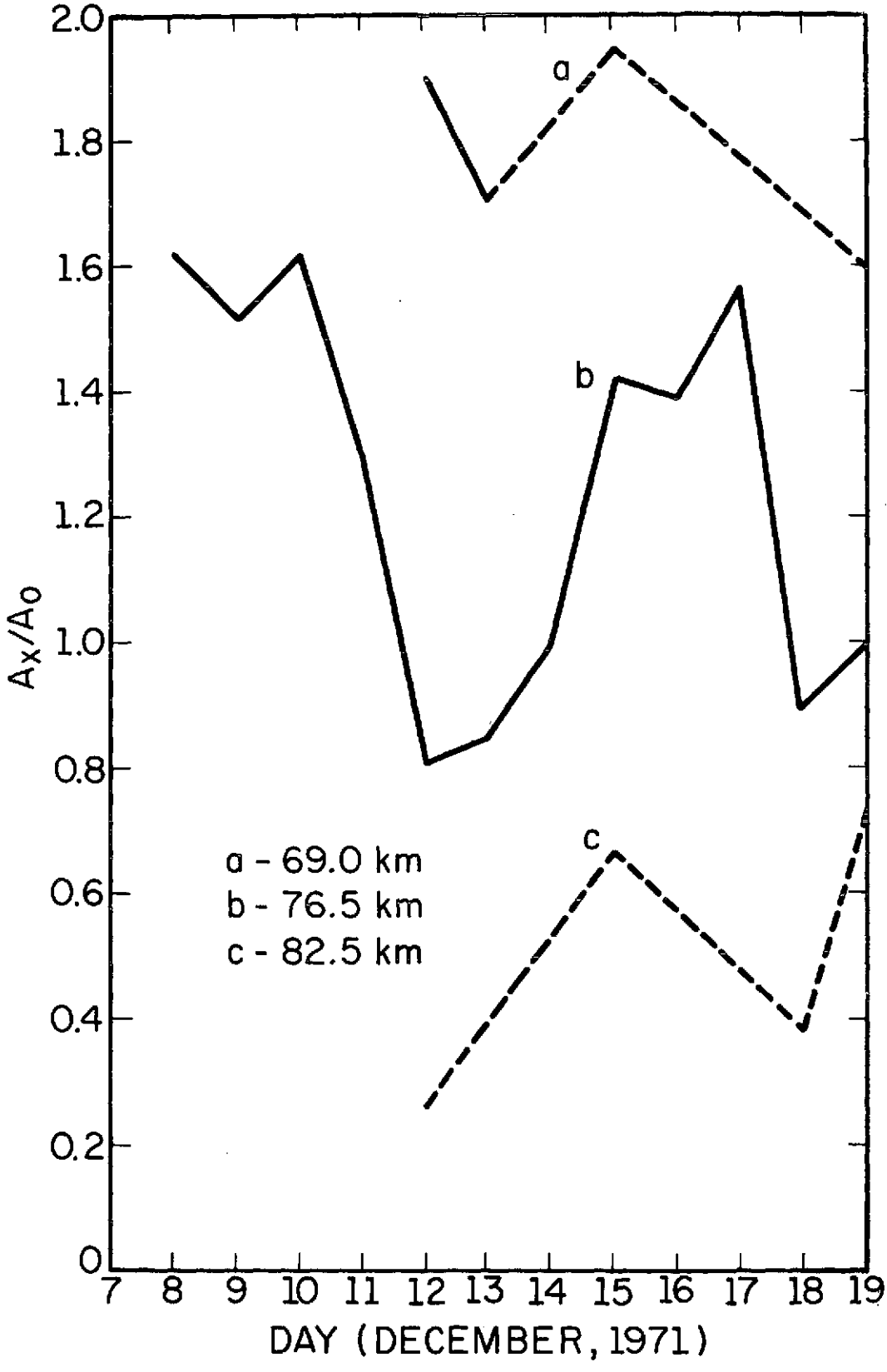

Figure 5.6 A_x/A_O ratios for the month of December, 1971, at 69, 76.5 and 82.5 km altitude, solar zenith angle of approximately 60°.

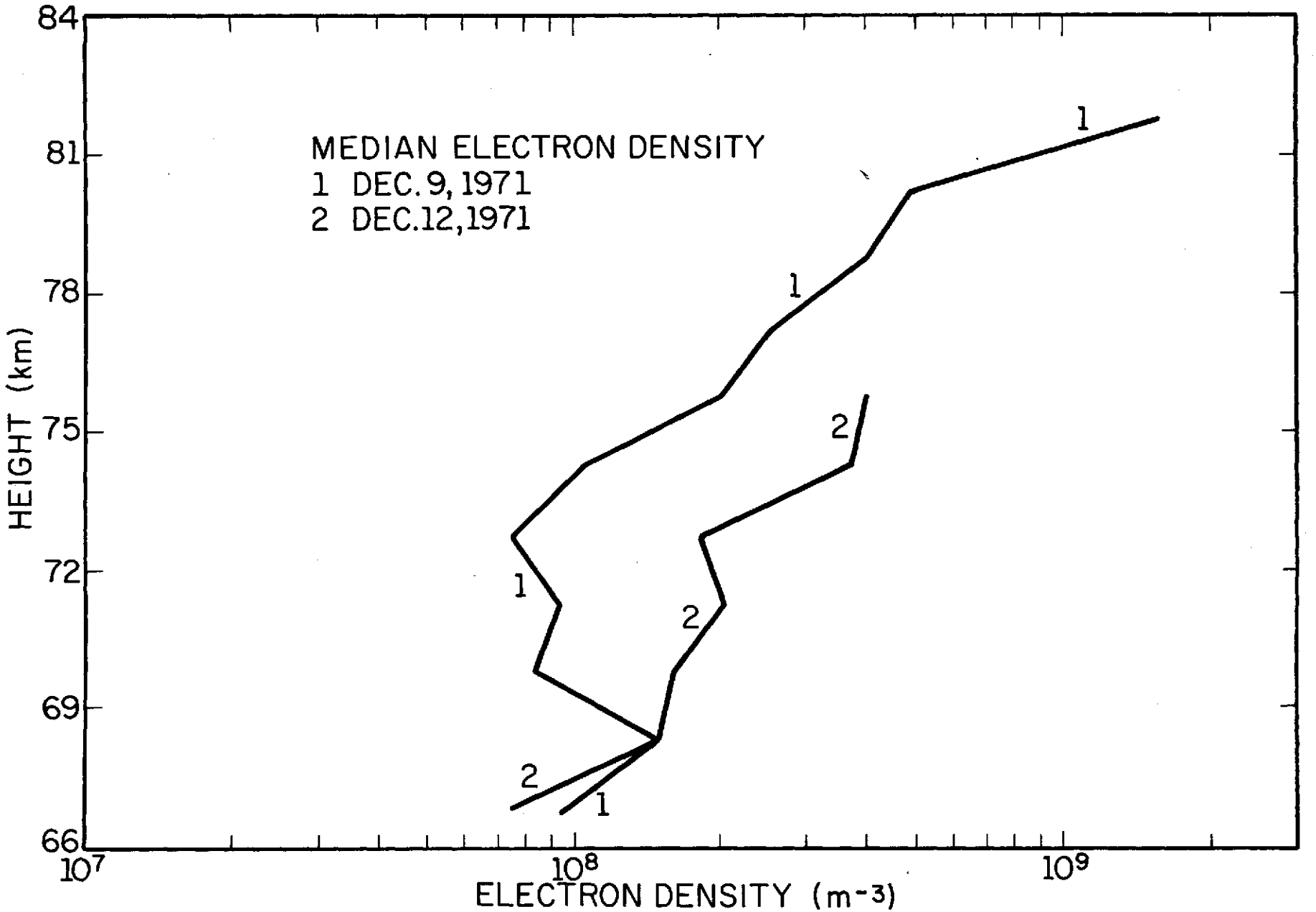

Figure 5.7 Median electron densities for a day of low absorption (December 9) and a day of high absorption (December 12).

be observed that the high absorption day is characterized by an increase of ionization all over the *D* region, from 69 to 76 km. Above this height no measurement was made on December 12, due to saturation of the receiver. At 74 km, the electron density on December 12 was approximately four times greater than on December 9.

The daily variation of the ionization was closely correlated to the variations of geomagnetic activity, as can be observed on Table 5.1, that gives the A_p indices. On December 12, 13, 18 and 19, days of high ionization, the A_p index was of 9, 13, 22 and 11, respectively. On December 8, 9, 10, 15, 16 and 17, days of low absorption, the A_p index was 3, 7, 3, 3, 8 and 67, respectively. December 17, although being a day of low absorption and high magnetic activity, was prior to a day of high ionization.

Such correlation suggests that the variations in ionization during December 71 were produced by geomagnetic effects.

The A_x/A_o profile of Figure 5.6 shows that the best indicator of the ionization is the A_x/A_o ratio at 76.5 km. Above this height, the A_x/A_o ratio is influenced principally by the strong gradient in electron density that appears near 80 km, and at lower altitudes, as 69 km, the differential absorption is too small, producing practically no variation in the A_x/A_o ratio.

5.3 *Partial Reflections in January and February, 1972*

The median electron densities at 70, 75 and 78 km, for solar zenith angles between 70 and 60°, for the months of January and February of 1972, are shown in Figures 5.8 and 5.9. The A_x/A_o ratios at 69, 76.5 and 82.5 km, solar zenith angle of approximately 60° are shown in Figures 5.10 and 5.11.

TABLE 5.1

A_p indices for the months of December 1971, January 1972, and February 1972.

Day	Dec A_p	Jan A_p	Feb A_p
1	6	7	7
2	5	8	13
3	12	6	9
4	8	10	9
5	3	6	6
6	1	2	6
7	3	4	8
8	7	4	7
9	3	5	4
10	3	7	10
11	6	15	7
12	9	6	4
13	13	4	22
14	3	3	15
15	3	19	13
16	8	29	8
17	67	20	22
18	22	19	12
19	11	11	14
20	3	8	12
21	10	22	9
22	19	25	4
23	12	32	6
24	7	10	33
25	6	17	16
26	12	22	6
27	4	15	4
28	4	23	6
29	15	14	2
30	16	9	
31	7	7	

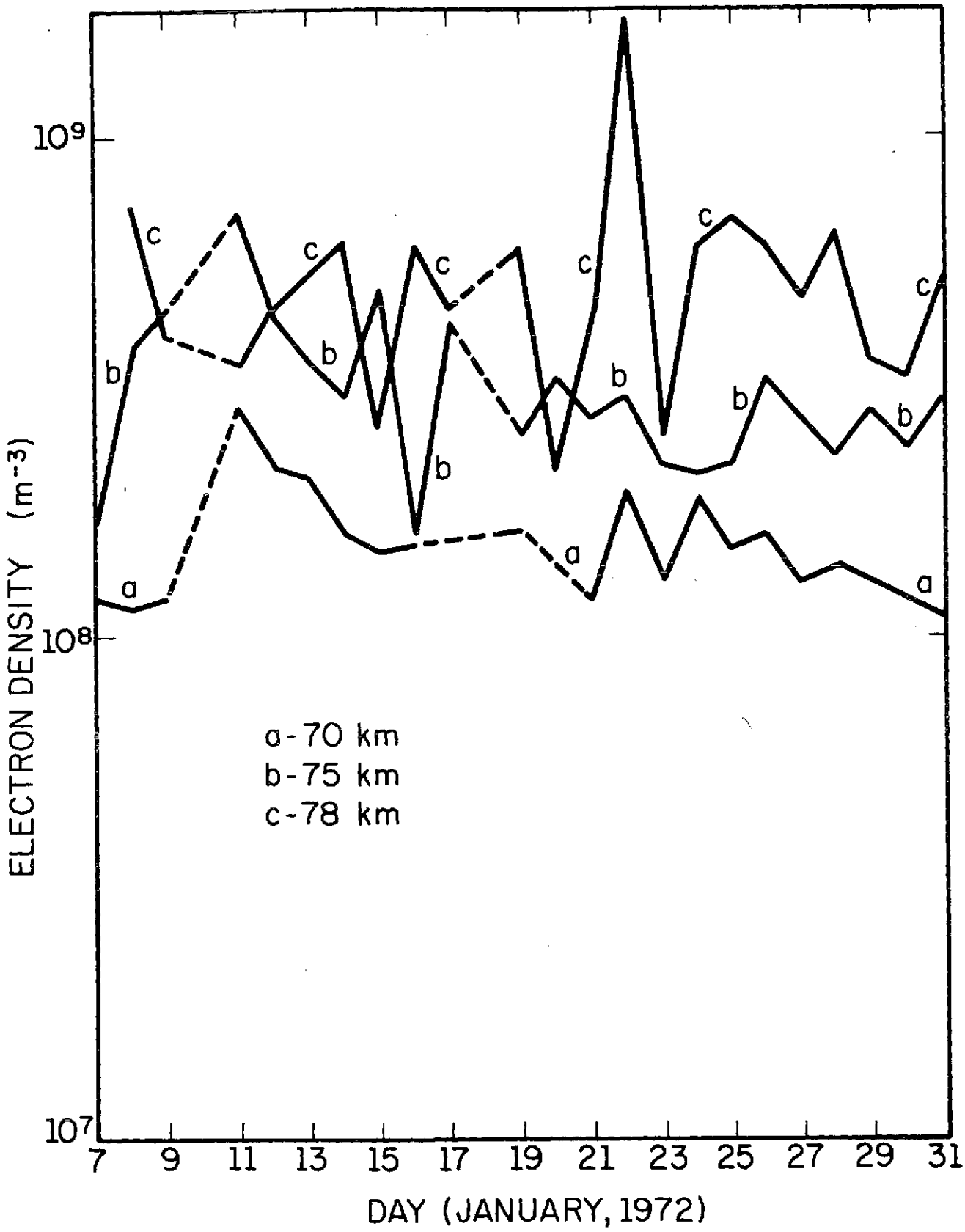

Figure 5.8 Daily median electron densities at 70, 75 and 78 km altitude, solar zenith angle between 70 and 60°, for the month of January, 1972.

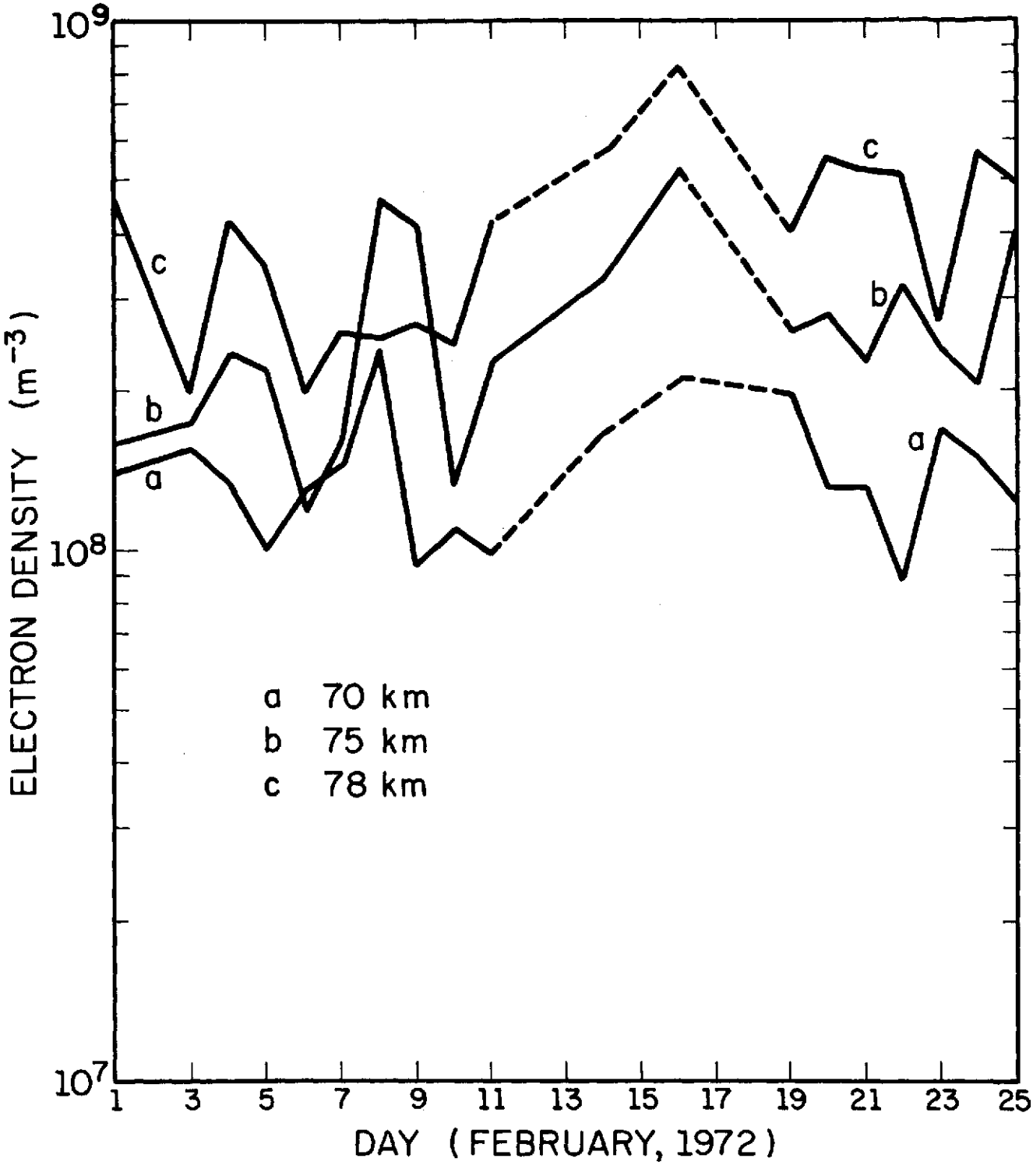

Figure 5.9 Daily median electron densities at 70, 75 and 78 km altitude, solar zenith angle between 70 and 60°, for the month of February, 1972.

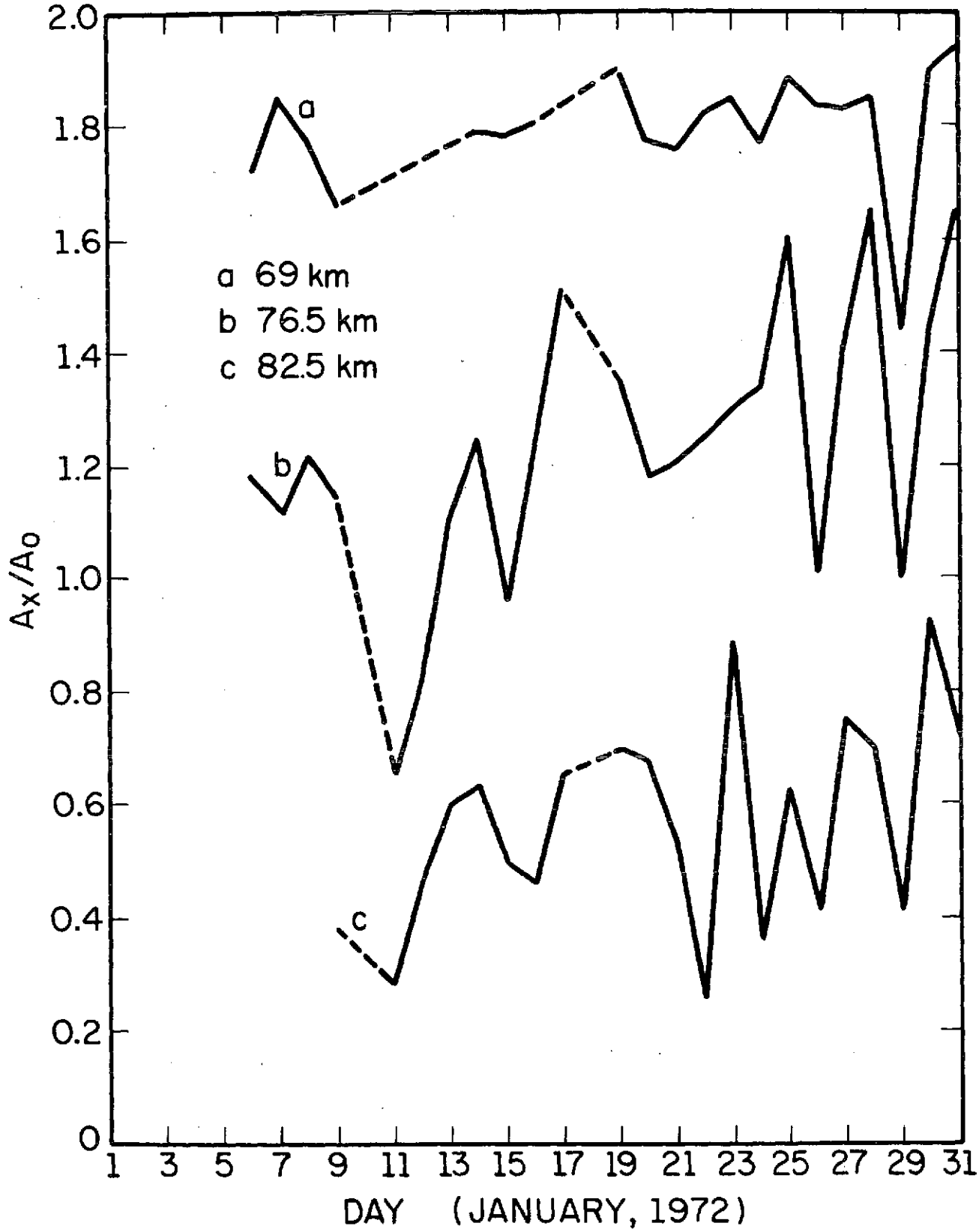

Figure 5.10 A_x/A_o ratios for the month of January, 1972, at 69, 76.5 and 82.5 km altitude, solar zenith angle of approximately 60°.

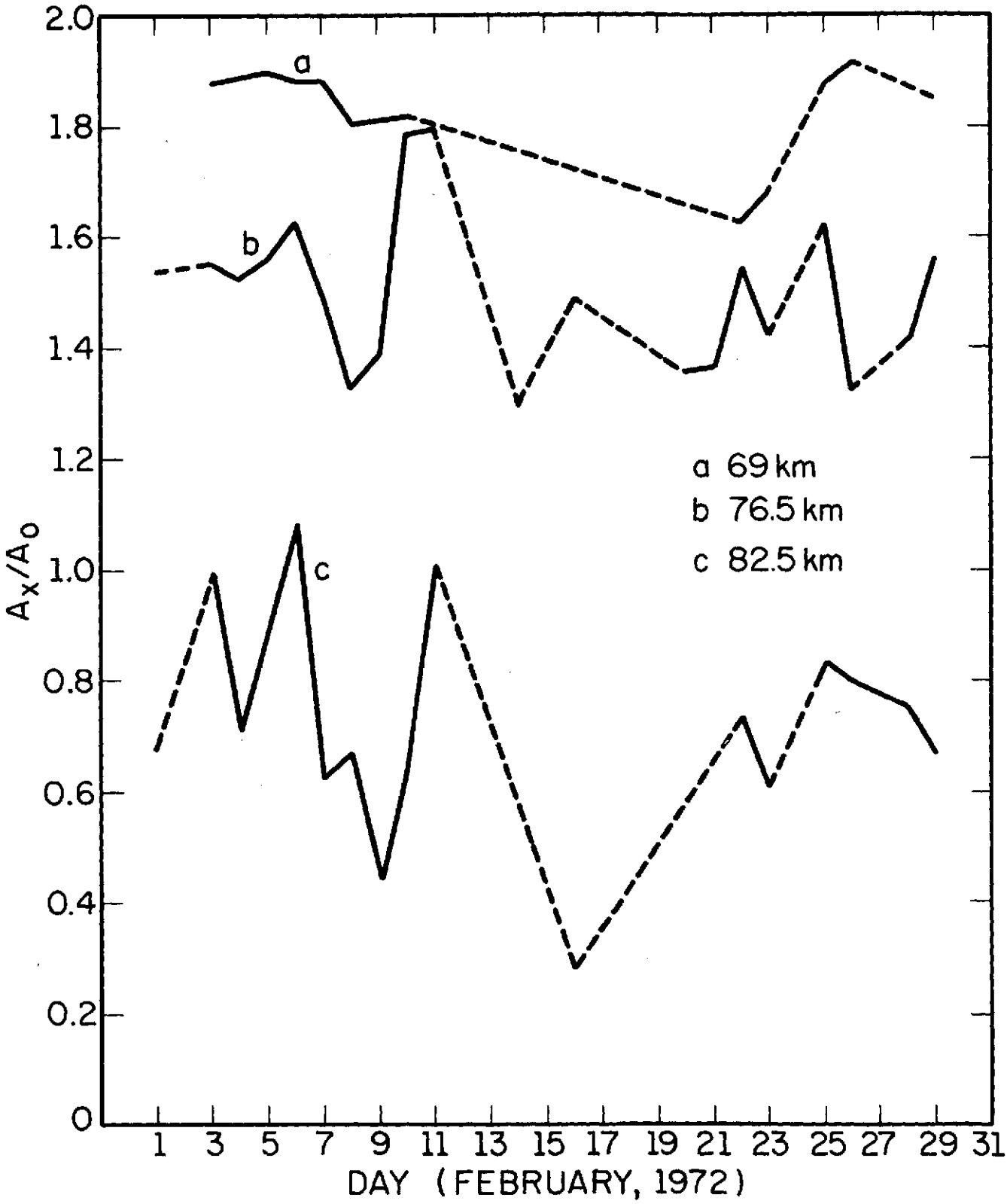

Figure 5.11 A_x/A_o ratios for the month of February, 1972, at 69, 76.5 and 82.5 km altitude, solar zenith angle of approximately 60°.

The behavior of the *D* region during the months of January and February of 1972 was quite different from that observed in December, 1971. Only one day of high absorption, on January 11, was observed. Low absorption days appeared more frequently, as on January 25, 28, 31 and February 10. The daily variations of electron densities were much smaller than in December.

The days of higher ionization on January 11, 15, 26 and 29, and on February 14, 20 and 26, were also associated to variations of geomagnetic activity, as can be observed in Table 5.1.

Such results indicate that variations of ionization during all the winter 1971-1972 were mainly due to geomagnetic effects.

Measurements of electron densities during the occurrence of solar flares were made several times. The flare that produced the most pronounced effects on the *D* region occurred on January 19, between 11:34 and 12:45 hours, local time. The electron-density profiles measured during this period are shown in Figure 5.12. The profile at 11:09 was taken before the flare. The ionization reached its maximum values on the profile measured at 11:47. All the *D* region, down to 63 km, was affected. The electron density produced between 63 and 64 km by the X-ray radiation was of approximately 3×10^8 m^{-3}. The X-ray solar fluxes during the flare are shown in Table 5.2. 1.8 vertical absorption measurements made at Greenbelt, Maryland [*S. Gnanalingam*, private communication] showed a good correlation to the A_x/A_o ratio at 76.5 km, measured at Wallops Island as can be observed on Figures 5.13 and 5.14, that show the scatter plot of the A_x/A_o ratio at 76.5 km versus 1.8 MHz vertical absorption, for the months of January and February, 1972, respectively.

TABLE 5.2

X-ray solar fluxes during the solar flare on January 19, 1972 between 11:34 and 12:45 hours, local time.

local time		11:34 (start)	11:45 (peak)	12:45 (end)
Solar fluxes ($erg.cm^{-2}$ sec)	0.5-3.A°	$3x10^{-6}$	$8x10^{-4}$	$1.7x10^{-6}$
	1-8 A°	$6x10^{-3}$	$2.3x10^{-2}$	$3.3x10^{-3}$

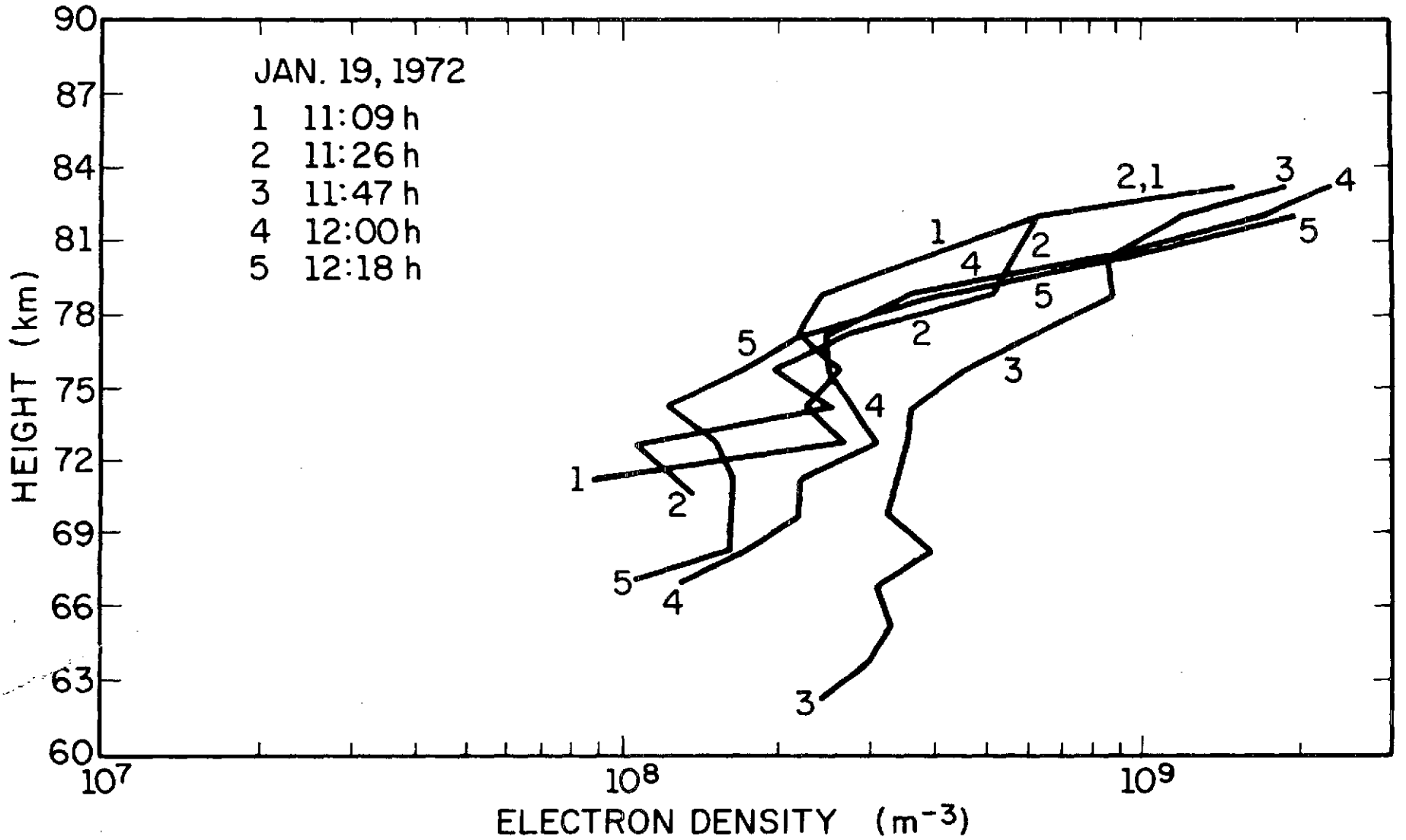

Figure 5.12 Electron-density profiles measured before and during the solar flare that occurred on January 19, 1972, between 11:34 and 12:45 hours, local time.

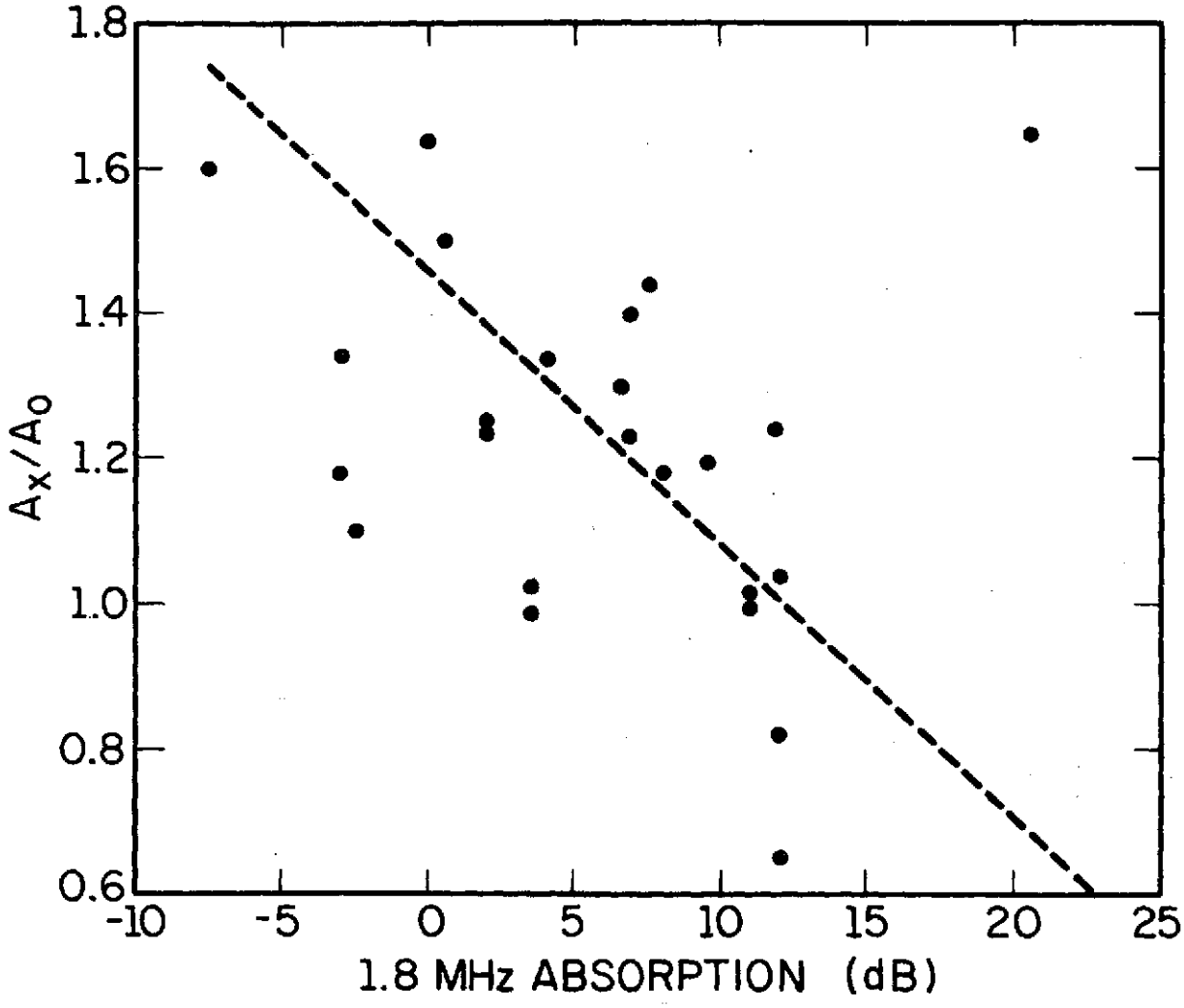

Figure 5.13 Scatter plot of A_x/A_o ratio at 76.5 km, measured at Wallops Island, Virginia versus 1.8 MHz vertical absorption measured at Greenbelt, Maryland, for the month of January, 1972.

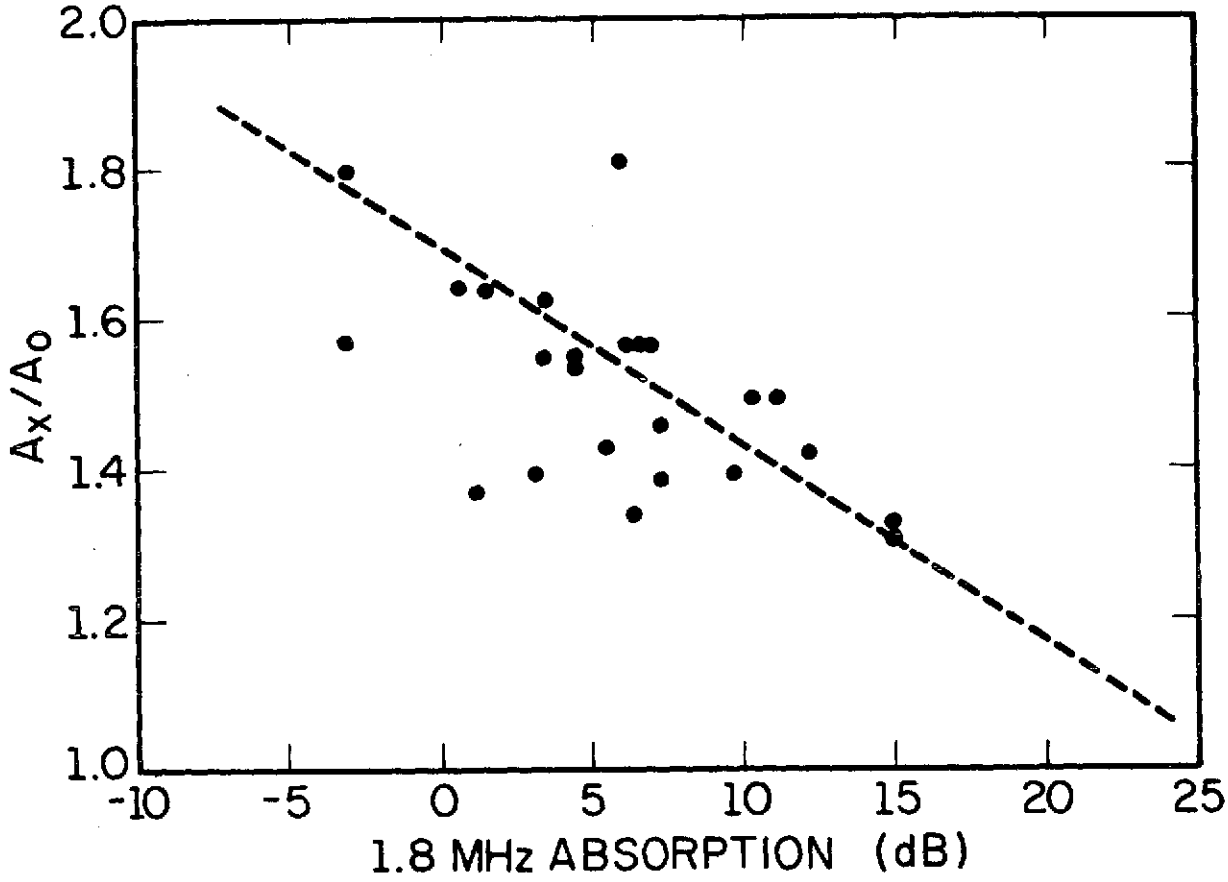

Figure 5.14 Scatter plot of A_x/A_o ratio at 76.5 km altitude, measured at Wallops Island, Virginia, versus 1.8 MHz vertical absorption measured at Greenbelt, Maryland, for the month of February, 1972.

Figure 5.15 shows the electron-density profiles measured on January 31, 1972, between 11:40 and 12:30 hours, local time. This day was chosen as the low day, and a Nike Apache rocket launched at 12:30 for the measurement of electron densities and collision frequencies, by Faraday rotation, differential absorption and current probe. The technique employed on the rocket measurement is the same as described by *Mechtly et al.* [1967]. The results of the rocket measurement are also shown, on the traced line, in Figure 5.15 [*E. A. Mechtly*, private communication]. As can be observed on Figure 5.15, the profile numbers 1 and 2, taken at 11:40 and 11:58 hours are lower than the profile numbers 3 and 4 taken at 12:12 and 12:30 hours. This difference is the consequence of a small flare, that occurred after 12:00 and was strong enough to change the ionization of the *D* region. Comparison of the rocket profile with partial-reflection profile number 4 shows good agreement above 79 km, with a difference in height between the two profiles of approximately 1.5 km, which is less than the precision of the partial-reflection measurements.

Below 72 km, the profiles will also be in good agreement if the partial-reflection profile is lowered by 3 km. Between 72 and 79 km, however, there is a complete disagreement. There is no explanation for such disagreement, unless the rocket profile suffered the influence of a sudden change in the solar X-ray radiation due to the flare cited above, and that this influence did not appear completely on the partial-reflection measurement, because this measurement was the result of an average over 12 minutes. The Solrad 9 satellite reported a flux of 1.0×10^{-3} erg. cm^{-2} s^{-1}, dropping rapidly, for the range of 1-8 Å, at 12:35. At 13:10 this flux dropped to 4×10^{-4} erg. cm^{-2} s^{-1}.

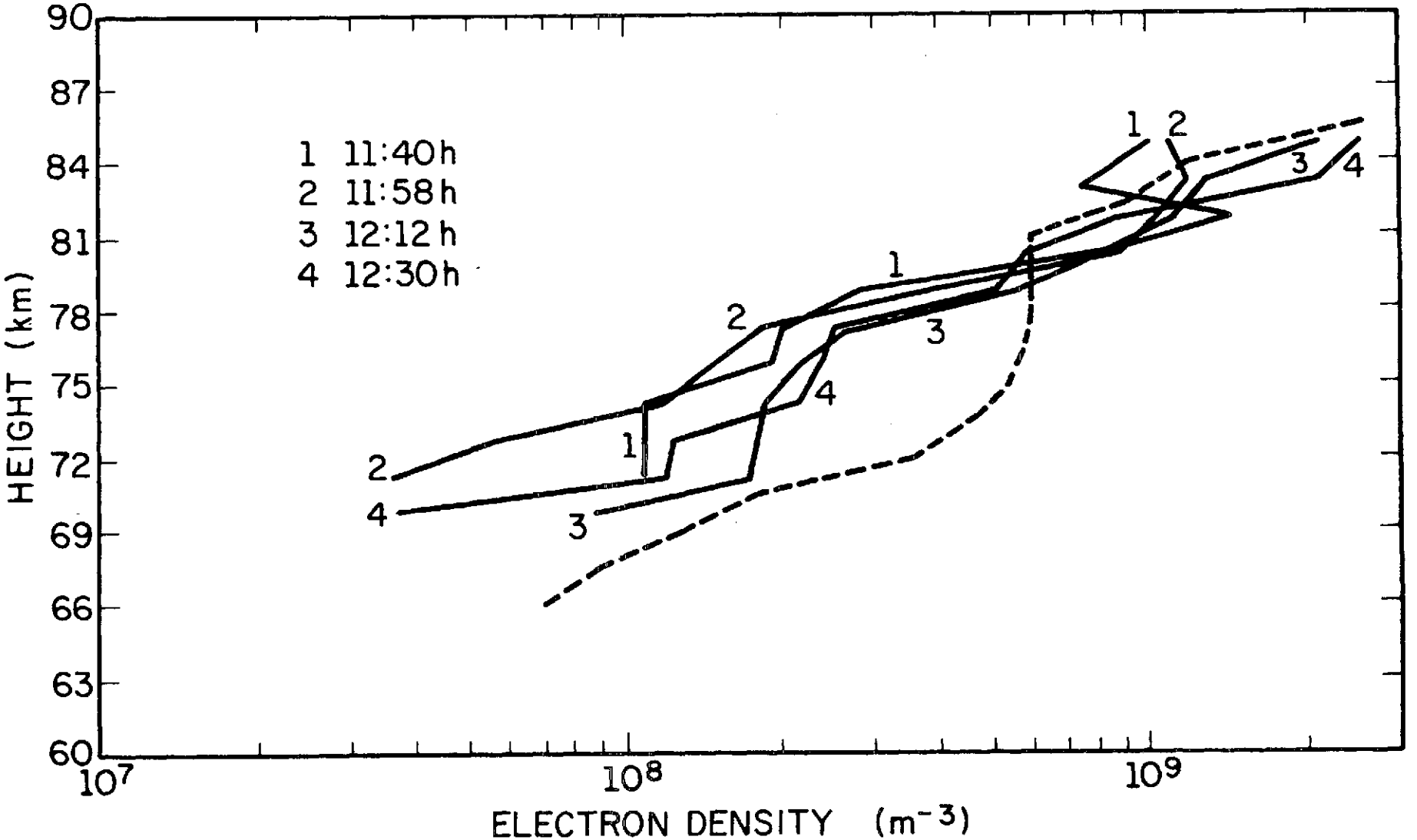

Figure 5.15 Electron-density profiles obtained from partial-reflection measurements (full line) and rocket measurements (traced line) at Wallops Island, Virginia, on January 31, 1972.

It should be noticed that no ground measurement made on January 31 indicated a day of high absorption, including the vertical absorption at 1.8 MHz. Finally, it is interesting to observe that the electron densities obtained by the rocket between 72 and 79 km are very high even for a day of high absorption.

In Figure 5.16, the profile shown in full line was obtained by taking at each height the maximum electron density measured by rockets on previous days of high absorption [*Mechtly et al.*, 1973; *Sechrist et al.*, 1969]. In traced line is the rocket profile obtained on January 31.

Between 72 and 75 km, the profile on January 31 is higher than any one obtained previously in high absorption days. The gradient in electron density, however, appears between 82 and 84 km, and not below 80 km, as normally happens on high absorption days. Such features suggest the influence of X-ray radiation on the ionization between 72 and 78 km.

5.4 *Measurements of Reflection Coefficients*

Since the gain of the antenna, approximately 16 dB, and the gain of the receiver were measured, it was possible to determine the values of the reflection coefficient as a function of height. The expression to determine the reflection coefficient is the following:

$$R_o = 10 \log(A_o^2/50) + L_a + L_p + L_h - G_a - P_t \qquad (5.1)$$

where R_o is the reflection coefficient for the ordinary mode, $(A_o^2/50)$ is the power at the input of the receiver, L_a is the ionospheric absorption, L_p is the path loss, L_h is the ohmic loss in the cables between the transmitter and the antenna and between the antenna and the receiver, G_a is the

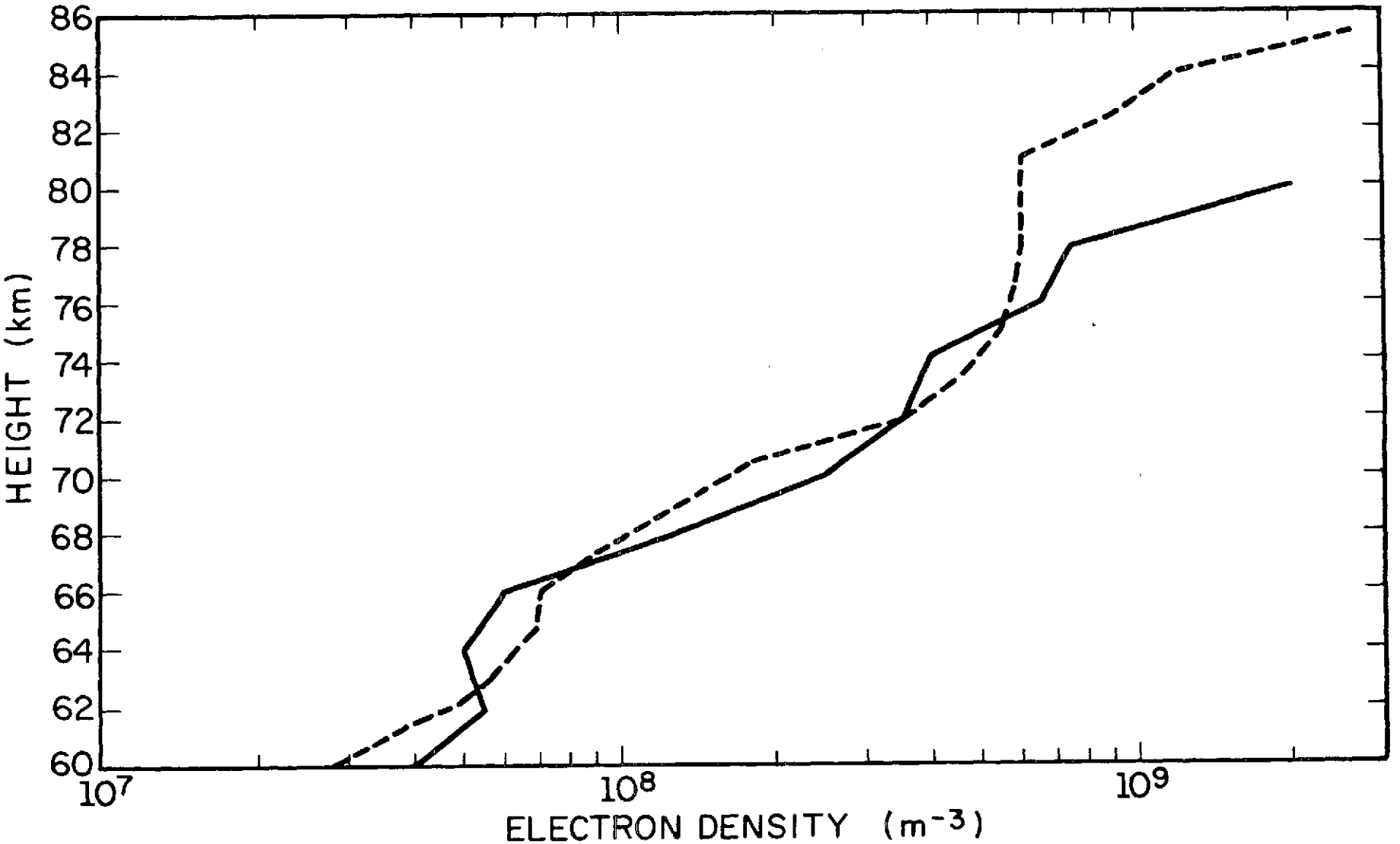

Figure 5.16 Electron-density profiles obtained by rocket measurement on January 31, 1972 (traced line), and by taking the maximum electron density at each height from previous measurements [*Sechrist et al.*, 1969; *Mechtly et al.*, 1972].

antenna gain and P_t is the transmitted power, all the above quantities given in dB.

The calculated R_o is the average reflection coefficient over a height interval of 7.5 km, since 50 μsec pulses were used on the measurements. Figure 5.17 shows the reflection coefficient profiles for the ordinary mode, measured on December, 1971, in two days of high absorption (Dec. 12 at 11:55 and Dec. 13 at 12:35), one day of low absorption (Dec. 15, 12:50) and one day of medium absorption (Dec. 19, 11:50). It can be observed that high absorption corresponds to higher reflection coefficients. The reflection coefficient at 69 km, for example, is approximately four times greater on December 3 than December 15. Near 80 km the reflection coefficient shows a steep gradient, that corresponds to the gradient in electron density at the same heights. On the high absorption day this gradient appeared at a height 4 km lower than on low absorption day.

Figure 5.18 shows the reflection coefficient profiles, for the ordinary mode, on several days of January 1972. It is observed a rather large variation of the reflection coefficient at a given height, for different days. At 75 km, for example, the reflection coefficient on January 7 at 11:25 was 3.5 times greater than on January 25 at 11:35.

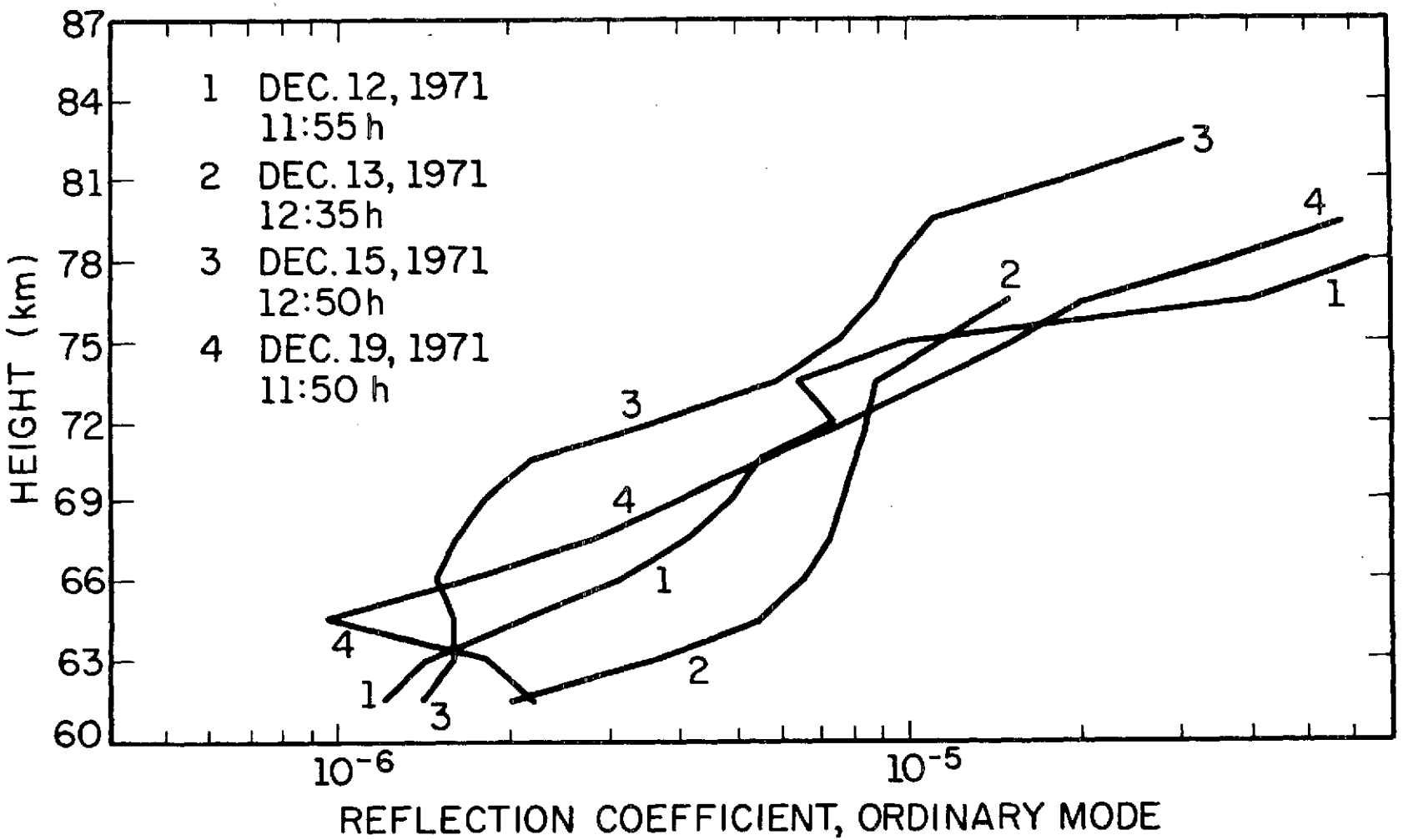

Figure 5.17 Reflection coefficient profiles for the ordinary mode, measured during the month of December, 1971.

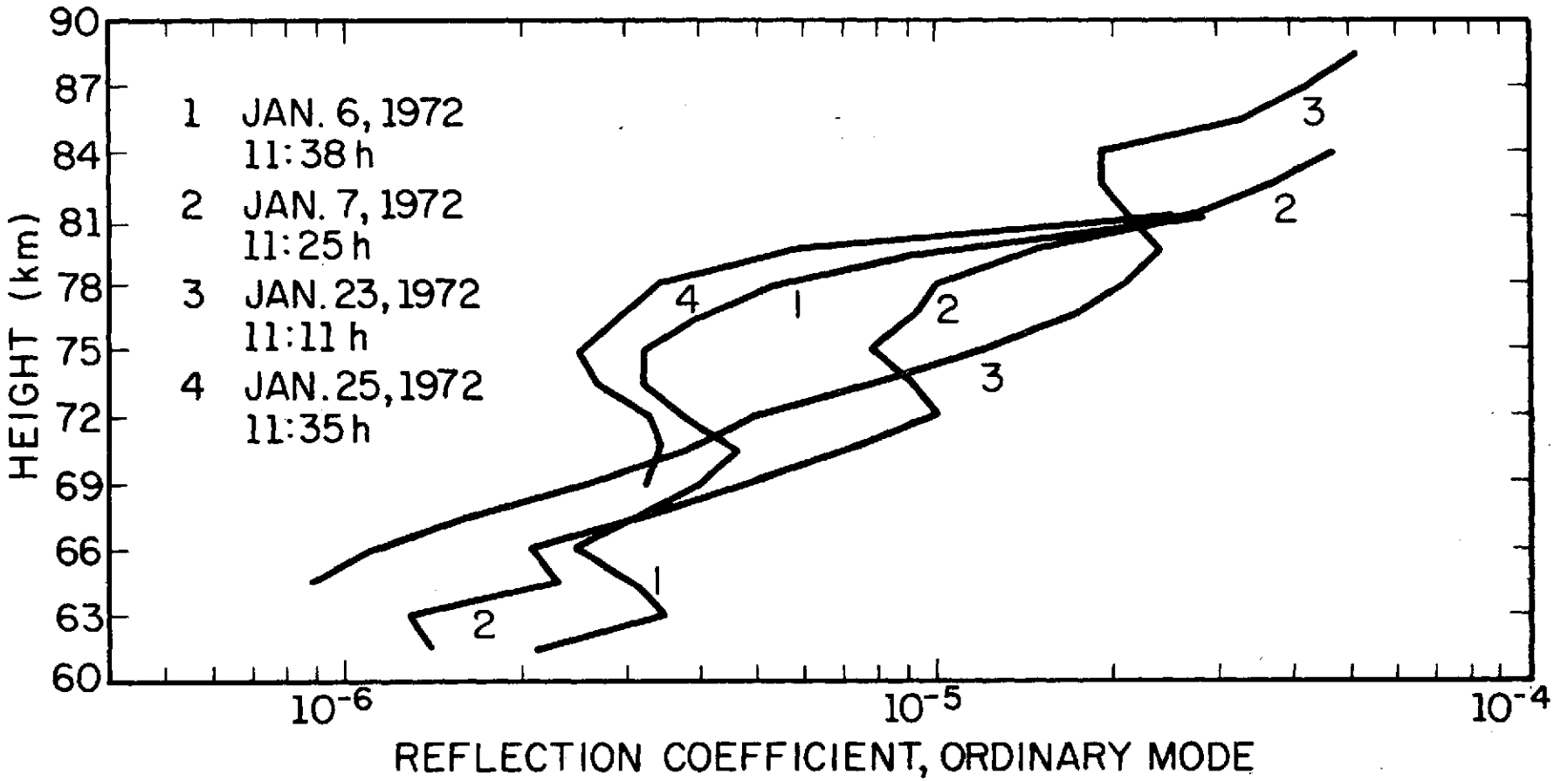

Figure 5.18 Reflection coefficient profiles for the ordinary mode, measured during the month of January, 1972.

6. CONCLUSIONS AND SUGGESTIONS FOR FURTHER WORK

6.1 *Conclusions*

The main objectives of the present work were to analyze the validity of the scattering theories and signal processing methods used in partial-reflection measurements, to suggest possible improvements, and to execute reliable measurements of the *D* region during the winter of 1971-1972.

In Chapter 4 partial reflections were studied for a region where the scattering cross section changes rapidly with height. Such a situation happens in the *D* region near 80 km altitude, at the same heights where electron-density profiles measured by rockets show a steep gradient. Figures 4.4 to 4.6 show A_o profiles measured during the month of August, 1971, where large gradients are observed between 75 and 80 km. The electron-density profiles corresponding to the A_o profiles of Figures 4.4 to 4.6 are shown in Figures 4.1 to 4.3. It is observed that at the heights where the A_o profiles change rapidly with height there appear valleys in the electron-density profiles. Such valleys cannot be considered as real, but a consequence of the finite pulse width of the transmitted pulses and of the changes of the scattering cross section with height. In Section 4.1, it was shown that in a region where the electron-density profile is a constant, but the scattering cross section changes with height, partial-reflection measurements will produce fictitious valleys in the electron-density profile, as shown in Figures 4.10, 4.11 and 4.13. Comparison of the model calculations of Figures 4.10, 4.11 and 4.13 with the measured profiles of Figures 4.1 to 4.3 shows a great similarity in the observed valleys. The corresponding A_o profiles show the same similarity.

Two possible mechanisms of reflection that can be responsible for the gradients in scattering cross section near 80 km were analyzed in Chapter 4:

reflections produced by gradients in electron density and by random irregularities with a locally homogeneous background medium. Reflections produced by gradients in electron density were analyzed in Section 4.2. The calculated reflection coefficient for a gradient similar to that observed on rocket profiles was 5.4×10^{-6}. Measured reflection coefficients, shown in Figures 5.25 to 5.29 are of the order of 10^{-5} near 80 km. This result indicates that at such heights the reflections are at least partially produced by gradients in electron density. The magnitude of the reflection coefficient near 60 km indicates that at low altitudes the gradients are also an important factor in the production of reflections. Further evidences of reflections produced by gradients in electron density are also presented in Chapter 2, Table 2.1, that shows that the correlation coefficient between A_o signals, 1.5 or 3.0 km apart, increases with height above 75 km, and is very high above 82 km, and in Chapter 4, Figures 4.18 and 4.19, that shows that the number of reflections observed at each height is a maximum near 80 km, and in Figures 4.4 and 4.6 that show that at the same heights where gradients in electron density are observed there is a sharp increase in the A_o profiles. Reflections produced by gradients in electron density can explain the existence of preferred heights of reflections, frequently observed in previous measurements, and confirmed in the measurements made at the University of Illinois

The dependence of the reflection coefficient on the size of the reflector, shown in Figure 4.15, indicates that resonances can appear, and that they are not the same for the ordinary and extraordinary modes. To overcome the influence of such resonances, a large number of samples (at

least 500) must be used in the calculation of one electron-density profile, and all samples must be used, without rejecting signals with low signal-to-noise ratio or signals that reached the saturation of the receiver. In case of saturation, the data cannot be used. The result of rejecting part of the received data is shown in Figure 4.17.

Reflections produced by random irregularities in a locally homogeneous background medium were discussed in Section 4.3. An expression of the scattering cross section for such a medium was developed and is presented in expression (4.74). Application of the developed expression to partial-reflection calculations shows that the measured electron density will depend on the power spectrum of the irregularities, at higher altitudes. Calculations of electron-density profiles, assuming that the real profile is that shown in Figure 4.26, for different power spectrums, are shown in Table 4.2. If the spectrum is a Gaussian spectrum with a correlation distance greater than 50 m, serious errors can be committed in partial-reflection measurements, producing fictitious valleys.

Possible contributions of random reflections to partial reflections near 80 km are discussed in Section 4.3.3. It is concluded that if the power spectrum is a Gaussian spectrum with a correlation distance less than 50 m, fluctuations of electron density of only 0.1 percent will be enough to produce reflections of the same order of magnitude of the observed ones.

The effects discussed above will be minimized if narrow pulses are used in the measurements. As a consequence, pulses with a period of 25 μsec or less are recommended. Besides reducing the pulse width, two possible improvements in the signal processing methods are discussed in

Section 4.5. The first one is to deconvolute the A_o and A_x profiles. In the attempts made during the present work no reliable result was obtained from deconvolution. The second one is to use only maximums of the A_o and A_x profiles at each height in the calculations of electron density. Figure 4.28 shows two electron-density profiles obtained from the same data, by using only maximums of the A_o and A_x profiles, or by averaging the signals at heights separated by 1.5 km. The two methods can produce quite different results.

Based on the theoretical studies described above, the partial-reflection system of the University of Illinois was set up to execute measurements of the *D* region during the winter 1971-1972. The results are presented in Chapter 5. The month of December, 1971 was characterized by a periodic variation of the absorption, with a period of approximately 6 days, and by a large difference between the absorption of a low and a high absorption day. In the days of high absorption there was an increase of electron density all over the *D* region, down to 63 km. During the months of January and February, 1972 , the behavior of the *D* region was quite different. The daily variations of absorption were small, and no day of high absorption was observed. The variations of ionization were closely correlated to variations in geomagnetic activity. Comparison between rocket and partial-reflection measurements made on January 31, 1973, shows good agreement between 78 and 84 km, but between 72 and 78 km the measurements did not agree. Possible influence of ionization by X-rays on the rocket measurement was suggested as a possible cause for this discrepancy. Measurements of the reflection coefficient, shown in Figures 5.17 and 5.18 indicate that its value changes on an average from 10^{-6} at 60 km to 10^{-5} at 80 km. Above 80 km a strong gradient is observed.

Measurements of electron density during sunrise, made on October 1971, at Urbana, Illinois show that strong reflections, probably produced by gradients in electron density, are observed from the *C* layer. Reflections from the *C* layer permitted the measurement of collision frequency at lower altitudes. At 63 km, a value of 2.0×10^{7} s^{-1} was obtained.

6.2 *Suggestions for Further Work*

For the improvement of the partial-reflection technique, a better understanding of the nature of the irregularities must be acquired. Statistical studies of the reflections can produce useful information. Direct measurements by rockets carrying current probes, designed to measure both the background electron density and the fluctuations, is another source of information.

The scattering theory developed in Chapter 4 should be extended to include an arbitrary geometry of the background medium, and not only a linear variation, as considered here.

Measurements made simultaneously with different pulse widths should be made frequently, in order to verify the influence of the measured pulse width on the measured profiles. Pulse widths of less than 25 μsec should be included in the measurements.

Techniques for deconvoluting the A_x and A_o profiles should be improved. Comparative analysis of profiles obtained by taking only maximums of the A_o and A_x profiles, or by taking averages at heights separated by 1.5 km should be made.

Simultaneous rocket and partial-reflection measurements on days of high absorption, when normally valleys are observed on the partial-reflection measurements, would permit a better study of the causes of existence of such valleys.

REFERENCES

Aikin, A. C. (1972), Ionization sources of the ionospheric *D* and *E* region, *Aeron. Rep. 48*, Aeron. Lab., Dep. Elec. Eng., Univ. Ill., Urbana-Champaign, 96-103.

Appleton, E. V. (1937), Regularities and irregularities in the ionosphere, *1, Proc. Royal Soc.*, A 162-451.

Appleton, E. V. and W. R. Piggott (1948), Ionospheric absorption measurements throughout a sunspot cycle, *Proc. Int. Scient. Radio Union 7*, 320.

Austin, G. L. (1971), A direct measuring differential phase experiment, *J. Atmos. Terr. Phys. 33*, 1667-1674.

Austin, G. L., G. T. Bennett and M. R. Thrope (1969), The phase of waves partially reflected from the lower ionosphere (70-120 km), *J. Atmos. Terr. Phys. 31*, 1099-1106.

Barth, C. A. (1966), Nitric oxide in the upper atmosphere, *Annls. Geophys. 22*, 198-207.

Bartman, F. L., L. W. Chany, L. M. Jones and V. C. Liu (1956), Upper-air density and temperature by the falling-sphere method, *J. Appl. Phys. 27*, 706-712.

Belrose, J. S. (1966), *Electron-density profiles in ionosphere and exosphere*, North-Holland, Amsterdam, 48.

Belrose, J. S. (1970), Radio wave probing of the ionosphere by partial reflection of radio waves (from height below 100 km), *J. Atmos. Terr. Phys. 32*, 567-596.

Belrose, J. S. (1971), Paper presented at the COSPAR Symposium on *D*- and *E*-Region Ion Chemistry, Urbana, Illinois, July 6-8.

Belrose, J. S. and M. J. Burke (1964), Study of the lower ionosphere using partial reflection, *J. Geophys. Res. 69*, 2799-2818.

Birley, M. H. and C. F. Sechrist, Jr. (1971), Partial-reflection data collection and processing using a small computer, *Aeron. Rep. 42*, Aeron. Lab., Dep. Elec. Eng., Univ. Ill., Urbana-Champaign.

Blamont, J. E. and C. De Jager (1961), Upper atmospheric turbulence near the 100 km level, *Ann. Geophys. 17*, 134-144.

Blamont, J. E. and T. M. Donahue (1964), The sodium dayglow: observation and interpretation of a large diurnal variation, *J. Geophys. Res. 69*, 4093-4127.

Booker, H. G. (1959), Radio scattering in the lower ionosphere, *J. Geophys. Res. 64*, 2164-2177.

Bossolasco, M. and A. Elena (1963), Absorption de la couche *D* et température de al mesosphefe, *C. R. Acad. Sci.*, Paris 256, 4491-4493.

Bowhill, S. A. (1969), *D*-region morphology and processes, *Aeron. Rep. 32*, Aeron. Lab., Dep. Elec. Eng., Univ. Ill., Urbana-Champaign, 12-17.

Budden, K. G. (1960), *Radio Waves in the Ionosphere*, Cambridge University Press.

Burke, M. J. and E. H. Hara (1963), Tables of semiconductor integrals $C_p(x)$ and their approximations for use with the generalized Appleton-Hartree formulas, *Defense Res. Board DRTE Rept. 1113*, Ottawa, Canada.

Carver, J. H., B. H. Horton and F. G. Burger (1966), Nocturnal ozone distribution in the upper atmosphere, *J. Geophys. Res. 71*, 4189-4191.

Cohen, J. C. (1971), Modeling the *D* region partial reflection experiment, *Sci. Rep. 378*, Ionospheric Res. Lab., Pennsylvania State Univ.

Collin, R. E. (1966), *Foundation for Microwave Engineering*, Mc Graw-Hill, Inc.

Connolly, D. J. and B. S. Tenenbaum (1972), Mode coupling in partial reflections from the ionosphere at vertical incidence, *Radio Sci. 7*, 457-464.

Coyne, T. N. R. and J. S. Belrose (1973), An investigation into the effects of limited height resolution in the differential-absorption partial-reflection experiment, *J. Geophys. Res. 78*, 8276-8288.

Davies, K. (1965), Ionospheric radio propagation, *National Bureau of Standards, Monograph 80*.

Dieminger, W. (1952), Uber dis ursache der excessiven absorption in der ionosphare an Wintertagen, *J. Atmos. Terr. Phys. 2*, 304-349.

Donahue, T. M. (1972), Positive-ion chemistry of the *D* and *E* regions, *Radio Sci. 7*, 73-80.

Donahue, T. M. and R. Meier (1967), Distribution of sodium in the daytime upper atmosphere as measured by rocket experiment, *J. Geophys. Res. 72*, 2803-2829.

Faucher, G. A., R. W. Procunier and F. S. Sherman (1963), Upper-atmosphere density obtained from measurements of drag on a falling sphere, *J. Geophys. Res. 68*, 3437-3450.

Faucher, G. A., J. F. Morrissey and C. N. Stark (1967), Falling sphere density measurements, *J. Geophys. Res. 72*, 299-305.

Fehsenfeld, F. C. and E. E. Ferguson (1969), Origin of water-cluster ions in the *D* region, *J. Geophys. Res. 74*, 2217-2222.

Fejer, J. A. (1970), Radio wave probing of the lower ionosphere by cross-modulation techniques, *J. Atmos. Terr. Phys. 32*, 597-607.

Ferguson, E. E. and F. C. Fehsenfeld (1969), Water vapor ion cluster concentrations in the *D* region, *J. Geophys. Res. 74*, 5743-5751.

Flood, W. A. (1968), Revised theory for partial reflection *D*-region measurements, *J. Geophys. Res. 73*, 5585-5598.

Fraser, G. J. and R. A. Vincent (1970), A study of *D*-region irregularities, *J. Atmos. Terr. Phys. 32*, 1591-1607.

Gallet, R. M. (1955), Aerodynamical mechanisms producing electronic density fluctuations in turbulent ionized layers, *Proc. IRE 43*, 1240-1252.

Gardner, F. F. and J. L. Pawsey (1953), Study of the ionospheric *D* region using partial reflections, *J. Atmos. Terr. Phys. 2*, 321-344.

Geisler, J. E. and R. E. Dickinson (1968), Vertical motions and nitric oxide in the upper atmosphere, *J. Atmos. Terr. Phys. 30*, 1205-1521.

Geller, M. A. and C. F. Sechrist, Jr. (1971), Coordinated rocket measurements on the *D*-region winter anomaly II. Some implications, *J. Atmos. Terr. Phys. 33*, 1027-1040.

Greenhow, J. S. and E. L. Neufeld (1959), Measurements of turbulence in the 80-100 km region from radio echo observations of meteors, *J. Geophys. Res. 64*, 2129.

Gregory, J. B. (1961), Radio wave reflections from the mesosphere, *J. Geophys. Res. 66*, 429-445.

Gregory, J. B. (1965), The influence of atmospheric circulation on mesospheric electron density, *J. Atmos. Sci. 22*, 217.

Grisson, J. T., D. R. Koehler and B. G. Gibbs (1966), Spectral information and the experimental resolution problem, *Nuclear Instruments and Methods 45*, 190-196.

Hale, L. C., D. P. Hoult and D. C. Baker (1968), A summary of blunt probe theory and experimental results, *Space Res. 8*, 320-331.

Hays, P. B., R. G. Roble and A. N. Shah (1972), Terrestrial atmospheric composition from stellar occultations, *Science 17b*, 793-794.

Henry, G. W., Jr. (1966), Instrumentation and preliminary results from shipboard measurements of vertical incidence ionospheric absorption, *Aeron. Rep. 13*, Aeron. Lab., Dep. Elec. Eng., Univ. Ill., Urbana-Champaign.

Huffman, R. E., P. E. Paulsen, J. C. Larrafee and R. B. Cairns (1971), Decrease in the $O_2(^1\Delta_g)$ photoionization rates resulting from CO_2, absorption, *J. Geophys. Res. 76*, 1028-1038.

Johnson, F. S., J. D. Purcell, R. Tousey and K. Watanabe (1952), Direct measurements of the vertical distribution of atmospheric ozone to 70 km altitude, *J. Geophys. Res. 57*, 156-176.

Krankowsky, D., F. Arnold, H. Wider, J. Kissel and J. Zähringer (1972), Positive-ion chemistry in the lower ionosphere, *Radio Sci. 7*, 93-98.

La Gow, H. E., R. Horowitz and J. Ainsworth (1959), Arctic atmospheric structure to 250 km, *Planet. Space Sci. 2*, 33-38.

Lighthill, M. J. (1960), Studies of magneto-hydrodynamic waves and other anisotropic wave motions, *Philos. Trans. Roy. Soc.*, London, A353, 397-430.

Liu, C. H. (1967), Wave propagation in a random medium with parabolic background, *Radio Sci.*, 961-976.

Maehlum, B. (1967), On the 'winter anomaly' in the midlatitude *D* region, *J. Geophys. Res. 72*, 2287-2297.

Mandel'stam, S. L. (1965), X-ray emission of the sun, *Space Sci. Rev. 4*, 587-665.

Manson, A. H., M. W. J. Merry and R. A. Vincent (1969), The relationship between the partial reflection of radio waves from the lower ionosphere and irregularities as measured by rocket probes, Paper presented at the 12th Plenary Meeting of COSPAR, Prague, Czechoslovakia.

Mechtly, E. A. and L. G. Smith (1968), Seasonal variation of the lower ionosphere at Wallops Island during the IQSY, *J. Atmos. Terr. Phys. 30*, 1555-1561.

Mechtly, E. A., S. A. Bowhill, L. G. Smith and H. W. Knoebel (1967), Lower ionosphere electron concentration and collision frequency from rocket measurements of Faraday rotation, differential absorption and probe current, *J. Geophys. Res. 72*, 5239-5245.

Mechtly, E. A., L. G. Smith and G. W. Henry (1973), Rocket observations of the winter anomaly, Paper presented at the 16th Plenary Meeting of COSPAR, Konstanz, F.R.G., May 1973.

Meira, L. G. (1971), Measurements of upper atmospheric nitric oxide and their consequences to the lower ionosphere, *J. Geophys. Res. 76*, 175-179.

Miller, D. E. and R. Ryder (1973), Measurement of the ozone concentration from 55 to 95 km at sunset, *Planet. Space Sci. 21*, 963-970.

Mitchell, J. D., L. C. Hale, R. O. Olsen, J. Randhawa and R. Rubio (1972), Positive ions and the winter anomaly, *Radio sci. 7*, 175-179.

Montbriand, L. E. and J. S. Belrose (1972), Effective electron loss rates in the lower *D* region during the decay of solar flare X-ray flare events, *Radio Sci. 7*, 133-142.

Narcisi, R. S. and A. D. Bailey (1965), Mass spectrometric measurements of positive ions at altitudes from 64 to 112 kilometers, *J. Geophys. Res. 70*, 3687-3700.

Narcisi, R. S., A. D. Bailey, L. E. Wlodyka and C. R. Philbrick (1972), Ion composition measurements in the lower ionosphere during the November 1966 and March 1970 solar eclipses, *J. Atmos. Terr. Phys. 34*, 647-658.

Nicolet, M. and A. C. Aikin (1960), The formation of the *D* region of the ionosphere, *J. Geophys. Res. 65*, 1469-1483.

Pearce, J. B. (1969), Rocket measurement of nitric oxide between 60 and 96 km, *J. Geophys. Res. 74*, 853-861.

Piggott, W. R. and E. V. Thrane (1966), The effect of irregularities in collision frequency on the amplitude of weak partial reflections, *J. Atmos. Terr. Phys. 28*, 311-314.

Pirnat, C. R. and S. A. Bowhill (1968), Electron densities in the lower ionosphere deduced from partial reflection measurements, *Aeron. Rep. 29*, Aeron. Lab., Dep. Elec. Eng., Univ. Ill., Urbana-Champaign.

Rarick, J. P. (1969), Deconvolution of physical data, *Scientific Rep. 344*, Ionosphere Res. Lab., Pennsylvania State Univ.

Reed, E. I. (1968), A night measurement of mesospheric ozone by observations of ultraviolet airglow, *J. Geophys. Res. 73*, 2951-2957.

Reid, G. C. (1970), Production and loss of electrons in the quiet daytime *D* region of the ionosphere, *J. Geophys. Res. 75*, 2551-2562.

Ritchie, R. H. and V. E. Anderson (1966), The use of Fourier transforms in the unfolding of experimental data, *Nuclear Instruments and Methods 45*, 277-281.

Sechrist, C. F., Jr. (1970), Interpretation of *D*-region electron densities, *Radio Sci. 5*, 663-671.

Sechrist, C. F., Jr. (1974), Comparisons of techniques for measurement of *D*-region electron densities, *Radio Sci. 9*, 137-149.

Sechrist, C. F., Jr., E. A. Mechtly and J. S. Shirke (1969), Coordinated rocket measurements on the *D*-region winter anomaly - I. Experimental results, *J. Atmos. Terr. Phys. 31*, 145-153.

Seddon, J. C. (1953), Propagation measurements in the ionospheric with the aid of rockets, *J. Geophys. Res. 58*, 323-335.

Sen, H. K. and A. A. Wyller (1960), Generalization of the Appleton-Hartree magnetoionic formulas, *J. Geophys. Res. 65*, 3931-3950.

Simonich, D. M. and K. C. Yeh (1971), Radio wave scattering from random fluctuations in an anisotropic medium, *Tech. Rep. 42*, Ionosphere Radio Lab., Univ. Ill., Urbana-Champaign.

Stone, H. (1962), Mathematical resolution of overlapping spectral lines, *J. Optical Soc. Am. 52*, 998-1003.

Strobel, D. F. (1972), Minor neutral constituents in the mesosphere and lower thermosphere, *Radio Sci. 7*, 1-21.

Stroud, W. G., W. Nordberg, W. P. Bandeen, F. L. Bartman and P. Titus (1960), Rocket-grenade measurements of temperatures and winds in the mesosphere over Churchill, Canada, *J. Geophys. Res. 65*, 2307-2323.

Tatarski, V. I. (1961), *Wave Propagation in a Turbulent Medium*, Dover Publications, Inc., New York.

Thomas, L. (1974), Recent developments and outstanding problems in the theory of the *D* region, *Radio Sci. 9*, 121-136.

Von Biel, H. A. (1971), Amplitude distribution of *D*-region partial reflections, *J. Geophys. Res. 76*, 8365-8367.

Von Biel, H. A., W. A. Flood and H. G. Camnitz (1970), Differential phase partial-reflection technique for the determination of *D*-region ionization, *J. Geophys. Res. 75*, 4863-4870.

Webber, W. (1962), The production of free electrons in the ionospheric *D* layer by solar and galactic cosmic rays and the resultant absorption of radio waves, *J. Geophys. Res. 67*, 5091-5106.

Weeks, L. H. and L. G. Smith (1968), A rocket measurement of ozone near sunrise, *Planet. Space Sci. 16*, 1189-1195.

Westcott, C. H. (1948), Transmission-line bridge, *Wireless Eng.*, 215-220.

Zimmerman, S. P. (1965), Turbulent atmospheric parameters by contaminant deposition, *J. App. Meteor.*, 279.

APPENDIX I. SIMPLIFICATION OF THE SCATTERED ELECTRIC FIELD

Let's take equation (4.53), that is repeated below:

$$\vec{E}_1 = -k_0^2 n(0)\ \frac{\exp(ikn(0)R)}{2\pi R}\ \vec{A}_o\ \int_v n_1(\vec{R}) n(h')^{1/2}\ \exp\{ik_0 \int_0^{h'} \bar{n}(h)dh\}\ \cdot$$

$$\exp\{-ik\bar{n}(0)\vec{m}\cdot\vec{R}'\}\ \cdot\ \exp\{ik_0 \int_0^{h'} [\bar{n}(h)-\bar{n}(0)]dh\}dv' - \frac{n(0)\exp(ik_0 n(0)R)}{2\pi R}\ \cdot$$

$$\cdot \int_{v'} \nabla\{\bar{n}(h')^{1/2}\ \exp[ik_0 \int_0^{h'} [\bar{n}(h)dh]\ \vec{A}_o\cdot\nabla \ln(n_1(\vec{R}'))\}\ \cdot\ \exp\{-ik_0\bar{n}(0)\vec{m}\cdot\vec{R}'\}\cdot$$

$$\cdot\ \exp\{ik_0 \int_0^{h'} [\bar{n}(h)\ -\ \bar{n}(0)]dh\}dv' \quad . \quad . \quad . \quad . \quad . \quad . \quad . \qquad (1.A)$$

Applying Gauss' theorem to the second term of the second member of equation (1.A) it results:

$$\vec{E}_1' = -k_0^2\bar{n}(0)\ \frac{\exp(ik_0\bar{n}(0)R)}{2\pi R}\ \vec{A}_o\ \int_{v'} n_1(\vec{R}')\bar{n}\ h')^{1/2}\ \exp\{ik_0 \int_0^{h'} \bar{n}(h)dh\}\ \cdot$$

$$\exp\{-ik_0 n(0)\vec{m}\ \vec{R}'\}\{ik_0 \int_0^{h'} [\bar{n}(h)\ -\ \bar{n}(0)]dh\}dv$$

$$+\ \bar{n}(0)\ \frac{\exp(ik_0 n(0)R)}{2\pi R} \int_v \{k_0\vec{m}\ \bar{n}(0) + [\bar{n}(h')\ -\ \bar{n}(0)]\}\ \cdot\ \bar{n}(h')^{-1/2}$$

$$\cdot\ \exp[ik_0 \int_0^{h'} \bar{n}(h)dh]\ \vec{A}_o\ \cdot\ \nabla \ln(n(R'))\ \cdot\ \exp\{-ik_0\bar{n}(0)\vec{m}\cdot\vec{R}'\}$$

$$\cdot\ \exp[ik_0 \int_0^{h'} [\bar{n}(h)\ -\ \bar{n}(0)]dh\}dv' \quad . \quad . \quad . \quad . \quad . \qquad (2.A)$$

Taking $\bar{n}(h') - \bar{n}(0) << 1$, equation (2.A) can be written as:

$$\vec{E}_1 = -k_0^2 n(0) \frac{\exp(ik_0 n(0)R)}{2\pi R} C_1 \vec{A}_o + ik\, n(0)^2 \frac{\exp(ik_0 n(0)R)}{2\pi R} C_2\, \vec{m} \tag{3.A}$$

Where

$$C_1 = \int_{v'} n_1(\vec{R}')\, \bar{n}(h')^{1/2} \exp\{ik_0 \int_0^{h'} \bar{n}(h)dh\} \cdot \exp\{-ik_0 n(0)\vec{m}\cdot\vec{R}'\}$$
$$\cdot \exp\{ik_0 \int_0^{h'} [\bar{n}(h) - \bar{n}(0)]dh\}dv' \tag{4.A}$$

$$C_2 = \int_{v'} \bar{n}(h')^{-1/2} \exp\{ik_0 \int_0^{h} \bar{n}(h)dh\} \cdot \exp\{-ik_0 \bar{n}(0)\vec{m}\cdot\vec{R}'\}$$
$$\exp\{ik_0 \int_0^{h'} [\bar{n}(h) - \bar{n}(0)]dh\} \cdot \vec{A}_o \cdot \nabla \ln(n(\vec{R}'))dv' \tag{5.A}$$

Applying Gauss' theorem to equation (5.A), it results:

$$C_2 = -ik_0(0)\, \vec{A}_o \cdot \vec{m} \int \bar{n}(h')^{-3/2}\, n(R') \exp\{ik_0 \bar{n}(0)\vec{m}\, \vec{R}'\} \cdot$$
$$\exp\{ik_0 \int_0^{h'} [\bar{n}(h) - \bar{n}(0)]dh\} \tag{6.A}$$

where it was assumed $\nabla \ln(n_1(\vec{R}')) = \nabla \ln[\bar{n}(h')\,(1 + \frac{\bar{n}_1(\vec{R}')}{\bar{n}(h')})] \cong \frac{1}{\bar{n}(h')} \nabla n_1(R')$

Substituting this expression on equation (3.A), and taking $\bar{n}(h')^{-3/2} \cong \bar{n}(h')^{1/2} \cdot \bar{n}(0)^{-2}$ the following expression is obtained for E_1:

$$E_1 = -k_0^2 n(0) \frac{\exp(k_0 \bar{n}(0) R)}{2\pi R} \vec{A}_o C_1 + \frac{k_0^2 \bar{n}(0)}{} \frac{\exp(ik_0 n(0) R)}{2\pi R} \cdot \vec{m} C_1 (\vec{A}_o \cdot \vec{m}) \qquad (7.A)$$

Equation (7.A) shows that the second term of the second member is longitudinal (direction of m), with same magnitude and in opposite direction to the longitudinal component of the first term of the second member.

APPENDIX II. COMPUTER PROGRAMS AND SUB-ROUTINES

```
C       **********PROAX**********
C       PROAX PRINTS AX/AO AND ELECTRON DENSITY PROFILES BETWEEN
C       60 AND 90 KM. VALUES OF AX AND AO ARE READ FROM DECTAPE.
C       AVERAGE POWER OF ORDINARY AND EXTRAORDINARY SIGNALS AND
C       OF NOISE ARE CALCULATED. THE AVERAGE POWER OF NOISE IS
C       SUBTRACTED FROM THE AVERAGE POWER OF SIGNAL AT EVERY
C       HEIGHT. FRAMES ARE REJECTED IF THE AVERAGE NOISE FOR BOTH
C       AX AND AO EXCEEDS A GIVEN NUMBER, BMXNS. IF THE DIFFERENCE
C       BETWEEN A SAMPLE AT A GIVEN HEIGHT AND THE SAMPLE AT THE
C       SAME HEIGHT IN THE FRAME IMEDIATELLY BEFORE EXCEEDS A VA-
C       LUE RE1 OR RE2, THE SAMPLE AT THAT HEIGHT, 1.5 KM ABOVE,
C       AND 1.5 KM BELOW ARE REJECTED.
C       **********
C
        DIMENSION FNAM(2),AO(21),AX(21),AVAO(21),AVAX(21),
        1XO(21),IRJO(21),IRJX(21),DIFNO(4),DIFNX(4),
        2BO(21),BX(21),BNO(4),BNX(4),BBNO(4),BBNX(4)
10      CALL HEAD(0)
C       INITIAL VALUES
        SNO=0.
        SNX=0.
        IR=0
        IRNO=0
        IRNX=0
        BMO=0.
        BMX=0.
        DO 16 I=1,21
        XO(I)=0.
        AVAO(I)=0.
        AVAX(I)=0.
        AO(I)=0.
        AX(I)=0.
        IRJO(I)=0
16      IRJX(I)=0
        DO 17 I=1,4
        BNO(I)=0.
17      BNX(I)=0.
        CALL VALUE
        CALL DINIT
        WRITE(6,20)
20      FORMAT(15H WHICH DATAFILE)
        READ(4,30)FNAM
30      FORMAT(2A5)
        CALL FSTAT(2,FNAM,LOG)
        IF(LOG.NE.0)GO TO 40
        WRITE(6,35)FNAM
35      FORMAT(6H FILE ,2A5,19H NOT FOUND ON DAT 2)
        GO TO 10
40      WRITE(6,41)
41      FORMAT(24H COLLISION FREQ. PROFILE/
        1 25H SUMMER,WINTER,OR EQUINOX)
        READ(4,42)RESP
42      FORMAT(A5)
        CALL SEEK(2,FNAM)
        WRITE(6,43)
43      FORMAT(14H MAXIMUM NOISE)
        READ(4,44)BMXNS
```

```
44      FORMAT(F10.0)
        WRITE(6,45)
45      FORMAT(21H REJECTION BELOW 72KM)
        READ(4,44)RE1
        WRITE(6,46)
46      FORMAT(21H REJECTION ABOVE 72KM)
        READ(4,44)RE2
        KEOFO=0
        KEOFX=0
        ID=0
50      DO 52 I=1,21
        BO(I)=AO(I)
52      BX(I)=AX(I)
        DO 54 I=1,4
        BBNO(I)=BNO(I)
54      BBNX(I)=BNX(I)
C       DREAD READS 21 VALUES OF SIGNAL, BETWEEN 60 AND 90 KM,
C       AND 4 VALUES OF NOISE TAKEN BETWEEN 45 AND 51 KM
        CALL DREAD(AO,BNO,IERR,ID,KEOFO)
        IF(KEOFO.EQ.1)GO TO 114
        CALL DREAD(AX,BNX,IERR,ID,KEOFX)
        IF(KEOFX.EQ.1)GO TO 112
C       AVERAGE POWER OF NOISE OF THE FRAME
        BMEANO=0.
        BMEANX=0.
        DO 56 I=1,4
        BMEANO=BMEANO+BNO(I)**2
56      BMEANX=BMEANX+BNX(I)**2
        BMEANO=SQRT(BMEANO/4.)
        BMEANX=SQRT(BMEANX/4.)
C       REJECTION OF FRAMES IF AVERAGE NOISE FOR BOTH AO AND AX
C       EXCEEDS A VALUE BMXNS
        IF(BMEANO.GT.BMXNS.AND.BMEANX.GT.BMXNS)GO TO 100
C       CALCULATION OF TOTAL AVERAGE NOISE
        DO 58 I=1,4
        DIFNO(I)=BNO(I)-BBNO(I)
58      DIFNX(I)=BNX(I)-BBNX(I)
        DO 66 I=1,2
        J=I+1
        K=I+2
C       REJECTION OF ORDINARY SAMPLE IF FADING EXCEEDS
C       RE1, OR IF SATURATION IS REACHED
        IF(DIFNO(I).GT.RE1.OR.DIFNO(J).GT.RE1.OR.DIFNO(K).GT.RE1.OR.
        1BNO(J).GT.510..OR.BNX(J).GT.510.)GO TO 60
        BMO=BMO+BNO(J)**2
        GO TO 62
C       NUMBER OR SAMPLES OF ORDINARY NOISE REJECTED
60      IRNO=IRNO+1
        IF(BNO(J).GT.510..OR.BNX(J).GT.510.)GO TO 64
62      IF(DIFNX(I).GT.RE1.OR.DIFNX(J).GT.RE1.OR.DIFNX(K).GT.RE1)
        1 GO TO 64
        BMX=BMX+BNX(J)**2
        GO TO 66
64      IRNX=IRNX+1
66      CONTINUE
68      DO 84 I=1,21
C       REJECTION OF SAMPLE OF ORDINARY SIGNAL IF FADING EXCEEDS
```

```
C       A VALUE RE1 OR RE2, OR IF SATURATION IS REACHED
        J=I+1
        L=I-1
        IF(L.EQ.0)L=1
        IF(J.GT.21)J=21
        DIFE=AO(I)-BO(I)
        DIFEA=AO(L)-BO(L)
        DIFEB=AO(J)-BO(J)
        IF(I.GT.9)GO TO 70
        IF(DIFE.GT.RE1.OR.DIFEA.GT.RE1.OR.DIFEB.GT.RE1.OR.
       1AO(I).GT.510..OR.AX(I).GT.510.)GO TO 74
        GO TO 72
70      IF(DIFE.GT.RE2.OR.DIFEA.GT.RE2.OR.DIFEB.GT.RE2.OR.
       1AO(I).GT.510..OR.AX(I).GT.510.)GO TO 74
C       AVERAGE POWER OF ORDINARY SIGNAL
72      AVAO(I)=AVAO(I)+AO(I)**2
        GO TO 76
C       NUMBER OF SAMPLES OF ORDINARY SIGNAL REJECTED
74      IRJO(I)=IRJO(I)+1
        IF(AO(I).GT.510..OR.AX(I).GT.510.)GO TO 82
76      DIFE=AX(I)-BX(I)
        DIFEA=AX(L)-BX(L)
        DIFEB=AX(J)-BX(J)
        IF(I.GT.9.AND.I.LT.16)GO TO 78
        IF(DIFE.GT.RE1.OR.DIFEA.GT.RE1.OR.DIFEB.GT.RE1)GO TO 82
        GO TO 80
78      IF(DIFE.GT.RE2.OR.DIFEA.GT.RE2.OR.DIFEB.GT.RE2)GO TO 82
80      AVAX(I)=AVAX(I)+AX(I)**2
        GO TO 84
82      IRJX(I)=IRJX(I)+1
84      CONTINUE
        GO TO 110
C       NUMBER OF FRAMES REJECTED DUE TO EXCESSIVE NOISE
100     IR=IR+1
110     SNO=BMEANO**2+SNO
        SNX=BMEANX**2+SNX
        GO TO 50
C       NUMBER OF SAMPLES TAKEN
112     ID=ID-1
114     ID=ID/2
        RID=ID
C       TOTAL NUMBER OF REJECTED SAMPLES AT EACH HEIGHT
        DO 116 I=1,21
        IRJO(I)=IRJO(I)+IR
116     IRJX(I)=IRJX(I)+IR
        IRNO=IRNO+2*IR
        IRNX=IRNX+2*IR
        AVNO=SQRT(SNO/RID)
        AVNX=SQRT(SNX/RID)
        RNO=ID*2-IRNO
        RNX=ID*2-IRNX
C       AVERAGE POWER OF SIGNAL SUBTRACTED FROM THE AVERAGE
C       POWER OF NOISE
        DO 118 I=1,21
        RSAMO=ID-IRJO(I)
        RSAMX=ID-IRJX(I)
        AVOC=AVAO(I)/RSAMO-BMO/RNO
```

```
      AVXC=AVAX(I)/RSAMX-BMX/RNX
      AVAO(I)=(ABS(AVOC)/AVOC)*SQRT(ABS(AVOC))
      AVAX(I)=(ABS(AVXC)/AVXC)*SQRT(ABS(AVXC))
118   CONTINUE
      BMO=SQRT(BMO/RNO)
      BMX=SQRT(BMX/RNX)
      CALL HEAD(1)
      WRITE(6,120)AVNO,AVNX,BMO,IRNO,BMX,IRNX
120   FORMAT(2X,17HAVERAGE NOISE ORD,F8.1/2X,17HAVERAGE NOISE EXT,1X
     1,F7.1//2X,9HNOISE ORD,F8.1,I5,11H REJECTIONS/2X,
     29HNOISE EXT,F8.1,I5,11H REJECTIONS)
      WRITE(6,122)ID,IR
122   FORMAT(//1X,I4,14H SAMPLES TAKEN,5X,I5,16H FRAMES REJECTED//
     19H REJECTED,2X,9H REJECTED,2X,6HHEIGHT,2X,6HAV. AO,2X,
     26HAV. AX/4X,3HORD,8X,3HEXT)
      HT=58.5
      DO 126 I=1,21
      HT=HT+1.5
      WRITE(6,124)IRJO(I),IRJX(I),HT,AVAO(I),AVAX(I)
124   FORMAT(3X,I4,7X,I4,3X,F5.1,3X,F6.1,2X,F6.1)
126   CONTINUE
      CALL HEAD(1)
C     AX/AO RATIOS
      DO 128 I=1,21
      IF(AVAO(I).LE.0.0.OR.AVAX(I).LE.0.0)GO TO 128
      XO(I)=AVAX(I)/AVAO(I)
128   CONTINUE
      MINIT=ID/150
C     AX/AO PROFILE
      CALL PLOTI(XO,1,21,MINIT)
C     CALC CALCULATES AND PRINTS ELECTRON DENSITY PROFILE
      CALL CALC(XO,1,20,RESP)
      GO TO 10
      STOP
      END
```

```
C       **********************PROAXC*********************************
C       PROAXC PRINTS AX/AO AND ELECTRON DENSITY PROFILES AND
C       NUMBER OF MAXIMUMS OBSERVED IN THE REFLECTED SIGNALS
C       AT EACH HEIGHT. THE SIGNAL PROCESSING METHOD IS THE
C       SAME AS USED IN THE PROGRAM PROAX.
C       ************************************************************
C
        DIMENSION FNAM(2),AO(21),AX(21),AVAO(21),AVAX(21),IREJ(21),
        1XO(21),HEIO(21),HEIX(21),IRJO(21),IRJX(21),
        2BO(21),BX(21),BNO(4),BNX(4),BBNO(4),BBNX(4),DIFNO(4),DIFNX(4)
10      CALL HEAD(0)
C       INITIAL VALUES
        SNO=0.
        SNX=0.
        IR=0
        IRNO=0
        IRNX=0
        BMO=0.
        BMX=0.
        DO 16 I=1,21
        HEIO(I)=0.
        HEIX(I)=0.
        XO(I)=0.
        AVAO(I)=0.
        AVAX(I)=0.
        AO(I)=0.
        AX(I)=0.
        IRJO(I)=0
16      IRJX(I)=0
        DO 17 I=1,4
        BNO(I)=0.
17      BNX(I)=0.
        CALL VALUE
        CALL DINIT
        WRITE(6,20)
20      FORMAT(15H WHICH DATAFILE)
        READ(4,30)FNAM
30      FORMAT(2A5)
        CALL FSTAT(2,FNAM,LOG)
        IF(LOG.NE.0)GO TO 40
        WRITE(6,35)FNAM
35      FORMAT(6H FILE ,2A5,19H NOT FOUND ON DAT 2)
        GO TO 10
40      WRITE(6,41)
41      FORMAT(24H COLLISION FREQ. PROFILE/
        1 25H SUMMER,WINTER,OR EQUINOX)
        READ(4,42)RESP
42      FORMAT(A5)
        CALL SEEK(2,FNAM)
        WRITE(6,43)
43      FORMAT(14H MAXIMUM NOISE)
        READ(4,44)BMXNS
44      FORMAT(F10.0)
        WRITE(6,45)
45      FORMAT(21H REJECTION BELOW 72KM)
        READ(4,44)RE1
        WRITE(6,46)
```

```
46      FORMAT(21H REJECTION ABOVE 72KM)
        READ(4,44)RE2
        KEOFO=0
        KEOFX=0
        ID=0
50      DO 52 I=1,21
        BO(I)=AO(I)
52      BX(I)=AX(I)
        DO 54 I=1,4
        BBNO(I)=BNO(I)
54      BBNX(I)=BNX(I)
C       DREAD READS 21 VALUES OF SIGNAL, BETWEEN 60 AND 90 KM,
C       AND 4 VALUES OF NOISE TAKEN BETWEEN 45 AND 51 KM.
        CALL DREAD(AO,BNO,IERR,ID,KEOFO)
        IF(KEOFO.EQ.1)GO TO 114
        CALL DREAD(AX,BNX,IERR,ID,KEOFX)
        IF(KEOFX.EQ.1)GO TO 112
C       AVERAGE POWER OF NOISE OF THE FRAME
        BMEANO=0.
        BMEANX=0.
        DO 56 I=1,4
        BMEANO=BMEANO+BNO(I)**2
56      BMEANX=BMEANX+BNX(I)**2
        BMEANO=SQRT(BMEANO/4.)
        BMEANX=SQRT(BMEANX/4.)
C       REJECTION OF FRAMES IF AVERAGE NOISE FOR BOTH AO AND AX
C       EXCEEDS A VALUE BMXNS
        IF(BMEANO.GT.BMXNS.AND.BMEANX.GT.BMXNS)GO TO 100
C       CALCULATION OF TOTAL AVERAGE NOISE
        DO 58 I=1,4
        DIFNO(I)=BNO(I)-BBNO(I)
58      DIFNX(I)=BNX(I)-BBNX(I)
        DO 66 I=1,2
        J=I+1
        K=I+2
C       REJECTION OF ORDINARY SAMPLE IF FADING EXCEEDS
C       RE1,OR IF SATURATION IS REACHED
        IF(DIFNO(I).GT.RE1.OR.DIFNO(J).GT.RE1.OR.DIFNO(K).GT.RE1.OR.
       1BNO(J).GT.510..OR.BNX(J).GT.510.)GO TO 60
        BMO=BMO+BNO(J)**2
        GO TO 62
C       NUMBER OF SAMPLES OF ORDINARY NOISE REJECTED
60      IRNO=IRNO+1
        IF(BNO(J).GT.510..OR.BNX(J).GT.510.)GO TO 64
62      IF(DIFNX(I).GT.RE1.OR.DIFNX(J).GT.RE1.OR.DIFNX(K).GT.RE1)
       1GO TO 64
        BMX=BMX+BNX(J)**2
        GO TO 66
64      IRNX=IRNX+1
66      CONTINUE
68      DO 84 I=1,21
C       REJECTION OF SAMPLE OF ORDINARY SIGNAL IF FADING EXCEEDS
C       A VALUE RE1 OR RE2, OR IF SATURATION IS REACHED
        J=I+1
        L=I-1
        IF(L.EQ.0)L=1
        IF(J.GT.21)J=21
```

```
      DIFE=AO(I)-BO(I)
      DIFEA=AO(L)-BO(L)
      DIFEB=AO(J)-BO(J)
      IF(I.GT.9)GO TO 70
      IF(DIFE.GT.RE1.OR.DIFEA.GT.RE1.OR.DIFEB.GT.RE1.OR.
     1AO(I).GT.510..OR.AX(I).GT.510.)GO TO 74
      GO TO 200
70    IF(DIFE.GT.RE2.OR.DIFEA.GT.RE2.OR.DIFEB.GT.RE2.OR.
     1AO(I).GT.510..OR.AX(I).GT.510.)GO TO 74
C     DETERMINATION OF MAXIMUMS IN THE REFLECTED SIGNAL
200   EJ=AO(I)-0.5*AO(L)-0.5*AO(J)
      IF(AO(I).GT.AO(J).AND.AO(I).GT.AO(L).AND.
     1EJ.GT..05*AO(I).AND.AO(I).GT.2.*BMEANO)GO TO 202
      GO TO 72
C     NUMBER OF MAXIMUMS
202   HEIO(I)=HEIO(I)+1.
C     AVERAGE POWER OF ARDINARY SIGNAL
72    AVAO(I)=AVAO(I)+AO(I)**2
      GO TO 76
C     NUMBER OF SAMPLES OF ORDINARY SIGNAL REJECTED
74    IRJO(I)=IRJO(I)+1
      IF(AO(I).GT.510..OR.AX(I).GT.510.)GO TO 82
76    DIFE=AX(I)-BX(I)
      DIFEA=AX(L)-BX(L)
      DIFEB=AX(J)-BX(J)
      IF(I.GT.9.AND.I.LT.16)GO TO 78
      IF(DIFE.GT.RE1.OR.DIFEA.GT.RE1.OR.DIFEB.GT.RE1)GO TO 82
      GO TO 204
78    IF(DIFE.GT.RE2.OR.DIFEA.GT.RE2.OR.DIFEB.GT.RE2)GO TO 82
204   EJ=AX(I)-0.5*AX(L)-0.5*AX(J)
      IF(AX(I).GT.AX(L).AND.AX(I).GT.AX(J).AND.EJ.GT..05*AX(I).
     1AND.AX(I).GT.2.*BMEANX)GO TO 206
      GO TO 80
206   HEIX(I)=HEIX(I)+1.
80    AVAX(I)=AVAX(I)+AX(I)**2
      GO TO 84
82    IRJX(I)=IRJX(I)+1
84    CONTINUE
      GO TO 110
C     NUMBER OF FRAMES REJECTED DUE TO EXCESSIVE NOISE
100   IR=IR+1
110   SNO=BMEANO**2+SNO
      SNX=BMEANX**2+SNX
      GO TO 50
112   ID=ID-1
114   ID=ID/2
      BID=ID
C     TOTAL NUMBER OF REJECTED SAMPLES AT EACH HEIGHT
      DO 116 I=1,21
      IRJO(I)=IRJO(I)+IR
116   IRJX(I)=IRJX(I)+IR
      IRNO=IRNO+2*IR
      IRNX=IRNX+2*IR
      AVNO=SQRT(SNO/BID)
      AVNX=SQRT(SNX/BID)
      NR=(ID/100)*30
      CALL HEAD(1)
```

```
      WRITE(6,208)
208   FORMAT(20X,25HHEIGHTS OF REFLECTION, AO)
      CALL PLOTF(60.,88.5,20,HEIO,NR)
      WRITE(6,210)
210   FORMAT(//20X,25HHEIGHTS OF REFLECTION, AX)
      CALL PLOTF(60.,88.5,20,HEIX,NR)
      RNO=ID*2-IRNO
      RNX=ID*2-IRNX
C     AVERAGE POWER OF SIGNAL SUBTRACTED FROM AVERAGE
C     POWER OF NOISE
      DO 118 I=1,21
      RSAMO=ID-IRJO(I)
      RSAMX=ID-IRJX(I)
      AVOC=AVAO(I)/RSAMO-BMO/RNO
      AVXC=AVAX(I)/RSAMX-BMX/RNX
      AVAO(I)=(ABS(AVOC)/AVOC)*SQRT(ABS(AVOC))
      AVAX(I)=(ABS(AVXC)/AVXC)*SQRT(ABS(AVXC))
118   CONTINUE
      BMO=SQRT(BMO/RNO)
      BMX=SQRT(BMX/RNX)
      CALL HEAD(1)
      WRITE(6,120)AVNO,AVNX,BMO,IRNO,BMX,IRNX
120   FORMAT(2X,17HAVERAGE NOISE ORD,F8.1/2X,17HAVERAGE NOISE EXT,1X
     1,F7.1//2X,9HNOISE ORD,F8.1,I5,11H REJECTIONS/2X,
     29HNOISE EXT,F8.1,I5,11H REJECTIONS)
      WRITE(6,122)ID,IR
122   FORMAT(//1X,I4,14H SAMPLES TAKEN,5X,I5,16H FRAMES REJECTED//
     19H REJECTED,2X,9H REJECTED,2X,6HHEIGHT,2X,6HAV. AO,2X,
     26HAV. AX/4X,3HORD,8X,3HEXT)
      HT=58.5
      DO 126 I=1,21
      HT=HT+1.5
      WRITE(6,124)IRJO(I),IRJX(I),HT,AVAO(I),AVAX(I)
124   FORMAT(3X,I4,7X,I4,3X,F5.1,3X,F6.1,2X,F6.1)
126   CONTINUE
      CALL HEAD(1)
C     AX/AO RATIOS
      DO 128 I=1,21
      IF(AVAO(I).LE.0.0.OR.AVAX(I).LE.0.0)GO TO 128
      XO(I)=AVAX(I)/AVAO(I)
128   CONTINUE
      MINIT=ID/150
C     AX/AO PROFILE
      CALL PLOTI(XO,1,21,MINIT)
C     CALC CALCULATES AND PRINTS ELECTRON DENSITY PROFILE
      CALL CALC(XO,1,20,RESP)
      GO TO 10
      STOP
      END
```

```
C       **********PROAT**********
C       PROAT PRINTS AX/AO AND ELECTRON DENSITY PROFILES FOR PAR-
C       TIAL REFLECTION DATA TAKEN WITH A PROGRAMMED ATTENUATOR
C       THAT OPERATES ON ALTERNATE FRAMES. THE AO SIGNALS USED
C       ABOVE A HEIGHT AHT ARE THE ATTENUATED SIGNALS. THE SIG-
C       NAL PROCESSING METHOD IS THE SAME AS USED IN PROGRAM
C       PROAX
C       ************************************************************
C
        DIMENSION FNAM(2),AO(21),AX(21),AVAO(21),AVAX(21),
        1XO(21),IRJO(21),IRJX(21),DIFNO(4),DIFNX(4),
        2BO(21),BX(21),BNO(4),BNX(4),BBNO(4),BBNX(4)
        3,IRJOT(21),BOT(21),BNXN(4),AXN(21),AOT(21),AXT(21)
        4,BNOT(4),BNXT(4),BBNOT(4),DIFNOT(4),AVAOT(21)
10      CALL HEAD(0)
C       INITIAL VALUES
        SNO=0.
        SNX=0.
        IR=0
        IRNO=0
        IRNX=0
        IRNOT=0
        BMO=0.
        BMOT=0.
        BMX=0.
        DO 16 I=1,21
        XO(I)=0.
        AVAO(I)=0.
        AVAX(I)=0.
        AO(I)=0.
        AX(I)=0.
        IRJO(I)=0
        IRJOT(I)=0
16      IRJX(I)=0
        DO 17 I=1,4
        BNO(I)=0.
17      BNX(I)=0.
        CALL VALUE
        CALL DINIT
        WRITE(6,20)
20      FORMAT(15H WHICH DATAFILE)
        READ(4,30)FNAM
30      FORMAT(2A5)
        CALL FSTAT(2,FNAM,LOG)
        IF(LOG.NE.0)GO TO 40
        WRITE(6,35)FNAM
35      FORMAT(6H FILE ,2A5,19H NOT FOUND ON DAT 2)
        GO TO 10
40      WRITE(6,41)
41      FORMAT(24H COLLISION FREQ. PROFILE/
        1 25H SUMMER,WINTER,OR EQUINOX)
        READ(4,42)RESP
42      FORMAT(A5)
        CALL SEEK(2,FNAM)
        WRITE(6,43)
43      FORMAT(14H MAXIMUM NOISE)
        READ(4,44)BMXNS
```

```
      WRITE(6,300)
300   FORMAT(22H HEIGHT STARTING ATTEN)
      READ(4,44)AHT
      IT=(AHT-58.5)/1.5-1.
44    FORMAT(F10.0)
      WRITE(6,45)
45    FORMAT(21H REJECTION BELOW 72KM)
      READ(4,44)RE1
      WRITE(6,46)
46    FORMAT(21H REJECTION ABOVE 72KM)
      READ(4,44)RE2
      KEOFO=0
      KEOFX=0
      ID=0
      CALL DREAD(AO,BNO,IERR,ID,KEOFO)
      CALL DREAD(AX,BNX,IERR,ID,KEOFX)
      CALL DREAD(AOT,BNOT,IERR,ID,KEOFO)
      CALL DREAD(AXT,BNXT,IERR,ID,KEOFX)
      IDM=4
      IF(AOT(9).LT.AO(9))GO TO 50
      CALL DREAD(AOT,BNOT,IERR,ID,KEOFO)
      CALL DREAD(AXT,BNXT,IERR,ID,KEOFX)
      IDM=6
50    DO 52 I=1,21
      BO(I)=AO(I)
      BOT(I)=AOT(I)
52    BX(I)=AX(I)
      DO 54 I=1,4
      BBNO(I)=BNO(I)
      BBNOT(I)=BNOT(I)
54    BBNX(I)=BNX(I)
C     DREAD READS 21 VALUES OF SIGNAL, BETWEEN 60 AND 90 KM,
C     AND 4 VALUES OF NOISE TAKEN BETWEEN 45 AND 51 KM
      CALL DREAD(AO,BNO,IERR,ID,KEOFO)
      IF(KEOFO.EQ.1)GO TO 326
      CALL DREAD(AX,BNX,IERR,ID,KEOFX)
      IF(KEOFX.EQ.1)GO TO 320
      CALL DREAD(AOT,BNOT,IERR,ID,KEOFO)
      IF(KEOFO.EQ.1)GO TO 322
      CALL DREAD(AXT,BNXT,IERR,ID,KEOFX)
      IF(KEOFX.EQ.1)GO TO 324
C     AVERAGE POWER OF NOISE OF THE FRAME
      BMEANO=0.
      BMEANX=0.
      DO 56 I=1,4
      BMEANO=BMEANO+BNO(I)**2
56    BMEANX=BMEANY+BNX(I)**2
      BMEANO=SQRT(BMEANO/4.)
      BMEANX=SQRT(BMEANX/4.)
C     REJECTION OF FRAMES IF AVERAGE NOISE FOR BOTH AO AND AX
C     EXCEEDS A VALUE BMXNS
      IF(BMEANO.GT.BMXNS.AND.BMEANX.GT.BMXNS)GO TO 100
C     CALCULATION OF TOTAL AVERAGE NOISE
      DO 58 I=1,4
      DIFNO(I)=BNO(I)-BBNO(I)
      DIFNOT(I)=BNOT(I)-BBNOT(I)
58    DIFNX(I)=BNX(I)-BBNX(I)
```

```
      DO 304 I=1,2
      J=I+1
      K=I+2
C     REJECTION OF ORDINARY SAMPLE IF FADING EXCEEDS
C     RE1, OR IF SATURATION IS REACHED
      IF(DIFNO(I).GT.RE1.OR.DIFNO(J).GT.RE1.OR.DIFNO(K).GT.RE1.OR.
     1BNO(J).GT.510..OR.BNX(J).GT.510.)GO TO 60
      BMO=BMO+BNO(J)**2
      GO TO 62
C     NUMBER OR SAMPLES OF ORDINARY NOISE REJECTED
60    IRNO=IRNO+1
      IF(BNO(J).GT.510..OR.BNX(J).GT.510.)GO TO 64
62    IF(DIFNX(I).GT.RE1.OR.DIFNX(J).GT.RE1.OR.DIFNX(K).GT.RE1)
     1 GO TO 64
      BMX=BMX+BNX(J)**2
      GO TO 66
64    IRNX=IRNX+1
66    IF(BNOT(J).GT.510..OR.BNXT(J).GT.510.)GO TO 302
      IF(DIFNOT(I).GT.RE1.OR.DIFNOT(J).GT.RE1.OR.DIFNOT(K).
     2GT.RE1)GO TO 302
      BMOT=BMOT+BNOT(J)**2
      GO TO 304
302   IRNOT=IRNOT+1
304   CONTINUE
68    DO 76 I=1,IT
C     REJECTION OF SAMPLE OF ORDINARY SIGNAL IF FADING EXCEEDS
C     A VALUE RE1 OR RE2, OR IF SATURATION IS REACHED
      J=I+1
      L=I-1
      IF(L.EQ.0)L=1
      IF(J.GT.21)J=21
      DIFE=AO(I)-BO(I)
      DIFEA=AO(L)-BO(L)
      DIFEB=AO(J)-BO(J)
      IF(I.GT.9)GO TO 70
      IF(DIFE.GT.RE1.OR.DIFEA.GT.RE1.OR.DIFEB.GT.RE1.OR.
     1AO(I).GT.510..OR.AX(I).GT.510.)GO TO 74
      GO TO 72
70    IF(DIFE.GT.RE2.OR.DIFEA.GT.RE2.OR.DIFEB.GT.RE2.OR.
     1AO(I).GT.510..OR.AX(I).GT.510.)GO TO 74
C     AVERAGE POWER OF ORDINARY SIGNAL
72    AVAO(I)=AVAO(I)+AO(I)**2
      GO TO 76
C     NUMBER OF SAMPLES OF ORDINARY SIGNAL REJECTED
74    IRJO(I)=IRJO(I)+1
76    CONTINUE
      DO 84 I=1,21
      IF(I.GT.IT)GO TO 306
      IF(AO(I).GT.510..OR.AX(I).GT.510.)GO TO 82
      GO TO 308
306   IF(AX(I).GT.510.)GO TO 82
308   J=I+1
      L=I-1
      IF(L.EQ.0)L=1
      IF(J.GT.21)J=21
      DIFE=AX(I)-BX(I)
      DIFEA=AX(L)-BX(L)
```

```
      DIFEB=AX(J)-BX(J)
      IF(I.GT.9.AND.I.LT.16)GO TO 78
      IF(DIFE.GT.RE1.OR.DIFEA.GT.RE1.OR.DIFEB.GT.RE1)GO TO 82
      GO TO 80
78    IF(DIFE.GT.RE2.OR.DIFEA.GT.RE2.OR.DIFEB.GT.RE2)GO TO 82
80    AVAX(I)=AVAX(I)+AX(I)**2
      GO TO 84
82    IRJX(I)=IRJX(I)+1
84    CONTINUE
      ITM=22-IT
      DO 314 I=1,ITM
      IJ=I+IT-1
      J=IJ+1
      L=IJ-1
      IF(L.EQ.0)L=1
      IF(J.GT.21)J=21
      DIFE=AOT(IJ)-BOT(IJ)
      DIFEA=AOT(L)-BOT(L)
      DIFEB=AOT(J)-BOT(J)
      IF(DIFEA.GT.RE1.OR.DIFEB.GT.RE1.OR.DIFE.GT.RE1.OR.
     2AOT(IJ).GT.510.)GO TO 312
      AVAOT(IJ)=AVAOT(IJ)+AOT(IJ)**2
      GO TO 314
312   IRJOT(IJ)=IRJOT(IJ)+1
314   CONTINUE
      GO TO 110
C     NUMBER OF FRAMES REJECTED DUE TO EXCESSIVE NOISE
100   IR=IR+1
110   SNO=BMEANO**2+SNO
      SNX=BMEANX**2+SNX
      GO TO 326
320   ID=ID-1
      GO TO 326
322   ID=ID-2
      GO TO 326
324   ID=ID-3
326   ID=(ID-IDM)/4
      BID=ID
C     TOTAL NUMBER OF REJECTED SAMPLES AT EACH HEIGHT
      DO 116 I=1,21
      IRJO(I)=IRJO(I)+IR
      IRJOT(I)=IRJOT(I)+IR
116   IRJX(I)=IRJX(I)+IR
      IRNO=IRNO+2*IR
      IRNOT=IRNOT+2*IR
      IRNX=IRNX+2*IR
      AVNO=SQRT(SNO/BID)
      AVNX=SQRT(SNX/BID)
      RNO=ID*2-IRNO
      RNX=ID*2-IRNX
      RNOT=ID*2-IRNOT
C     AVERAGE POWER OF SIGNAL SUBTRACTED FROM THE AVERAGE
C     POWER OF NOISE
      DO 118 I=1,21
      IF(I.GT.IT)GO TO 328
      RSAMO=ID-IRJO(I)
      AVOC=AVAO(I)/RSAMO-BMO/RNO
```

```
      AVAO(I)=(ABS(AVOC)/AVOC)*SQRT(ABS(AVOC))
328   RSAMX=ID-IRJX(I)
      AVXC=AVAX(I)/RSAMX-BMX/RNX
      AVAX(I)=(ABS(AVXC)/AVXC)*SQRT(ABS(AVXC))
118   CONTINUE
      DO 330 I=1,ITM
      IJ=I+IT-1
      RSAMO=ID-IRJOT(IJ)
      AVOC=AVAOT(IJ)/RSAMO-BMOT/RNOT
      AVAOT(IJ)=(ABS(AVOC)/AVOC)*SQRT(ABS(AVOC))
330   IRJO(IJ)=IRJOT(IJ)
      CORR=AVAO(IT)/AVAOT(IT)
      DCOR=20.*ALOG10(CORR)
      ITC=21-IT
      DO 332 I=1,ITC
      IJC=IT+I
332   AVAO(IJC)=AVAOT(IJC)*CORR
      BMO=SQRT(BMO/RNO)
      BMX=SQRT(BMX/RNX)
      CALL HEAD(1)
      WRITE(6,120)AVNO,AVNX,BMO,IRNO,BMX,IRNX
120   FORMAT(2X,17HAVERAGE NOISE ORD,F8.1/2X,17HAVERAGE NOISE EXT,1X
     1,F7.1//2X,9HNOISE ORD,F8.1,I5,11H REJECTIONS/2X,
     29HNOISE EXT,F8.1,I5,11H REJECTIONS)
      WRITE(6,122)ID,IR,DCOR
122   FORMAT(//1X,I4,14H SAMPLES TAKEN,5X,I5,16H FRAMES REJECTED/
     2F6.2,15H DB ATTENUATION//
     39H REJECTED,2X,9H REJECTED,2X,6HHEIGHT,2X,6HAV. AO,2X,
     26HAV. AX/4X,3HORD,8X,3HEXT)
      HT=58.5
      DO 126 I=1,21
      HT=HT+1.5
      WRITE(6,124)IRJO(I),IRJX(I),HT,AVAO(I),AVAX(I)
124   FORMAT(3X,I4,7X,I4,3X,F5.1,3X,F6.1,2X,F6.1)
126   CONTINUE
      CALL HEAD(1)
C     AX/AO RATIOS
      DO 128 I=1,21
      IF(AVAO(I).LE.0.0.OR.AVAX(I).LE.0.0)GO TO 128
      XO(I)=AVAX(I)/AVAO(I)
128   CONTINUE
      MINIT=ID/150
C     AX/AO PROFILE
      CALL PLOTI(XO,1,21,MINIT)
C     CALC CALCULATES AND PRINTS ELECTRON DENSITY PROFILE
      CALL CALC(XO,1,20,RESP)
      GO TO 10
      STOP
      END
```

```
C       **********SUBROUTINE DREAD**********
C       DREAD READS 21 SAMPLES OF SIGNAL AND 4 SAMPLES OF NOISE
C       FROM DECTAPE. THE OUTPUT VOLTAGES ARE TRANSFORMED INTO
C       INPUT VOLTAGES BY LINAP.
C       ************************************************************
C
        SUBROUTINE DRFAD(A,BMEAN,IERR,ID,KEOF)
        DIMENSION A(21),IDAT(26),BMEAN(4)
        KEOF=0
        CALL DUMPR(IDAT,NEGF)
C CHECK ID CONSECUTIVE
        IF(ID-IDAT(1)+1) 10,15,10
C CHECK FOR EOF
10      IF(IDAT(1).NE.77777) GO TO IERR
C       E.O.F.
        KEOF=1
        GO TO 210
15      ID=IDAT(1)
40      DO 42 MIN=6,26
        MFVE=MIN-5
        A(MFVE)=IDAT(MIN)
        A(MFVE)=A(MFVE)*100./51.
        CALL LINAP(A(MFVE))
42      CONTINUE
C       SAMPLES OF NOISE
        DO 130 J=1,4
        JEL=J+1
        BMEAN(J)=IDAT(JEL)
        BMEAN(J)=BMEAN(J)*100./51.
        CALL LINAP(BMEAN(J))
130     CONTINUE
210     CONTINUE
        RETURN
        END



C       **********SUBROUTINE LINAP**********
C       LINAP TRANSFORMS OUTPUT VOLTAGES INTO INPUT VOLTAGES OF
C       THE RECEIVER. THE CALIBRATION DATA IS CONTAINED IN SUB-
C       ROUTINE VALUE.
C       ************************************************************
C
C       INPUT AND OUTPUT:
C       A IS THE OUTPUT VOLTAGE THAT IS TRANSFORMED INTO
C       INPUT VOLTAGE
C
        SUBROUTINE LINAP(A)
        COMMON / / S(29),TU(29),TUO(30)
        IF(A.GT.1000.0)A=1000.0
        DO 5 I=1,29
        J=I+1
        IF(A.GT.TUO(I).AND.A.LE.TUO(J)) GO TO 10
5       CONTINUE
        A=0.
        RETURN
10      A=(A-TUO(I))*S(I)+TU(I)
        IF(A.LT.0.0)A=0.0
        RETURN
        END
```

```
C       **********SUBROUTINE CALC**********
C       SUBROUTINE CALC CALCULATES AND PRINTS ELECTRON DENSITY
C       PROFILES BETWEEN 60 AND 90KM.
C       ************************************************
C
C       INPUT DATA:
C       ARRAY(I)= AX/AO RATIOS FROM 60 TO 90KM
C       LL=LOWER LIMIT IN THE CALCULATION (1=60.7KM)
C       LH=UPPER LIMIT IN THE CALCULATION (20=89.2KM)
C       RESP=COLLISION FREQUENCY PROFILE (SUMMER,WINTER OR EQUINOX)
C
        SUBROUTINE CALC(ARRAY,LL,LH,RESP)
        DIMENSION ARRAY(21),P(21),R(3),CF(3),EL(20)
        DATA SUM,WIN,EQU/5HSUMME,5HWINTE,5HEQUIN/
        IF (RESP.EQ.SUM) GO TO 100
        IF (RESP.EQ.WIN) GO TO 200
        IF (RESP.EQ.EQU) GO TO 300
C       COLLISION FREQUENCY PROFILES
100     P(1)=240.
        P(2)=182.
        P(3)=140.
        P(4)=108.
        P(5)=83.
        P(6)=63.
        P(7)=49.
        P(8)=38.
        P(9)=29.
        P(10)=22.
        P(11)=17.
        P(12)=12.9
        P(13)=10.1
        P(14)=7.7
        P(15)=6.
        P(16)=4.6
        P(17)=3.5
        P(18)=2.7
        P(19)=2.02
        P(20)=1.55
        P(21)=1.20
        GO TO 400
200     P(1)=183.
        P(2)=145.
        P(3)=110.
        P(4)=89.5
        P(5)=68.
        P(6)=56.
        P(7)=44.
        P(8)=35.
        P(9)=27.5
        P(10)=21.5
        P(11)=17.
        P(12)=13.2
        P(13)=10.4
        P(14)=7.8
        P(15)=6.1
        P(16)=4.6
        P(17)=3.5
```

```
      P(18)=2.65
      P(19)=2.1
      P(20)=1.5
      P(21)=1.2
      GO TO 400
300   P(1)=220.
      P(2)=172.
      P(3)=132.
      P(4)=104.
      P(5)=80.
      P(6)=62.
      P(7)=48.
      P(8)=37.
      P(9)=28.5
      P(10)=22.
      P(11)=17.
      P(12)=13.
      P(13)=10.
      P(14)=7.8
      P(15)=6.0
      P(16)=4.6
      P(17)=3.6
      P(18)=2.75
      P(19)=2.12
      P(20)=1.65
      P(21)=1.35
400   DO 401 I=1,21
      P(I)=P(I)*(10.**5)
401   CONTINUE
      CALL HEAD(1)
      K=0
      DO 20 I=LL,LH
C     CALCULATION OF ELECTRON DENSITIES
      R(1)=ARRAY(I)
      R(2)=ARRAY(I+1)
      K=K+1
      CF(1)=P(K)
      CF(2)=P(K+1)
      IF(R(1).EQ.0.0.OR.R(2).EQ.0.0) GO TO 20
C     FUNCTION ELDEN CALCULATES ELECTRON DENSITIES
      EL(K)=ELDEN(R,CF,1.5E+3)/(10.**6)
20    CONTINUE
C     PLOT(J) PLOTS THE ELECTRON DENSITY PROFILE
      CALL PLOTJ (EL)
      RETURN
      END
```

```
C       **********SUBROUTINE VALUE**********
C       VALUE CONTAINS THE CALIBRATION OF THE RECEIVER AND IS
C       CALLED BY LINAP, TO CORRECT THE PARTIAL REFLECTION DATA
C       FROM NONLINEARITY OF THE RECEIVER.
C       ************************************************
C
C       S(I)=RATIO OF INCREMENTS AT INPUT AND OUTPUT OF RECEIVER
C       TU(I)=INPUT OF RECEIVER
C       TUO(I)=OUTPUT OF RECEIVER
C
        SUBROUTINE VALUE
        COMMON / / S(29),TU(29),TUO(30)
        S(1)=4.467
        S(2)=1.722
        S(3)=1.247
        S(4)=1.115
        S(5)=.988
        S(6)=.797
        S(7)=.668
        S(8)=.639
        S(9)=.569
        S(10)=.493
        S(11)=.451
        S(12)=.427
        S(13)=.414
        S(14)=.391
        S(15)=.398
        S(16)=.363
        S(17)=.344
        S(18)=.348
        S(19)=.360
        S(20)=.393
        S(21)=.432
        S(22)=.492
        S(23)=.511
        S(24)=.583
        S(25)=.689
        S(26)=.676
        S(27)=.796
        S(28)=.839
        S(29)=1.112
        TU(1)=0.
        TU(2)=4.467
        TU(3)=6.310
        TU(4)=7.943
        TU(5)=8.913
        TU(6)=10.0
        TU(7)=12.589
        TU(8)=14.125
        TU(9)=15.849
        TU(10)=17.783
        TU(11)=19.953
        TU(12)=22.387
        TU(13)=25.119
        TU(14)=28.184
        TU(15)=31.623
        TU(16)=35.481
```

```
TU(17)=44.668
TU(18)=70.795
TU(19)=112.202
TU(20)=125.893
TU(21)=158.489
TU(22)=199.526
TU(23)=251.189
TU(24)=281.838
TU(25)=316.228
TU(26)=354.813
TU(27)=398.107
TU(28)=446.684
TU(29)=501.187
TUO(1)=-.4
TUO(2)=.6
TUO(3)=1.67
TUO(4)=2.98
TUO(5)=3.85
TUO(6)=4.95
TUO(7)=8.2
TUO(8)=10.5
TUO(9)=13.2
TUO(10)=16.6
TUO(11)=21.
TUO(12)=26.4
TUO(13)=32.8
TUO(14)=40.2
TUO(15)=49.
TUO(16)=58.7
TUO(17)=84.
TUO(18)=160.
TUO(19)=279.
TUO(20)=317.
TUO(21)=400.
TUO(22)=495.
TUO(23)=600.
TUO(24)=660.
TUO(25)=719.
TUO(26)=775.
TUO(27)=839.
TUO(28)=900.
TUO(29)=965.
TUO(30)=1020.
RETURN
END
```

```
C       **********VALS**********
C       VALS CALCULATES ELECTRON DENSITIES AS WOULD BE MEA-
C       SURED FROM PARTIAL REFLECTIONS, IN A REGION WHERE
C       THE SCATTERING CROSS-SECTION PER UNIT VOLUME CHAN-
C       GES IN STEPS AS A FUNCTION OF HEIGHT.
C       **************************************************
C
C       INPUT:
C       S1=SCATTERING CROSS-SECTION BELOW A HEIGHT ZA
C       S2=SCATTERING CROSS-SECTION BETWEEN HEIGHTS ZA AND ZB
C       S3=SCATTERING CROSS-SECTION ABOVE A HEIGHT ZB
C       ZA,ZB=HEIGHTS DEFINDED ABOVE
C       CF=COLLISION FREQUENCY, ASSUMED INDEPENDENT OF HEIGHT
C       EDR=REAL ELECTRON DENSITY OF THE REGION, ASSUMED CONS-
C       TANT
C       W=PULSE WIDTH OF THE TRANSMITTED PULSE FOR P.R. MEASUREMENT
C
        DIMENSION RO(100),RX(100),RA(100)
        C52(X)=(X*(X*(X+6.69459)+16.90100)+1.16306)/(X*(X*(X*(X*(X+
        16.63145)+35.35526)+68.92050)+64.09346)+4.36057)
        C=2.99792E8
1       WRITE(6,10)
10      FORMAT(3H S1)
        READ(4,11)S1
11      FORMAT(F10.2)
        WRITE(6,12)
12      FORMAT(3H S2)
        READ(4,11)S2
        WRITE(6,13)
13      FORMAT(3H S3)
        READ(4,11)S3
        WRITE(6,14)
14      FORMAT(13H CF, FORMAT E)
        READ(4,15)CF
        WRITE(6,16)
16      FORMAT(13H ED, FORMAT E)
        READ(4,15)EDR
15      FORMAT(E10.2)
        WRITE(6,17)
17      FORMAT(3H ZA)
        READ(4,11)ZA
        WRITE(6,18)
18      FORMAT(3H ZB)
        READ(4,11)ZB
        WRITE(6,19)
19      FORMAT(12H PULSE WIDTH)
        READ(4,11)W
        C0=2.59614E7/CF
        CX=7.3886E6/CF
        FO=((5./4.)*(3182.601/C)*C52(C0))/C0
        FX=((5./4.)*(3182.601/C)*C52(CX))/CX
        AFO=FO*EDR
        AFX=FX*EDR
        Z1=ZA-W/4.-2000.
        N=(ZB-ZA+W/2.+3000.)*2.E-3+2.
        AOP=EXP(AFO*W)
        AON=EXP(-1.*AFO*W)
```

```
      AXP=EXP(AFX*W)
      AXN=EXP(-1.*AFX*W)
      C1=ZA-W/4.
      C2=ZB-W/4.
      C3=ZA+W/4.
      C4=ZB+W/4.
C     CALCULATION OF THE REFLECTED SIGNALS, AO AND AX
      WRITE(6,20)
20    FORMAT(//7X,2HRA,19X,2HRO,10X,2HRX,10X,2HZ1/)
      DO 45 I=1,N
      Z1=Z1+500.
      IF(Z1.GT.C1.AND.Z1.LE.C2)GO TO 31
      IF(Z1.GT.C2.AND.Z1.LE.C3)GO TO 32
      IF(Z1.GT.C3.AND.Z1.LE.C4)GO TO 33
      IF(Z1.GT.C4)GO TO 34
      RO(I)=(S1/(4.*AFO))*(AOP-AON)*EXP(-4.*AFO*Z1)
      RX(I)=(S1/(4.*AFX))*(AXP-AXN)*EXP(-4.*AFX*Z1)
      GO TO 304
31    RO(I)=((S2-S1)/(4.*AFO))*EXP(-4.*AFO*ZA)+((S1*AOP-S2*AON)/
     1(4.*AFO))*EXP(-4.*AFO*Z1)
      RX(I)=((S2-S1)/(4.*AFX))*EXP(-4.*AFX*ZA)+((S1*AXP-S2*AXN)/
     1(4.*AFX))*EXP(-4.*AFX*Z1)
      GO TO 304
32    RO(I)=((S2-S1)/(4.*AFO))*EXP(-4.*AFO*ZA)+((S3-S2)/
     1(4.*AFO))*EXP(-4.*AFO*ZB)+((S1*AOP-S3*AON)/(4.*AFO))*EXP(-4.*
     2AFO*Z1)
      RX(I)=((S2-S1)/(4.*AFX))*EXP(-4.*AFX*ZA)+((S3-S2)/
     2(4.*AFX))*EXP(-4.*AFX*ZB)+((S1*AXP-S3*AXN)/(4.*AFX))*EXP(-4.*
     2AFX*Z1)
      GO TO 304
33    RO(I)=((S3-S2)/(4.*AFO))*EXP(-4.*AFO*ZB)+((S2*AOP-S3*
     1AON)/(4.*AFO))*EXP(-4.*AFO*Z1)
      RX(I)=((S3-S2)/(4.*AFX))*EXP(-4.*AFX*ZB)+((S2*AXP-S3*
     2AXN)/(4.*AFX))*EXP(-4.*AFX*Z1)
      GO TO 304
34    RO(I)=(S3/(4.*AFO))*(AOP-AON)*EXP(-4.*AFO*Z1)
      RX(I)=(S3/(4.*AFX))*(AXP-AXN)*EXP(-4.*AFX*Z1)
304   IF(RO(I).EQ.0.)GO TO 305
      RA(I)=SQRT(RX(I)/RO(I))
      GO TO 306
305   RA(I)=1000.
306   WRITE(6,307)RA(I),RO(I),RX(I),Z1
307   FORMAT(4E12.3)
45    CONTINUE
C     CALCULATION OF ELECTRON DENSITIES AS OBSERVED FROM
C     PARTIAL REFLECTIONS
      ZZ=ZA-W/4.-1250.
      WRITE(6,47)
47    FORMAT(//7X,2HED,10X,2HZM/)
      J=N-3
      DO 46 K=1,J
      L=K+3
      CCL=K
      ZM=ZZ+500.*CCL
      ED=ALOG(RA(K)/RA(L))/(3000.*(FX-FO))
      WRITE(6,310)ED,ZM
310   FORMAT(2E12.3)
46    CONTINUE
      GO TO 1
      STOP
      END
```

```
C       ********************VALEX**************************
C       VALEX CALCULATES ELECTRON DENSITIES AS WOULD BE MEA-
C       SURED FROM PARTIAL REFLECTIONS, IN A REGION WHERE
C       THE SCATTERING CROSS-SECTION PER UNIT VOLUME CHANGES
C       EXPONENTIALLY
C       ****************************************************
C
C       INPUT:
C       S1=SCATTERING CROSS-SECTION BELOW A HEIGHT ZA
C       S3=SCATTERING CROSS-SECTION ABOVE A HEIGHT ZB
C       B=EXPOENT OF THE SCATTERING CROSS-SECTION,S=EXP(BZ),
C       BETEWEEN HEIGHTS ZA AND ZB
C       ZA,ZB=HEIGHTS DEFINED ABOVE
C       CF=COLLISION FREQUENCY, ASSUMED INDEPENDENT OF HEIGHT
C       EDR=REAL ELECTRON DENSITY OF THE REGION, ASSUMED
C       CONSTANT
C       W=PULSE WIDTH OF THE TRANSMITTED PULSE FOR P.R. MEASUREMENT
C
        DIMENSION RO(100),RA(100),RX(100)
        C52(X)=(X*(X*(X+6.69459)+16.90100)+1.16306)/(X*(X*(X*(X*(X+
        116.63145)+35.35526)+68.92050)+64.09346)+4.36057)
        C=2.99792E8
1       WRITE(6,8)
8       FORMAT(3H S1)
        READ(4,11)S1
        WRITE(6,10)
10      FORMAT(24H B (S=EXP(BZ)), FORMAT E)
        READ(4,11)B
11      FORMAT(F10.2)
        WRITE(6,16)
16      FORMAT(20H S3, IF NEG=EXP(BZB))
        READ(4,11)S3
        WRITE(6,17)
17      FORMAT(3H ZA)
        READ(4,11)ZA
        WRITE(6,19)
19      FORMAT(3H ZB)
        READ(6,11)ZB
        WRITE(6,12)
12      FORMAT(5H CF-E)
        READ(4,20)CF
20      FORMAT(E10.2)
        WRITE(6,13)
13      FORMAT(12H PULSE WIDTH)
        READ(4,11)W
        WRITE(6,14)
14      FORMAT(5H ED-E)
        READ(4,20)EDR
        IF(S3.LT.0.)S3=EXP(B*ZB)
C       CALCULATION OF REFLECTED SIGNALS, AO AND AX
        CO=2.59614E7/CF
        CX=7.3886E6/CF
        FO=((5./4.)*(3182.601/C)*C52(CO))/CO
        FX=((5./4.)*(3182.601/C)*C52(CX))/CX
        AFO=FO*EDR
        AFX=FX*EDR
        BO=B-4.*AFO
```

```
      BX=B-4.*AFX
      C1=ZA-W/4.
      C2=ZB-W/4.
      C3=ZA+W/4.
      C4=ZB+W/4.
      Z1=ZA-W/4.-2000.
      N=(ZB-ZA+3000.+W/2.)*2.E-3+2.
      WRITE(6,21)
21    FORMAT(//7X,2HRA,10X,2HRO,10X,2HRX,10X,2HZ1/)
      DO 45 I=1,N
      Z1=Z1+500.
      IF(Z1.GT.C1.AND.Z1.LE.C2)GO TO 51
      IF(Z1.GT.C2.AND.Z1.LE.C3)GO TO 52
      IF(Z1.GT.C3.AND.Z1.LE.C4)GO TO 53
      IF(Z1.GT.C4)GO TO 54
      RO(I)=(S1/(4.*AFO))*(EXP(AFO*W)-EXP(-1.*AFO*W))*EXP(-4.*AFO*Z1)
      RX(I)=(S1/(4.*AFX))*(EXP(AFX*W)-EXP(-1.*AFX*W))*EXP(-4.*AFY*Z1)
      GO TO 42
51    RO(I)=(S1/(4.*AFO))*(EXP(-4.*AFO*(Z1-W/4.))-EXP(-4.*AFO*ZA))
     1+(1./BO)*(EXP(BO*(Z1+W/4.))-EXP(BO*ZA))
      RX(I)=(S1/(4.*AFX))*(EXP(-4.*AFX*(Z1-W/4.))-EXP(-4.*AFX*ZA))
     1+(1./BX)*(EXP(BX*(Z1+W/4.))-EXP(BX*ZA))
      GO TO 42
52    RO(I)=(S1/(4.*AFO))*(EXP(-4.*AFO*(Z1-W/4.))-EXP(-4.*AFO*ZA))
     1+(S3/(4.*AFO))*(EXP(-4.*AFO*ZB)-EXP(-4.*AFO*(Z1+W/4.)))
     2+(1./BO)*(EXP(BO*ZB)-EXP(BO*ZA))
      RX(I)=(S1/(4.*AFX))*(EXP(-4.*AFX*(Z1-W/4.))-EXP(-4.*AFX*ZA))
     1+(S3/(4.*AFX))*(EXP(-4.*AFX*ZB)-EXP(-4.*AFX*(Z1+W/4.)))
     2+(1./BX)*(EXP(BX*ZB)-EXP(BX*ZA))
      GO TO 42
53    RO(I)=(1./BO)*(EXP(BO*ZB)-EXP(BO*(Z1-W/4.)))+(S3/(4.*AFO))*(
     1EXP(-4.*AFO*ZB)-EXP(-4.*AFO*(Z1+W/4.)))
      RX(I)=(1./BX)*(EXP(BX*ZB)-EXP(BX*(Z1-W/4.)))+(S3/(4.*AFX))*(
     1EXP(-4.*AFX*ZB)-EXP(-4.*AFX*(Z1+W/4.)))
      GO TO 42
54    RO(I)=(S3/(4.*AFO))*(EXP(AFO*W)-EXP(-1.*AFO*W))*EXP(-4.*AFO*Z1)
      RX(I)=(S3/(4.*AFX))*(EXP(AFX*W)-EXP(-1.*AFX*W))*EXP(-4.*AFY*Z1)
42    IF(RO(I).EQ.0.)GO TO 44
      RA(I)=SQRT(RX(I)/RO(I))
      GO TO 43
44    RA(I)=1000.
43    WRITE(6,41)RA(I),RO(I),RX(I),Z1
41    FORMAT(4E12.3)
45    CONTINUE
C     CALCULATION OF ELECTRON DENSITIES AS WOULD BE
C     MEASURED FROM PARTIAL REFLECTIONS
      ZZ=ZA-W/4.-1250.
      WRITE(6,47)
47    FORMAT(//7X,2HED,10X,2HZM/)
      J=N-3
      DO 46 I=1,J
      L=I+3
      CCL=I
      ZM=ZZ+500.*CCL
      ED=ALOG(RA(I)/RA(L))/((FX-FO)*3000.)
      WRITE(6,310)ED,ZM
310   FORMAT(2E12.3)
46    CONTINUE
      GO TO 1
      STOP
      END
```

```
C       ************************ADIST*****************************
C       ADIST PRINTS A HISTOGRAM OF THE  DISTRIBUTION OF VALUES
C       OF AO, AX, OR AX/AO.
C       ***********************************************************
C
        DIMENSION FNAM(2),AO(21),AX(21),BNO(4),BNX(4),IFA(31,21),
       2IR(21),AXAO(21),AO2(21),AX2(21)
10      CALL HEAD(0)
        IRNO=0
        IRNX=0
        CALL VALUE
        CALL DINIT
        WRITE(6,20)
20      FORMAT(15H WHICH DATAFILE)
        READ(4,30)FNAM
30      FORMAT(2A5)
        CALL FSTAT(2,FNAM,LOG)
        IF(LOG.NE.0)GO TO 40
        WRITE(6,35)FNAM
35      FORMAT(6H FILE ,2A5,19H NOT FOUND ON DAT 2)
        GO TO 10
40      CALL SEEK(2,FNAM)
51      FORMAT(F10.0)
C       CV IS THE CENTRAL VALUE OF THE HISTOGRAM
        WRITE(6,52)
52      FORMAT(14H CENTRAL VALUE)
        READ(4,51)CV
C       STEP IS THE INTERVAL IN VALUES OF AO, AX OR AX/AO
C       TO BE USED IN THE HISTOGRAM
        WRITE(6,54)
54      FORMAT(11H WHICH STEP)
        READ(4,51)STEP
C       SAMPLES WILL BE REJECTED IF NOISE IN THE ORDINARY
C       OR EXTRAORDINARY FRAME EXCEEDS A VALUE BMXNS
        WRITE(6,56)
56      FORMAT(10H MAX NOISE)
        READ(4,51)BMXNS
C       SAMPLES WILL BE REJECTED IF THE SIGNAL TO NOISE RATIO
C       IS BELOW A VALUE SNR
        WRITE(6,57)
57      FORMAT(19H SIGNAL-NOISE RATIO)
        READ(4,51)SNR
C       SAMPLES WILL BE REJECTED IF THEY INCREASE BY MORE
C       THAN A VALUE RE, IN RELATION TO THE SAMPLE TAKEN
C       AT THE SAME HEIGHT, IMMEDIATELLY BEFORE
        WRITE(6,58)
58      FORMAT(11H MAX FADING)
        READ(4,51)RE
        WRITE(6,62)
62      FORMAT(24H AO, AX OR AX/AO (1,2,3))
        READ(4,63)IS
63      FORMAT(I1)
        KEOFO=0
        KEOFX=0
        ID=0
        DO 64 IN=1,21
        IR(IN)=0
```

```
      AO(IN)=0.
64    AX(IN)=0.
      DO 65 I=1,31
      DO 65 J=1,21
65    IFA(I,J)=0
      CVS=CV-STEP*16.
      CMIN=CV-15.*STEP
      CMAX=CV+15.*STEP
48    DO 66 I=1,21
      AO2(I)=AO(I)
66    AX2(I)=AX(I)
      CALL DREAD(AO,BNO,IERR,ID,KEOFO)
      IF(KEOFO.EQ.1)GO TO 50
      CALL DREAD(AX,BNX,IERR,ID,KEOFX)
      IF(KEOFX.EQ.1)GO TO 50
      BMEANO=0.
      BMEANX=0.
      DO 61 I=1,4
      BMEANO=BMEANO+BNO(I)**2
61    BMEANX=BMEANX+BNX(I)**2
      BMEANO=SQRT(BMEANO/4.)
      BMEANX=SQRT(BMEANX/4.)
      IF(IS.EQ.1)BMEANX=0.
      IF(IS.EQ.2)BMEANO=0.
      BLO=SNR*BMEANO
      BLX=SNR*BMEANX
      DO 95 IN=1,21
      IF(IS.EQ.1)AX(IN)=500.
      IF(IS.EQ.2)AO(IN)=500.
      IF(BMEANO.GT.BMXNS.OR.BMEANX.GT.BMXNS.OR.AO(IN).LT.BLO.OR.
     1AX(IN).LT.BLX)GO TO 81
      DIFE=AO(IN)-AO2(IN)
      IF(DIFE.GT.RE.OR.AO(IN).GT.510..OR.AX(IN).GT.510.)GO TO 81
79    DIFE=AX(IN)-AX2(IN)
      IF(DIFE.GT.RE)GO TO 81
      GO TO 82
81    IR(IN)=IR(IN)+1
      GO TO 95
82    AXAO(IN)=AX(IN)/AO(IN)
      IF(IS.EQ.1)AXAO(IN)=AO(IN)
      IF(IS.EQ.2)AXAO(IN)=AX(IN)
      IF(AXAO(IN).LE.CMIN)GO TO 91
      IF(AXAO(IN).GE.CMAX)GO TO 92
      DO 84 I=1,31
      CI=I
      C=CVS+CI*STEP
      CM=C-STEP/2.
      CP=C+STEP/2.
      IF(AXAO(IN).GE.CM.AND.AXAO(IN).LT.CP)GO TO 90
84    CONTINUE
90    IFA(I,IN)=IFA(I,IN)+1
      GO TO 95
91    IFA(1,IN)=IFA(1,IN)+1
      GO TO 95
92    IFA(31,IN)=IFA(31,IN)+1
95    CONTINUE
      GO TO 48
```

```
      ID=ID/2
      HT=60.
      CALL HEAD(1)
      DO 120 I=1,21
      WRITE(6,110)HT,ID,IR(I)
110   FORMAT(///2X,6HHEIGHT,F4.1/2X,I4,1X,13HSAMPLES TAKEN,3X,I4,
      21X,8HREJECTED/)
      CS=CMIN
      WRITE(6,112)
112   FORMAT(4X,5HVALUE,3X,4HFREQ,4X,5HVALUE,3X,4HFREQ,4X,
      25HVALUE,3X,4HFREQ,4X,5HVALUE,3X,4HFREQ/)
      DO 118 J=1,29,4
      CS1=CS+STEP
      CS2=CS1+STEP
      CS3=CS2+STEP
      IF(J.EQ.29)GO TO 113
      WRITE(6,114)CS,IFA(J,I),CS1,IFA(J+1,I),CS2,IFA(J+2,I)
      2,CS3,IFA(J+3,I)
      GO TO 118
113   WRITE(6,114)CS,IFA(J,I),CS1,IFA(J+1,I),CS2,IFA(J+2,I)
114   FORMAT(4(F9.2,I7))
118   CS=CS+STEP*4.
120   HT=HT+1.5
      GO TO 10
      STOP
      END
```

```
C       ************************ADISTT*****************************
C       ADISTT PRINTS A HISTOGRAM OF THE  DISTRIBUTION OF VALUES
C       OF AO, AX, OR AX/AO, FOR DATA TAKEN WITH A PROGRAMED ATTE-
C       NUATOR, THAT OPERATES ON ALTERNATE FRAMES.
C       ************************************************************
C
        DIMENSION FNAM(2),AO(21),AX(21),BNO(4),BNX(4),IFA(31,21),
       2IR(21),AXAO(21),AOT(21),AXT(21),BNOT(4),BNXT(4),AO2(21),
       3AX2(21)
10      CALL HEAD(0)
        IRNO=0
        IRNX=0
        CORR=1.
        DO 15 I=1,31
        DO 15 J=1,21
15      IFA(I,J)=0
        CALL VALUE
        CALL DINIT
        WRITE(6,20)
20      FORMAT(15H WHICH DATAFILE)
        READ(4,30)FNAM
30      FORMAT(2A5)
        CALL FSTAT(2,FNAM,LOG)
        IF(LOG.NE.0)GO TO 40
        WRITE(6,35)FNAM
35      FORMAT(6H FILE ,2A5,19H NOT FOUND ON DAT 2)
        GO TO 10
40      CALL SEEK(2,FNAM)
51      FORMAT(F10.0)
C       CV IS THE CENTRAL VALUE OF THE HISTOGRAM
        WRITE(6,52)
52      FORMAT(14H CENTRAL VALUE)
        READ(4,51)CV
C       STEP IS THE INTERVAL IN VALUES OF AO, AX OR AX/AO
C       TO BE USED IN THE HISTOGRAM
        WRITE(6,54)
54      FORMAT(11H WHICH STEP)
        READ(4,51)STEP
C       SAMPLES WILL BE REJECTED IF NOISE IN THE ORDINARY
C       OR EXTRAORDINARY FRAME EXCEEDS A VALUE BMXNS
        WRITE(6,56)
56      FORMAT(13H MAX NOISE)
        READ(4,51)BMXNS
C       SAMPLES WILL BE REJECTED IF THE SIGNAL TO NOISE RATIO
C       IS BELOW A VALUE SNR
        WRITE(6,57)
57      FORMAT(19H SIGNAL-NOISE RATIO)
        READ(4,51)SNR
C       SAMPLES WILL BE REJECTED IF THEY INCREASE BY MORE
C       THAN A VALUE RE, IN RELATION TO THE SAMPLE TAKEN
C       AT THE SAME HEIGHT, IMMEDIATELLY BEFORE
        WRITE(6,58)
58      FORMAT(11H MAX FADING)
        READ(4,51)RE
        WRITE(6,41)
41      FORMAT(23H HEIGHT STARTING ATT AO)
        READ(4,51)AHO
```

```
      WRITE(6,42)
42    FORMAT(23H HEIGHT STARTING ATT AX)
      READ(4,51)AHX
      WRITE(6,43)
43    FORMAT(22H CORRECTION ATT SIGNAL)
      READ(4,51)CORR
      WRITE(6,62)
62    FORMAT(24H AO, AX OR AX/AO (1,2,3))
      READ(4,63)IS
63    FORMAT(I1)
      IHO=(AHO-58.5)/1.5
      IHX=(AHX-58.5)/1.5
      KEOFO=0
      KEOFX=0
      ID=0
      IDM=4
      CALL DREAD(AO,BNO,IERR,ID,KEOFO)
      CALL DREAD(AX,BNX,IERR,ID,KEOFX)
      CALL DREAD(AOT,BNOT,IERR,ID,KEOFO)
      CALL DREAD(AXT,BNXT,IERR,ID,KEOFX)
      IF(AOT(9).LT.AO(9))GO TO 210
      IDM=6
      CALL DREAD(AOT,BNOT,IERR,ID,KEOFO)
      CALL DREAD(AXT,BNXT,IERR,ID,KEOFX)
210   DO 64 IN=1,21
      IR(IN)=0
      AO(IN)=0.
64    AX(IN)=0.
      CVS=CV-STEP*16.
      CMIN=CV-15.*STEP
      CMAX=CV+15.*STEP
48    DO 66 I=1,21
      AO2(I)=AO(I)
66    AX2(I)=AX(I)
      CALL DREAD(AO,BNO,IERR,ID,KEOFO)
      IF(KEOFO.EQ.1)GO TO 50
      CALL DREAD(AX,BNX,IERR,ID,KEOFX)
      IF(KEOFX.EQ.1)GO TO 50
      CALL DREAD(AOT,BNOT,IERR,ID,KEOFO)
      IF(KEOFO.EQ.1)GO TO 50
      CALL DREAD(AXT,BNXT,IERR,ID,KEOFX)
      IF(KEOFX.EQ.1)GO TO 50
      BMEANO=0.
      BMEANX=0.
      DO 61 I=1,4
      BMEANO=BMEANO+BNO(I)**2
61    BMEANX=BMEANX+BNX(I)**2
      BMEANO=SQRT(BMEANO/4.)
      BMEANX=SQRT(BMEANX/4.)
      IF(IS.EQ.1)BMEANX=0.
      IF(IS.EQ.2)BMEANO=0.
      BLO=SNR*BMEANO
      BLX=SNR*BMEANX
      DO 95 IN=1,21
      IF(IN.GE.IHO)AO(IN)=AOT(IN)/CORR
      IF(IN.GE.IHX)AX(IN)=AXT(IN)/CORR
      SAT=510./CORR
```

```
      IF(IS.EQ.1)AX(IN)=300.
      IF(IS.EQ.2)AO(IN)=300.
      IF(BMEANO.GT.BMXNS.OR.BMEANX.GT.BMXNS.OR.AO(IN).LT.BLO.OR.
      1AX(IN).LT.BLX)GO TO 81
      DIFE=AO(IN)-AO2(IN)
      IF(DIFE.GT.RE.OR.AO(IN).GT.SAT.OR.AX(IN).GT.SAT)GO TO 81
79    DIFE=AX(IN)-AX2(IN)
      IF(DIFE.GT.RE)GO TO 81
      GO TO 82
81    IR(IN)=IR(IN)+1
      GO TO 95
82    AXAO(IN)=AX(IN)/AO(IN)
      IF(IS.EQ.1)AXAO(IN)=AO(IN)
      IF(IS.EQ.2)AXAO(IN)=AX(IN)
      IF(AXAO(IN).LE.CMIN)GO TO 91
      IF(AXAO(IN).GE.CMAX)GO TO 92
      DO 84 I=1,31
      CI=I
      C=CVS+CI*STEP
      CM=C-STEP/2.
      CP=C+STEP/2.
      IF(AXAO(IN).GE.CM.AND.AXAO(IN).LT.CP)GO TO 90
84    CONTINUE
90    IFA(I,IN)=IFA(I,IN)+1
      GO TO 95
91    IFA(1,IN)=IFA(1,IN)+1
      GO TO 95
92    IFA(31,IN)=IFA(31,IN)+1
95    CONTINUE
      GO TO 48
50    ID=(ID-IDM)/4
      HT=60.
      CALL HEAD(1)
      DO 120 I=1,21
      WRITE(6,110)HT,ID,IR(I)
110   FORMAT(2X,6HHEIGHT,F4.1/2X,I4,1X,13HSAMPLES TAKEN,3X,I4,1X,
      28HREJECTED)
      CS=CMIN
      WRITE(6,112)
112   FORMAT(4X,5HVALUE,3X,4HFREQ,4X,5HVALUE,3X,4HFREQ,4X,
      25HVALUE,3X,4HFREQ,4X,5HVALUE,3X,4HFREQ/)
      DO 118 J=1,31,4
      CS1=CS+STEP
      CS2=CS1+STEP
      CS3=CS2+STEP
      IF(J.EQ.29)GO TO 113
      WRITE(6,114)CS,IFA(J,I),CS1,IFA(J+1,I),CS2,IFA(J+2,I)
      2,CS3,IFA(J+3,I)
      GO TO 118
113   WRITE(6,114)CS,IFA(J,I),CS1,IFA(J+1,I),CS2,IFA(J+2,I)
114   FORMAT(4(F9.2,I7))
118   CS=CS+STEP*4.
120   HT=HT+1.5
      GO TO 10
      STOP
      END
```

```
C       **********RETARD**********
C       RETARD CALCULATES ELECTRON DENSITIES FROM 72 TO 90
C       KM, CORRECTING THE VALUES OF AX, DUE TO THE DIFFE-
C       RENT GROUP VELOCITIES OF THE ORDINARY AND EXTRAOR-
C       DINARY MODES.
C       ************************************************************
C
        DIMENSION CF(13),ED(12),A0(13),AX(13)
        C3(X)=(X*(X*(X*(X+2.465311E1)+1.139416E2)+1.128751E1)+
        22.398347E-2)/(X*(X*(X*(X*(X*(X+2.465681E1)+1.204951E2)+
     2  32.895808E2)+1.492125E2)+9.387737)+1.806412E-2)
        C5(X)=(X*(X*(X+6.69459)+16.90100)+1.16306)/(X*(X*(X*(X*(X+
        26.63145)+35.35526)+68.92050)+64.09346)+4.36057)
1       CALL HEAD(0)
C       COLLISION FREQUENCY MODEL
        CF(1)=27.5E5
        CF(2)=21.5E5
        CF(3)=17.E5
        CF(4)=13.2E5
        CF(5)=10.4E5
        CF(6)=7.8E5
        CF(7)=6.1E5
        CF(8)=4.6E5
        CF(9)=3.5E5
        CF(10)=2.65E5
        CF(11)=2.1E5
        CF(12)=1.5E5
        CF(13)=1.2E5
C       INITIAL CONDITIONS AND CONSTANTS
        HT0=72.E3
        TOR=0.
        TXR=0.
        C=2.997925E8
        TP=6.28318
        W=2.66E6*TP
        F=2.66E6
        W0=2.5961E7
        WX=7.3886E6
        A4=2.398347E-2
        A3=1.128751E1
        A2=1.139416E2
        A1=2.465311E1
        B6=1.806412E-2
        B5=9.387737
        B4=1.492125E2
        B3=2.895808E2
        B2=1.204951E2
        B1=2.465681E1
        D3=1.163064
        D2=1.690100E1
        D1=6.694593
        E5=4.360573
        E4=6.409346E1
        E3=6.892050E1
        E2=3.535525E1
        E1=6.631449
C       READ VALUES OF A0,AX AND ELECTRON DENSITIES CALCULATED
```

```
C       WITHOUT CORRECTION FOR THE RETARDATION OF THE X MODE,
C       BETWEEN 72 AND 90 KM.
        WRITE(6,11)
11      FORMAT(20H ED, 72.7 TO 89.2 KM)
        READ(4,12)(ED(I),I=1,12)
12      FORMAT(E10.2)
        WRITE(6,13)
13      FORMAT(15H AO,72 TO 90 KM)
        READ(4,15)(AO(I),I=1,13)
15      FORMAT(F10.2)
        WRITE(6,14)
14      FORMAT(3H AX)
        READ(4,15)(AX(I),I=1,13)
        CALL HEAD(1)
        WRITE(6,10)
10      FORMAT(4X,2HED,8X,2HHT,8X,3HMUO,7X,3HMUX,7X,2HTO,
        28X,2HTX,7X,5HAX/AO)
        DO 30 I=1,11
        HT=HT0+1.5E3
        CFM=(CF(I)+CF(I+1))/2.
        O=WO/CFM
        Y=WX/CFM
C       DERIVATIVES OF THE FUNCTIONS C3/2(X) AND C5/2(X)
        ANO=O*(O*(O*(O+A1)+A2)+A3)+A4
        DO=O*(O*(O*(O*(O*(O+B1)+B2)+B3)+B4)+B5)+B6
        ANOD=4.*O**3+3.*A1*O**2+2.*A2*O+A3
        DOD=6.*O**5+5.*O**4*B1+4.+B2*O**3+3.*B3*O**2+2.*B4*O+B5
        ANX=X*(X*(X*(X+A1)+A2)+A3)+A4
        DX=X*(X*(X*(X*(X*(X+B1)+B2)+B3)+B4)+B5)+B6
        ANXD=4.*X**3+3.*A1*X**2+2.*A2*X+A3
        DXD=6.*X**5+5.*B1*X**4+4.*B2*X**3+3.*B3*X**2+2.*B4*X+B5
        ANO5=O**3+D1*O**2+D2*O+D3
        DO5=O**5+E1*O**4+E2*O**3+E3*O**2+E4*O+E5
        ANO5D=5.*O**4+4.*E1*O**3+3.*E2*O**2+2.*E3*O+E4
        DO5D=5.*O**4+4.*E1*O**3+3.*E2*O**2+2.*E3*O+E4
        ANX5=X**3+D1*X**2+D2*X+D3
        DX5=X**5+E1*X**4+E2*X**3+E3*X**2+E4*X+E5
        ANX5D=3.*X**2+2.*D1*X+D2
        DX5D=5.*X**4+4.*E1*X**3+3.*E2*X**2+2.*E3*X+E4
        C3OD=TP*(DO*ANOD-ANO*DOD)/(CFM*DO**2)
        C3XD=TP*(DX*ANXD-ANX*DXD)/(CFM*DX**2)
        C5OD=TP*(DO5*ANO5D-ANO5*DO5D)/(CFM*DO5**2)
        C5XD=TP*(DX5*ANX5D-ANX5*DX5D)/(CFM*DX5**2)
C       CALCULATION OF RX/RO
        O1=WO/CF(I)
        X1=WX/CF(I)
        O2=WO/CF(I+1)
        X2=WX/CF(I+1)
        RX1=(Y1*C3(X1))**2+(2.5*C5(X1))**2
        RO1=(O1*C3(O1))**2+(2.5*C5(O1))**2
        RX2=(Y2*C3(X2))**2+(2.5*C5(X2))**2
        RO2=(O2*C3(O2))**2+(2.5*C5(O2))**2
        ABB=(1.25*3182.6*(C5(X)-C5(O)))/(C*CFM)
        DLOGR=ALOG(RX2/RO2)/2.-ALOG(RX1/RO1)/2.
        AXAO1=AX(I)/AO(I)
18      WN2=3182.6*ED(I)
C       GROUP VELOCITIES FOR THE ORDINARY AND EXTRAORDINARY
```

```
C       MODES
        REO=-1.*F*WN2*O*C3OD/(TP*CFM)-WN2*C3(O)*(WO+W)/(TP*CFM**2)
        REX=-1.*F*WN2*X*C3XD/(TP*CFM)-WN2*C3(X)*(WX+W)/(TP*CFM**2)
        AIMO=(5./2.)*WN2*C5(O)/(TP*CFM)+(5./2.)*F*WN2*C5OD/(TP*CFM)
        AIMX=(5./2.)*WN2*C5(X)/(TP*CFM)+(5./2.)*F*WN2*C5XD/(TP*CFM)
        AN2OR=1.-WN2*WO*C3(O)/(W*CFM**2)
        AN2OI=(5./2.)*WN2*C5(O)/(W*CFM)
        AN2XR=1.-WN2*WX*C3(X)/(W*CFM**2)
        AN2XI=(5./2.)*WN2*C5(X)/(W*CFM)
        TGO2=AN2OI/AN2OR
        TGX2=AN2XI/AN2XR
        COSO2=SQRT(1./(1.+TGO2**2))
        COSX2=SQRT(1./(1.+TGX2**2))
        SINO=SQRT((1.-COSO2)/2.)
        COSO=SQRT((1.+COSO2)/2.)
        SINX=SQRT((1.-COSX2)/2.)
        COSX=SQRT((1.+COSX2)/2.)
        AMODO=SQRT(AN2OI**2+AN2OR**2)
        AMODX=SQRT(AN2XI**2+AN2XR**2)
        ANOR=AMODO*COSO
        ANOI=AMODO*SINO
        ANXR=AMODX*COSX
        ANXI=AMODX*SINX
        AMUO=(ANOR*(REO+2.*F)+AIMO*ANOI)/(2.*F*(ANOR**2+ANOI**2))
        AMUX=(ANXR*(REX+2.*F)+AIMX*ANXI)/(2.*F*(ANXR**2+ANXI**2))
        VO=C/AMUO
        VX=C/AMUX
C       CORRECTION OF AX/AO, BY USING A LINEAR INTERPOLATION
        DH=(HT-HTØ)
        TIO=DH/VO
        TIX=DH/VX
        TO=TOR+TIO
        TX=TXR+TIX
        DT=TX-TO
        DAX=AX(I+2)-AX(I+1)
        AXC=AX(I+1)+DAX*DT/(DH/C)
        AXAO2=AXC/AO(I+1)
C       CORRECTED ELECTRON DENSITIES
        DLOGA=ALOG(AXAO2)-ALOG(AXAO1)
        ED1=(DLOGR-DLOGA)/(ABB*DH*2.)
        DED=ABS((ED1-ED(I))/ED(I))
        IF(DED.LE.Ø.15)GO TO 21Ø
        IF(DAX.LE.Ø.)GO TO 12Ø
        ED(I)=(ED1+ED(I))/2.
        WRITE(6,9ØØ)ED1,ED(I)
9ØØ     FORMAT(3H  1,2E12.3)
        IF(ED(I).LT.5.E7.OR.ED(I).GT.1.E1Ø)GO TO 21Ø
        GO TO 18
12Ø     IF(ED1.GT.ED(I))ED(I)=1.1*ED(I)
        IF(ED1.LT.ED(I))ED(I)=.9*ED(I)
        IF(ED(I).LT.5.E7.OR.ED(I).GT.1.E1Ø)GO TO 21Ø
        WRITE(6,9Ø1)ED1,ED(I)
9Ø1     FORMAT(3H  2,2E12.3)
        GO TO 18
21Ø     TOR=TO
        TXR=TX
        HTØ=HT
```

```
      WRITE(6,28)ED(I),HT,AMUO,AMUX,TO,TX,AXA02
28    FORMAT(1P7E10.2)
30    CONTINUE
      GO TO 1
      STOP
      END
```

```
C       **********DECONM**********
C       DECONM CALCULATES DECONVOLUTION OF AO AND AX, AND
C       ELECTRON DENSITIES, USING A LEAST SQUARE APPROXIMATION
C       **************************************************
C
        DOUBLE PRECISION A
        DIMENSION AO(26),AX(26),G(21),CO(21),CX(21),A(21,21),
        2SOS(21),SXS(21),AOD(21),AXD(21),XO(21)
        CALL HEAD(0)
C       G(I) ARE SAMPLES OF THE TRANSMITED POWER TAKEN EVERY
C       1.5KM
        WRITE(6,8)
8       FORMAT(17H PULSE, 5 SAMPLES)
        READ(4,15)(G(I),I=1,5)
        DO 10 I=1,16
        K=I+5
10      G(K)=0.
        WRITE(6,12)
12      FORMAT(14H AO, 21 VALUES)
        READ(4,15)(AO(I),I=1,21)
15      FORMAT(F10.2)
        WRITE(6,17)
17      FORMAT(3H AX)
        READ(4,15)(AX(I),I=1,21)
        WRITE(6,18)
18      FORMAT(24H COLLISION FREQ. PROFILE/
        2 25H SUMMER,WINTER,OR EQUINOX)
        READ(4,19)RESP
19      FORMAT(A5)
        WRITE(6,20)
20      FORMAT(16H GAMMA, FORMAT E)
        READ(4,22)GAM
22      FORMAT(E10.2)
        DO 25 I=1,5
        K=I+21
        AO(K)=0.
25      AX(K)=0.
C       CALCULATION OF EQ (A(N,M)+GAM*B(N,M))*S(N)=C(N)
C       DEFINE A(N,M)
1       DO 35 N=1,21
        DO 35 M=1,21
35      A(N,M)=0.
        DO 40 N=1,17
        DO 40 M=1,5
        KI=N+M-1
        K=N-M+1
        DO 36 L=1,5
        LM=L+M-1
36      A(N,KI)=A(N,KI)+G(L)*G(LM)
        IF(K.LE.0)GO TO 40
        A(N,K)=A(N,KI)
40      CONTINUE
        DO 43 NM=1,4
        N=MM+17
        NM4=N-4
        A(N,NM4)=G(1)*G(5)
        NM3=N-3
```

```
      A(N,NM3)=G(1)*G(4)+G(2)*G(5)
      IF(N.GT.20)A(N,NM3)=G(1)*G(4)
      NM2=N-2
      A(N,NM2)=G(1)*G(3)+G(2)*G(4)+G(3)*G(5)
      IF(N.EQ.20)A(N,NM2)=G(1)*G(3)+G(2)*G(4)
      IF(N.EQ.21)A(N,NM2)=G(1)*G(3)
      NM1=N-1
      LN=22-N
      DO 42 L=1,LN
      L1=L+1
42    A(N,NM1)=A(N,NM1)+G(L)*G(L1)
      DO 43 MM=1,LN
      M=MM+N-1
      KL=LN-MM+1
      DO 43 L=1,KL
      LM=L+MM-1
43    A(N,M)=A(N,M)+G(L)*G(LM)
C     ADD GAM*B(N,M)
      DO 50 N=1,15
      M=N+3
      NM3=M-3
      NM2=M-2
      NM1=M-1
      N0=M
      N1=M+1
      N2=M+2
      N3=M+3
      A(M,NM3)=GAM*(-1./2.)+A(M,NM3)
      A(M,NM2)=GAM*(13./4.)+A(M,NM2)
      A(M,NM1)=GAM*(-17./2.)+A(M,NM1)
      A(M,N0)=GAM*49./4.+A(M,N0)
      A(M,N1)=GAM*(-17./2.)+A(M,N1)
      A(M,N2)=GAM*13./4.+A(M,N2)
50    A(M,N3)=GAM*(-1./2.)+A(M,N3)
      A(1,1)=GAM*1./4.+A(1,1)
      A(1,2)=GAM*(-1.)+A(1,2)
      A(1,3)=GAM*5./4.+A(1,3)
      A(1,4)=GAM*(-1./2.)+A(1,4)
      A(2,1)=GAM*(-1.)+A(2,1)
      A(2,2)=GAM*17./4.+A(2,2)
      A(2,3)=GAM*(-6.)+A(2,3)
      A(2,4)=GAM*13./4.+A(2,4)
      A(2,5)=GAM*(-1./2.)+A(2,5)
      A(3,1)=GAM*5./4.+A(3,1)
      A(3,2)=GAM*(-6.)+A(3,2)
      A(3,3)=GAM*42./4.+A(3,3)
      A(3,4)=GAM*(-17./2.)+A(3,4)
      A(3,5)=GAM*13./4.+A(3,5)
      A(3,6)=GAM*(-1./2.)+A(3,6)
      A(19,16)=A(19,16)+GAM*(-1./2.)
      A(19,17)=A(19,17)+GAM*13./4.
      A(19,18)=A(19,18)+GAM*(-17./2.)
      A(19,19)=A(19,19)+GAM*45./4.
      A(19,20)=A(19,20)+GAM*(-15./2.)
      A(19,21)=A(19,21)+GAM*2.
      A(20,17)=A(20,17)+GAM*(-1./2.)
      A(20,18)=A(20,18)+GAM*13./4.
```

```
      A(20,19)=A(20,19)+GAM*(-15./2.)
      A(20,20)=A(20,20)+GAM*(29./4.)
      A(20,21)=A(20,21)+GAM*(-5./2.)
      A(21,18)=A(21,18)+GAM*(-1./2.)
      A(21,19)=A(21,19)+GAM*2.
      A(21,20)=A(21,20)+GAM*(-5./2.)
      A(21,21)=A(21,21)+GAM
      DO 52 I=1,21
      CO(I)=0.
52    CX(I)=0.
      DO 58 N=1,21
      DO 55 K=1,5
      L=K+N-1
      CO(N)=CO(N)+G(K)*AO(L)**2
55    CX(N)=CX(N)+G(K)*AX(L)**2
58    CONTINUE
C     INVERSION OF EQUATIONS
      CALL MATINV(A,21,DET)
      DO 61 N=1,21
      SOS(N)=0.
61    SXS(N)=0.
      DO 62 N=1,21
      DO 62 M=1,21
      SOS(N)=A(N,M)*CO(M)+SOS(N)
62    SXS(N)=A(N,M)*CX(M)+SXS(N)
      CALL HEAD(1)
      DO 68 I=1,21
      AOD(I)=0.
68    AXD(I)=0.
      DO 70 N=1,21
      DO 69 M=1,5
      MN=N-M+1
      IF(MN.LE.0)GO TO 70
      AOD(N)=AOD(N)+G(M)*SOS(MN)
69    AXD(N)=AXD(N)+G(M)*SXS(MN)
70    CONTINUE
      DO 72 N=1,21
      SOS(N)=(ABS(SOS(N))/SOS(N))*SQRT(ABS(SOS(N)))
      SXS(N)=(ABS(SXS(N))/SXS(N))*SQRT(ABS(SXS(N)))
      AOD(N)=(ABS(AOD(N))/AOD(N))*SQRT(ABS(AOD(N)))
72    AXD(N)=(ABS(AXD(N))/AXD(N))*SQRT(ABS(AXD(N)))
      DO 74 I=1,19
      N=22-I
      SOS(N)=SOS(N-2)
      SXS(N)=SXS(N-2)
74    XO(N)=ABS(SXS(N)/SOS(N))
      WRITE(6,75)GAM
75    FORMAT(6H GAMMA,1PE12.2)
      WRITE(6,80)(SOS(I),I=1,21),(SXS(I),I=1,21),(AOD(I),I=1,21),
     2(AXD(I),I=1,21)
80    FORMAT(1P7E10.2/1P7E10.2/1P7E10.2//)
      WRITE(6,80)(XO(I),I=1,21)
      CALL CALC(XO,1,20,RESP)
      GAM=GAM*1000.
      GO TO 1
      STOP
      END
```

```
C       ********************SUBROUTINE MATINV**********************
C       MATINV INVERTS A SYMMETRIC MATRIX AND CALCULATES ITS DE-
C       TERMINANT.
C       ************************************************************
C
C     USAGE
C       CALL MATINV (ARRAY, NORDER, DET)
C
C     DESCRIPTION OF PARAMETERS
C       ARRAY  - INPUT MATRIX WHICH IS REPLACED BY ITS INVERSE
C       NORDER - DEGREE OF MATRIX (ORDER OF DETERMINANT)
C       DET    - DETERMINANT OF INPUT MATRIX
C
C     SUBROUTINES AND FUNCTION SUBPROGRAMS REQUIRED
C       NONE
C
C     MODIFICATIONS FOR FORTRAN II
C       OMIT DOUBLE PRECISION SPECIFICATIONS
C       CHANGE DABS TO ABSF IN STATEMENT 23
C
C     COMMENTS
C       DIMENSION STATEMENT VALID FOR NORDER UP TO 21
C
      SUBROUTINE MATINV (ARRAY, NORDER, DET)
      DOUBLE PRECISION ARRAY, AMAX, SAVE
      DIMENSION ARRAY(21,21), IK(21), JK(21)
   10 DET = 1.
   11 DO 100 K=1, NORDER
C
C        FIND LARGEST ELEMENT ARRAY(I,J) IN REST OF MATRIX
C
      AMAX = 0.
   21 DO 30 I=K, NORDER
      DO 30 J=K, NORDER
   23 IF (DABS(AMAX) - DABS(ARRAY(I,J))) 24, 24, 30
   24 AMAX = ARRAY(I,J)
      IK(K) = I
      JK(K) = J
   30 CONTINUE
C
C        INTERCHANGE ROWS AND COLUMNS TO PUT AMAX IN ARRAY(K,K)
C
   31 IF (AMAX) 41, 32, 41
   32 DET = 0.
      GO TO 140
   41 I = IK(K)
      IF (I-K) 21, 51, 43
   43 DO 50 J=1, NORDER
      SAVE = ARRAY(K,J)
      ARRAY(K,J) = ARRAY(I,J)
   50 ARRAY(I,J) = -SAVE
   51 J = JK(K)
      IF (J-K) 21, 61, 53
   53 DO 60 I=1, NORDER
      SAVE = ARRAY(I,K)
      ARRAY(I,K) = ARRAY(I,J)
   60 ARRAY(I,J) = -SAVE
```

```
C
C          ACCUMULATE ELEMENTS OF INVERSE MATRIX
C
   61 DO 70 I=1, NORDER
      IF (I-K) 63, 70, 63
   63 ARRAY(I,K) = -ARRAY(I,K) / AMAX
   70 CONTINUE
   71 DO 80 I=1, NORDER
      DO 80 J=1, NORDER
      IF (I-K) 74, 80, 74
   74 IF (J-K) 75, 80, 75
   75 ARRAY(I,J) = ARRAY(I,J) + ARRAY(I,K)*ARRAY(K,J)
   80 CONTINUE
   81 DO 90 J=1, NORDER
      IF (J-K) 83, 90, 83
   83 ARRAY(K,J) = ARRAY(K,J) / AMAX
   90 CONTINUE
      ARRAY(K,K) = 1. / AMAX
  100 DET = DET * AMAX
C
C          RESTORE ORDERING OF MATRIX
C
  101 DO 130 L=1, NORDER
      K = NORDER - L + 1
      J = IK(K)
      IF (J-K) 111, 111, 105
  105 DO 110 I=1, NORDER
      SAVE = ARRAY(I,K)
      ARRAY(I,K) = -ARRAY(I,J)
  110 ARRAY(I,J) = SAVE
  111 I = JK(K)
      IF (I-K) 130, 130, 113
  113 DO 120 J=1, NORDER
      SAVE = ARRAY(K,J)
      ARRAY(K,J) = -ARRAY(I,J)
  120 ARRAY(I,J) = SAVE
  130 CONTINUE
  140 RETURN
      END
```